INTEGRATED MODELING OF MIXED SURFACTANTS DISTRIBUTION AND CORROSION INHIBITION PERFORMANCE IN OIL PIPELINES

by

Yakun Zhu

A dissertation submitted to the faculty of
The University of Utah
in partial fulfillment of the requirements for the degree of

Doctor of Philosophy

Department of Metallurgical Engineering

The University of Utah

December 2015

The University of Utah Graduate School

STATEMENT OF THESIS APPROVAL

The dissertation of **Yakun Zhu**

has been approved by the following supervisory committee members:

Michael L. Free	, Chair	**08/21/2015** Date Approved
Milind Deo	, Member	**08/21/2015** Date Approved
Vladimir Hlady	, Member	**08/21/2015** Date Approved
Jan D. Miller	, Member	**08/21/2015** Date Approved
Hong Yong Sohn	, Member	**08/21/2015** Date Approved

and by **Manoranjan Misra** , Chair of

the Department of **Metallurgical Engineering**

and by David B. Kieda, Dean of The Graduate School.

ABSTRACT

Among the existing corrosion control methods, surfactant inhibitors have widely been used for corrosion inhibition of pipelines in water-oil-steel pipe (WOS) environments. This dissertation includes a systemic review of the causes of pipeline corrosion in WOS environments containing carbon dioxide (CO_2), general corrosion control using surfactant inhibitors and associated concerns, and commonly used classes of surfactants and their properties, various processes and phenomena that affect overall surfactant performance. This dissertation also provides a review of experimental evaluation techniques and various developed models (semi-empirical model, mechanistic model, and multiphysics model) in evaluation of surfactant inhibition efficiency. An integrated corrosion inhibition (ICI) model is proposed, developed, and validated based on the current understanding of the inhibition of CO_2 corrosion in WOS environments using surfactants.

The developed ICI model for the modeling and prediction of corrosion inhibition efficiency of mixed surfactant inhibitors is a multiphysics model, based on the fundamentals from many areas of corrosion science, electrochemistry, metallurgical engineering, and chemical and analytical engineering, etc., and the integration of several submodels, including a water-oil surfactant distribution submodel, the aqueous cmc prediction submodel, and the modified Langmuir adsorption (MLA)/ modified quantitative structure activity relation (MQSAR) submodel. Software is developed based on the ICI model and the use of computational and programming resources.

The phenomena and processes integrated into the ICI model include surfactant partitioning between oil and water, micellization and precipitation, adsorption/desorption at surfaces and interfaces, surfactant-solvent interactions, surfactant-counterion pairing, lateral interactions between surfactant molecules, and fluid flow. These phenomena are incorporated into three main processes and associated modeling: partitioning between oil and water, micellization/precipitation, and effective adsorption on metal substrate and water/oil interface.

The framework of multiphysics ICI model is intended to serve as a basic framework in the understanding of mixed surfactant inhibitor performance with a focus on the application in salt-containing WOS environments. Beyond this, other potential applications may be extended to the design of surfactants, selection of optimal surfactants for specific applications, experimental validation of developed models, simulation of conceivable processes and phenomena, and the integration into more comprehensive lifetime prediction models in which all the surfactant efficiency-affecting factors may be evaluated.

TABLE OF CONTENTS

LIST OF TABLES

LIST OF FIGURES

LIST OF SYMBOLS

a: area per surfactant molecule i at micellar core-water interface.

a_{ch}: area per surfactant molecule at the micelle surface of charge.

a_{hi}: effective cross-sectional area of the hydrated headgroup of surfactant i.

a_{ij}: effective cross-sectional area of the headgroup of surfactant i associated with counterion j.

a_{M}, a_{mi}, and a_{mj}: the activities of micelle $\mathrm{M}_{\mathrm{N,}}$ monomeric surfactant i, and counterion j, respectively.

a_{oi}: area per surfactant molecule i at the interface shielded by the headgroup and equal to min (L_{o}^2, a_{hi}).

$\vec{A}'$: a vector of regression coefficients.

$\bar{B}'$: a regression constant.

C: concentration of total surfactants in solution. When *C* is lower than cmc, it represents monomer concentration; when *C* is higher than cmc, it represents monomeric and micellar form.

C_{m}: overall concentration of total monomers in mixed water-oil environment. C_{mi}: concentration of total mixed surfactant i, including monomeric form and micellar form. If not specified, C_{mi} is default to the concentration in aqueous phase.

$C_{\mathrm{mw:}}$ molar concentration of water.

C_{mo}: molar concentration of oil.

C_j: concentration of counterion j.

C_s: the salt concentration in unit M.

C_{tol}: initial concentration (not at equilibrium) of total surfactants in water phase.

C^o: concentration of total surfactants in oil phase.

C^w: concentration of total surfactants in water phase.

C_i^w: overall concentration of total surfactant 'i' in water phase.

C_i^o: overall concentration of total surfactant 'i' in oil phase.

C_m^o: concentration of total monomers in oil phase.

C_m^w: concentration of total monomers in water phase.

C_{mi}^w: concentration of monomeric surfactant 'i' in water phase.

C_{mi}^o: concentration of monomeric surfactant 'i' in oil phase.

$\bar{C}$: overall average concentration of total surfactants in water-oil environment.

C^-: counterion in aqueous solution, not concentration.

$\bar{C}_{mi}$: overall concentration of monomeric surfactant 'i' in water-oil environment at saturation.

D_f: average value of the diffusion coefficients of diffusing species in unit $cm^2 \cdot s^{-1}$.

D_i: intercept of the plot of $\ln(\Gamma_i)$ vs. $\ln(\gamma_c(C_c + \Gamma_i))$ based on surfactant i in aqueous solutions containing different concentrations of electrolyte.

D' and D'': fitted dimensionless parameters specific to homologous surfactants.

e: the elementary positive charge.

E_{corr}: open circuit potential.

E_{HOMO}: energy of highest occupied molecular orbital.

E_{LUMO}: energy of lowest unoccupied molecular orbital.

E_{pzc}: potential of zero charge.

f: ordinary frequency in unit Hz of electrochemical impedance spectroscopy (EIS) measurement.

f_{i}: activity coefficient of surfactant 'i' in micelles.

$\Delta G_{\mathrm{ad}}^{\mathrm{o}}$: equilibrium adsorption free energy.

i_{corr}: corrosion current density with surfactants in solution.

i_{ocorr}: corrosion current density without surfactants in solution.

I: ionic strength of solution.

j: ion j, including cation and anion, dissociated from 1:1 salt.

k: Boltzmann constant.

k_{s}: Setchenov coefficient.

K_{ad}: equilibrium adsorption constant.

K_{i}: partitioning coefficient of surfactant 'i'.

K_{mix}: apparent partitioning coefficient of mixed surfactants.

$K_{\upsilon}(d)$: modified Bessel function of the second kind.

K': a regression constant, equal to the adsorption constant K_{ad} multiplied by the cmc.

l_{c}: micelle core minor radius.

l_{sp}: optimized core minor radius of spherical micelle.

l_{oi}: extended hydrocarbon tail length of surfactant i.

L: inductance of inductor in unit $\mathrm{H \cdot cm^{-2}}$ in EIS measurement.

L_{i}: the hydrocarbon chain length of surfactant i, which represents the number of carbon atoms in chain.

L_o: the characteristic segment length of hydrocarbon tail (L_o=0.46 nm).

m_i: monomer of surfactant i (i=1, 2, or 3 …).

m_j: monomer of counterion j (j=1, 2, or 3 …).

m_i^+: monomer of cationic surfactant i in dissociated form.

$M_{k'}$ (k' = 1, 2, or 3): k^{th} momentum related to aggregation number and applicable to N_n, N_w, and N_z.

M_N: micelle of an aggregation number N, micelle composition α_i, and a counterion binding coefficient δ_j.

$M^{N(1-\delta_i)^+}$: micelle of surfactant i with aggregation number of N and counterion binding coefficient δ_i.

n: phase shift in EIS measurement. The subscript cpedl, cpe1, or cpe2 represents electrical double layer, surfactant monolayer, or surfactant bilayers/multilayers, respectively.

n_s: average number of segments in hydrocarbon tail.

N: aggregation number of micelle.

N_n, N_w, N_z, and N_Q: the number-based, weight-based, z-based, and quencher-based aggregation number, respectively.

N_{sp}: aggregation number of spherical micelle.

P: parameter in unit $s^{1/2}$ used for fitting the impedance of porous Warburg element w. The subscript 1 or 2 represents porous element w1 or w2, respectively.

P_p: packing factor of surfactant. P_p =1/3 for spherical micelle; P_p =1/2 for cylindrical micelle; P_p =1 for planar micelle.

q: surface charge of micelle.

$\vec{Q}$: a vector of quantum chemical descriptors for a particular surfactant or surfactant mixture.

r_{ch}: the radius of the micelle surface of charge.

R: gas constant.

R_{ct}: charge transfer resistance in in the presence of surfactants.

R_{cto}: charge transfer resistance in in the absence of surfactants.

R_L: resistance of an inductor.

R_p: linear polarization resistance in the presence of surfactants.

R_{po}: linear polarization resistance in the absence of surfactants.

R_s: solution resistance.

R_1: resistance of covered monolayer on electrode surface.

R_2: resistance of covered bilayers/multilayers on electrode surface.

s: as subscript, it represents salt s.

S: shape factor. S=3 for spherical micelle; S=2 for cylindrical micelle; S=1 for planar micelle.

$S_{i:}$ slope of the plot of $\ln(\Gamma_i)$ vs. $\ln\left(\gamma_c(C_c + \Gamma_i)\right)$ based on surfactant i in aqueous solutions containing different concentrations of electrolyte.

t: a function of micelle surface charge density in molecular thermodynamic cmc model.

T: temperature.

v_{CH_2}: volume of methylene group.

v_{CH_3}: volume of methyl group.

v_h: the average volume of hydrated headgroups of mixed surfactants.

v_{hi}: the volume of headgroup of surfactant i.

v_{t}: the average volume of hydrocarbon tails of mixed surfactants.

v_{ti}: volume of a hydrocarbon tail of surfactant i with tail length of L_{i}.

v_{tsp}: optimized average hydrocarbon tail volume in spherical micelle.

V_{sm}: molar volume of surfactant molecule.

V_{o}: volume of oil phase.

V_{w}: volume of water phase.

W: parameter in unit Ω^{-1} $s^{1/2}$ ·cm^{-2}or $S{\cdot}s^{1/2}{\cdot}cm^{-2}$ used for fitting porous Warburg element w. The subscript 1 or 2 represents porous element w1 or w2, respectively.

x_{i}: mole fraction of surfactant i in the total amount of mixed surfactants in bulk solution of discussed. The bulk solution may be pure water, pure oil, or mixture of water and oil.

x_{mi}: the molar fraction of monomeric surfactant i in total mixed monomeric surfactants in bulk solution, which means the bulk mixed molar fraction.

X: mole fraction of total surfactants added in the solution.

X_{c}: mole fraction of counterion in the total amount of species, including water molecules, surfactant molecules, and all ions dissociated from added salts, in bulk aqueous solution.

X_{i}: mole fraction of monomeric surfactant i in the total amount of species in bulk aqueous solution.

X_{mcy}: mole fraction of monomeric surfactant in bulk solution at critical cylindrical micelle concentration.

X_{msp}: mole fraction of monomeric surfactant in bulk solution at critical spherical micelle concentration.

X_{m}: mole fraction of total monomeric surfactants in bulk solution.

X_{M}, X_{mi}, and X_{mj}: the mole fractions of micelle $\mathrm{M_N}$, monomeric surfactant i, and

counterion j in solution, respectively.

X_{Msp}: spherical micelle size distribution.

$X_{\mathrm{mi}}^{\mathrm{w}}$: molar fraction of surfactant 'i' in total amount of molecules in water phase.

$X_{\mathrm{mi}}^{\mathrm{o}}$: molar fraction of surfactant 'i' in total amount of molecules in oil phase.

$X_{\mathrm{j}}^{\mathrm{w}}$: molar fraction of counter 'j' in total amount of molecules in water phase.

Y: pseudo capacitance characterizing constant phase element (cpe) in unit of $\Omega^{-1}\cdot cm^{-2}\cdot s^{n}$. The subscript cpedl, cpe1, or cpe2 represents electrical double layer, surfactant monolayer, or surfactant bilayers/multilayers, respectively.

z_i and z_j: the valences of ionic surfactant i in dissociated form and counterion j, respectively.

Z_{cpe}: impedance of a cpe.

α_i: composition of surfactant i in the micelle, which means mixed molar fraction in micelle. For pure surfactant it is equal to 1.

α_s: mole fraction of salt s in total added salts. $\alpha_s = 1$ for pure salt; $0 < \alpha_s < 1$ multiple salts.

β_{a} : anodic Tafel slope.

β_c: cathodic Tafel slope.

γ_c: mean activity coefficient of ions in aqueous solution.

γ_{hmi}: functional headgroup activity coefficient.

γ_i: activity coefficient of monomeric surfactant i in aqueous solution.

γ_{M}, γ_{mi}, and γ_{mj}: the activity coefficients of micelle M_N, monomeric surfactant i, and counterion j, respectively.

γ_{tmi}: hydrocarbon chain tail activity coefficient.

$\gamma_{\mathrm{mi}}^{\mathrm{w}}$: activity coefficient of monomeric surfactant 'i' in water phase.

γ_{mi}^{o}: activity coefficient of monomeric surfactant 'i' in oil phase.

γ_{mj}^{w}: activity coefficient of counterion 'j' in water phase.

γ_{hmi}^{w}: functional headgroup activity coefficient of surfactant 'i' in water phase.

γ_{tmi}^{w}: hydrocarbon chain tail activity coefficient of surfactant 'i' in water phase.

Γ_{app}: the average concentration in water-oil environments of mixed surfactants at which mixed micelles start to form.

$\Gamma_{app,i}$: the average concentration in water-oil environments of surfactant 'i' at which micelles start to form.

Γ^{w}: the aqueous cmc of surfactant mixture. However, for pure surfactant system, Γ^{w} reduces to the cmc of corresponding pure surfactant.

Γ_{i}^{p}: cmc of surfactant i in pure water.

Γ_{i}^{o}: cmc of surfactant i in oil phase.

Γ_{i}^{w}: cmc of pure surfactant i in aqueous phase.

$\bar{\Gamma}$: surface aggregation concentration of mixed surfactants testing system in aqueous solution in the present work. However, for pure surfactant system, $\bar{\Gamma}$ reduces to sac of corresponding pure surfactant.

δ_i: counterion binding coefficient of surfactant i in traditional cmc model. δ_i barely changes for a series of homologous surfactants. The mean value δ_m is more appropriate to use for mixed homologous surfactants.

δ_i: binding coefficient to micelles of counterion 'j' in molecular thermodynamic cmc model.

δ_m: mean value of counterion binding coefficient calculated from all δ_i of a series of homologous surfactants.

δ_s: the dielectric decrement of added salt s.

ΔE: difference between E_{HOMO} and E_{LUMO}.

ΔH_{tri}^{o}: enthalpy change of transfer of surfactant 'i' from aqueous phase to organic phase.

ΔN: the fraction of electrons transferred from the surfactant to the metal surface.

ΔS_{tri}^{o}: entropy change of transfer of surfactant 'i' from aqueous phase to organic phase.

$\Delta\mu_{act}^{o}$: standard free energy contribution from the activity of surfactant and counterion.

$\Delta\mu_{ch2}^{o}$: standard free energy contribution of methylene group from pure water to organic micelle.

$\Delta\mu_{ch3}^{o}$: standard free energy contribution of methyl group from pure water to organic micelle.

$\Delta\mu_{elec}^{o}$: standard free energy contribution from electrostatic interaction.

$\Delta\mu_{ent}^{o}$: standard free energy contribution from entropy gain associated with headgroup-counterion mixing.

$\Delta\mu_{ich2}^{o}$: standard free energy change of micellization per methylene group of surfactant i.

$\Delta\mu_{ich3}^{o}$: standard free energy change of micellization per methyl group of surfactant i.

$\Delta\mu_{if}^{o}$: standard free energy change of micellization of functional group of surfactant i.

$\Delta\mu_{int}^{o}$: standard free energy contribution from formation of micellar core-water interface.

$\Delta\mu_{i,s/w}^{o}$: standard free energy contribution from the hydrocarbon tail transfer of surfactant i from aqueous solution containing salts to pure water.

$\Delta\mu_{i,w/o}^{o}$: standard free energy contribution from the hydrocarbon tail transfer of surfactant i from pure water to organic micelle.

$\Delta\mu_{m}^{o}$: standard micellization free energy per surfactant molecule with consideration of solution composition of surfactant and with incorporation of surfactant activity and

counterion activity.

$\Delta\mu^{o}_{mic}$: standard free energy change of micellization.

$\Delta\mu^{o}_{mcy}$: minimized standard free energy of micellization for infinite cylindrical micelle.

$\Delta\mu^{o}_{msp}$: minimized standard free energy of micellization for spherical micelle.

$\Delta\mu^{o}_{mic}$: standard micellization free energy per surfactant molecule without consideration of activity.

$\Delta\mu^{o}_{pack}$: standard free energy contribution from hydrocarbon tail packing in the micelle.

$\Delta\mu^{o}_{st}$: standard free energy contribution from surfactant headgroup steric interaction.

$\Delta\mu^{o}_{tri}$: standard free energy change of transfer of surfactant 'i' from aqueous phase to organic phase.

$\Delta\mu^{o}_{trhi}$: standard free energy change of transfer of head group of surfactant 'i' from salt water to organic phase.

$\Delta\mu^{o}_{trt}$: standard free energy contributions from hydrocarbon transfer from salt water into micelle.

$\Delta\mu^{o}_{trti}$: standard free energy change of transfer of hydrocarbon chain of surfactant 'i' from salt water to organic phase.

ϵ, ϵ_w, and ϵ_o: the dielectric constant of solvent, water, and vacuum, respectively.

ζ: Nernst diffusion layer thickness in unit cm.

η: corrosion inhibition efficiency.

θ: electrode surface coverage.

ι: imaginary unit.

κ: the inversed Debye length.

λ_B: the Bjerrum length.

μ_c: chemical potential of counterion.

μ_i: chemical potential of monomeric surfactant i. Please note that all chemical potential and free energy terms are in unit $J \cdot mol^{-1}$or $kJ \cdot mol^{-1}$.

μ_c^o: standard chemical potential of counterion in infinitely dilute solution.

μ_M^o, μ_{mi}^o and μ_{mj}^o: the standard chemical potentials of micelle M_N, monomeric surfactant i, and counterion j, respectively. The standard state of water is defined as pure liquid while the standard state of all other species is defined for an infinitely dilute solution.

μ_{Mi}^o: standard chemical potential of monomeric surfactant i in micelle.

μ_i^w: chemical potential of monomeric surfactant 'i' in water phase.

μ_i^m: chemical potential of surfactant 'i' in mixed micelles.

μ_i^o: chemical potential of monomeric surfactant 'i' in oil/organic phase.

μ_i^{pm}: chemical potential of surfactant 'i' in pure micelles.

$\mu_i^{o,o}$: standard chemical potential of monomeric surfactant 'i' in organic phase.

$\mu_i^{w,o}$: standard chemical potential of monomeric surfactant 'i' in water phase.

μ_j^w: chemical potential of counterion 'j' in water phase.

$\mu_j^{w,o}$: standard chemical potential of counterion 'j' in water phase.

$\bar{\mu}$: dipole moment of surfactant molecule.

υ: factor associated with shape factor *S* and equal to (*S*-2)/2.

σ: micelle surface charge density.

σ_{ini}: the interfacial tension between water and surfactant i in micelle phase.

σ_s: the surface tension of aqueous solution with added salt s.

σ_{sui}: the surface tension of normal alkane tails from surfactant i.

σ_w: the surface tension of pure water.

$\varphi(d_{\mathrm{o}})$: the value of $\varphi(d)$ at $d = d_{\mathrm{o}}$, that is the surface electrical potential at the micelle surface of charge.

ω: angular frequency rad·s^{-1} in EIS measurement.

ACKNOWLEDGEMENTS

The work presented in this dissertation was carried out in the Department of Metallurgical Engineering, University of Utah, under the supervision of Prof. Michael L. Free. Thanks to BP for providing research funding.

Firstly, I would like to give great thanks to my supervisor, Prof. Michael L. Free, for the chance to work with him, and for his help, support, discussions, and encouragement over the last five years. Working with him is my great opportunity to learn that enthusiasm, devotion, and creative thinking are keys to success.

I would also like to thank Prof. Milind Deo, Prof. Vladimir Hlady, Prof. Jan D. Miller, and Prof. H. Y. Sohn for their guidance, discussion, and invaluable suggestions for the completion of my dissertation.

Mass spectrometry tests were performed using the Mass Spectrometry Facility at the Department of Chemistry at the University of Utah. Great thanks are delivered to Dr. Jim Muller and Mr. George Russell for the success of the testing work and the subsequent data analysis.

Thanks also to everyone in Prof. Michael L. Free's research group, for their encouragement, discussions, and suggestions throughout the research project.

Last but not least, I would like to express sincere appreciation and love to all of my family members for their support and encouragement along all the years of my education.

CHAPTER 1

INTRODUCTION*

1.1 General introduction

As an important component of the economy, the oil and gas industry has received considerable attention from researchers because oil mining and transportation have become increasingly expensive due in part to equipment damage caused by corrosive media, such as media containing dissolved H_2S, Cl^-, and CO_2 [1-5]. As a specific oil and gas industry example, pipeline made of carbon steel is easily corroded in environments that contain water and carbon dioxide (CO_2) [4-6]. The annual direct cost of corrosion in United State has been estimated to be around $276 billion or 3.1% of the gross domestic product (GDP). About 3.7% out of the total cost comes from the oil and gas industry [3, 8], which is much of due to the CO_2 corrosion of carbon steel. One piece of corroded X65 pipe steel is shown in Fig. 1.1 for visual evaluation.

CO_2 is usually present in produced "sweet" fluids in the form of a dissolved gas and carbonic acid [9, 10]. Corrosion occurs when steel comes in contact with carbonic acid, which leads to the failure of pipelines, accidents, and economic losses. CO_2 corrosion is affected by many factors based on studies over the past several decades [8,11]: the change in temperature can lead to a change in CO_2 corrosion [12-14] and chemical

* Part of a review manuscript submitted to Corrosion Sci.

composition of corrosion product [9,15]; the increase in CO_2 partial pressure [13,16] and fluid flow rate [17-19] accelerate CO_2 corrosion; the increase in pH [9,12,16], solution salt concentration such as Cl^- [20], and Cr [21] content in the steel matrix can decrease the uniform corrosion rate. In addition, O_2 can enhance CO_2 corrosion rate by acting as a catalyst [22] and H_2S can increase corrosion through its synergistic action with CO_2 [23].

These concerns have led to great interest in industry and academia to control CO_2-related corrosion of pipeline in various oilfields around the world. A widely used corrosion control method is to use organic inhibitors, many of which are surfactants with hydrophilic and hydrophobic molecular sections [24-26]. It is usually assumed that the corrosion inhibition is equal to the effective surface coverage of surfactant inhibitor on steel [27-29]. However, there are many other factors that influence the performance and inhibition efficiency of surfactant, such as surfactant molecule structure, mixed composition of surfactant mixture, water/oil partitioning, the material the surfactant is applied to and surface conditions (roughness, defects, etc.), and the environment in which the surfactants are used (fluid flow, salt concentration, temperature, pressure, etc.), etc.

Extensive research work has been performed in the understanding of these processes but many challenges remain [30-36]. Regarding partitioning, for example, research over a wide surfactant concentration range of various mixed homologous/nonhomologous surfactants has not been systemically reported [37]. A comprehensive theory or model to adequately describe the effects of ions and binding mechanisms on micellization of mixed surfactants over a wide concentration range of salt has not been well developed [29,32,33].

At present, the modeling of corrosion inhibition efficiency η (%) of surfactant

inhibitors is limited to traditional methods, including Langmuir, Temkin, and Frumkin etc. [29, 38-41]. First-principles modeling, which is actually semi-empirical modeling based on best-fit of experimental data such as quantitative structure activity relation (QSAR) [42-46], combined QSAR and mechanistic approaches, is also established. Multiphysics modeling, based on various processes that affect inhibition efficiency, such as fluid flow, pH, speciation, and partitioning [34, 47-49], is also available. However, each of these techniques is at different stages of maturity and has potential limitations.

The emergence and quick development of modeling tools from molecule design, molecular interactions, chemical reaction evaluation, microstructure evolution, device physics, thermodynamics, electrochemical kinetics, fluid mechanics, and process control provides a fundamental basis for integrated predictive modeling of the performance of corrosion inhibitors in industrial settings. Therefore, an integrated corrosion inhibition (ICI) model, following a brief review and discussion of the current understanding of CO_2 corrosion in brine solution, CO_2 corrosion control methods, general properties of inhibitors, various factors affecting efficiency of inhibitors in water-oil pipeline, evaluation techniques of inhibition efficiency, general introduction about modeling consideration and application, and existing models for the evaluation of corrosion inhibitors, is proposed, constructed, and validated to evaluate performance and associated processes of various pure and mixed surfactant inhibitors used in a WOS environments.

1.2 CO_2 corrosion electrochemistry

CO_2 corrosion in aqueous phase, normally initiated as pitting corrosion, is an electrochemical process involving electron transfer that leads to the dissolution of iron at

the anode and the evolution of hydrogen at the cathode. Corrosion products within the pits mainly consist of $FeCO_3$ [16,17,50,51], regardless of the surrounding CO_2 pressure [12]. Upon local anodic iron dissolution, a corrosion product layer of $FeCO_3$ grows on the pit surface due to its low solubility in water (p_{Ksp} = 10.54 at 25 ℃) [50,52,53]. The overall reaction is:

$$Fe + CO_2\,(g) + H_2O\,(l) \rightarrow FeCO_3 + H_2\,(g) \quad 1.1$$

In acidic solution, the anodic reaction follows a general multistep mechanism [12,16,17,50-53]:

$$Fe \rightarrow Fe^{2+} + 2e^- \quad 1.2$$

$$Fe^{2+} + CO_3^{2+} \rightarrow FeCO_3 \quad 1.3$$

$$Fe^{2+} + 2HCO_3^- \rightarrow Fe(HCO_3)_2 \quad 1.4$$

$$Fe(HCO_3)_2 \rightarrow FeCO_3 + CO_2 + H_2O \quad 1.5$$

at the cathode,

$$CO_2 + H_2O \rightarrow H_2CO_3 \quad 1.6$$

$$2HCO_3^- + 2e^- \rightarrow H_2 + 2CO3^{2-} \quad 1.7$$

$$HCO_3^- \rightarrow H^+ + CO3^{2-} \quad 1.8$$

Based on these corrosion processes (Eqs. (1.2)-(1.8)) under appropriate conditions, a corrosion scale $FeCO_3$ is expected to deposit on the surface of the carbon steel.

There are many factors that affect the anodic dissolution of iron in CO_2-saturated solution, such as microstructural features [14, 50], temperature [12-14,54,55], and salt concentration [20,56-59], CO_2 partial pressure [13,16], fluid flow rate [17-19], pH [9,12,16], etc., and thus the dissolution mechanism of iron would be slightly different depending on the specific environment where the steel is deployed. Certain examples are

given for the illustration of various parameter effects on iron dissolution in a CO_2 environment.

For a surface with microcracking due to the characteristic microstructure such as high energy phase/grain boundaries, carbide precipitations, and coarsened dislocations etc., it is reported that the formation of the $FeCO_3$ scale in geothermal water generally takes place in two reaction steps: 1) the Fe[II] compounds in which ferrous hydroxide $Fe(OH)_2$ film forms in the first step [50,53] as shown in Eq. (1.9), leading to an increase of the local pH. 2) At the saturation dissolution of ferrous hydroxide, a $Fe(OH)_2$-passivating film can form followed by the precipitation of a ferrous carbonate scale $FeCO_3$ in Eqs. (1.10) and (1.11) due to the low solubility of $FeCO_3$ in water [50,59,60]. The growth of the corrosion layer depends on the carbon and oxygen partial pressures. If the ferrous carbonate film is highly porous, it may initiate the depassivating of the steel locally, leaving the activated surface susceptible to local corrosion-induced microcracking [50].

$$Fe + 2H_2O \rightarrow [Fe(OH)_2]_{ads} + 2H^+ + 2e^- \quad 1.9$$

$$[Fe(OH)_2]_{ads} + [H_2CO_3]_{ads} \rightarrow FeCO_3 + 2H_2O \quad 1.10$$

$$Fe + CO_3^{2+} \rightarrow FeCO_3 + 2e^- \quad 1.11$$

The characteristics and morphology of corrosion product film $FeCO_3$ are heavily dependent on environmental temperature which, in turn, influences the CO_2 corrosion process [12-14,54,55]. At modest temperature (<70 ℃), anodic dissolution of iron progressively increases with temperature [61]. It is believed that the increase of corrosion rate in the low-temperature range is attributed to an increase of mass-transfer rate due to flow effects and slow $FeCO_3$ formation [14,61]. The corrosion rate gradually diminishes with $FeCO_3$ growth. However, the corrosion process proceeds unhindered at sites of

$FeCO_3$ breakdown, which may lead to severe localized attack [61]. At temperatures above 80 ℃, the solubility of $FeCO_3$ in aqueous solution decreases which eventually leads to $FeCO_3$ precipitation in solution and coverage on steel surface [14, 61]. Therefore, a diffusion process may become the rate-determining step in CO_2 corrosion of iron after the formation of the protective scale. On the other hand, the above discussion does not rule out the possibility of the occurrence of localized corrosion or the formation of nonprotective corrosion scales considering that the diffusion barrier and the porous layer $FeCO_3$ may be superseded by the liquid surface states [14].

The geological formation water in oil and gas wells usually contains dissolved salts at high concentration and it is necessary to investigate the CO_2 corrosion mechanism at high salt concentrations to simulate the commercial environment. It has been found that the corrosion rate of iron is inhibited with the increase of Cl^- concentration [62-64] probably because of the decreased solubility of CO_2 in aqueous phase. However, it is also reported that Cl^- content is important in the onset of localized corrosion and the presence of a small amount of Cl^- could significantly reduce the passivating tendency of steel due to the increased ionic strength and solution conductivity [65,66]. Very recently it has been reported that the maximum iron corrosion rate (around 86μA cm^{-2}) in simulated CO_2-saturated oil well environments is reached at Cl^- (or NaCl) concentration of 25g/L [20]. Below the maximum corrosion rate, CO_2 corrosion is promoted with increasing Cl^- concentration. Above the maximum corrosion rate, however, CO_2 corrosion is inhibited with increasing Cl- concentration because of the significantly reduced CO_2 solubility and the decreased opportunities of H^+, H_2O, H_2CO_3, and HCO_3^- to participate in corrosion. Moreover, Cl^- can destroy the corrosion product films and change the morphology of

corrosion product films, which are in line with previous findings [58,67]. Despite these studies, research on the effect of Cl^- over wide concentration range on CO_2 corrosion is limited. The catalytic mechanism of Cl^- in promoting anodic dissolution is summarized as follows [20,68,69]:

$$Fe + Cl^- + H_2O \rightarrow [FeCl(OH)^-]_{ad} + H^+ + e^- \quad 1.12$$

$$[FeCl(OH)^-]_{ad} \rightarrow FeClOH + e^- \quad 1.13$$

$$FeClOH + H^+ \rightarrow Fe^{2+} + Cl^- + H_2O \quad 1.14$$

The number of holes and cracks in the corrosion product films increases as the Cl^- content increases, and the corrosive medium can pass through these areas to penetrate the films. Consequently, the corrosion of the metallic matrix is accelerated [20].

1.3 Corrosion inhibition using inhibitors

A widely used corrosion control method is to use organic surfactant inhibitors, many of which are surfactants with hydrophilic and hydrophobic molecular sections [24-29]. One example of a surfactant molecule of homologous benzalkonium chlorides (BAC), hexadecyl trimethyl ammonium bromide (C16), is shown in Fig. 1.2 [29]. C16 has a N-based aromatic functional group which is hydrophilic, and a hydrophobic hydrocarbon tail with 16 linear CH_2 and CH_3 sections. The hydrophilic group strongly prefers interaction with polar entities such as water or other ions, whereas the hydrophobic section strongly prefers interaction with other hydrophobic entities such as hydrocarbons. This dual nature of surfactants determines their interactions with surfaces and interfaces.

1.3.1 Hydrophilicity and hydrophobicity of surfactants

The hydrophilic functional group of surfactant molecules strongly prefers interaction with polar entities such as water, metals, and other ions. Generally, surfactants adsorb on the metal surface, block the active sites exposed to corrosive media, and thereby reduce corrosion attack [12,13,29,70,71]. It is believed that the structure of heterocyclic surfactant molecules plays a dominant role in the corrosion inhibition. The presence and structure of specific atoms in these molecules strongly influences the adsorption mechanism and corrosion inhibition efficiency [35,45,70,71]. The atoms N and O functional groups, for example, have tendency to donate electrons to metal substrates which inhibits metal dissolution because of electron lose [29,72].

The hydrophobic portion, which is nonpolar, strongly prefers interaction with hydrophobic entities such as hydrocarbon phase [29,37,71]. Therefore, surfactant molecules are prone to adsorb at and cover the surfaces/interfaces, such as air-liquid surface and liquid-solid interface, to escape from polar solvent such as water by associating and packing hydrocarbon chains together. The surfactant concentration at which a monolayer of surfactant molecules adsorbs on and covers metal surface is termed the surface aggregation concentration (sac) which is critical to corrosion inhibition [22-25,29,71,72]. As surfactant concentration increases, bilayers/multilayers are likely to form on metal surface. Surfactant molecules can also form aggregates in aqueous phase at solubility saturation in a way that they usually orient their hydrophobic tails toward those of neighboring surfactant molecules and their hydrophilic head groups toward water or hydrophilic surfaces. The surfactant concentration at which surfactant molecules start to form aggregates such as micelles in solution is termed the critical micelle concentration

(cmc) [22-25,29,71,72]. It has been shown that the sac is usually much lower than the cmc and that high efficiency of corrosion inhibition is usually achieved at the sac provided that the surfactant is a good corrosion inhibitors [29,71,72].

Surfactant inhibitors usually tend to adsorb on substrates (various metallic materials, such as steel pipe) and behave as a barrier which protects metallic materials from corrosion. It is usually assumed that corrosion inhibition in the presence of low surfactant concentration (usually lower than micelle formation concentration) can be represented by the number of active surface sites of substrate covered by surfactant adsorption [27-29]. More and more active surface area is covered by surfactants and protected against corrosion as surfactant concentration increases. Near the sac or the cmc, the metal surface is assumed to be covered by one monolayer or multilayers of surfactants, respectively [27-29]. As it is previously mentioned that surfactants form micelles at solubility saturation in aqueous phase, the surfactant may form reversed micelles in oil phase at a certain concentration which is termed the oil cmc (Γ^{o}). The cmc in aqueous phase is termed the aqueous cmc (Γ^{w}). The overall average concentration at which the micelle starts to form in the entire oil-water environment is termed the apparent cmc (Γ). The surface coverage θ is given by

$$\theta = \frac{i_{\mathrm{ocorr}} - i_{\mathrm{corr}}}{i_{\mathrm{ocorr}}} \qquad 1.15$$

where i_{ocorr} and i_{corr} are the corrosion current density without and with surfactant inhibitors in solution, respectively.

Schematic representation of the correlation between surface coverage and surfactant concentration based on reported work [28,29,73] is shown in Fig. 1.3. When the surfactant concentration is low, there is only slight adsorption of surfactants on substrate.

At intermediate concentration, surfactants start to aggregate on the substrate but are loosely distributed. At the concentration around the sac, a relatively uniform and porous film of adsorbed surfactants distributed on the substrate, where the substrate is relatively well protected from corrosion [29]. Further increase of surfactant concentration up to and beyond the cmc, the growth of aggregates on substrate occurs mainly by bilayers/multilayers adsorption and hemi-micelles/micelles aggregation, which slightly contributes to additional corrosion inhibition [29].

1.3.2 Adsorption mechanism

The adsorption mechanism of surfactant is usually determined by the adsorption energy $\Delta G_{\mathrm{ad}}^{\mathrm{o}}$, which is correlated to the adsorption constant using the equation below [29,34,71]:

$$K_{\mathrm{ad}} = \frac{1}{C_{\mathrm{mw}}} \exp\left(-\frac{\Delta G_{\mathrm{ad}}^{\mathrm{o}}}{RT}\right) \quad 1.16$$

where K_{ad} is the equilibrium adsorption constant, which is usually calculated based on various adsorption isotherms [34] which will be discussed in the later sections, C_{mw} is molar concentration of water which is 55.5 M, R is the gas constant, and T is absolute temperature. Generally, a negative value of $\Delta G_{\mathrm{ad}}^{\mathrm{o}}$ demonstrates that the adsorption of surfactant on the steel surface is a spontaneous process and shows a strong interaction between surfactant molecules and steel surface [74,75]. If $\Delta G_{\mathrm{ad}}^{\mathrm{o}}$ is more positive than -20 kJ·mol^{-1}, the interaction between surfactant and metal is often classified as physisorption due to electrostatic interaction. When $\Delta G_{\mathrm{ad}}^{\mathrm{o}}$ is more negative than -40 kJ·mol^{-1}, the adsorption usually involves charge sharing or transfer between the surfactant molecules and the metal surface to form coordination bonds, which is also classified as

chemisorption [75,76]. However, physisorption can sometimes be energetically favorable and significant whereas chemisorption may sometimes have relatively weak binding energy due to various factors that influence adsorption [77,78].

1.3.3 Common surfactant inhibitors

The most widely used cationic surfactants are quaternary ammonium salts and amines (when protonated), in which the cation acts as a surface active specie [29,79]. These surfactants usually perform well as inhibitors in low pH solutions because these surfactants should be in the protonated state and low pH is helpful to ensure protonation. It is reported that certain pure and mixed long-chain quaternary ammonium bromides were used as efficient corrosion inhibitors for steel materials [29,71,72,80]. Other typical surfactants commonly used in oilfields include alkyl phenol ethoxylate such as nonylphenol ethoxylate (NPE) [80-83], ethoxylated alcohols [84], polyethylene glycol esters of fatty acids [82], and ethoxylated alkyl phenols [82].

1.3.4 Surfactant mixtures

It has been a practical observation that pure surfactant inhibitor is usually either not available at low cost or not effective enough for corrosion inhibition and a proper mixture containing additional surfactants, intensifiers, solvents, and co-solvents is desired [29,71,72,79,84,85]. In practical applications surfactant mixtures have received wide attention because of their superior physicochemical properties and capabilities in efficient adsorption, solubilization, dispersion, suspension, and transportation [29,87,88]. Solutions containing mixed surfactants can often be conveniently tuned to achieve

desired properties by adjusting the mixture composition. More surface-active and expensive surfactants are usually mixed with less surface-active and less expensive surfactants to reduce cost [29,71].

It is believed that there is a synergistic effect of mixed surfactants on corrosion inhibition of metals [29,71,75,89], which results in an improved performance of mixed surfactants relative to individual surfactants. The synergistic inhibition has been shown to be an effective method of improving the inhibition efficiency, decreasing the amount of dosage, and diversifying the application of surfactants [29,71,75,89]. In addition, a co-operative effect in corrosion inhibition of metals occurs upon introduction of halide ions to corrosive media which contains surfactant inhibitors. However, the addition of halide ions may either stimulate or inhibit corrosion of metal, depending on concentration. It has been reported that the inhibitive effects of halides follow the order of $I^- >> Br^- > Cl^-$. The strong synergistic effect of iodide ion can be explained the chemisorption with metal surface because of its larger size and polarizability [75,90-92]

A synergistic parameter S_{sn}, is introduced to describe the combined inhibition behaviour of amines and halide ions [89]. The synergistic parameter S_{sn} is determined as follows for the interaction of inhibitors 1 and 2

$$S_{sn} = \frac{1-\theta_{1,2}^{calc}}{1-\theta_{1,2}^{meas}} \quad 1.17$$

where $\theta_{1,2}^{meas}$ is the experimentally measured surface coverage of mixed surfactant inhibitors 1 and 2. $\theta_{1,2}^{calc}$ is the calculated surface coverage based on additivity assuming no interaction between the inhibitors and is given by

$$\theta_{1,2}^{calc} = \theta_1 + \theta_2 - \theta_1\theta_2 \quad 1.18$$

where θ_1 and θ_2 are surface coverages based on individual surfactant inhibitors 1 and 2,

respectively.

It is generally agreed that if S approaches 1 no interaction between the two inhibitors exists, if S > 1 a synergistic effect applies, and that if S<1 an antagonistic interaction predominates [89-94].

One example of corrosion inhibition utilization of surfactant mixture is shown in Fig. 1.4. According to the authors [29,72], C16 has good corrosion inhibition for X65 steel but poor solubility in aqueous phase. In contrast, C12 is very easy to dissolve in aqueous phase but can only provide good corrosion inhibition at much higher concentration (~ two orders of higher) and pure C12 is much more expensive than C16. The overall performance of C14 lies in between that of C12 and C16. In addition, the cost to isolate individual surfactant from industrially produced surfactants which are usually mixtures of homologous surfactants is another consideration. Therefore, it is wise to mix the three of them to achieve good corrosion inhibition at the minimized economic investment. It is interesting to find in Fig. 1.4 that the corrosion current density is low at the sac, and additional increase in surfactant concentration above the sac does not contribute much to extra corrosion inhibition.

Certain additional studies on mixed surfactant inhibitor can be found elsewhere [95-97], such as the report using cinnamaldehyde, benzalacetone, and chalcone with propargyl alcohol to protect steel from corrosion in 20% HCl at 90 ℃ [97]; however, the majority of the well-documented work [6,79,98-101] is focused on single compounds as corrosion inhibitors for steel materials, and the corrosion inhibition is usually not effective enough or too costly for industrial applications. Therefore, the development of a comprehensive theory or model is needed to adequately predict steel corrosion inhibition

using various mixed surfactants in WOS environments.

1.4 Various determining factors of inhibitor efficiency

Upon addition to a WOS environment, surfactant inhibitors can be involved in many processes, including adsorption on steel surfaces, water/oil partitioning, precipitation, surfactant interactions, and micellization, etc., which, in turn, affect the availability of monomeric surfactants in aqueous phase, which directly influences corrosion inhibition efficiency [29,34,37,71,72,102]. Other factors, such as environmental temperature and fluid flow rate in pipeline, also need to be considered [34,37]. Therefore, it is not a straightforward task to evaluate the effect of available monomeric surfactants on metal corrosion.

Many corrosion inhibition modeling approaches are available in the literature. These approaches vary from the use of simple inhibitor factors and inhibition efficiency to the application of complicated molecular modeling techniques to describe inhibitor interactions with the steel surface and iron carbonate scale [14,24-29,34,38-49,51,71,72,84-94]. The most used approach is based on the assumption that corrosion protection is achieved by surface coverage and slows down one or more electrochemical reactions, as mentioned previously [29,34,51,71,72]. The criteria to evaluate the efficiency of pure or mixed surfactant inhibitors that are deployed in a WOS environment is summarized in six areas [14,29,34,51,79,103-105]: 1) high corrosion inhibition efficiency η; 2) effective oil/water partitioning; 3) minimal tendency of emulsion formation; 4) availability and stability of surfactant inhibitors; 5) materials compatibility; 6) feasible monitoring and continuous injection of inhibitors. For comprehensive design,

selection, utilization, and performance improvement and prediction of surfactant inhibitors in an industrial WOS environment, the consideration of the above criteria is highly recommended.

Various processes and phenomena which generally occur upon the injection of surfactant inhibitors to a WOS environment are shown in Fig. 1.5 [106]. Certain processes play a dominant role in the determination of corrosion inhibition, such as adsorption on metal surface and oil/water partitioning, while other processes such as adsorption at oil/water interface slightly affect corrosion inhibition. These processes and associated effects on corrosion inhibition will be reviewed one-by-one as follows.

1.4.1 Adsorption at steel/water and water/oil interface

Steel corrosion inhibition is directly determined by the effective adsorption of surfactant monolayers and bilayer/multilayers on the steel substrate/surface due to the physical and chemical blockage of the surface active sites exposed to corrosive media [27-29,72,106]. Physisorption is usually accomplished through van der Waals forces and electrostatic interactions between polar or charged functional groups and charged/polar steel (or other metal substrate) surface [29,72]. The adsorbed surfactant chemically modifies steel in a way that the functional groups partially donate electrons to iron and link the steel substrate by forming a partial chemical bond, leaving the hydrocarbon tails pointing outwards and forming a densely packed hydrophobic barrier which is believed to inhibit the diffusion of water, carbonate ions, halide ions (if there is any), hydrogen ions, and oxygen etc. to the surface [34,106]. Adsorption behavior can usually be evaluated using experimental methods, such as Fourier transform infrared spectroscopy (FTIR) and

polarization modulation infrared reflection absorption spectroscopy (PM-IRRAS) [5,107,108], or using computational approaches such as density functional theory (DFT) and classical molecular dynamics simulation [35,36,41-45,109,110].

The adsorption of a surfactant molecule at a steel surface (it is actually steel/solution interface) can be presented as a substitution adsorption process between the surfactant molecules in aqueous solution, (Sur_{aq}), and the water molecules on the metallic surface (H_2O_{ad}) [111,112]:

$$Sur_{aq} + \varsigma \cdot H_2O_{ads} \leftrightarrow Sur_{ad} + \varsigma \cdot H_2O_{aq} \quad 1.19$$

where ς is an empirical fitting parameter, which is interpreted as the number of water molecules displaced by one surfactant molecule.

Surfactant adsorption is dependent on adsorption energy, lateral interactions of surfactant molecules, and associated entropy change [29,34,38]. As discussed previously, the corrosion inhibition efficiency is assumed to be equal to the effective surface coverage, and thus adsorption models have been constructed from the change of the corrosion rate or equivalent parameters such as polarization resistance and charge transfer resistance from electrochemical measurements as a function of surfactant concentration [29,71,72,113]. The most frequently used adsorption models are the Langmiur, Temkin, Freundlich, Frumkin, Flory-Huggins, Dhar-Flory-Huggins, and Bockris-Swinkels models [29,71,114-119], which are introduced below

Langmuir isotherm

$$K_{\mathrm{ad}} C_{\mathrm{m}}^{\mathrm{w}} = \frac{\theta}{1-\theta} \quad 1.20$$

Temkin isotherm

$$K_{\mathrm{ad}} C_{\mathrm{m}}^{\mathrm{w}} = \exp(\xi\theta) \quad 1.21$$

Freundlich isotherm

$$K_{\mathrm{ad}} C_{\mathrm{m}}^{\mathrm{w}\,1/\varsigma} = \theta \qquad 1.22$$

Frumkin isotherm

$$K_{\mathrm{ad}} C_{\mathrm{m}}^{\mathrm{w}} = \frac{\theta}{(1-\theta)} \exp(-\xi\theta) \qquad 1.23$$

Flory-Huggins isotherm

$$K_{\mathrm{ad}} C_{\mathrm{m}}^{\mathrm{w}} = \frac{\theta}{\varsigma(1-\theta)^{\varsigma}} \qquad 1.24$$

Dhar-Flory-Huggins

$$K_{\mathrm{ad}} C_{\mathrm{m}}^{\mathrm{w}} = \frac{\theta}{(1-\theta)^{\varsigma} \exp(\varsigma-1)} \qquad 1.25$$

Bockris-Swinkels

$$K_{\mathrm{ad}} C_{\mathrm{m}}^{\mathrm{w}} = \frac{\theta}{(1-\theta)^{\varsigma}} \frac{(\theta+\varsigma(1-\theta))^{(\varsigma-1)}}{\varsigma^{\varsigma}} \qquad 1.26$$

where K_{ad} is the equilibrium adsorption constant, $C_{\mathrm{m}}^{\mathrm{w}}$ is the concentration of monomeric surfactant in the electrolyte (aqueous phase), and ξ is the molecular interaction constant ($\xi < 0$ indicates lateral attraction interactions between adsorbed surfactant molecules; and $\xi > 0$ indicates lateral repulsion interactions between adsorbed surfactant molecules). Based on the experimental data, an appropriate adsorption isotherm can be selected for a particular surfactant inhibitor of interest and the associated application can be found elsewhere [29,71,114-119]. Please note that all the isotherms are based on best-fit of experimental data, and they are only partially theoretically sound except the Langmuir isotherm. The best-fit empirical parameters ς and ξusually cannot be extrapolated to other surfactants which include homologous and nonhomologous surfactants.

Recently a multi-interaction (MI) isotherm which describes monolayer adsorption and lateral interactions between adsorbed surfactant molecules and the formation of surface

aggregates based on the combination of Langmuir isotherm and the aqueous cmc has been developed and described as follows [120]

$$\Lambda = \Lambda_{\max,1} \frac{\frac{C_m^w}{\Gamma^w}}{K_{haf,1}+\frac{C_m^w}{\Gamma^w}} + \Lambda_{\max,2} \frac{\left(\frac{C_m^w}{\Gamma^w}\right)^{\varsigma}}{K_{haf,2}+\left(\frac{C_m^w}{\Gamma^w}\right)^{\varsigma}} \quad 1.27$$

where Λ is the equilibrium amount of adsorption concentration (10^7 molecules/colony forming unit (CFU)); $\Lambda_{\max,1}$ and $\Lambda_{\max,2}$ are the maximum adsorption concentrations for the two interactions; $K_{haf,1}$ and $K_{haf,2}$ are half saturation constants for each interaction (unit less); Γ^w is the aqueous cmc. The first term in Eq. (1.27) is a Langmuir isotherm describing monolayer adsorption on the substrate surface, and the second term accounts for lateral interactions between the adsorbed surfactants and formation of the surface aggregates. The multi-interaction isotherm adsorption has been validated for linear polyoxyethylene (POE) alcohol surfactants of the form C_xE_y onto the surface of a *Sphingomonas* sp [120] and an example of the model application to $C_{12}E_9$ is given in Fig. 1.6. The fitting of MI isotherm is excellent over the entire concentration above and below the aqueous cmc while Langmuir isotherm fails to fit well. However, please note that the MI isotherm has three best-fit parameters (ς, $K_{haf,1}$, and $K_{haf,2}$) and that these parameters have the same limitation as those in the regular adsorption isotherms discussed above. Correspondingly, the extrapolation of the fitting parameters to other surfactants usually leads to unreliable results.

As mentioned in the former section, the aqueous sac (represented using $\bar{\Gamma}$) and cmc (represented using Γ^w) are important parameters characterizing corrosion inhibition efficiency of surfactants. Therefore, a new adsorption isotherm termed the modified Langmuir adsorption (MLA) has been reported by incorporating the aqueous cmc into the

regular Langmuir model to evaluate surfactant adsorption and corrosion inhibition efficiency of surfactants under various solution conditions. This approach benefits from the consideration that the cmc is easier to measure and predict than the sac [29,37,71,72,106]. However, the concentration range is usually confined between zero and the sac for accurate evaluation. The MLA is presented below

$$\frac{1}{1-\theta} = 1 + K' \frac{C_{\mathrm{m}}^{\mathrm{w}}}{\Gamma^{\mathrm{w}}}, (C_{\mathrm{m}}^{\mathrm{w}} \leq \bar{\Gamma}) \quad 1.28$$

where K' is equal to the adsorption constant K_{ad} multiplied by Γ^{w}. Note homologous surfactants tend to achieve similar levels of surface coverage at similar ratios of surfactant concentration to surfactant cmc, so the value of K' barely varies for homologous surfactants and can be used as a universal constant for such homologous surfactants [29,72]. Note that the $C_{\mathrm{m}}^{\mathrm{w}}$ can increase up to the aqueous cmc Γ^{w} or above, but the deviation of the prediction from experimental data will increase to some extent (within acceptable range) and not be as good as the prediction for $C_{\mathrm{m}}^{\mathrm{w}}$ below the sac, as shown in following sections, which show that the sac is a transition point in characterizing the effectiveness of adsorbed surfactants for corrosion inhibition. On the other hand, the corrosion inhibition is usually high enough at the sac, and therefore, the continuous increase of surfactant concentration up to the cmc or above does not contribute much to additional corrosion inhibition and thus the deviation between MLA prediction and experimental results at or above the cmc should be small.

The essence of Eq. (1.28) is that the incorporation of cmc can successfully adjust for the effect of solution conditions and surfactant properties, such as salt concentration, solution temperature, hydrocarbon chain length, lateral surfactant interactions, and counterion binding, on surfactant adsorption and thus on corrosion inhibition efficiency.

It is interesting to note that the regression parameter K' in MLA for one surfactant can be transferred (extrapolated) to the corresponding homologous surfactants and other surfactants with similar head groups (usually characterized by quantum descriptors) [29,72]. It is therefore easy to understand that the best-fit parameter of K' of any surfactant mixture can be used for the mixtures of similar surfactants [29,72].

The plots of MLA and some commonly used adsorption models based on the electrochemical measurements for the mixture (C12/C14/C16=0.70/0.25/0.05 in 0.171M NaCl aqueous media with CO_2 saturation and pH=4 at 40 ℃) are presented in Fig. 1.7, in which only MLA shows clearly the feature of the aqueous sac [29,72]. The MLA plot of $\frac{1}{1-\theta}$ vs. $\frac{C_m^w}{\Gamma^w}$ yields a slope of fit parameter K'=13.74, and an intercept of 1 which is in the absence of surfactant inhibitors, as shown in Fig. 1.7(d). There is one abrupt transition around the concentration of the aqueous sac, which indicates that when the surfactant concentration is below the aqueous sac, surface coverage increases rapidly and linearly with the increases in surfactant concentration; above the sac, the increase in concentration does not contribute much to further surface coverage increase. The K'=13.74 can be extrapolated to other mixtures of BAC surfactants and provides predicted surface coverage and inhibition which is comparable to experimental data, as shown in Fig. 1.8 [29,72].

It has been shown that the amount of surfactants adsorbed at the water-oil interface, which is orders of magnitude less than that of monomeric surfactants in the bulk phase provided that there is no turbulent flow of water-oil mixture, is unlikely to significantly impact the mass balance [121] and therefore, this amount of surfactants as well as the effect on the availability of monomeric surfactants in the bulk solution for adsorption on

steel surface and associated corrosion inhibition can be neglected.

1.4.2 Surface aggregation and the aqueous cmc

As discussed in the former section, the incorporation of the aqueous cmc into MLA is a big improvement in the modeling of surfactant adsorption in that this method can describe surfactant adsorption on substrate surface and account for lateral interactions between the adsorbed surfactants and formation of aggregates as well as the environmental effects such as salt concentration, solution temperature, etc.. Therefore, the accurate evaluation of the aqueous cmc of pure and mixed surfactants of interest is critical to the application of MLA. On the other hand, the aggregation process consumes most of surfactants added to the aqueous phase above the aqueous cmc, which inevitably affects the availability of monomeric surfactants for adsorption on metal surface and associated corrosion inhibition [106].

Assuming the monomeric surfactant m_i (i=1, 2, or 3...) is completely dissociated in aqueous solution containing counterion m_j (j=1, 2, or 3…) but in the micelle form the surfactant is associated to some extent with counterions, therefore, the surfactant micellization is described by the following process [72,122-126]

$$N\sum_i \alpha_i m_i^{z_i} + N\sum_j \delta_j m_j^{z_j} \leftrightarrow M_N^{N(\sum_i \alpha_i z_i + \sum_j \delta_j z_j)} \quad 1.29$$

where α_i is the molar fraction of surfactant i in the micelle, M_N, which has an aggregation number N, micelle composition α_i, and an ion binding coefficient δ_j [72,122-126]. For micelles of pure surfactant, $\alpha_i = 1$; for mixed micelles, $0 < \alpha_i < 1$. z_i and z_j are the valences of ionic surfactant i in dissociated form and counterion j. For nonionic surfactant i, $z_i = 0$ and $\delta_j = 0$.

One of the challenges in the study of the aqueous cmc comes from the effects of specific ions and added salts on the aggregation properties of surfactants. Different counterions usually present different effects on the aqueous cmc, micelle shape, micelle growth, micelle size and distribution, mixed micelle composition (for mixed surfactants), and phase separation [122- 124,127-134]. It is reported that the counterion effect on the aggregation properties of cationic surfactants is usually stronger than that of anionic surfactants [131,132]. In addition, the cmc depression due to the counterion effect usually follows the Hofmeister series: OH^- < F^- < Cl^- < Br^- < NO_3^- < ClO_3^- < I^- < benzoate$^-$ < salicylate$^-$ for cationic surfactants; and Li^+ < Na^+ < K^+ < Cs^+ for anionic surfactants [122,131,132]. The specific counterion effects on micelle size and sphere-to-rod transition is usually in the same order as shown previously for cmc [132]. The counterion binding mechanism, however, is not clear and has been a controversial issue [135].

At low salt concentration, the coion effect on cmc, aggregation number, and sphere-to-rod transition is negligible [122,136,137]. However, as salt concentration increases, the coion effect becomes increasingly noticeable [122,136,137]. Particularly at relatively high salt concentration, the coion effect on aggregation properties becomes dramatic, as discussed in the text below.

In the approach proposed by Nagarajan and Ruckenstein [138] based on the work from Evans and Ninham [139], Nagarajan [138] successfully incorporates a parameter which is the distance between the surface of a hydrophobic/micellar core (the micellar core is the micelle with hydrophobic chain and without headgroup) and the center of counterions. This parameter, according to Nagarajan [139], is dependent on headgroup

size, hydrated counterion size, and the distance from the counterion to the charge of ionic surfactant. However, Nagarajan does not provide more details about these dependencies. The molecular thermodynamic theory (MTT) [128, 140-142] provides a great step in progress toward the understanding and modeling of counterion specificity on ionic surfactant micellization. In the theory, the counterion is assumed to bind to the micelle surface in terms of fractional coverage between 0 and 1, and it affects the magnitude of various free energy contributions to the micellization process. The predicted cmc as well as some other properties such as aggregation number and mixed micelle composition are in relatively good agreement with experiment. However, the theory does not clarify the specificity of headgroup-counterion pair interactions. More recently, Moreira and Firoozabadi (MF) [136] improved to some extent the existing MTT [128, 138, 140-143] by the introduction of solvent-shared specific counterion-headgroup pairs. However, the MF model only applies to the spherical and globular micelles in a very narrow range of added salt concentration and does not take into account the sphere-to-rod transition and growth of micelles to long cylinders. Koroleva and Victorov (KV) [144] developed a model that introduces the specific headgroup-counterion pair in which a geometric parameter, called the distance of the closest approach of the ion to the core, is added to take into account hydration effects. Moreover, they adopted a modified Poisson-Boltzmann (PB) equation [145] that incorporates the dispersion interactions between ions and micelles to differentiate the polarizability of different ions, which has also been considered by recently reported work [146]. The predicted cmc, aggregation number, and sphere-to-rod transition are in reasonably good agreement with experiment. However, the incorporation of the dispersion interaction between counterion and micelle in the

modified PB equation does not adequately reflect the effect of counterion specificity on cmc [136].

It is reported that an alternative molecular thermodynamic (AMT) model for the prediction of the aqueous cmc [72,122-124] based on existing MTT [136-143] is developed which incorporates the surfactant activity, counterion activity, and ion effects on surfactant aggregation. In the developed model, the activity coefficient of ions is evaluated using Pitzer's method [147,148] or Davies [149] equation depending on the salt concentration, the activity coefficient of surfactants is evaluated from the Setchenov equation [150], and the specificity of headgroup-counterion pair is considered to reflect hydration effects and the degree of counterions binding to micelles. The counterion binding coefficient is initially set as a variable and finds its optimal value by minimizing micellization free energy. The effect of coion is evaluated from salt-dependent factors [72,122-124,135], including the Setchenov coefficient, the dielectric decrement of salt, and the correlation between the change of surface tension and the change of salt concentration in aqueous solution.

The aqueous cmc of pure surfactant i ($\Gamma_{\mathrm{i}}^{\mathrm{w}}$), or of surfactant mixture (Γ^{w}), is calculated using the equation below (Γ^{w} is used for illustration) [72,122-124]

$$\Gamma^{w} = (C_{\mathrm{mw}} + C_{\mathrm{s}})\exp^{\left(\frac{1}{kT}\Delta\mu_{\mathrm{m}}^{\mathrm{o}}\right)} \tag{1.30}$$

where C_{mw} is molar concentration of water, C_{s} is concentration of salt, k is the Boltzmann constant, T is temperature, and $\Delta\mu_{\mathrm{m}}^{\mathrm{o}}$ is micellization free energy which is calculated from several contributing thermodynamic terms.

$$\Delta\mu_{\mathrm{m}}^{\mathrm{o}} = \Delta\mu_{\mathrm{trt}}^{\mathrm{o}} + \Delta\mu_{\mathrm{int}}^{\mathrm{o}} + \Delta\mu_{\mathrm{pack}}^{\mathrm{o}} + \Delta\mu_{\mathrm{st}}^{\mathrm{o}} + \Delta\mu_{\mathrm{ent}}^{\mathrm{o}} + \Delta\mu_{\mathrm{elec}}^{\mathrm{o}} + \Delta\mu_{\mathrm{act}}^{\mathrm{o}} \tag{1.31}$$

The first three terms on the right side of Eq. (1.31) are associated with the packing and

interactions of hydrocarbon tails and the formation of hydrophobic micellar core: $\Delta\mu^{o}_{trt}$, $\Delta\mu^{o}_{int}$, and $\Delta\mu^{o}_{pack}$ represent free energy contributions from hydrocarbon transfer from water into micelle, formation of micellar core-water interface, and hydrocarbon tail packing in micelle, respectively. The next three terms are associated with surfactant headgroups and counterions in the micelle-water interfacial region: $\Delta\mu^{o}_{st}$, $\Delta\mu^{o}_{ent}$, and $\Delta\mu^{o}_{elec}$ represent surfactant headgroup steric interactions, headgroup-counterion mixing, and electrostatic interactions, respectively [72,122-124]. The last term $\Delta\mu^{o}_{act}$ represents the contribution from surfactant activity and counterion activity in the bulk solution [72,122-124].

The application of this model has been validated using various pure and mixed surfactants in salt solutions [72,122-124]. The model application to pure alkyltrimethylammonium surfactant C_nTABr in solution with added salt (NaBr, NaCl, or KCl) to evaluate chain length effects, counterion effects, and coion effects on aggregation properties is shown in Fig. 1.9 [72,122-124,151-158]. The aqueous cmc (Fig. 1.9(a)) and sphere-to-rod transition threshold (Fig. 1.9(b)) decreases as chain length increases whereas N_w (Fig. 1.9(b)) increases as chain length increases. The predicted aqueous cmc for all surfactants in Fig. 1.9 match very well with experimental data except that a slight deviation appears for C_{12}TABr with added NaBr above 1 M. An excellent agreement is observed between predicted and experimental N_w. The sphere-to-rod transition is manifested by the sharp change of aggregation number, counterion binding coefficient, and core minor radius (not shown here) as a function of salt concentration. The comparison of model predicted transition (salt concentration threshold) and deduced transition from experiment [151-158] match reasonably well. For C_{16}TABr with added

salt KBr, for example, the predicted threshold is 0.08 M and the experimental threshold is 0.1 M [156-158].

The Hofmeister series, which indicates $Cl^-<Br^-$ for cationic surfactant aggregation, is reflected by the effect of counterion on the depression of the aqueous cmc and of counterion binding coefficient, and on the increment of N_w by comparing C_{16}TABr and C_{16}TACl (see Fig. 1.9) [72,122-124]. The effect of coion is examined by adding different salts (NaBr and KBr) to the aqueous solutions containing C_{16}TABr: the coion effect on cmc and on N_w is minor at low salt concentration, whereas increasing salt concentration increases the coion effect becomes increasingly noticeable, as shown in Fig. 1.9 [72,122-124].

It is reported that the AMT model can also be applied to ternary surfactant mixtures, such as cationic/cationic/nonionic mixture: C_{16}TABr/C_{16}BzCl/$C_{16}E_{20}$ with added NaCl in the aqueous solution, as shown in Fig. 1.10 [72,122-124]. Fig. 1.10(a) gives the comparison of predicted cmc from various models, including the Clint model [160], Rubingh and Holland (R-H) model [161-162], and the AMT model [72,122-124], and experimental cmc [159]. The AMT model gives the best prediction while there is an overestimation from the Clint model and an underestimation from R-H model. The predicted aggregation number is only calculated from the AMT model, which gives slightly overestimated but acceptable values.

An improved traditional model [29,71] over the work of a similar kind [27,28] for the prediction of the aqueous cmc is also reported and given below for various pure, binary, ternary, and multiple homologous/nonhomologous surfactant mixtures with i components:

$$\Gamma^{w} = \frac{1}{\sum_i x_i (\gamma_c C_c)^{\delta_i} \left(\frac{1}{\Gamma_i^p}\right)^{(1+\delta_i)}} \qquad 1.32$$

where x_i is the bulk mixed molar fraction of surfactant i. Γ_i^p is the aqueous cmc of surfactant i in pure water (i represents surfactant 1, 2, or 3, …). δ_i is counterion binding coefficient with respect to surfactant i based on best-fit of experimental data. δ_i barely changes for a series of homologous surfactants and is also constant as a function of salt concentration (low to medium depending on specific surfactant class: 0~1) [29,72]. Note that the counterion binding coefficient δ_j in the advanced cmc model is with respect to counterion j and different from δ_i. C_c is the concentration of ion dissociated from electrolyte and from ionic surfactant in aqueous solution. γ_c is the mean activity coefficient of ions in aqueous solution and is usually calculated using Pitzer's method [147,148] or Davies [149] equation. Eq. (1.32) is supported by the report that the cmc is heavily dependent on and exponentially related to electrolyte concentration [125,126,146,163]. The application of this improved traditional model for the aqueous cmc prediction is shown in Fig. 1.11 and details can be found elsewhere [72].

It is clear that the aqueous cmc, which is usually predicted with existing model [29,71,72,122-124], takes into account the ion/salt effect on aggregation/adsorption, headgroup-counterion pair and associated hydration effect, hydrocarbon chain length, van der Waals interactions between surfactant molecules, steric interactions between head groups, electrostatic interactions at the interfacial region of micelles, and the interactions between solvent and surfactant. Therefore, the insertion of the aqueous cmc into the Langmuir isotherm, which is the MLA, can accurately describe the adsorption phenomena and adsorption of surfactants on substrates and associated effects of physical and chemical properties of surfactants and solvent environments. Beyond the applicability of the MLA model for pure surfactant and mixed homologous surfactants, a

valuable part lies in its potential to evaluate the corrosion inhibition of various surfactant mixtures of different classes under various solution conditions using only one set of fit experimental data. Examples are given in Fig. 1.12 with the assumption that the corrosion inhibition efficiency is equal to the effective metal surface coverage [5,27, 29,71,72,122-124].

1.4.3 Kinetics of surfactant adsorption and desorption

The corrosion inhibition efficiency of adsorbed surfactants is also a function of packaging efficiency of surfactant molecules and the competition with other species that promote corrosion (water molecules, halides, and organic acids, etc.). Reports are available using mechanistic modeling [29,71,72,122-124] and molecular modeling perspectives [169-171] regarding the packing efficiency, however, none of these studies assesses the kinetics aspect of surfactant adsorption which actually affects the stability and availability of adsorbed surfactants in a way that if the adsorbed molecules are loosely packed with pores the penetration of corrosive species may occur and promote corrosion [34,172-174]. Therefore, the comprehensive evaluation of the transport of water, halides, carbonate ions, hydrogen and metal-complexes etc. through the porous adsorbed surfactants in the kinetics aspect should be performed. On the other hand, the surfactant concentration in aqueous solution will decrease as a function of time due to their dynamic nature and the surfactant molecules may desorb. Understanding desorption kinetics of surfactants is critical in the optimization of injection frequency of surfactants to ensure effective corrosion inhibition [34,175,176]. The electrochemical tests which are performed in the laboratory to simulate corrosion inhibition performance of surfactants,

however, usually run only a few hours (h) to a few days and that all the tests generally follow the same procedures, so that the effect of kinetics is minimized.

1.4.4 Water/oil partitioning

When an aqueous surfactant solution comes into contact with an immiscible organic liquid, such as oil, surfactant monomers may prefer partitioning into organic liquid until equilibrium is reached between the two liquids [30,37,106,177,178]. Considering the complicity of water/oil partitioning of surfactants in WOS environment and associated interfacial phenomena, the determination of surfactant partitioning between water and oil usually serves as the basis of the hydrophobic-hydrophilic balance [37,106,177-180], which further affects the availability of monomeric surfactants in aqueous phase and the associated adsorption on metal surface for corrosion inhibition [37,106].

For pure surfactant, the partitioning is usually characterized by the partitioning coefficient, which is defined as the ratio of monomeric surfactant concentration in oil to that in aqueous phase (pure water or salt-containing water) [37,106,121,178,179,181]:

$$K_{\mathrm{i}} = \frac{C_{\mathrm{mi}}^{\mathrm{o}}}{C_{\mathrm{mi}}^{\mathrm{w}}} \tag{1.33}$$

where K_{i} is the partitioning coefficient of surfactant i, $C_{\mathrm{mi}}^{\mathrm{o}}$ and $C_{\mathrm{mi}}^{\mathrm{w}}$ are monomeric concentration of surfactant i in oil phase and aqueous phase, respectively.

Extensive research has been performed on low concentration (typically lower than the aqueous cmc) partitioning of nonionic surfactants [37,121,178-180,182-189]. The partitioning research on higher surfactant concentration systems, however, has been rarely reported and limited [31,37,121,190,191]. The relevant report on the partitioning of ionic surfactant at high concentration levels is even less than that for nonionic surfactants

[37,106,192]. The investigation of partitioning above the aqueous cmc and the apparent cmc is important (the apparent cmc is the average concentration in water and oil environment at which the micelle starts to form): the portioning is a monomer process, and the partitioning coefficient is determined by monomer concentrations in the two phases, which are limited by micelle formation [37,106].

For surfactant mixtures, the partitioning becomes more complicated in terms of equilibrium mixture composition in each phase, because of the effect of individual mixed species on the partitioning, and the adsorption of mixture at the oil/water interface [37,106]. It has been shown that for some pure surfactants, a plateau concentration of monomer is reached either in oil phase or in aqueous phase with increasing total surfactant concentration beyond the aqueous cmc [31,193,194]. However, it is also reported for mixed surfactants that the amount of surfactants partitioned into the oil phase continues to increase beyond aqueous cmc [121,191,193]. The partitioning change of mixed surfactants above the aqueous cmc is reported to arise from the selective partitioning of more hydrophobic components into oil phase, which makes the experimental investigation and quantitative modeling work more challenging [31,121,193].

Before moving onto the discussion of partitioning modeling, it is necessary to clarify the relation between partitioning and the aqueous cmc. The aqueous cmc of pure surfactant or mixed surfactants in the absence of oil phase is assumed to be equal to the aqueous cmc in the presence of nonpolar oil phase, which is confirmed by related reports [37,106]. On the other hand, the nonpolar oil phase does not contribute to the micelle formation in aqueous phase. It is actually reported that for nonionic surfactants with non-

polar heptane as oil phase, the aqueous cmc has been observed to be very similar to the corresponding aqueous cmc without oil phase [195] and that for certain anionic surfactants with heptane as the oil phase, the aqueous cmc has also been found to be very close to the cmc measured in water in the absence of oil [196]. For certain cationic surfactants with a more polar oil phase (dichloromethane), however, the aqueous cmc is significantly different from the corresponding cmc with oil phase [102].

It has been reported that the partition coefficients of surfactant in pure water/oil environment can be predicted using semi-empirical modeling [179,187] and quantum chemical methods [34,197,198]. One quantum prediction of partitioning coefficient has been reported to take into account the effect of protonation in aqueous phase [199,200], which is, however, far away from realistic conditions in oilfields where the aqueous phase contains multiple classes of inorganic salts and the crude oils are complex mixtures of organic solvents. It is a challenging task to estimate partitioning from aqueous phase containing various salts into organic mixtures using the partition coefficient for pure water/oil despite the availability of developed theories which are at different stages of maturity [201-206].

Very recently, an improved surfactant partitioning prediction model termed water/oil surfactant distribution model has been reported for the evaluation of partitioning and distribution of mixed surfactants in water (containing salts) and oil (pure toluene, heptane, or mixture of the both) environment [37,106], which is briefly described below and details of model derivation and application can be found elsewhere [37,106].

With this model, the partitioning coefficient K_i of surfactant i is predicted using the following equation [37]

$$K_{\mathrm{i}} = \frac{\gamma_{\mathrm{mi}}^{\mathrm{w}} C_{\mathrm{mo}}}{\gamma_{\mathrm{mi}}^{\mathrm{o}} C_{\mathrm{mw}}} \exp\left(-\frac{\Delta\mu_{\mathrm{tri}}^{\mathrm{o}}}{RT}\right) \quad 1.34$$

where $\gamma_{\mathrm{mi}}^{\mathrm{o}}$ and $\gamma_{\mathrm{mi}}^{\mathrm{w}}$ are activity coefficients of monomeric surfactant i in oil phase and water phase, respectively. $\gamma_{\mathrm{mi}}^{\mathrm{o}}$ is assumed to be unity. $\gamma_{\mathrm{mi}}^{\mathrm{w}}$ is calculated using Pitzer's method [147,148] or Davies [149] equation to take into account the effect of dissolved salt in water on the partitioning process. C_{mo} and C_{mw} are molar concentrations of oil and water, respectively. The standard free energy change of transfer of surfactant i, $\Delta\mu_{\mathrm{tri}}^{\mathrm{o}}$, from water to oil is estimated from the free energy transfer method [37] or reported quantum chemical method [34]. An excellent agreement is observed between predicted and experimental values of K_{i} in Fig. 1.13 for various surfactants [37,106].

The partitioning coefficient of surfactant mixtures is termed the apparent partitioning coefficient and is given by

$$K_{\mathrm{mix}} = \frac{\sum K_{\mathrm{i}} x_{\mathrm{i}} / (V_{\mathrm{w}} + V_{\mathrm{o}} K_{\mathrm{i}})}{\sum x_{\mathrm{i}} / (V_{\mathrm{w}} + V_{\mathrm{o}} K_{\mathrm{i}})} \quad 1.35$$

where x_{i} is molar fraction of surfactant i in the total amount of mixed surfactants. V_{w} and V_{o} are volumes of water and oil phase, respectively.

The apparent aqueous cmc of mixed surfactants is given by

$$\Gamma_{\mathrm{app}} = \frac{1}{\sum \frac{x_{\mathrm{i}}}{f_{\mathrm{i}} \Gamma_{\mathrm{i}}^{\mathrm{w}} V_{\mathrm{w}} / (V_{\mathrm{w}} + V_{\mathrm{o}}) + f_{\mathrm{i}} K_{\mathrm{i}} \Gamma_{\mathrm{i}}^{\mathrm{w}} V_{\mathrm{o}} / (V_{\mathrm{w}} + V_{\mathrm{o}})}} \quad 1.36$$

where f_{i} is activity coefficient of surfactant i in micelles (assumed to be unit). $\Gamma_{\mathrm{i}}^{\mathrm{w}}$ is the aqueous cmc value of surfactant i.

Concentration of total monomeric surfactants, C_{m}, in water and oil phases can be calculated by solving the following equation when there is micelle formation in water/oil environment:

$$\sum \frac{x_{\mathrm{i}} C_{\mathrm{tol}}}{C_{\mathrm{tol}} - C_{\mathrm{m}}(1 + V_{\mathrm{o}}/V_{\mathrm{w}}) + f_{\mathrm{i}} \Gamma_{\mathrm{i}}^{\mathrm{w}} + f_{\mathrm{i}} K_{\mathrm{i}} \Gamma_{\mathrm{i}}^{\mathrm{w}} V_{\mathrm{o}} / V_{\mathrm{w}}} = 1 \quad 1.37$$

where C_{tol} is initial concentration (not at equilibrium) of total surfactants added to water phase. With the calculated C_m and K_i, the distribution of monomeric surfactant i in both water and oil can be determined.

Molar fraction of surfactant i in mixed micelles is written as

$$\alpha_i = \frac{x_i C_{tol} V_w - (C_{mi}^o V_o + C_{mi}^w V_w)}{C_{tol} V_w - C_m (V_o + V_w)} \quad 1.38$$

With this developed model, the partitioning coefficient K_i of surfactant i, the aqueous cmc of surfactant i, the apparent cmc of mixed surfactants in water-oil environment, Γ_{app}, monomer concentration of surfactant i in water and in oil phase, C_{mi}^w and C_{mi}^o, and molar fraction of surfactant i in the mixed micelles, α_i, can be predicted in water (containing salts)-oil (nonpolar) at given inputs which include total surfactant concentration and mixed molar ratio x_i in bulk solution. If experimental data for cmc and partitioning coefficient of surfactant i are available, use the experimental data; if no experimental data are available, use the methods introduced above to predict the aqueous cmc and the partitioning coefficient and then substitute these values into surfactant distribution model. Examples of model validation can be found in Fig. 1.14 and Fig. 1.15 [37]. As can be seen from the figures, all predicted partitioning associated properties match experimental data very well.

However, there are some limitations regarding this model in ways that the oil phase should be nonpolar or slightly polar organic solvents which do not or affect only slightly the aqueous cmc of surfactants and that no vigorous stirring is allow in the partitioning process to avoid microemulsion formation. These problems should be addressed in the future modeling work.

1.4.5 Precipitation with corrosion products

It has been reported that [34] the ions Fe^{2+} and Fe^{3+} from iron dissolution can combine with surfactant molecules to form complexes or ligands which affect the availability of monomeric surfactants in bulk solution and thus compromise adsorption on metal surface and the corrosion inhibition efficiency of surfactants. It is also likely that the surfactant adsorption consists of such ligands or complexes that affect the packing efficiency of SAM/multiplayers [209]. Other components, such as sand, can also compromise the efficiency of surfactant inhibitors in a way that these components can act as an alternative adsorption sink for the surfactant inhibitors [34]. Besides the characterization of the specific complex formation processes using experimental techniques, mechanistic models, which are usually based on a combination of the best-fit of experimental data and associated theory, may become more useful in a way that the developed model can be extrapolated to similar testing systems, such as the previously mentioned MLA [27, 29,71,72,122-124]. Please note that the quantum chemical methods may be used to evaluate complex formation [34,210-213], but it is difficult to simulate the conditions in realistic WOS environments.

1.4.6 Fluid flow in WOS environment

It is necessary to take into account the flowing water/oil fluid in WOS environments for the evaluation of surfactant corrosion inhibition efficiency because the inhibitor concentration profile will change over time and thus affects corrosion inhibition [34]. The flow rate can be simulated using an experimental setup, such as a flow loop [214] or simply a rotating disk electrode [29,71,215], multiphysics modeling, such as finite

element modeling [216], or the combined mechanistic modeling with experimental evaluation [29,71], so that a relation between the flow rate and surfactant injection frequency can be set up for effective corrosion inhibition. Another challenge is that the vigorous flow may cause formation of microemulsions in either aqueous or oil phase or both, which are difficult to evaluate through modeling.

1.4.7 Salt/ion effects

The aqueous phase in oilfields generally contains mixtures of various inorganic salts, which not only promote the corrosion of metal in ways as discussed previously but also affect surfactant-associated processes, including aggregation, adsorption, partitioning, surfactant-ion pair, hydration, and thus affect the corrosion inhibition. Any experimental evaluation and modeling work should take this into account. Alternatively, the ion effects on the efficiency of surfactant adsorption may be incorporated into certain processes associated with surfactants, such as aggregation and micellization which are well accounted for by the above mentioned MLA [27, 29,71,72,122-124] and partitioning which is evaluated by a surfactant water/oil distribution model [37,106]. At present, these mechanistic modeling methods are well developed to describe the effect of simple 1:1 salts (such as NaCl). More complicated salts (such as $Fe(NO_3)_3$) [27, 29,37,71,72,106122-124] will require more work so that the model can be tuned for application in more complicated systems with mixtures of salts.

1.4.8 Microstructure of metal

In the evaluation of corrosion inhibition efficiency of surfactants, it is recommended that for experiment, the metal surface conditions should be consistent and for modeling work, certain thermodynamic and kinetics parameters should be considered to describe the metal surface state and microstructure evaluation as a function of time. The cathodic and anodic reactions may be changed in ways that the state of metal surface is inevitably affected by the corrosive media, such as pH, salts, and temperature and that the metal surface is generally inhomogeneous and contains defects and contaminants which preferentially initiate local corrosion attack ahead of uniform metal corrosion. Corrosion inhibition may be affected by surfactant adsorption and preferential adhesion to certain microstructural features which promotes either the cathodic or anodic reaction. For example, the interaction between surfactants and metal surface defects may alter the steady state of protective oxide film which defines the long-term corrosion inhibition [217-220].

To minimize the error introduced by microstructure of metal surface, it is recommended all tests follow the same procedures for sample surface preparation and cleaning and that try to avoid the preferential corrosion attack introduced by these procedures [221-225]: for example, minimization of the edge effects when samples are cut from bulk metal [221] and avoidance of deep scratches when metal surface is polished [226-228]. Furthermore, the degreasing agent should not be corrosive to metal samples [221], and cleaning of corrosion products should follow standard method such as ASTM G1 standard [225], etc. More details about the role of metal surface and microstructure and surface preparation in the corrosion inhibition have been reported

elsewhere [34,79].

With all the points (1-8) discussed in mind, it is realized that the evaluation of surfactant performance in WOS environment is never a trivial work and that experimental characterization and mechanistic modeling should incorporate at least most of the major processes, such as adsorption, partitioning, aggregation, and salt effects, and neglect the so-called “unknown unknowns” [229]: for example, if the discussed oil itself plays a role in corrosion inhibition and if so how and to what extent.

1.5 Corrosion inhibition evaluation: experiment

A suite of laboratory tests is recommended and performed for specific applications of pure or mixed surfactant inhibitors to evaluate the associated corrosion inhibition performance before deployment in actual oilfields [79, 85,223]. The test conditions in the laboratory should be the same or as close as possible to the actual conditions in the oil pipelines, such as the composition of tested metallic material, the temperature, salt concentration, etc. Tests are usually performed in flow loop which simulate the realistic oil pipe [214] or simply a rotating disk electrode in glass cell [29,71,215] with real or simulated environment. Commonly used test techniques in corrosion inhibition evaluation include linear polarization resistance [29,71,72,123], potentiodynamic scans [29,71,72,123], electrochemical impedance spectroscopy [29,71,72,123], electrochemical noise [223], and weight loss measurement [230].

1.6 Corrosion inhibition evaluation: modeling

Many different mathematical models have been developed for the evaluation of corrosion inhibition using surfactant inhibitors in WOS environment, including semi-empirical models [42-46], mechanistic models [29,38-41,71,72,114-119,123], combined semi-empirical and mechanistic models [49,231], and multiphysics models [34, 47-49,72], which will be reviewed in this section.

1.6.1 Semi-empirical models

Semi-empirical models are usually based on best-fit of the experimental data using partially theoretical basis. Before the use of these models, model calibration should be performed with a sufficiently large and reliable experimental data set so that they can be extrapolated to other testing systems with confidence. However, the calibration usually leads to the appearance of certain constants with sound physical meaning but others constants as arbitrary best-fit parameters. It is, therefore, very likely that extrapolation can lead to unreliable and sometimes physically unrealistic results because of these best-fit parameters. Another issue with semi-empirical models is that they only focus on the effective surface coverage and adsorption energy while ignore other aspects that are essential for evaluation of corrosion inhibition of surfactants, such as salt effect, micelle formation, and packing efficiency, etc.

One model of this kind is the quantitative structure activity relation (QSAR) approach [42-46] which assumes that corrosion inhibition efficiency can be evaluated as linear/nonlinear coupling of quantum chemical descriptors with experimentally determined inhibitor efficiencies. The coupling based on best-fit of experimental data

yields a set of regression parameters which has no theoretical basis at all and can hardly be extrapolated to other surfactants or testing systems even of similar kind due to a very small and thus unreliable calibration data set, which severely limits their utility [34,72,123].

Other types of semi-empirical models may include various developed adsorption isotherms, the details of which can be found in the section of "Adsorption at steel surface and water/oil interface".

1.6.2 Mechanistic models

Mechanistic models have a sound theoretical basis in ways that they can describe the mechanisms of corrosion inhibition using surfactant. Most constants in these models have a clear physical meaning, despite the fact that the determination of some constants still requires best-fits of limited experimental data. When established using one set or limited sets of reliable experimental data, these models can produce accurate predictions with sound physical meaning, as well as reliable extrapolated predictions to other systems. Improvement of these models is feasible by adding parameters or coupling with other approaches.

One such model is introduced in the section of "Adsorption at steel surface and water/oil interface", which is the mechanistic MLA model [29,37,71,72,106,123]. Similarly, a modified QSAR model, the MQSAR model [72,123], is an improvement over most existing QSAR models in surfactant inhibitor studies in that the aqueous cmc is coupled with the regular QSAR models to take into account various physical phenomena and solution environments.

The cmc, which is usually determined by one rigorous thermodynamic model as mentioned above [72,122-124], actually takes into account the various physical phenomena such as surfactant aggregation/adsorption, difference in chain length, and van der Waals interactions between surfactant molecules, etc., and solution environments such as salt concentration and ionic species [72,122-124]. Therefore, the insertion of the aqueous cmc into the regular Langmuir adsorption and QSAR can accurately describe the adsorption phenomena of surfactants on substrates (metal electrode) and associated effects of physical and chemical properties of surfactants and solvent environment. The set of regression parameters which is obtained from the best-fit of experimental data of only one surfactant can be extrapolated to various pure and mixed homologous series of this surfactant class and to various pure and mixed surfactants of similar class [29,72,123]. The more valuable part lies in its potential to evaluate the corrosion inhibition of various surfactant mixtures of different classes at various solution conditions using only one set of experimental data. Examples of comparison of MLA- or MQSAR-based predictions and experimental data are given in Fig. 1.16 for corrosion inhibition evaluation assuming corrosion inhibition is equal to effective surface coverage [72,123]. The experimental parameters of associated different testing systems are summarized in Table 1.1.

1.6.3 Multiphysics models

The basic idea of a multiphysics model in the evaluation of the corrosion inhibition performance of surfactants in WOS environment is that all the conceivable processes and phenomena that affect the overall surfactant corrosion inhibition should be considered

and incorporated into one integrated model in which connections between various processes and resulting effects on ultimate corrosion inhibition is explored with submodels associated with critical processes that are integrated and evaluated. Unknown factors that may affect surfactant performance are uncovered and incorporated, and software package is utilized, based on the fundamentals from many areas of corrosion science, electrochemistry, metallurgical engineering, and chemical and analytical engineering, etc. Existing models/submodels and computational and programming resources are used for the description of associated processes. Other potential applications of such a model may be extended to the design of surfactants, selection of optimal surfactants for specific applications, experimental validation of developed models, and simulation of conceivable processes and phenomena. Such modeling can be integrated into comprehensive lifetime prediction models in which all the surfactant efficiency-affecting factors may be evaluated.

It has been reported recently that a multiphysics perspective for the performance of surfactant inhibitors in WOS environment is proposed following the systematic domains and processes approach, in which, according to the authors, several physical and chemical processes contributing to the ultimate surfactant inhibitor efficiency are evaluated [34]. However, data reported for the validation of such a model is very limited and, tremendous amount of experimental and modeling work remains to be implemented before ultimate application.

1.7 Objectives of the present research

With all the above discussed points in mind, an integrated corrosion inhibition (ICI) model, in this work, has been proposed for the modeling and prediction of corrosion inhibition efficiency of mixed surfactant inhibitors based on the integration of several thermodynamic or mechanistic submodels. The submodels include: 1) the water-oil surfactant distribution submodel which evaluates the surfactant partitioning in water/oil environment; 2) the aqueous cmc prediction submodel which takes into account the effects of various physical and chemical properties of surfactants and solution environments on aggregation and micellization; and 3) the MLA/ MQSAR submodel which considers the effects of major processes such as partitioning and aggregation on surfactant adsorption and determines the ultimate effective surface coverage.

The phenomena and processes integrated into the ICI model include surfactant partitioning between oil and water, micellization and precipitation, adsorption/desorption at surface/interface, fluid flow, surfactant-solvent interactions, surfactant-counterion pair, and lateral interactions between surfactant molecules (see Fig. 1.5). These phenomena are incorporated into three main processes and associated modeling considering the feasibility of experimental evaluation and model validation: partitioning between oil and water, micellization/precipitation, and effective adsorption on metal substrate and water/oil interface. Fluid flow is simulated using rotating disc electrode test. The last three phenomena in the domain of multilayer/micelle-water interfaces are incorporated into an effective adsorption process using associated modeling. The metal electrode surface is prepared consistently following standard procedures to minimize systemic error on ultimate corrosion inhibition. The ICI model does not focus on the surfactant injection

process/frequency, such as the modeling of the evolution of total surfactant concentration through a flowing water/oil mixture as a function of time from injection, nor does it consider surfactant migration along the length of the pipeline although these kinetics-related issues will be addressed in an improved version of this model in the future.

In the next few chapters of this thesis, the development of each of the submodels as well as the ICI model will be introduced one-by-one in detail and each is followed by the validation using existing experimental data from this work and literature reported results to demonstrate the applicability and robustness of ICI model in corrosion inhibition prediction of various pure and mixed surfactants in WOS environment. Beyond this, the framework of ICI model is intended to serve as a basic framework for development of more powerful predictive models/tools in the understanding of design, selection, optimization, and utilization of various pure and mixed surfactant inhibitors with a focus on the application in salt-containing WOS environments.

The following chapters are organized as below:

Chapter 2: corrosion inhibition of various mixed surfactants

Chapter 3: MLA and MQSAR models for corrosion inhibiton prediction

Chapter 4: effects of micellization and aggregation on corrosion inhibition

Chapter 5: effects of surfactant partitioning and distribution on corrosion inhibition

Chapter 6: integrated modeling of surfactant corrosion inhibition performance

Chapter 7: Conclusions

Table 1.1 Experimental conditions for different surfactant testing systems. cmc and sac are estimated values based on experiment [72, 123].

Testing system	Surfactant Mixed ratio	Salt *C*(M)	*T* (℃)	pH	Electrode	Rotation (RPM)	cmc (μM)	sac (μM)
I	$C_{14}BzCl/C_{14}BzCl/C_{16}BzCl$ 0.70/0.25/0.05	NaCl 0.171	40	4	X65 steel	300	140	72
II	$C_{14}BzCl/C_{14}BzCl/C_{16}BzCl$ 0.33/0.33/0.33	NaCl 0.599	40	5	X65 steel	100	16.5	9
III	AAOA 1	NaCl 0.856	25	6	1018 steel	low	15	8.2
IV	CPC 1	HCl 1	31	0	1018 steel	1000	1.5	1
V	$C_{16}TAB$ 1	$Fe(NO_3)_3$ 0.03	32	---	copper	1000	30	20

*AAOA: N-[2-[(2-aminoethyl) amino] ethyl]-9-octadecenamide; CPC: cetylpyridinium chloride; C16TAB: Hexadecyl trimethyl ammonium bromide.

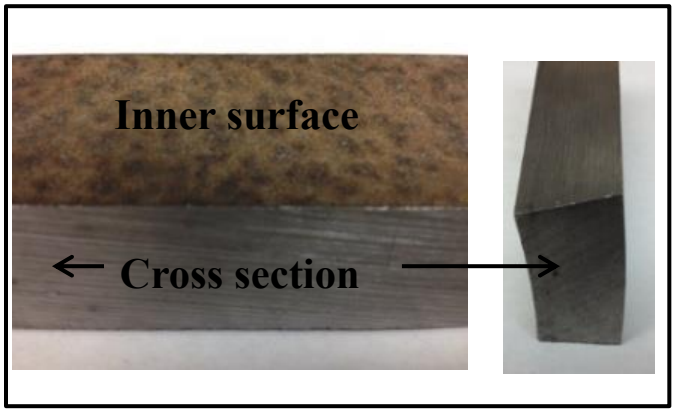

Fig. 1.1 One piece of sample corroded X65 pipe steel used in oilfields

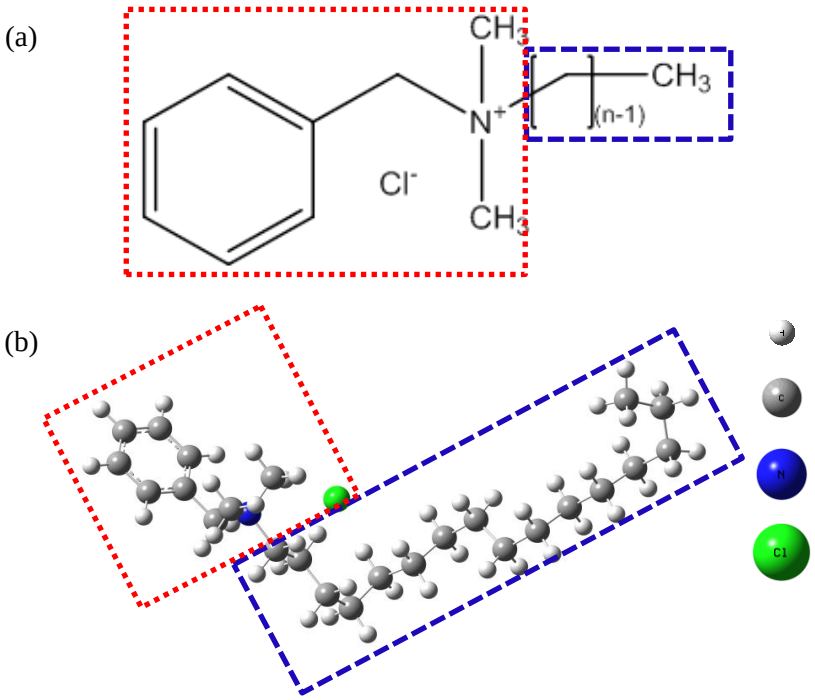

Fig. 1.2 Chemical formula of benzyl dimethyl hexadecyl ammonium chloride (C16, $C_{16}Cl$, or $C_{16}BzCl$) (a) and optimized molecular geometry (b) [29]. Dotted line region: functional group; dashed line region: hydrocarbon tail.

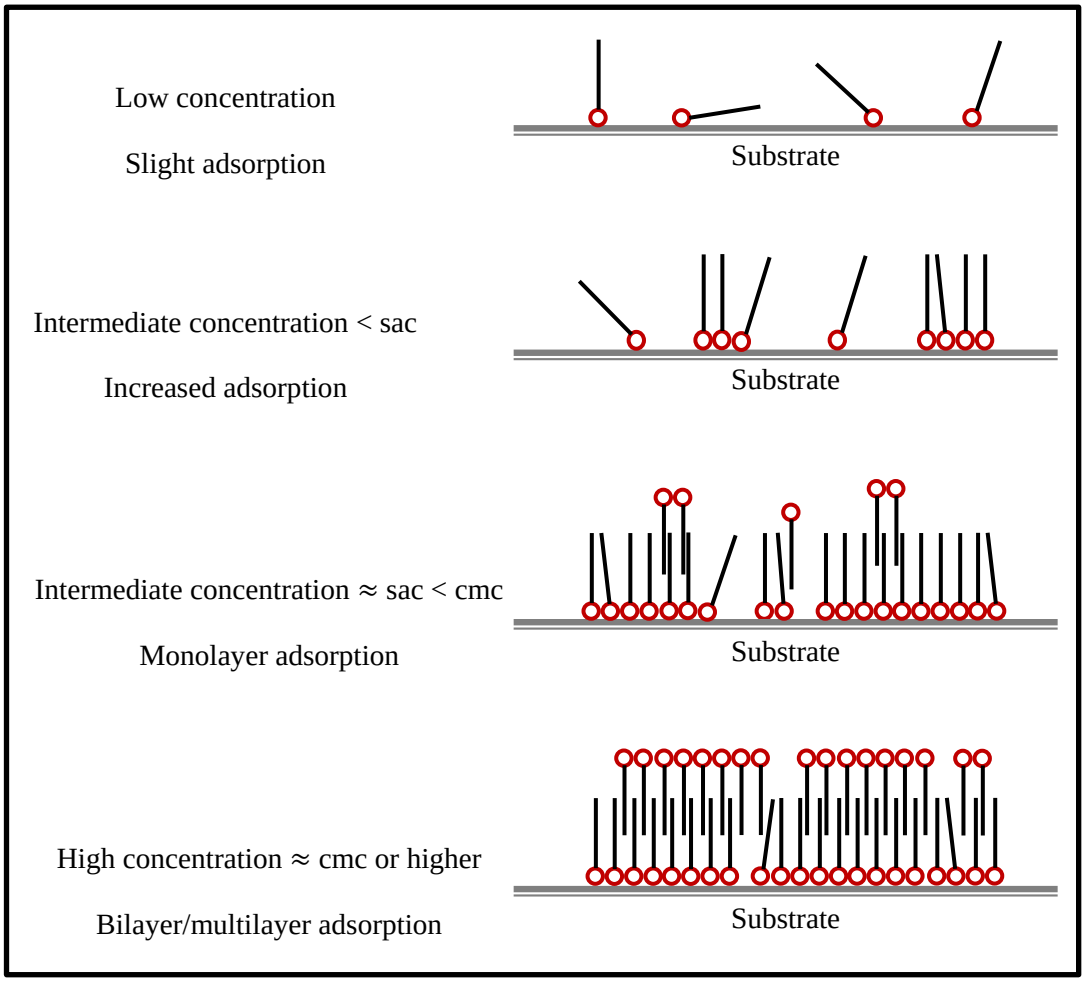

Fig. 1.3 Schematic representation of the correlation between surface coverage and surfactant concentration [28,29,73].

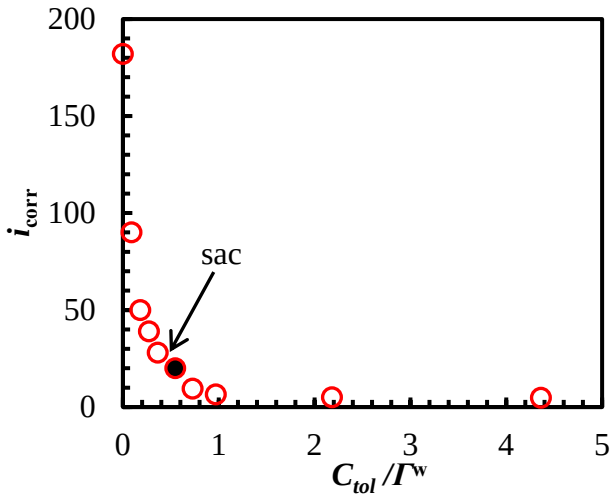

Fig. 1.4 Corrosion current density as a function of total concentration of mixed BAC surfactants (C12/C14/C16=1:1:1) divided by the aqueous cmc Γ^{w} in 0.599 M NaCl containing aqueous solution at 40 ℃ and pH=5 [29].

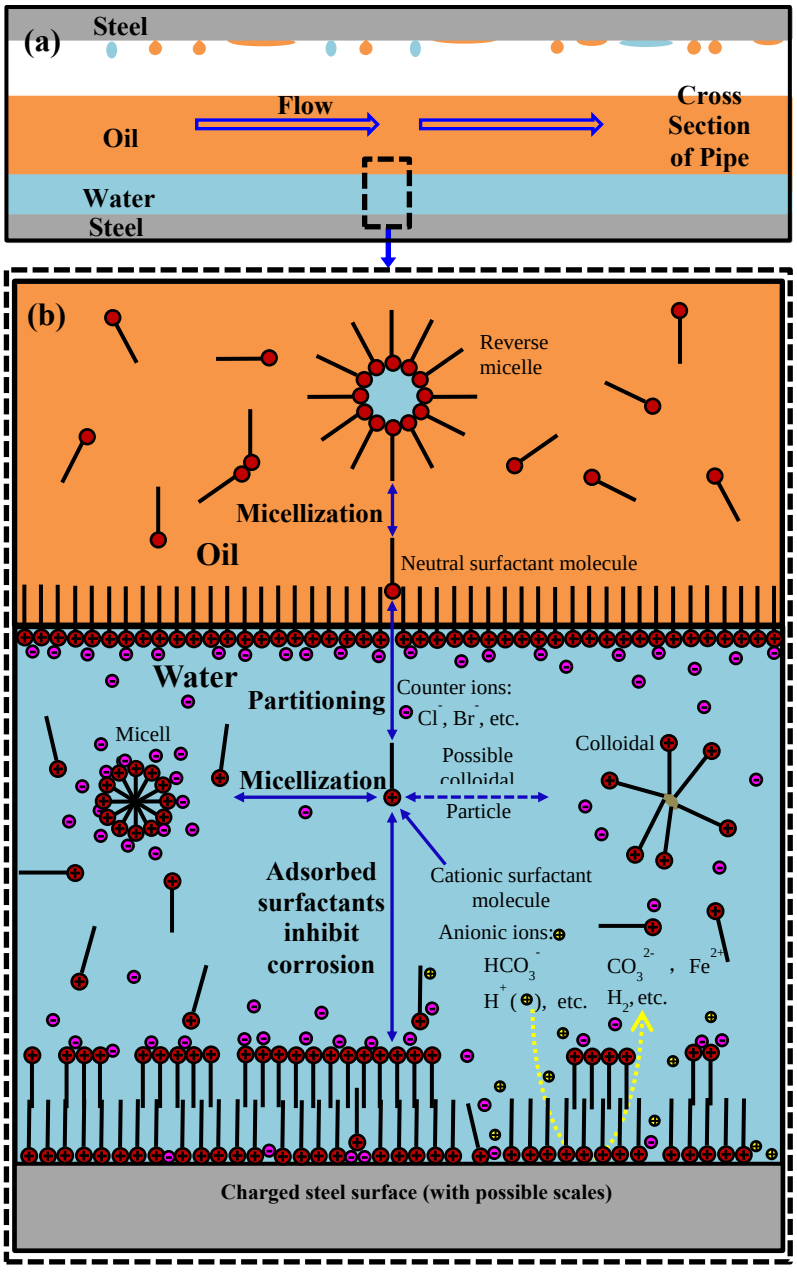

Fig. 1.5 Surfactant distribution in WOS environments: (a) cross-section of steel pipe containing water, oil, and some oil vapor; (b) schematic illustration of cationic surfactant distribution and various processes in a WOS environment with dissolved CO_2 at the average surfactant concentration above the apparent cmc [106].

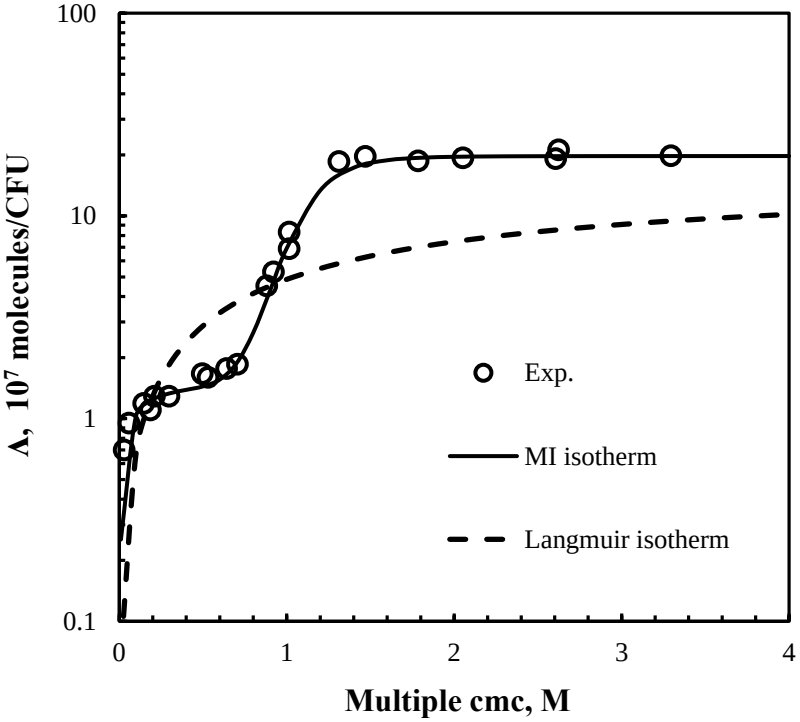

Fig. 1.6 Comparison of experimental and fitted adsorption isotherms for $C_{12}E_9$ onto the Sphingomonas sp [120].

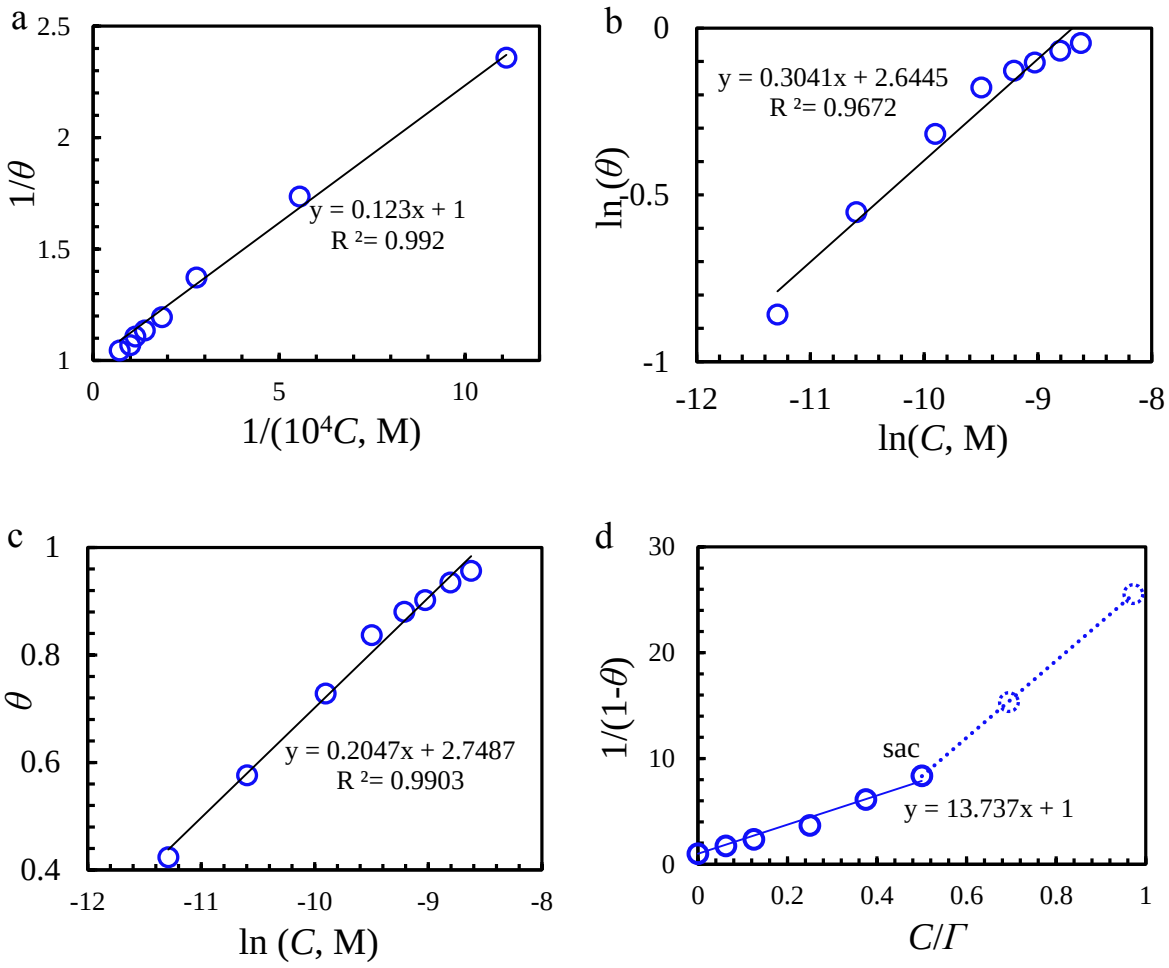

Fig. 1.7 The adsorption isotherms on X65 steel electrode of mixed BAC (C12/C14/C16=0.70/0.25/0.05) in 0.171M NaCl aqueous media with CO2 saturation and pH=4 at 40 ℃: (a) Langmuir adsorption; (b) Freundlich adsorption; (c) Temkin adsorption; (d) Modified Langmuir adsorption (MLA) [29,72].

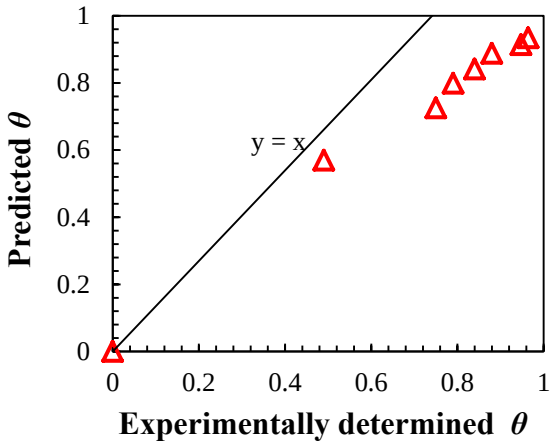

Fig. 1.8 The comparison of experimentally determined surface coverage and predicted surface coverage based on MLA and extrapolated parameter $\boldsymbol{K'}$=13.74 on X65 steel electrode of mixed BAC (C12/C14/C16=1/1/1) in 0.599M NaCl aqueous media with CO_2 saturation and pH=5 at 40 ℃ [29,72].

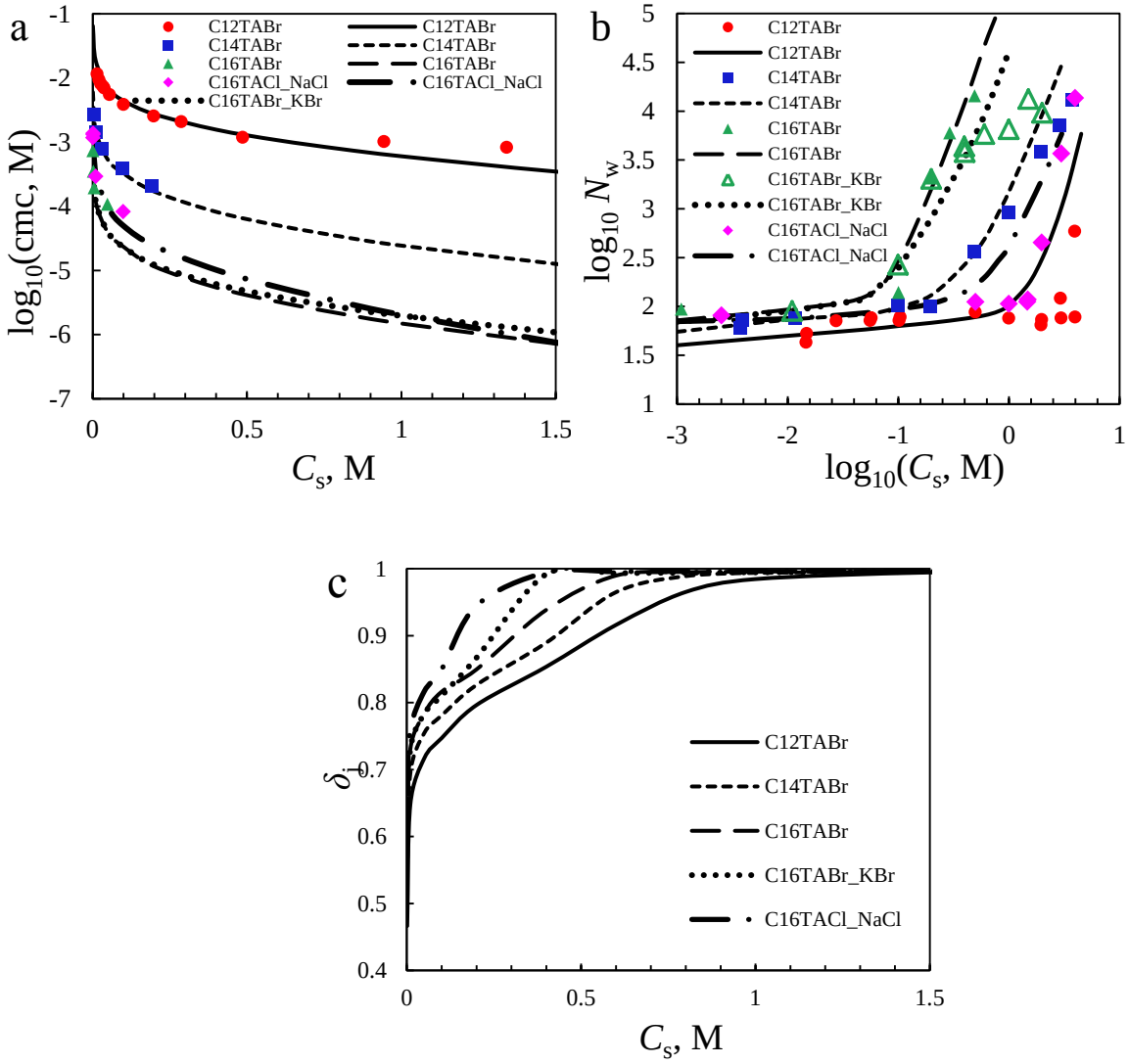

Fig. 1.9 Comparison of predicted and experimental aggregation properties: (a) cmc, (b) weight-based aggregation number N_w, and (c) counterion binding coefficient of alkyltrimethylammonium bromide/chloride C_nTAX (X=Br^-, Cl^-) vs. salt concentration. The salt type is specified in the legend; if not specified, the default salt is NaBr. Solid and dashed lines represent model prediction; symbols represent experimental data cited from references [72, 122, 151-158]. Model inputs based on experimental conditions: 35 ℃, and total solution concentration of surfactant set at 10 mM for $C_{14}TABr$ and $C_{16}TABr/Cl$, and at 30 mM for $C_{12}TABr$.

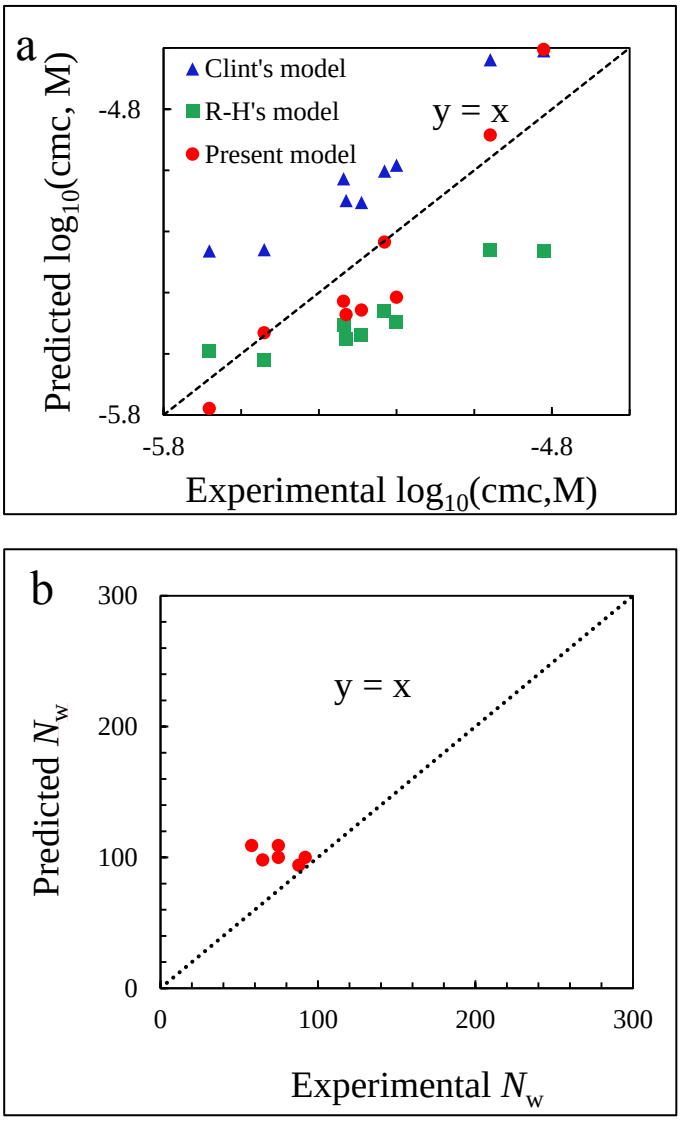

Fig. 1.10 Predicted (a) cmc, and (b) aggregation number of ternary mixed surfactants C_{16}TABr, C_{16}BzCl, and $C_{16}E_{20}$ vs. experimental results. In (a) solid and dashed lines represent model prediction; symbols represent experimental data cited from reference [122]. Predicted values in (b) are from AMT model. Inputs of model according to experiment conditions: 30 mM NaCl, 25 ℃, and total solution concentration of surfactant set at cmc.

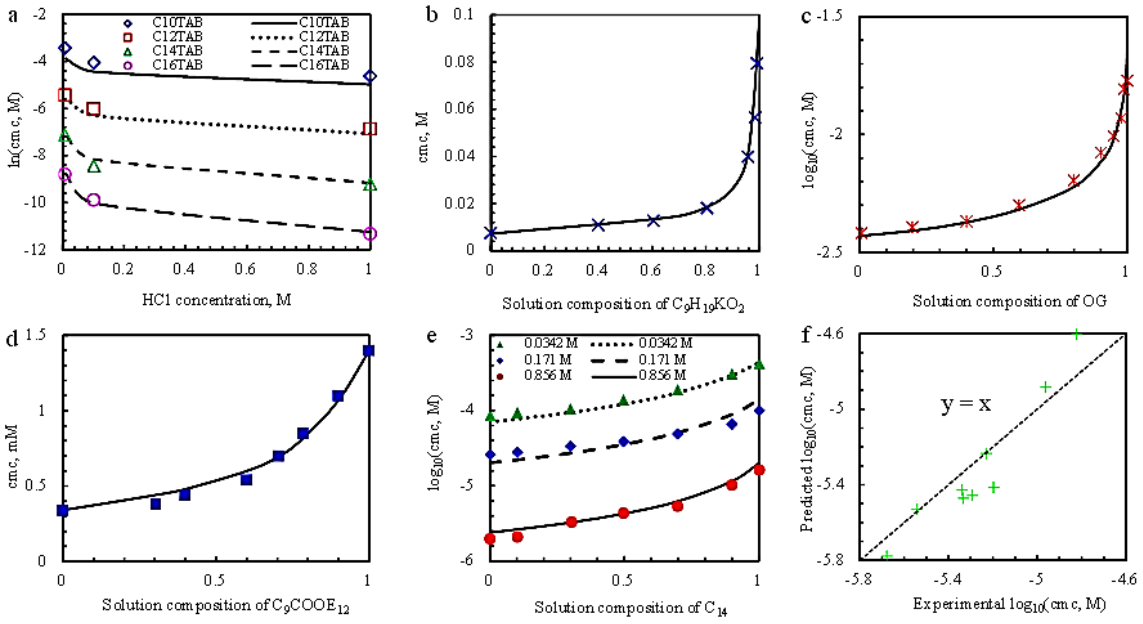

Fig. 1.11 Comparison between predicted and experimental cmc: (a) cmc of pure CnTAB as a function of HCl concentration in solution at T = 25 ℃; (b) cmc of binary mixed nonionic surfactants ($C_9H_{19}KO_2$ and $C_{11}H_{23}KO_2$) as a function of bulk mixed molar fraction of $C_9H_{19}KO_2$ at T = 25 ℃; (c) cmc of binary mixed anionic and nonionic surfactants (SDS and OG) as a function of mixed bulk solution composition of OG with 20 mM NaCl at T = 25 ℃; (d) cmc of binary mixed nonionic surfactants (C_9COOE_{12} and $C_{11}COOE_{12}$) as a function of bulk mixed molar fraction of C_9COOE_{12} at T = 25 ℃ without salt; (e) cmc of ternary mixed homologous cationic surfactants BAC (C12, C14, & C16) as a function of mixed molar fraction of C14 with NaCl concentrations of 0.0342 M, 0.171 M, or 0.856 M at T = 40 ℃; C12 & C16 are equal-molar mixed; (f) predicted cmc vs. experimental cmc of ternary mixed cationic, cationic, and nonionic surfactants (C16, C_{16}TAB, and $C_{16}E_{20}$) at various mixed molar ratios with 30 mM NaCl in solution at T = 25 ℃. Symbols represent experimental data; lines represent model predicted data. Experimental data of cmc in Figures (a)-(d) & (f) is cited from references [98,159,164-167]. C_nTAB: n-alkyl trimethyl ammonium bromide; $C_nH_{(2n+1)}KO_2$: potassium alkanoate; OG: octylglucoside; SDS: sodium dodecyl sulfate; C_nCOOE_{12}: $C_nH_{(2n+1)}COO(CH_2CH_2O)_{12}CH_3$; C_n: n-benzalkonium chloride or BAC; $C_{16}E_{20}$: polyoxythylene cetyl ether. Data are cited from [72].

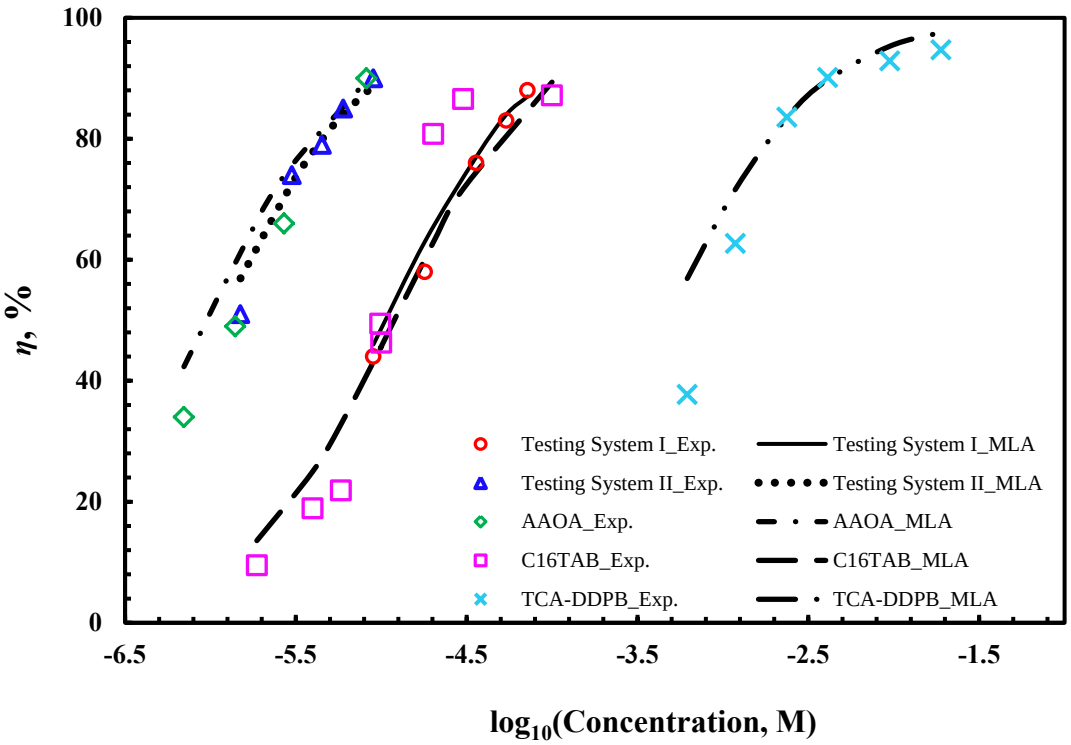

Fig. 1.12 Comparison between experimental inhibition efficiency and predicted inhibition efficiency for different testing systems of mixed BAC-X65 steel at 40 ℃ [71] and reported testing system using surfactant AAOA [5], surfactant C_{16}TAB [27] , and surfactant mixture of TCA-DDPB [168] based on MLA. *K′* are 15.73 for AAOA-1018 steel system in 0.856 M NaCl aqueous solution at 25 ℃, 2.52 for C16TAB-copper system in 0.03 M $Fe(NO_3)_3$ aqueous solution at 32 ℃, 20.26 for TCA-DDPB-J55 steel in 10% HCl aqueous solution at 30 ℃. AAOA: N-[2-[(2-aminoethyl) amino] ethyl]-9-octadecenamide; TCA: trans-cinnamaldehyde; DDPB: dodecylpyridinium bromide. Data are cited from reference [71].

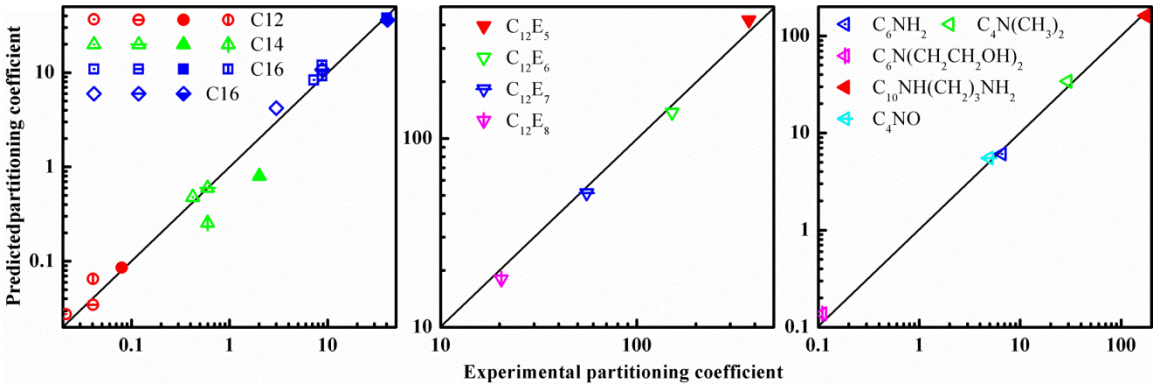

Fig. 1.13 Comparison of predicted partitioning coefficient and experimental partitioning coefficient [37]. (a) Pure C12, C14, and C16 partitioning in water and oil (toluene) environment at 40 ℃. Open symbols: 0 M NaCl water and oil partitioning; open symbols with center dot: 0.0342 M NaCl water and oil partitioning; open symbols with (vertical and horizontal) center cross line: 0.171 M NaCl water and oil partitioning; half-filled symbols: 0.804 M NaCl water and oil partitioning; solid-filled symbols: 0.856 M NaCl water and oil partitioning. (b) Polyoxyethylene glycol n-dodecyl ether ($C_{12}E_n$) partitioning in pure water and isooctane environment at 25 ℃. (c) Alkyl amines partitioning in 0.1 M NaOH water and heptane at 20 ℃. Experimental data cited from reference [37,186,194,207].

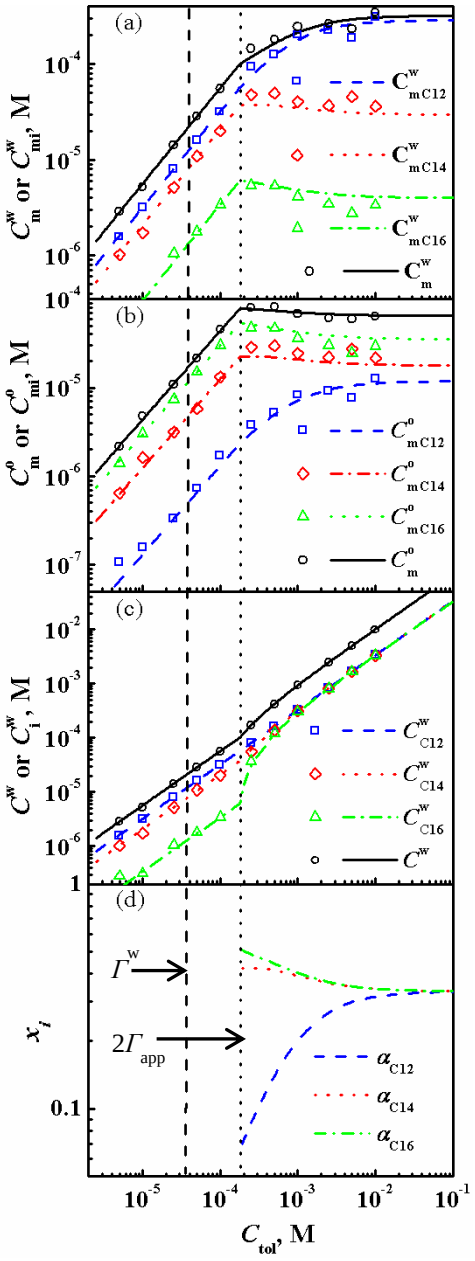

Fig. 1.14 Equilibrium partitioning properties of equal-molar mixed BAC surfactants (C12, C14, and C16) in water (0.171 M NaCl)-oil environment at 40°C: (a) equilibrium concentration of monomeric surfactants in water, (b) in oil, (c) equilibrium concentration of total surfactants in water, including monomer and micellized form, and (d) micelle composition of surfactant i as functions of total initial concentration of surfactants added to water. Symbols: experiment; lines: model prediction. Vertical dash line represents the cmc of surfactant mixture in aqueous phase: Γ^w; vertical dot line represents twice of the apparent cmc of surfactant mixture in water-oil environment: $2\Gamma_{app.}$ Data are cited from reference [37].

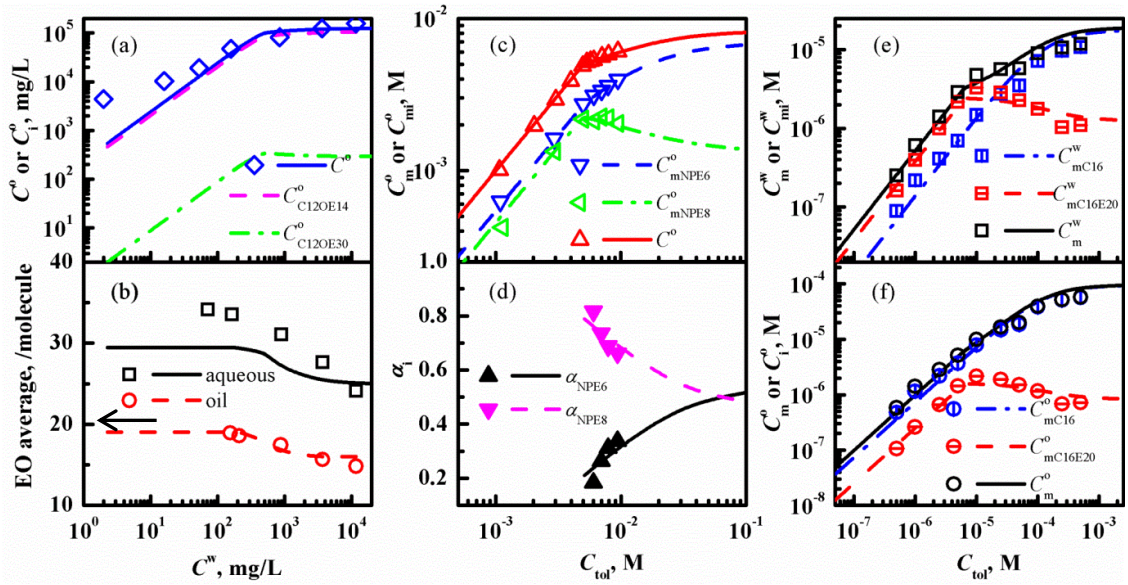

Fig. 1.15 Comparison between predicted and experimental partitioning properties of surfactants. (a) and (b) are equilibrium partitioning properties of mixed $C_{12}OE_{14}$ and $C_{12}OE_{30}$ surfactants in water-oil (trichloroethylene) environment at 25°C: (a) concentration of surfactants (b) average ethoxylate group (EO) distribution in aqueous and oil phase as a function of equilibrium aqueous concentration C^w. The values of aqueous cmc are 123.2 mg/L and 560 mg/L for $C_{12}OE_{14}$ and $C_{12}OE_{30}$, respectively. Mixed ratio: 0.475/0.525. The arrow in (b) indicates the initial EO average in water-oil environment. (c) and (d) are equilibrium partitioning properties of mixed NPE_6 and NPE_8 surfactants in water-oil (cyclohexane) environment at 25°C: (c) concentration of monomeric surfactants in oil phase (d) molar fraction of surfactants in mixed micelles as a function of C_{tol}. The values of aqueous cmc and partitioning coefficients are 2.70×10^{-5} M and 4.05×10^{-5} M, and 481 and 70 for NPE_6 and NPE_8, respectively. Mixed ratio: 0.542/0.458. (e) and (f) are equilibrium partitioning properties of mixed C16 and $C_{16}E_{20}$ surfactants in water-oil (heptane) environment at 25°C: (e) concentration of monomeric surfactants in 0.03 M NaCl aqueous phase (f) in oil phase as a function of C_{tol}. The predicted values of aqueous cmc and partitioning coefficients from previous work are 3.61×10^{-5} M and 2.47×10^{-6} M, and 5.32 and 0.66 for C16 and $C_{16}E_{20}$, respectively. Mixed ratio: 0.542/0.458. Lines: model prediction; symbols: reported data. Reported data in Figs. (a)-(f) are cited from literature [31,37,121,193,208].

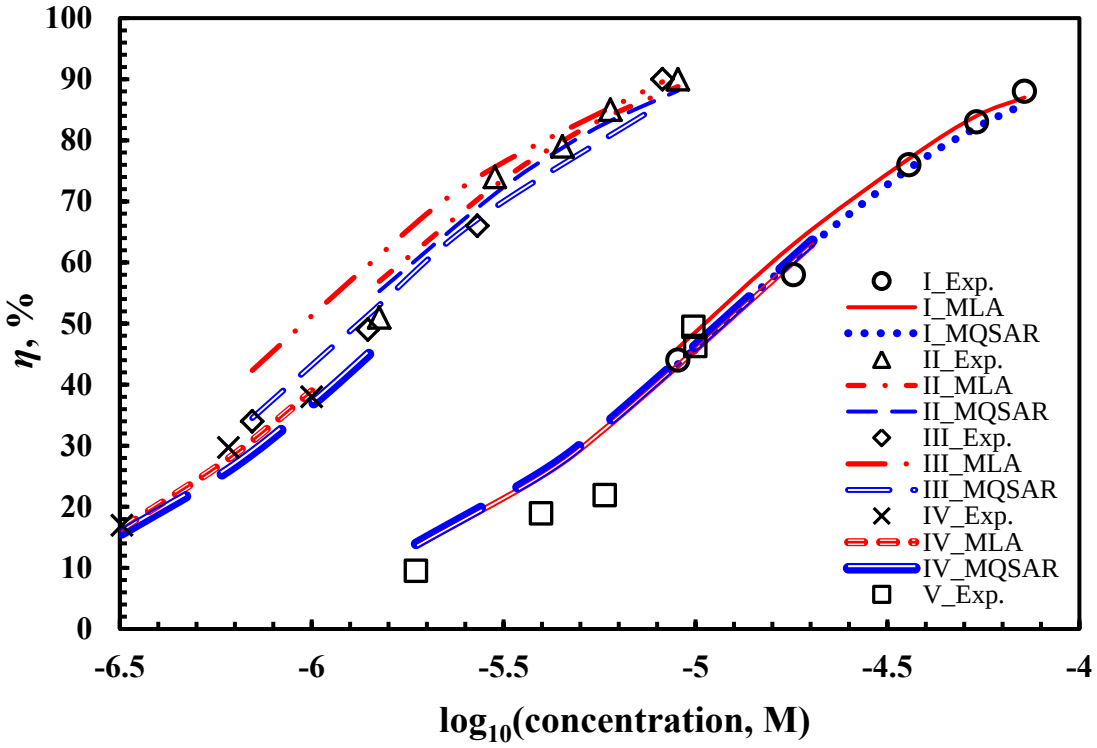

Fig. 1.16 Comparison of MQSAR model predicted inhibition efficiency and experimental inhibition efficiency as functions of surfactant concentration for various testing systems I-V. I: mixture of C12/C14/C16 = 0.70/0.25/0.05 in 0.171 M NaCl aqueous media with pH = 4 and electrode of X65 steel at 40 ℃ [72,123]; II: mixture of C12/C14/C16 = 1/1/1 in 0.599 M NaCl aqueous media with pH = 5 and electrode of X65 steel at 40 ℃ [72,123]; III: AAOA in 0.856 M NaCl aqueous media with pH=6 and electrode of 1018 steel at 25 ℃ [5,117]; IV: cetylpyridinium chloride in 1 M HCl aqueous media with electrode of 1018 steel at 31 ℃ [98]; V: C_{16}TAB in 0.03 M $Fe(NO_3)_3$ aqueous media with electrode of copper at 32 ℃ [232]. Regression coefficients are the same for testing systems I and II.

1.8 References

[1] B. Tribollet, J. Kittel, A. Meroufel, F. Ropital, F. Grosjean, E. M. M. Sutter, Electrochim. Acta 124 (2014) 46.

[2] S. Zou, X. Li, C. Dong, K. Ding, K. Xiao, Electrochim. Acta 114 (2013) 363.

[3] P. Bai, H. Zhao, S. Zheng, C. Chen, Corrosion Sci. 93 (2015) 109.

[4] Y. Zhou, Y. Zuo, Electrochim. Acta 154 (2015) 157.

[5] D.A. López, S.N. Simison, S.R. de Sánchez, Electrochim. Acta 48 (2003) 845.

[6] K.S. George, S. Nešić, Corrosion 63 (2007) 178.

[7] B.R. Linter, G.T. Burstein, Corrosion Sci. 41 (1999) 117.

[8] N. G. Thompson, Y. Mark, D. Daniel, Corrosion Rev. 25 (2007) 247.

[9] C. de Waard, D.E. Milliams, Corrosion 31 (1975) 177.

[10] G.I. Ogundele, W.E. White, Corrosion 43 (1987) 665.

[11] A. Ikeda, S. UedaM, Mukai, NACE International Corrosion Conference, New Orleans, 1984, Paper No. 289.

[12] K. Videm, A. Dugstad, Mater. Perform. 4 (1989) 46.

[13] B. Mishra, S. Al-Hassan, D.L. Olson, M.M. Salama, Corrosion 53 (1997) 852.

[14] M.B. Kermani, A. Morshed, Corrosion 59 (2003) 659.

[15] M.H. Ezuber, Mater. Des. 30 (2009) 3420.

[16] S. Nešić, J. Postlethwaite, S. Olsen, Corrosion 52 (1996) 280.

[17] S. Nešić, L. Lunde, Corrosion 50 (1994) 717.

[18] C. de Waard, U. Lotz, A. Dugstad, NACE International Corrosion Conference, Houston, 1995, Paper No. 128.

[19] J.C. Cardoso Filho, M.E. Orazem, NACE International Corrosion Conference, Houston, 2001, Paper No. 1058.

[20] Q.Y. Liu, L.J. Maoa, S.W. Zhou, Corrosion Sci. 84 (2014) 165.

[21] C.F. Chen, M.X. Lu, D.B. Sun, Z.H. Zhang, W. Chang, Corrosion 61 (2005) 594.

[22] K. Videm, A. M. Koren, Corrosion 49 (1993) 746.

[23] B. Brown, S.R. Parkala, S. Nesic, NACE International Corrosion Conference, 2003, Paper No. 4736.

[24] R. Fuchs-Godec, Electrochim. Acta 54 (2009) 2171.

[25] D. Gelman, D. Starosvetsky, Y. Ein-Eli, Corrosion Sci. 82 (2014) 271.

[26] B. Kronberg, Surfactant mixtures, Curr. Opin. Colloid Interface Sci. 2 (1997) 456.

[27] M. L. Free, Corrosion. Sci. 46 (2004) 3101.

[28] M. L. Free, Corrosion. Sci. 44 (2002) 2865.

[29] Y. Zhu, M. L. Free, G. Yi, Corrosion Sci. 98 (2015) 417.

[30] S. Endo, K. Goss, Environ. Sci. Technol. 48 (2014) 2776.

[31] M. A. Cowell, T. C. G. Kibbey, J. B. Zimmerman, K. F. Hayes, Environ. Sci. Technol. 34 (2000) 1583.

[32] J. Iyer, D. Blankschtein, J. Phys. Chem. B 118 (2014) 2377.

[33] L. Moreira, A. Firoozabadi, Langmuir 26 (2010) 15177.

[34] C. D. Taylor, A. Chandra, J. Vera, N. Sridhar, J. Electrochem. Soc. 162 (2015) 369.

[35] A. Kokalj, S. Peljhan, M. Finsgar, I Milosev, J. Am. Chem. Soc. 132 (2010) 16657.

[36] A. Kokalj, Corrosion Sci. 68 (2013) 195.

[37] Y. Zhu, M. L. Free, J. Electrochem. Soc. submitted.

[38] K. Y. Foo, B. H. Hameed, Chem. Eng. J. 156 (2010) 2.

[39] R. Fuchs-Godec, Colloid. Sur. A: Physical. Eng. Aspects 280 (2006) 130.

[40] M. Farsak, H. Keles, M. Keles, Corrosion Sci. 98 (2015) 223.

[41] M. P. Kern, D. Landolt, Corrosion Sci. 47 (2005) 485.

[42] I. B. Obot, D. D. Macdonald, Z. M. Gasem, Corrosion Sci. (2015).

[43] G. Gece, Corrosion Sci. 50 (2008) 50, 2981.

[44] Sonu, A. K. Tiwari, S. K. Saha, Ind. Eng. Chem. Res. 52 (2013) 5895.

[45] G.Gece, Corrosion Sci. 53 (2011) 3873.

[46] H. Zhao, X. Zhang, L. Ji, H. Hu, and Q. Li, Corrosion Sci. 83 (2014) 261.

[47] D. A. Winkler, M. Breedon, A. E. Hughes, F. R. Burden, A. S. Barnard, T. G. Harvey, I. Cole, Green Chem. 16 (2014) 3349.

[48] L. Li, X. Zhang, S. Gong, H. Zhao, Y. Bai, Q. Li, L. Ji, Corrosion Sci. (2015).

[49] S. K. Mondal, S. R. Taylor, J. Electrochem. Soc. 161 (2014) C476.

[50] A. Pfennig, R. Wiegand, M. Wolf, C.-P. Bork, Corrosion Sci. 68 (2013) 134.

[51] S. Nešić, Corrosion Sci. 49 (2007) 4308.

[52] L.J. Mu, W.Z. Zhao, Corros. Sci. 52 (2010) 82.

[53] J. Banas, U. Lelek-Borkowska, B. Mazurkiewicz, W. Solarski, Electrochim. Acta 52 (2007) 5704.

[54] S. Al-Hassan, B. Mishra, D. L. Olson, M. M. Salama, Corrosion 54 (1998) 480.

[55] J. M. Medina Huerta, J. G. God ínez, J. L. Gonz ález, Corrosion 68 (2012) 1.

[56] Ya. B. Unigovski, G. Lothongkum, E. M. Gutman, D. Alush, R. Cohen, Corros. Sci. 51 (2009) 3014.

[57] Q. Qu, J. Ma, L. Wang, L. Li, W. Bai, Z.T. Ding, Corrosion Sci. 53 (2011) 1186.

[58] B. Ingham, M. Ko, N. Laycock, J. Burnell, P. Kappen, J.A. Kimpton, D.E. Williams, Corrosion Sci. 56 (2012) 96.

[59] J. Han, J.W. Carey, J. Zhang, J. Appl. Electrochem. 41 (2011) 741.

[60] A. Pfennig, R. B äßler, Corrosion Sci. 51 (2009) 931.

[61] J.L. Crolet, "Corrosion in Oil and Gas Production," in Corrosion and Anticorrosion, eds. G. Beranger, H. Mazille, France: Hermes Science, 2002.

[62] C.F. Chen, M.X. Lu, D.B. Sun, Z.H. Zhang, W. Chang, Corrosion 61 (2005) 594.

[63] H. Fang, B. Brown, S. Nešić, NACE Corrosion Conference, Houston, 2010, Paper No. 276.

[64] J. Han, J.W. Carey, J. Zhang, J. Appl. Electrochem. 41 (2011) 741.

[65] X. Mao, X. Liu, R.W. Revie, Corrosion 50 (1994) 651.

[66] Y. Sun, K. George, S. Nešić, NACE Corrosion Conference, Houston, 2003, Paper No. 3327.

[67] L.Niu, K. Nakada, Corrosion Sci. 96 (2015) 171.

[68] G.T. Burstein, D.H. Davies, Corrosion Sci. 20 (1980) 1143.

[69] G.T. Burstein, D.H. Davies, J. Electrochem. Soc. 128 (1981) 33.

[70] J.O. Bockris, A.K.N. Reddy, Modern Electrochemistry, 2nd ed., Kluwer Academic/Plenum Publishers, New York, 2000.

[71] Y. Zhu, M. L. Free, Corrosion Sci. (2015) in press.

[72] Y. Zhu, M. L. Free, G. Yi, J. Electrochem. Soc. 168 (2015) C582.

[73] R. Zhang, P. Somasundaran, Adv. Colloid Interface Sci. 123-126 (2006) 213.

[74] M. Christov, A. Popova, Corrosion. Sci. 46 (2004) 1613.

[75] P. C. Okafor, Y. Zheng, Corrosion. Sci. 51 (2009) 850.

[76] M. Behpour, S.M. Ghoreishi, N. Soltani, M. Salavati-Niasari, M. Hamadanian, A. Gandomi, Corrosion. Sci. 50 (2008) 2172.

[77] X. Shi, R. Zhang, C. Minot, K. Hermann, M. A. Van Hove, W. Wang, N. Lin, J. Phys. Chem. Lett. 1 (2010) 2974.

[78] J. N. Israelachvili, Intermolecular and Surface Forces, 3rd ed., Academic Press, San Diego, 2011.

[79] M. Finšgar, J. Jackson, Corrosion Sci. 86 (2014) 17.

[80] M.A. Malik, M.A. Hashim, F. Nabi, S.A. AL-Thabaiti, Int. J. Electrochem. Sci. 6 (2011) 1927.

[81] D.A. Williams, P.K. Holifield, J.R. Looney, L.A. McDougall, US Patent 5,200,096, Exxon Chemicals Patents, Inc., 1993.

[82] S. Ali, J.S. Reyes, M.M. Samuel, F.M. Auzerais, US Patent 2010/0056405 A1, Schlumberger Technology Corporation, 2010.

[83] H.A. Nasr-El-Din, A.M. Al-Othman, K.C. Taylor, A.H. Al-Ghamdi, J. Petrol. Sci. Eng. 43 (2004) 57.

[84] D.G. Hill, H. Romijn, NACE Corrosion Conference, 2000, Paper No. 00342.

[85] D. I. Horsup, J. C. Clark, B. P. Binks, P. D. I. Fletcher, J.T. Hicks, Corrosion 66 (2010) 036001.

[86] E.R. Fischer, J.E. Parker, Corrosion 53 (1997) 62.

[87] R. M. Hill, Mixed Surfactant systems, Marcel Dekker, New York, 1993.

[88] M. J. Rosen, Surfactants and Interfacial Phenomena, 3rd ed., John Wiley, New Jersey, 2004.

[89] M. Heydari, M. Javidi, Corrosion Sci. 61 (2012) 148.

[90] P. C. Okafor, C .B. Liu, X. Liu, Y. G. Zheng, Appl. Electrochem. 39 (2009) 2535.

[91] E. E. Oguzie, Y. Li, F.H. Wang, Corros. Sci. 310 (2007) 90.

[92] E.E. Ebenso, H. Alemu, S.A. Umoren, I.B. Obot, Int. J. Electrochem. Sci. 3 (2008) 1325.

[93] M. Bouklah, B. Hammouti, A. Aouniti, M. Benkaddour, A. Bouyanzer, Appl. Surf. Sci. 252 (2006) 6236.

[94] L. Larabi, Y. Harek, M. Traisnel, A. Mansri, J. Appl. Electrochem. 34 (2004) 833.

[95] J. Gao, Y. Weng, S. Salitanate, L. Feng, H. Yue, Petrol. Sci. 6 (2009) 201.

[96] V.S. Sastri, Corrosion Inhibitors: Principles and Applications, John Wiley & Sons, Chichester, 2001.

[97] A.L.d.Q. Baddini, S.P. Cardoso, E. Hollauer, J.A.d.C.P. Gomes, Electrochim. Acta 53 (2007) 434.

[98] M. L. Free, W. Wang, D. Y. Ryu, Corrosion 60 (2004) 837.

[99] E.A. Flores, O. Olivares, N.V. Likhanova, M.A. Dom ńguez-Aguilar, N. Nava, D. Guzman Lucero, M. Corrales, Corros. Sci. 53 (2011) 3899.

[100] J. Aljourani, K. Raeissi, M.A. Golozar, Corros. Sci. 51 (2009) 1836.

[101] K.F. Khaled, K. Babić-Samardžija, N. Hackerman, J. Appl. Electrochem. 34 (2004) 697.

[102] R. Tadmouri, C. Zedde, C. Routaboul, J-C. Micheau, V. Pimienta, J. Phys. Chem. B 112 (2008) 12318.

[103] J. A. Dougherty, Y. S. Ahn, NACE Corrosion Conference, San Antonio, 1999, Paper No. 4.

[104] L. Wang, W. Chen, Journal of Natural Gas Chemistry, 19 (2010) 21.

[105] H. Liu, B.Wang, M. Fan, N. Henson, Y. Zhang, B. F. Towler, H. Gordon Harris, Fuel, 113(2013) 712.

[106] Y. Zhu, M. L. Free, J. Cho, Langmuir, Submitted.

[107] W. W. Focke, N. S. Nhlapo, E. Vuorinen, Corrosion Sci. 77 (2013) 88.

[108] M. Knag, J. Sjoblom, G. Oye, E. Gulbrandsen, Colloids Surf. A: Physicochem. Eng. Aspects, 250 (2004) 269.

[109] K. F. Khaled, Electrochim. Acta 53 (2008) 3484

[110] K. F. Khaled, J. Solid State Electrochem. 13 (2009) 1743.

[111] S. Zhang, Z. Tao, S. Liao, F. Wu, Corrosion Sci. 52 (2010) 3126.

[112] A.H. Esmaeel Naderi, M. Jafari, M.G. Ehteshamzadeh, G. Hosseini, Mater. Chem. Phys. 115 (2009) 852.

[113] Whitmire, N. Hackerman, Electrochim. Acta 53 (2008) 6024.

[114] W. Durnie, R. De Marco, A. Jefferson, B. Kinsella, J. Electrochem. Soc. 146 (1999) 1751.

[115] M. A. Amin, M. A. Ahmed, H. A. Arida, T. Arslan, M. Saracoglu, F. Kandemirli, Corrosion Sci. 53 (2011) 540.

[116] R. Fuchs-Godec, M. G. Pavlovic, Corrosion Sci. 58 (2012) 192-201.

[117] M.P. Desimone, G. Gordillo, S.N. Simison, Corrosion Sci. 53 (2011) 4033.

[118] D. Do, Adsorption Analysis: Equilibria and Kinetics, Imperial College Press. London, 1980.

[119] J. O' M. Bockris, D. A. J. Swinkels, J. Electrochem. Soc. 111 (1964) 736.

[120] D, G. Brown, K. S. Al Nuaimi, Langmuir 21 (2005) 11368.

[121] T. C. G. Kibbey, L. Chen, Colloids Surf. A: Physicochem. Eng. Aspects 326 (2008) 73.

[122] Y. Zhu, M. L. Free, Colloids Surf. A: Physicochem. Eng. Aspects submitted.

[123] Y. Zhu, M. L. Free, ECS Trans. 66 (2015) 53.

[124] Y. Zhu, M. L. Free, Department of Defense-Allied Nations Technical Corrosion Conference (2015).

[125] J. N. Phillips, Trans. Faraday Soc. 51 (1955) 561.

[126] M. Bourrel, R. S. Schechter, Microemulsions and Related Systems: Formation, Solvency, and Physical Properties, Marcel Dekker, Inc.: New York, NY, 1988.

[127] S. Ikeda, S. Hayashi, T. Imae, J. Phys. Chem. 85 (1981) 106.

[128] A. Goldsipe, D. Blankschtein, Langmuir 21 (2005) 9850.

[129] F. S. Lima, I. M. Cuccovia, D. Horinek, L. Q. Amaral, K. A. Riske, S. Schreiber, R. K. Salinas, E. L. Bastos, P. A. R. Pires, J. C. Bozelli, D. C. Favaro, A. C. B. Rodriguez, L. G. Dias, O. A. El Seoud, H. Chaimovich, Langmuir 29 (2013) 4193.

[130] F. S. Lima, F. A. Maximiano, I. M. Cuccovia, H. Chaimovich, Langmuir 27 (2011) 4319.

[131] L. Abezgauz, K. Kuperkar, P. A. Hassan, O. Ramon, P. Bahadur, D. Danino, J. Colloid Interface Sci. 342 (2010) 83.

[132] C. Oelschlaeger, P. Suwita, N. Willenbacher, Langmuir 26 (2010) 7045.

[133] N. Vlachy, B. Jagoda-Cwiklik, R. Vácha, D. Touraud, P. Jungwirth, W. Kunz, Adv. Colloid Interface Sci. 146 (2009) 42.

[134] L. J. Magid, J. Phys. Chem. B 102 (1998) 4064.

[135] R. R. Netz, D. Horinek, Annu. Rev. Phys. Chem. 63 (2012) 401.

[136] L. Moreira, A. Firoozabadi, Langmuir 26 (2010) 15177.

[137] S. V. Koroleva, A. I. Victorov, Phys. Chem. Chem. Phys.16 (2014) 17422.

[138] R. Nagarajan, E. Ruchenstein, Langmuir 7 (1991) 2934.

[139] R. Nagarajan, In Theory of Micelle Formation, K. Esumi, M. Ueno, CRC Press: Boca Raton, FL, 2003.

[140] V. Srinivasan, D. Blankschtein, Langmuir 19 (2003) 9932.

[141] V. Srinivasan, D. Blankschtein, Langmuir 19 (2003) 9946.

[142] V. Srinivasan, D. Blankschtein, Langmuir 21 (2005) 1647.

[143] V. A. Andreev, A. I. Victorov, Langmuir 22 (2006) 8298.

[144] S. V. Koroleva, A. I. Victorov, Langmuir 30 (2014) 3387.

[145] M. Manciu, E. Ruckenstein, Langmuir 21 (2005) 11312.

[146] B. Lukanov, A. Firoozabadi, Langmuir 30 (2014) 6373.

[147] J. F. Zemaitis, D. M. Clark, M. Rafal, N. C. Scrivner, Handbook of Aqueous Electrolyte Thermodynamics, AlChE, New York, 1986.

[148] K. S. Pitzer, Activity Coefficients in Electrolyte Solutions, 2nd ed., CRC Press, Boca Raton, 1991.

[149] J. N. Butler, Ionic Equilibrium: Solubility and pH Calculations, Wiley, New York, 1998.

[150] R. P. Schwarzenbach, P. M. Gschwend, D. M. Imboden, Environmental Organic Chemistry, 2nd ed., John Wiley and Sons, New York, 2001.

[151] M. N. Jo Nomuranes, J. Piercy, J. Chem. Soc., Faraday Trans. 1 68 (1972) 1839.

[152] S. Ozeki, S. Ikeda, Colloid Polym. Sci. 262 (1984) 409.

[153] T. Imae, R. Kamiya, S. Ikeda, J. Colloid Interface Sci. 108 (1985) 215.

[154] T. Imae, S. Ikeda, J. Phys. Chem. 90 (1986) 5216.

[155] H. Nomura, S. Koda, T. Matsuoka, T. Hiyama, R. Shibata, S. Kato, J. Colloid Interface Sci. 230 (2000) 22.

[156] Z. Weican, L. Ganzuo, M. Jianhai, S. Qiang, Z. Liqiang, L. Haojun, W. Chi, Chin. Sci. Bull. 45 (2000) 1854.

[157] A. Khatory, F. Lequeux, F. Kern, S.J. Candau, Langmuir 9 (1993) 1456.

[158] L. Magid, Z. Han, Z. Li, P. Butler, Langmuir 16 (2000) 149.

[159] A. A. Dar, G. M. Rather, S. Ghosh, A. R. Das, J. Colloid Interface Sci. 322 (2008) 572.

[160] J. H. Clint, J. Chem. Soc. Faraday Trans. 1 71 (1975) 1327.

[161] P. M. Holland, D. N. Rubingh, J. Phys. Chem. 87 (1983) 1984.

[162] A. D. Burman, T. Dey, B. Mukherjee, A. R. Das, Langmuir 16 (2000) 10020.

[163] U. P. Preiss, P. Eiden, J. Luczak, C. Jungnickel, J. Colloid Interface Sci. 412 (2013) 13.

[164] K. Shinoda, J. Phys. Chem. 58 (1954) 541.

[165] K. Shinoda, T. Nakagawa, Colloidal Surfactants, Academic Press, New York, 1963.

[166] K. Kameyama, A. Muroya, T. Takagi, J. Colloid Interface Sci. 196 (1997) 48.

[167] H. P. Moises de Oliveira, M. H. Gehlen, Langmuir 18 (2002) 3792.

[168] F. B. Growcock, W. W. Frenier, J. Electrochem. Soc. 135(1988) 817.

[169] A. Edwards, C. Osborne, S. Webster, D. Klenerman, M. Joseph, P. Ostovar, M. Doyle, Corrosion Sci., 36 (1994) 315.

[170] S. Ramachandran, B. L. Tsai, M. Blanco,H. J.Chen,Y. Tang, W. A. Goddard III, in New Techniques for Characterizing Corrosion and Stress Corrosion, R. H. Jones, D. R. Bear, The Minerals, Metals and Materials Society, 1996.

[171] S. Ramachandran, B. Tsai, M. Blanco, H. Chen, Y. Tang, W. A. Goddard, Langmuir 12 (1996) 6419.

[172] R. H. Hausler, Corrosion 42 (1986) 729.

[173] A. Ulman, Chem. Rev. 96 (1996) 1533.

[174] D. K. Schwartz, Annu. Rev. Phys. Chem. 52 (2001) 107.

[175] S. Ramachandran, C. Menendez, V. Jovancicevic, J. Long, J. Petrol. Explor. Prod. Technol. 2 (2012) 125.

[176] R. DeMarco, W. Durnie, A. Jefferson, B. Kinsella, A. Crawford, Corrosion 58 (2002) 354.

[177] M. Ben Ghoulam, N. Moatadid, A. Graciaa, J. Lachaise, Langmuir 20 (2004) 2584.

[178] A. Graciaa, J. Andérez, C. Bracho, J. Lachaise, J. Salager, L. Tolosa, F. Ysambertt,

Adv. Colloid Interface Sci. 123-126 (2006) 63-73.

[179] J. Salager, N. Marquez, A. Graciaa, J. Lachaise, Langmuir 16 (2000) 5534.

[180] J. Gomez del Rio, D. Hayes, V. S. Urban, J. Colloid Interface Sci. 352 (2010) 424.

[181] E. H. Crook, D. B. Fordyce, G. F. Trebbi, J. Colloid Interface Sci. 20 (1965) 191.

[182] B. W. Brooks, H. N. Richmond, J. Colloid Interface Sci. 162 (1994) 59.

[183] B. W. Brooks, H. N. Richmond, J. Colloid Interface Sci. 162 (1994) 67.

[184] J. L. Salager, N. Marquez, R. E. Anton, A. Graciaa, J. Lachaise, Langmuir 11 (1995) 37.

[185] F. Ravera, M. Ferrari, L. Liggieri, R. Miller, A. Passerone, Langmuir 13 (1997) 4817.

[186] M. Ben Ghoulam, N. Moatadid, A. Graciaa, J. Lachaise, Langmuir 18 (2002) 4367.

[187] Y. Zhu, V. Molinier, M. Durand, A. Lavergne, J. Aubry, Langmuir 25 (2009) 13419.

[188] A. Van de Voorde, C. Lorgeous, M. Gromaire, G. Chebbo, Environ. Pollution 164 (2012) 150.

[189] G. G. Warr, F. Grieser, T. W. Healy, J. Phys. Chem. 87 (1983) 4520.

[190] A. Graciaa, J. Lachaise, J. G. Sayous, P. Grenier, S. Yiv, R. S. Schechter, W. Wade, J. Colloid Interface Sci. 93 (1983) 474.

[191] M. Balcan, D. Anghel, Colloid Polym. Sci. 283 (2005) 982.

[192] V. Pradines, S. Despous, C. Claparols, N. Martins, J. Micheau, D. Lavabre, V. Pimienta, J. Phys. Org. Chem. 19 (2006) 350.

[193] F. Harusawa, T. Saito, H. Nakajima, S. Fukushima, J. Colloid Interface Sci. 74 (1980) 435.

[194] P. Alaei, B. P. Binks, P. D. I. Fletcher, NACE Corrosion Conference, 2013, Orlando, Paper No. 2158.

[195] R. Aveyard, B. P. Binks, S. Clark, P. D. I. Fletcher, J. Chem. Soc. Faraday Trans. 1 86 (1990) 3111.

[196] [196]R. Aveyard, B. P. Binks, S. Clark and J. Mead, J. Chem. Soc. Faraday Trans.

1, 82, (1986): p.125.

[197] A. V. Marenich, C. J. Cramer, D. G. Truhlar, Journal of Physical Chemistry B 113 (2009) 6378.

[198] G. Scalmani, M. J. Frisch, J. Chem. Phys. 132 (2010) 114110.

[199] C. D. Taylor, J. Electrochem. Soc. 162 (2015) C340.

[200] C. D. Taylor, A. Chandra, J. Vera, N. Sridhara, J. Electrochem. Soc. 162 (2015) C347

[201] M. D. Ellegaard, J. Abildskov, J. P. O'Connell, AICHE Journal 55 (2009) 1256 .

[202] P. E. Smith, R. M. Mazo, J. Phys. Chem. B. 112 (2008) 7875.

[203] N. F. A. Van der Vegt, W. F. van Gunsteren, J. Phys. Chem. B 108 (2004) 1056 .

[204] Y. Marcus, Pure & Appl. Chem. 62 (1990) 2069.

[205] N. A. Williams, G. L. Amidon, Pharm. Res. 5 (1988) 193.

[206] A. C. Chamberlin, D. G. Levitt, C. J. Cramer, D. G. Truhlar, Mol. Pharm. 5 (2008) 1064.

[207] A. D. James, J. M. Wates, E. W. Jones, J. Colloid Interface Sci. 160 (1993) 158.

[208] F. Harusawa, M. Tanaka, J. Phys. Chem. 85 (1981) 882.

[209] V. Jovancicevic, Y. S. Ahn, J. A. Dougherty, B. Alink, NACE Corrosion Conference, Orlando, 2000, Paper No. 7.

[210] A. C. T. van Duin, S. Dasgupta, F. Lorant, W. A. Goddard III, J. Phys. Chem. A 105 (2001) 9396.

[211] M. Raju, S.-Y. Kim, A. C. T. van Duin, K. A. Fichthorn, The Journal of Physical Chemistry C 117(2013) 10558.

[212] P. Selvam, H. Tsuboi, M. Koyama, M. Kubo, A. Miyamoto, Catalysis Today 100 (2005) 11.

[213] P. Valentini, T. E. Schwartzentruber, I. Cozmuta, Surface Sci. 605 (2011) 1941.

[214] T Hong, W.P Jepson, Corrosion Sci. 43 (2001) 1839.

[215] E. Barmatov, T. Hughes, M. Nagl, Corrosion Sci. 92 (2015) 85.

[216] L.Y. Xu, Y. F. Cheng, Corrosion Sci. 73 (2013) 150.

[217] D. D. Macdonald, J. Electrochem. Soc. 153 (2006) B213.

[218] C. Y. Chao, L. F. Lin, D. D. Macdonald, J. Electrochem. Soc. 128 (1981) 1187.

[219] L. F. Lin, C. Y. Chao, D. D. Macdonald, J. Electrochem. Soc. 128 (1981) 1194.

[220] D. D. Macdonald, Electrochim. Acta 56 (2011) 1761.

[221] E. Barmatov, J. Geddes, T. Hughes, M. Nagl, NACE Corrosion Conference, Salt Lake City, 2012, Paper No. 1573.

[222] W.W. Frenier, US Patent 5,096,618, Dowell Schlumberger Incorporated, Tulsa, Okla, 1992.

[223] S. Papavinasam, R.W. Revie, M. Attard, A. Demoz, K. Michaelian, Corrosion 59 (2003) 1096.

[224] B. B. Paty, D. D. N. Singh, Corrosion 48 (1992) 442.

[225] G1-03 Standard Practice for Preparing, Cleaning, and Evaluating Corrosion Test Specimens, ASTM International, 2003.

[226] M. Finšgar, Corrosion Sci. 72 (2013) 82.

[227] M. Finšgar, Corrosion Sci. 72 (2013) 90.

[228] M. Finšgar, Corrosion Sci. 68 (2013) 51.

[229] B. Saassouh, Z. Lounis, Cement & Concrete Composites 34 (2012) 1082.

[230] G. S. Vasyliev, Corrosion Sci. (2015).

[231] S. Mondal, S. R. Taylor, Research in Progress Symposium, NACE Corrosion Conference, San Antonio, 2014.

[232] W. Wang, M. L. Free, Corrosion Sci. 46 (2004) 2601.

CHAPTER 2

CORROSION INHIBITION OF VARIOUS MIXED SURFACTANTS*

2.1 Introduction

As an important component of the economy, the oil and gas industry has received considerable attention from researchers. However, oil mining and transportation have become increasingly expensive due to equipment damage caused by corrosive media, such as media containing dissolved H_2S, Cl^-, and CO_2 [1-5]. As a specific oil and gas industry example, carbon steel is easily corroded in environments that contain water and carbon dioxide (CO_2) [4-6]. Dissolved CO_2 in water and crude oil can cause tremendous damage to pipelines and structural components [4, 6, 7]. The annual direct cost of corrosion in the United States has been estimated to be around $276 billion or 3.1% of the gross domestic product (GDP). About 3.7% out of the total cost comes from oil and gas industry [3, 8], which is mainly due to the corrosion of carbon steel. These problems have led to great interest in industry and academia to control CO_2-related corrosion in various oilfields around the world. A widely used corrosion control method is to use organic inhibitors, many of which are surfactants with hydrophilic and hydrophobic molecular sections [9-11].

The hydrophilic functional group of surfactant molecules strongly prefers interaction

* Paper published in Corros. Sci. 98 (2015) 417-429 and Corros. Sci. (2015) doi:10.1016/j.corsci.2015.10.012.

with polar entities such as water, metals, and other ions. Generally, surfactants adsorb on the metal surface, block the active sites exposed to corrosive media, and thereby reduce corrosion attack [12, 13]. It is believed that the structure of heterocyclic surfactant molecules plays a dominant role in the corrosion inhibition performance. The presence and structure of specific atoms, such as C, H, N, and O, in these molecules, strongly influences the adsorption mechanism and corrosion inhibition efficiency [14, 15]. In practical applications, surfactant mixtures have received wide attention because of their superior physicochemical properties and capabilities in efficient solubilization, dispersion, suspension, and transportation [16, 17]. Solutions containing mixed surfactants can often be conveniently tuned to achieve desired properties by adjusting the mixed composition. More surface-active and expensive surfactants are usually mixed with less surface-active and less expensive surfactants to reduce cost [18]. However, the authors are not aware of a completely established theory or model to adequately predict the steel corrosion inhibition using various pure and mixed surfactants despite extensive research work [6, 19-25].

Surfactant molecules tend to adsorb at the air-liquid interface, liquid-solid interface, or liquid-liquid interface to escape from water by associating and aggregating hydrocarbon chains together. The concentration at which a monolayer forms at a surface is known as the surface aggregation concentration (sac). Surfactant molecules can also form aggregate structures to orient their hydrophobic tails toward those of neighboring surfactant molecules and their hydrophilic head groups toward water or hydrophilic surfaces. The concentration at which the surfactants start to form aggregates such as micelles in solution is termed the critical micelle concentration (cmc) [22-25].

It is usually assumed that the corrosion rate in the presence of low concentration of surfactants (usually lower than the cmc or the sac) can be represented by the number of active surface sites remaining after limited surfactant adsorption [22-27]. More and more active surface area is covered by surfactants and protected against corrosion as surfactant concentration increases. Near the sac or the cmc, the metal surface is assumed to be covered by one monolayer or multilayers of surfactants, respectively [23-28]. In this regard, sac and cmc are important characteristics in the evaluation of surfactant concentration effects on steel corrosion inhibition.

In the present study, a potential model for the prediction of metal corrosion inhibition using relevant pure and mixed surfactants in salt solution has been developed and validated. The collected experimental data from mixed homologous benzalkonium chloride (BAC) surfactants as corrosion inhibitors were used for the model derivation and illustration. The effects of temperature, surfactant concentration, and surfactant adsorption and aggregation on steel corrosion inhibition are discussed. The adsorption mechanism of BAC surfactants on a steel surface was investigated through the measurement of potential of zero charge and density functional theory (DFT) calculation. The sac, instead of cmc, is shown from experimental measurements, and it is utilized in a modified Langmuir adsorption (MLA) model as a characteristic of monolayer formation at the electrode-solution interface. A new cmc prediction model for various pure, binary, and ternary mixed surfactants in salt solution was developed and validated based on recently reported work [26]. This cmc prediction model is simple, easy to apply, and has few assumptions. The model outputs include cmc values of pure or various mixed surfactants over a wide range of dissolved salt concentrations. Mixed micelle

composition of mixed surfactants can also be predicted. Based on the electrochemical measurement results and by the incorporation of the cmc prediction model into the MLA, the corrosion inhibition efficiency over wide ranging conditions of pure and mixed surfactant inhibitors is accurately predicted.

2.2 Materials and experiments

The chemical formulas of various surfactant molecules used in the present work are shown in Fig. 2.1. The molecular structure and electronic properties of the surfactants are optimized in the presence of water as solvent using the Gasussian09 simulation package with the method of B3LYP and the basis set of 6-311G (d, p) based on DFT.

The test samples for surface tension measurements were prepared by sequential dilution of concentrated aqueous solutions of surfactants using double deionized water, made through a water purification system (Simplicity® UV made by EMD Millipore). The stock solution was prepared at a total surfactant concentration of 25 mM for electrochemical measurements using deionized water.

A piece of X65 steel, purchased from Metal Samples®, was used as the working electrode in electrochemical measurements with a surface area of 0.196 cm^2. The composition (wt %) was C 0.06%, Mn 1.33%, P 0.007%, S 0.005%, Si 0.30%, Cu 0.30%, Ni 0.10%, V 0.022%, Cb 0.046%, Al 0.019%, Cr 0.05%, Mo 0.03%, Ti 0.017%, Ca 0.0033%, and Fe (balance).

The surface of the X65 electrode was polished using SiC paper in the sequence of 400-600-800-1200 grit, and followed by polishing using MicroCloth™ with a particle size of ~ 5 μm supplied by Buehler. A platinum ring electrode and a single junction

saturated calomel electrode (SCE) were employed as counter and reference electrodes, respectively. Test solutions contained 0.171 or 0.599 M NaCl and were purged with Ar (>99.999%) for 2 h to remove oxygen followed by a purge of CO_2 (>99.999%) for 2 h to ensure CO_2 saturation prior to measurements. A flow of CO_2 was maintained during the experiments to keep a positive pressure inside the cell to avoid air ingress. The concentration of dissolved oxygen was monitored before electrochemical measurements using an Oxygen ULR CHEMets® Kit, and the concentration was measured and found to be below 20 ppb. The pH was adjusted to 4 - 5 for different mixtures by the addition of 1.0 M $NaHCO_3$ or diluted HCl. The surfactants were added at the beginning of each measurement. The test solutions were then kept at open circuit potential, E_{corr}, for 2 h for equilibration. Test conditions for different mixed surfactant systems are listed in Table 2.1. Testing System I is used as the primary example for the results discussion and inhibition efficiency prediction model derivation.

A Gamry reference 600 potentiostat was used for electrochemical measurements. Polarization resistance R_p was measured using the linear polarization resistance (LPR) method by polarizing the working electrode +/- 0.010 V (SCE) vs. E_{corr} with a sweep rate of 0.1 mV/s. Potentiodynamic scans were performed with a sweep rate of 1mV/s from -0.9 V (SCE) to -0.35 V (SCE). Electrochemical impedance spectroscopy (EIS) measurements were made with an applied alternating current (AC) potential of +/-0.010 V rms vs. E_{corr} in the frequency range of 100,000 - 0.010 Hz. The direct current (DC) potential was set as zero relative to E_{corr}. Each test was repeated at least three times as an independent measurement. The temperature was maintained at 40 ± 0.2 ℃, 50 ± 0.2 ℃, or 60 ± 0.2 ℃ for all electrochemical tests. The collected electrochemical data were

analyzed using software package Gamry Echem Analyst.

The surface tension of test solutions was measured within a precision of 0.1 mN/m by the platinum ring method using a Krüss K10 ST digital tensiometer, equipped with an isothermal vessel holder. All the measurements were performed at a constant temperature of 40 ± 0.2 ℃, which has been shown to be higher than the Krafft point of the surfactants and their mixtures in aqueous media containing various concentrations of NaCl. The constant temperature was maintained through a water circulation bath using a Polystat temperature controller, purchased from Cole-Parmer®. The platinum ring was rinsed with water and heated to an orange color using a Bunsen burner between tests to ensure the complete removal of contaminants. Triplicate measurements were used to confirm reproducibility. All values of reported surface tension were determined through the aforementioned procedures.

2.3 Results and discussion

2.3.1 Linear polarization measurement and potentiodynamic scan

The LPR measurements were performed on Testing System I with various concentrations of surfactants at different temperatures and the results were used to evaluate corrosion inhibition efficiency, η (%), using Eq. (2.1) with the Tafel slopes estimated from potentiodynamic scans [29].

$$\eta(\%) = 100 \times \frac{R_{\mathrm{p}} - R_{\mathrm{po}}}{R_{\mathrm{p}}} \qquad 2.1$$

where R_{po} and R_{p} are polarization resistances in the absence and presence of surfactant inhibitors, respectively.

The potentiodynamic scans were performed on Testing System I with various

concentrations of surfactants at different temperatures. Fig. 2.2 presents selected potentiodynamic scan curves. It can be seen that both anodic and cathodic reaction rates were increased with the increase in temperature. As can be seen from Fig. 2.2, the Tafel behavior of both branches of the polarization curves does not change much as a function of temperature. The shift of both branches to the right is in agreement with the increase of steel corrosion at higher temperatures.

The shape of the anodic branch changes when the surfactant concentration increases from below 72 μM to above 72 μM, which is consistent with the previously reported results [26]. This phenomenon may be explained by the first monolayer coverage on the steel surface where the monolayer effectively protects steel again corrosion. The concentration at 72 μM is the sac of mixed surfactants in Testing System I as shown in the next few sections. Above the sac, the anodic branch shape does not change much as the concentration continues to increase to the cmc or even higher values. The small change in the shape above the sac is due to the fact that steel surface is covered by surfactant bilayers/multilayers and possible hemi-micelles/micelles [22-26, 30].

For each studied temperature, an increase in current density is observed in the anodic branch (see dash-circled area in Fig. 2.2(b)). At certain relatively positive potential vs. E_{corr}, there is an abrupt change in slope, which is usually termed desorption potential [31]. Desorption potential decreases as temperature increases, suggesting that surfactant adsorption is favored at lower temperature as expected.

The Tafel slopes were estimated from potentiodynamic scan curves. For those curves without anodic Tafel dependence above the sac, the anodic Tafel slopes are derived from the cathodic branches and cathodic Tafel slopes [29]. The corrosion current density was

calculated using Tafel slope method [29]. The corrosion inhibition efficiency was calculated using Eq. (2.2) [29].

$$\eta\ (\%) = 100 \times \frac{i_{\mathrm{ocorr}} - i_{\mathrm{corr}}}{i_{\mathrm{ocorr}}} \qquad 2.2$$

where i_{ocorr} and i_{corr} are the corrosion current density without and with surfactant inhibitors in solution, respectively.

The results of Tafel slopes, polarization resistance, corrosion rate, and inhibition efficiency are summarized in Table 2.2 for the Testing System I surfactant mixture. As can be seen, the corrosion inhibition efficiency measured from potentiodynamic scans and LPR match very well. At each temperature, the inhibition efficiency increases rapidly to around 90% with the increase in surfactant concentration from 0 up to around 72 μM. Further increase in concentration does not effectively enhance inhibition efficiency even when the concentration is much higher than the cmc, Γ. The concentration of 72 μM is interpreted as the value of sac, $\bar{\Gamma}$, at which a complete monolayer usually forms at the electrode-solution interface, and above which, bilayers/multilayers or hemi-micelles/micelles usually form at the electrode-solution interface [26, 32, 33]. Note that the sac and the cmc barely change over a narrow range of low temperatures [22-26]. As mentioned in the introduction section, corrosion inhibition is usually directly related to the electrode surface coverage. Therefore, the monolayer is more effective with respect to corrosion inhibition and the formation of bilayers/multiplayers or hemi-micelles/micelles does not contribute much to additional corrosion inhibition after monolayer covers most active sites.

Regarding the temperature effect, the corrosion rate without surfactants increases as temperature increases due to the accelerated chemical and physical processes, such as

electrochemical reactions and transfer of reaction species [20]. Within the surfactant concentration range of 0-72 μM, the inhibition efficiency decreases by increasing the temperature from 40 to 60 °C. This phenomenon can be explained by a physisorption mechanism in which the adsorption of surfactants on steel becomes weaker as temperature increases. For surfactant concentration above the sac, the inhibition efficiency barely changes (see Table 2.2) over all studied temperatures and remains at a high level.

2.3.2 EIS measurements

Nyquist curves and Bode phase curves based on EIS measurements of X65 steel after immersion in aqueous media containing different surfactant concentrations of Testing System I at different temperatures are illustrated in Fig. 2.3 and Fig. 2.4, respectively. At each studied temperature, it was found that, without surfactant or with lower surfactant concentration, typically lower than the sac, the impedance plots feature a capacitive semicircle at high frequency and an inductive semicircle at low frequency; see Figs. 2.3(a) and 2.3(b). The diameter of capacitive semicircle which is usually believed to represent charge transfer resistance increases with increased surfactant concentration and this is in good agreement with the results of LPR measurements. The inductive semicircle is a characteristic of frequency dispersion, probably due to the surface roughness and inhomogeneity [26, 34, 35]. The adsorption of species, such as ion $[H^+]_{ads}$ or intermediate product $(FeOH)_{ads}$ on the electrode surface, may also contribute to the inductive semicircle formation during the relaxation process [36, 37]. As surfactant concentration increases to the sac, the inductive semicircle gradually disappeared at low frequency and

a 2nd capacitive semicircle started to form and overlap with the 1st capacitive semicircle in the middle of the frequency range (Figs. 2.3(c)). It is believed that the emerging 2nd semicircle at low frequency represents the formation of a porous monolayer film. At the surfactant concentrations above the sac, the 2nd semicircle is clearly seen, indicating the surfactant coverage above the monolayer level as bilayers or multilayers on the electrode surface.

At each studied temperature, only one phase angle peak (the 1st time constant) was observed at around 15 Hz in the phase angle plot at surfactant concentrations less than the sac ($\bar{\Gamma}$ = 72 μM) in Fig. 2.4(a) and 4(b), indicating that less than a complete monolayer formed. The maximum phase angle at this time constant increased with the increase of surfactant concentration up to the sac. Above the sac, the 2nd peak (the 2nd time constant) started to emerge at around 40 mHz (Figs. 4(c) and 4(d)). The maximum phase angle of the 1st time constant remains almost constant, indicating the likely formation of a complete protective film. The maximum phase angle of the 2nd time constant increased as the concentration increased, indicating the likely formation of a surfactant film of bilayers or multilayers.

At each studied surfactant concentration, the diameter of the 1st capacitive semicircle in the Nyquist curves mentioned above decreases as temperature increases. The phase angle peak corresponding to the 1st time constant around 15 Hz in the Bode phase curves experiences decrease as temperature increases, which indicates less adsorption of surfactants on the steel sample. All these results are in good agreement with LPR measurements and potentiodynamic scans.

Four different electrochemical equivalent circuits are used to fit the electrochemical

behavior of mixed surfactants in Testing System I (see Fig. 2.5) based on the EIS measurements and the previous discussion. The different circuits demonstrate the mechanistic changes in the corrosion process. In these equivalent circuits, an ideal capacitor is usually replaced by constant phase element (cpe) to represent the heterogeneity of the real system. The impedance of a cpe is defined as [38]

$$Z_{\mathrm{cpe}} = Y^{-1}(\iota\omega)^{-n} \tag{2.3}$$

where Y is pseudo capacitance characterizing cpe in unit $\Omega^{-1}\cdot s^{n}\cdot cm^{-2}\cdot$, ι is imaginary unit, n represents phase shift, ω is angular frequency in unit $rad\cdot s^{-1}$ and equal to $2\pi f$, and f is ordinary frequency in unit Hz in EIS plots. When n=1, cpe represents a capacitor with capacitance of Y^{-1}; when n=0.5, it represents a Warburg element; when n=0, it represents a resistor with resistance of Y^{-1}; and when $0<n<1$, it represents a non-ideal capacitor.

For the tests with surfactant concentrations lower than the sac, an inductor is introduced into the circuits to account for the inductive semicircle; near the sac, one porous bounded Warburg impedance element is added to the circuit to account for the diffusion process through the surfactant monolayer on electrode surface; above the sac, another porous bounded Warburg element is introduced to represent the diffusion through bilayers or multilayers. The impendence of a porous bounded Warburg element w is calculated using the equation:

$$Z_{\mathrm{w}} = \frac{\tanh\left(P\sqrt{(\iota\omega)}\right)}{W\sqrt{(\iota\omega)}} \tag{2.4}$$

with

$$P = \frac{\zeta}{D_{\mathrm{f}}^{1/2}} \tag{2.5}$$

where ζ is Nernst diffusion layer thickness in cm. D_{f} is an average value of the diffusion

coefficients of diffusing species in $cm^2 \cdot s^{-1}$. Parameters used for fitting this element are W in $\Omega^{-1}\ s^{1/2} \cdot cm^{-2}$or $S \cdot s^{1/2} \cdot cm^{-2}$, and P in $s^{1/2}$.

In the equivalent circuits presented in Fig. 2.5, R_s is solution resistance, R_{ct} is charge transfer resistance which is used to evaluate corrosion inhibition efficiency of surfactants, R_L is inductor resistance, R_1 and R_2 are resistances of the formed monolayers and bilayers/multilayers, Y_{cpe1} and Y_{cpe2} are pseudo capacitances of cpe1 and cpe2 corresponding to monolayers and bilayers/multilayers, respectively, L is inductance of an inductor, R_L is resistance of an inductor, and Y_{cpedl} is the pseudo capacitance of cpedl which represents the electric double layer. Z_{w1} and Z_{w2} represent the impendence of porous bounded Warburg elements w1 and w2, which are characterized by parameters W_1 and P_1, and W_2 and P_2, respectively. The fitted curves of equivalent circuits are presented in Figs. 2.3 and 2.4 and the values of fitted impedance parameters are summarized in Table 2.3.

As can be seen from Table 2.3, R_{ct} decreases with the increase of temperature at each studied concentration due to the decreased corrosion inhibition. n_{cpedl} generally decreases with increasing temperature, indicating the rougher surface at higher temperatures [39]. On the contrary, Y_{cpedl} increases with increasing temperature, suggesting less surfactant adsorbed on steel surface [39]. The resistances R_1 and R_2 of the inner and outer porous surfactant layer decreases at elevated temperatures due to the increased number of pores or the increased size of pores penetrated by electrolyte. At each temperature and concentration, R_1 is higher than R_2 probably because of denser surfactant coverage on the electrode surface. At each studied concentration, the decrease in diffusion related parameters P_1 and P_2 with increased temperature suggests increased diffusion of ions in

the porous surfactant layers at higher temperatures, which is in agreement with the fact that the diffusion coefficient increases with temperature increase. Similarly, the higher value of P_1 (compared to P_2) reflects the same trend in adsorbed surfactant density on electrode surface as reflected by the change in charge transfer resistance values.

The corrosion inhibition efficiency of the studied surfactant was calculated using the following formula for EIS measurements [29, 41]

$$\eta(\%) = 100 \times \frac{R_{\mathrm{ct}} - R_{\mathrm{cto}}}{R_{\mathrm{ct}}} \qquad 2.6$$

where R_{cto} and R_{ct} are polarization resistance in the absence and presence of surfactant inhibitors, respectively.

The calculated inhibition efficiency from EIS is summarized in Table 2.3, which is in agreement with the inhibition efficiency measured by LPR and potentiodynamic scans. Note that all the tests for Testing System I were performed with the rotation speed of 300 RPM. According to Oguzie et al. and Jiang et al. [42, 43], the dissolution of the iron metal from an electrode and the mass transport of iron ions from the electrode to bulk solution probably were accelerated upon rotation.

2.3.3 Temperature effect on steel corrosion activation

The dependence of corrosion rate on temperature can be evaluated using the Arrhenius equation below:

$$i_{\mathrm{corr}} = \lambda \exp\left(-\frac{E_{\mathrm{act}}}{RT}\right) \qquad 2.7$$

where i_{corr} is the corrosion current density measured from potentiodynamic scans, λ is an Arrhenius pre-exponential factor, E_{act} is the apparent activation energy of corrosion reaction, T is temperature, and R is gas constant [44]. The corresponding Arrhenius plots

based on the corrosion current density measurement without and with surfactants at different temperatures are shown in Fig. 2.6(a). The associated values of apparent activation energy of corrosion process in CO_2-saturated solution are determined from the slopes of such plots and are summarized in Table 2.4.

The value of E_{act} without surfactant is 17.9 kJ mol^{-1}, which is lower than the value reported [45, 46] probably because of the more aggressive aqueous environment with lower pH and higher electrode rotation speed in the present work. It is found that E_{act} is much higher in the presence of surfactants for the concentration range of 9 - 72 μM than in the absence of surfactants. The increase in E_{act} in the presence of surfactants jointly with the decreased inhibition efficiency at higher temperatures is often attributed to the formation of a physically adsorbed surfactant film on electrode surface [39, 47]. At the surfactant concentrations higher than 72 μM, a significant decrease in E_{act} is observed, which indicates a change of the adsorption behavior with the increase in surfactant concentration as was previously described in Sections 3.2 and 3.3. This is most likely explained by the blocking of surface active sites of electrode primarily by physisorption at the lower concentration range [48, 49].

Enthalpy change ΔH_{act} and entropy change ΔS_{act} of the corrosion process were also evaluated based on the transition state theory in Eq. (2.8)

$$i_{\text{corr}} = \frac{RT}{Nh} \exp\left(\frac{\Delta S_{\text{act}}}{R}\right) \exp\left(-\frac{\Delta H_{\text{act}}}{RT}\right) \qquad 2.8$$

where N is Avogadro's number, and h is the Plank constant. The values of ΔH_{act} and ΔS_{act} are determined from the slope and the intercept of the plot of $\ln(i_{corr}/T)$ vs. $1/T$ in Fig. 2.6(b), and are summarized in Table 2.4. The positive values of ΔH_{act} indicate the endothermic process of corrosion process while the negative values often indicate that the

activated complex in the rate determining step represents an association step instead of dissociation step [44].

2.3.4 Adsorption isotherm and thermodynamic parameter

Attempts were made to fit experimental data to various adsorption isotherms, including Langmuir, Frumkin, Temkin, and Freundlich isotherms. The fitting results are comparable. However, the Langmuir model is adopted due to its simplicity with only one parameter fitting. Langmuir model is described below

$$\frac{1}{\theta} = \frac{1}{K_{\mathrm{ad}} C} + 1 \tag{2.9}$$

K_{ad} is given by

$$K_{\mathrm{ad}} = \frac{1}{C_{\mathrm{wm}}} \exp\left(-\frac{\Delta G^{\mathrm{o}}_{\mathrm{ad}}}{RT}\right) \tag{2.10}$$

where C is the concentration of total surfactants in the bulk solution, C_{wm} is the molar concentration of water which is 55.5 M, K_{ad} is equilibrium adsorption constant, $\Delta G^{\mathrm{o}}_{\mathrm{ad}}$ is the standard free energy of adsorption process, R is the gas constant, and T is temperature. Note that for pure surfactant, C and Γ represent the concentration of pure surfactant in solution and the corresponding cmc, respectively; for mixed-surfactant, C and Γ represent the total concentration of mixed surfactants in solution and the corresponding mixed cmc, respectively.

Plots of $(1/\theta)$ vs. $1/C$ (for $C < \Gamma$) at different temperatures using Eq. (2.9) based on EIS measurements for Testing System I are shown in Fig. 2.7(a). The values of equilibrium constant K_{ad} are determined from the intercepts and are summarized in Table 2.5. It is found that K_{ad} decreases with the increasing temperature which suggests that the mixed BAC is physically adsorbed on the metal surface in the discussed concentration

range [50], in which the van der Waals and electrostatic forces dominate the adsorption. In contrast, the attraction force between the adsorbate and the adsorbent in chemisorption is dominated by covalent bonding and is very strong. Higher values of K_{ad} suggest strong interactions occur between the adsorbed surfactants and the electrode surface and that the adsorbed surfactants are not easily removable. In this regard, a strong covalent bonding of chemisorption could be implicated.

ΔG_{ad}^{o} is calculated using Eq. (2.10) and the values are listed in Table 2.5. The negative value demonstrates that the adsorption of surfactant on the steel surface is a spontaneous process and shows a strong interaction between surfactant molecules and an X65 steel surface [51, 52]. Generally, if adsorption free energy is more positive than -20 kJ mol^{-1}, the interaction between surfactant and metal is classified as physisorption due to electrostatic interaction. When the adsorption free energy is more negative than -40 kJ mol^{-1}, the adsorption involves charge sharing or transfer between surfactant molecules and metal surface to form coordination bonds, which is also classified as chemisorption [52, 53]. Based on the calculated value of adsorption free energy in the temperature range of 40-60 ℃, the adsorption mechanism of the discussed mixture can be classified as the combination of chemisorption and physisorption.

The adsorption enthalpy and entropy is correlated to adsorption free energy through the relation:

$$\Delta G_{ad}^{o} = \Delta H_{ad}^{o} - T\Delta S_{ad}^{o} \qquad 2.11$$

The plot of ΔG_{ad}^{o} vs. T in Fig. 2.7(b) gives a slope of ΔS_{ad}^{o} and an intercept of ΔH_{ad}^{o}, which are summarized in Table 2.5.

For the chemisorption process, ΔH_{ad}^{o} approaches -100 kJ mol^{-1} while for the

physisorption process, it is higher than -40 kJ mol^{-1} [54]. The calculated ΔH_{ad}^{o} value of -50.9 kJ mol^{-1} in this study, which is larger than the critical value of physisorption but smaller than the one for chemisorption, indicates the adsorption mechanism of mixed BAC involved both physisorption and chemisorption at total concentrations less than 72 μM. The negative value of ΔS_{ad}^{o} indicates a reduction in the translational degrees of freedom of adsorbed surfactant molecules compared to those in the bulk solution.

2.3.5 Mechanism of surfactant adsorption and corrosion inhibition

As discussed previously, the adsorption of mixed BAC involve both physisorption and chemisorption. The first step during the surfactant molecule adsorption process is physical interaction, which is companied by chemisorption in which charge sharing or electron transfer between d orbitals of the iron and the surfactant molecule occurs. The adsorption is usually affected by many factors, including the charge or dipole moment of surfactant molecule, the chemical structure of surfactant molecule, and the surface charge of the metal (iron). The surface charge of iron in aggressive aqueous media is usually evaluated according to the equation below:

$$E_r = E_{corr} - E_{pzc} \qquad 1.12$$

where E_r is the Antropov's "rational" corrosion potential, E_{corr} is open circuit potential, and E_{pzc} is potential of zero charge [55].

The E_{corr} value of mixed BAC surfactants at total concentration of 72 μM and E_{pzc} value are shown in Fig. 2.8 which presents the value of charge transfer resistance as a function of corrosion potential. The excess surface charge of steel can be determined by comparing E_{corr} with E_{pzc} (the maximum R_{ct} value corresponds to minimum C_{dl} value)

based on Eq. (2.12). The positive value of E_r indicates that the steel surface is positively charged with surfactants. Therefore, it is inferred that Cl^- ions take the first step to adsorb on the steel surface and make the surface negatively charged. After that, the positively charged $C14Bz^+$ which is dissociated from ionic BAC surfactants interacts electrostatically with the Cl^- ions that had already adsorbed on steel surface. With the increased concentration, the adsorbed surfactant molecules form a protective film against steel corrosion [56, 57].

For better illustration of the adsorption mechanism of BAC surfactants on steel surface, several theoretical parameters, such as the energies of molecular frontier orbitals (HOMO and LUMO), Mulliken charge distribution on the backbone atoms, dipole moment of the surfactant molecule, and surface electrostatic potential based on electron density of the molecule, were determined based on DFT using Gaussian09 as shown in Fig. 2.9. The surfactants used are homologous series and that the electronic properties of homologous series should be similar, thus the example of calculated results is given only based on $C_{14}BzCl$ for qualitative illustration in Fig. 2.9.

Frontier orbital (HOMO and LUMO) theory is useful in the prediction of adsorption centers and corrosion inhibition efficiency of the surfactant molecules on steel surface [19, 21, 55]. HOMO tends to donate electrons to suitable acceptor substances on the steel surface and the inhibition efficiency increases with the increase in HOMO energy while LUMO tends to accept electrons from steel surface and lower LUMO energy usually indicates stronger capability to accommodate electrons [19, 58]. The Milliken charges and surface electrostatic potential are usually shed light on the electron distribution of surfactant molecules and electrostatic interaction between molecules and iron (steel

surface) [44, 59]. It is generally agreed that dipole moment is a predictor of the direction of a corrosion inhibition reaction and that the adsorbed polar surfactants possessing high dipole moment on metal surface lead to better corrosion inhibition [44, 60].

Based on the calculation results presented in Fig. 2.9, it is inferred that the adsorption of BAC surfactants on an X65 steel surface involve both physical and chemical adsorption. The electron-rich atoms, such as N, in the surfactant molecules can accept protons and lead to the cationic forms of molecules, which interact with negatively charged metal surface (due to adsorption of Cl^- as discussed previously) through electrostatic forces. In the concentration range of 0-72 μM, surfactant molecules can lay horizontally to the surface and can also be oriented perpendicularly with the headgroup attached to the surface. At higher concentrations, surfactant molecules tend to perpendicularly adsorb on the surface to form protective bilayers/multilayers and hemi-micelles/micelles. Chemisorption of the BAC molecules is made possible by the link between the d orbital of iron atoms and the lone sp_2 electron pairs of the N atoms of the surfactant molecules. The electron-sharing between the benzene ring of the surfactant molecules and the d orbital of the iron atoms on steel surface also contributes to the chemisorption.

2.3.6 Corrosion inhibition efficiency modeling

As discussed in previous sections, sac and cmc are important parameters characterizing the corrosion inhibition efficiency of surfactants. Therefore, a modified Langmuir adsorption model (MLA) [26] is introduced for the corrosion inhibition prediction of homologous surfactants under various solution conditions by the

incorporation of cmc considering that cmc is easier to obtain than sac. The MLA is presented below

$$\frac{1}{1-\theta} = 1 + K' \frac{C}{\Gamma^{w}}, (C \leq \bar{\Gamma}) \quad 2.13$$

where K' is equal to the adsorption constant K_{ad} multiplied by Γ^{w} of surfactant. Note homologous surfactants tend to achieve similar levels of surface coverage at similar ratios of surfactant concentration to surfactant cmc, so the value of K' does not vary a lot for homologous surfactants [26]. Note that *C* could increase above the sac or the cmc, but the fitting would not be as good as the fitting for *C* below the sac for reasons discussed previously, indicating the sac is a transition point in characterizing the effectiveness of surfactants as corrosion inhibitors.

The plots of MLA and commonly used adsorption models based on the electrochemical measurements for Testing System I at 40 ℃ are presented in Fig. 2.10, in which only MLA shows clearly the feature of sac. The measured cmc for the mixture, 0.70/0.25/0.05 in 0.171M NaCl aqueous media at 40 ℃, is 144 μM. The plot of $\frac{1}{1-\theta}$ vs. $\frac{C}{\Gamma^{w}}$ yields a slope of constant K'=13.74, and an intercept of 1 which is in the absence of surfactant inhibitors, as shown in Fig. 2.10(d). There is one abrupt transition around the concentration of the sac, which indicates that when the inhibitor concentration is below the sac, inhibition efficiency increases rapidly and linearly with the increases in surfactant concentration; above the sac, the increase in concentration does not contribute much to further inhibition efficiency increase. The data for N-[2-[(2-aminoethyl) amino] ethyl]-9-octadecenamide (AAOA) are cited from literature [5].

Since corrosion inhibition is related to the cmc, it is expected that calculation of the cmc based on a predictive model instead of experimental measurement will aid in

corrosion inhibition determination. The predicted cmc can be used in the MLA to predict corrosion inhibition at surfactant concentrations lower than the sac. For pure surfactant i, the cmc prediction model is written as indicated in Eq. (2.14) (Details of model derivation and parameter calculation are presented in Appendix A.1 and Appendix A.2.):

$$\ln(\Gamma_{\mathrm{i}}^{\mathrm{w}}) \approx -\delta_{\mathrm{i}} \ln(\gamma_{\mathrm{c}} C_{\mathrm{c}}) + (L_{\mathrm{i}} - 1)\frac{\Delta\mu_{\mathrm{ch2}}^{\mathrm{o}}}{RT} + \frac{\Delta\mu_{\mathrm{ch3}}^{\mathrm{o}}}{RT} + \frac{\Delta\mu_{\mathrm{f}}^{\mathrm{o}}}{RT} + (1 + \delta_{\mathrm{i}})\ln C_{\mathrm{mw}} \qquad 2.14$$

where $\Gamma_{\mathrm{i}}^{\mathrm{w}}$ is the cmc of surfactant i in aqueous solution (i represents homologous surfactant 1, 2, or 3, …). δ_{i} is an experimental constant for surfactant i, usually interpreted as counterion binding coefficient. δ_{i} barely changes for a series of homologous surfactants. The mean value, δ_{m}, is more appropriate for homologous surfactants. C_{c} is the concentration of ion dissociated from electrolyte and from ionic surfactant in aqueous solution. γ_{c} is mean activity coefficient of ions in aqueous solution and is usually calculated using Davies equation [61] or Pitzer's method [62, 63]. L_{i} is hydrocarbon chain length of monomeric surfactant i. C_{12}BzCl, for example, has a chain length of 12, including 11 methylene groups and one methyl group. $\Delta\mu_{\mathrm{ch2}}^{\mathrm{o}}$ is standard free energy change of micellization per methylene group. $\Delta\mu_{\mathrm{ch3}}^{\mathrm{o}}$ is standard free energy change of micellization per methyl group. $\Delta\mu_{\mathrm{f}}^{\mathrm{o}}$ is standard free energy change of micellization of functional group. Eq. (2.14) is supported by the report that the cmc is heavily dependent on and exponentially related to electrolyte concentration [64-67].

The cmc prediction model of binary homologous surfactant mixture is given by

$$\Gamma^{\mathrm{w}} = \left(\frac{1}{\gamma_{\mathrm{c}} C_{\mathrm{c}}}\right)^{\delta_{\mathrm{m}}} \frac{1}{x_1\left(\frac{1}{\Gamma_1^{\mathrm{p}}}\right)^{(1+\delta_{\mathrm{m}})} + x_2\left(\frac{1}{\Gamma_2^{\mathrm{p}}}\right)^{(1+\delta_{\mathrm{m}})}} \qquad 2.15$$

where $\Gamma_{\mathrm{i}}^{\mathrm{p}}$ is the cmc of surfactant i in pure water. x_{i} is mole fraction of surfactant i in the total amount of mixed surfactants.

The cmc prediction model of ternary and multiple homologous surfactant mixture is given by

$$\Gamma^{\mathrm{w}} = \left(\frac{1}{\gamma_{\mathrm{c}} C_{\mathrm{c}}}\right)^{\delta_{\mathrm{m}}} \frac{1}{\sum_{\mathrm{i}} x_{\mathrm{i}} \left(\frac{1}{\Gamma_{\mathrm{i}}^{\mathrm{p}}}\right)^{(1+\delta_{\mathrm{m}})}} \tag{2.16}$$

For binary, ternary, and multiple nonhomologous surfactant mixture with i components, cmc and is given by

$$\Gamma^{\mathrm{w}} = \frac{1}{\sum_{\mathrm{i}} x_{\mathrm{i}} (\gamma_{\mathrm{c}} C_{\mathrm{c}})^{\delta_{\mathrm{i}}} \left(\frac{1}{\Gamma_{\mathrm{i}}^{\mathrm{p}}}\right)^{(1+\delta_{\mathrm{i}})}} \tag{2.17}$$

Eq. (2.17) is actually an universal cmc prediction model for various pure, binary, ternary, and multicomponent mixed surfactants.

For various cmc prediction models introduced above, the inputs include bulk mixed molar fraction x_{i}, counterion binding coefficient δ_{i}, activity coefficient of counterion γ_{c}, concentration of counterion C_{c}, and the cmc of surfactant i (in pure water) $\Gamma_{\mathrm{i}}^{\mathrm{p}}$ which can be directly measured or cited from literature. x_{i} and C_{c} are known parameters, γ_{c} can be easily calculated given solution conditions, and δ_{i} and $\Gamma_{\mathrm{i}}^{\mathrm{p}}$ are usually readily available in existing literature. The outputs include cmc and mixed micelle composition. Please note that the model derivation is based on ionic surfactant. However, the developed model is also applicable to nonionic surfactant with counterion binding coefficient fixed at zero.

The model validation using various pure and mixed surfactants at various salt concentrations is shown in Fig. 2.11. The associated model parameters are summarized in Table 2.6. Experimental data of cmc values in Figs. 2.11(a)-(d) and (f) is cited from references [22, 68, 69, 72-74]. As can be seen, the predicted cmc and experimental cmc for pure surfactant (Fig. 2.11(a)), mixed homologous nonionic surfactants (Figs. 2.11(b)

and 2.11(d)), mixed anionic and nonionic surfactants (Fig. 2.11(c)), and ternary mixed homologous cationic surfactants (Fig. 2.11(e)) are in excellent agreement. For ternary mixed cationic, cationic, and nonionic surfactants, the predicted cmc and experimental cmc match reasonably well (Fig. 2.11(f)).

Substitution of the cmc prediction model of Eq. (2.17) into Eq. (2.13) leads to

$$\frac{1}{1-\theta} = 1 + K'C \sum_i x_i (\gamma_c C_c)^{\delta_i} \left(\frac{1}{\Gamma_i^p}\right)^{(1+\delta_i)} \quad 2.18$$

Assuming the corrosion inhibition efficiency η is equal to surface coverage θ, η is then estimated using:

$$\eta(\%) = 100\left(1 - \frac{1}{1+K'C \sum_i x_i (\gamma_c C_c)^{\delta_i} \left(\frac{1}{\Gamma_i^p}\right)^{(1+\delta_i)}}\right) \quad 2.19$$

Fig. 2.12 presents the comparison of predicted inhibition efficiency and experimental inhibition efficiency for different testing systems using both MLA and Langmuir adsorption (LA). The K' value for mixed BAC is obtained by fitting the model to the experimental data of Testing System I, as shown in Fig. 2.10(d). The model is validated using the data obtained from Testing System II. As mentioned earlier, the value of K' in Eq. (13) remains almost constant for homologous surfactants and thus the fitting K' value from Testing System I is used for inhibition efficiency prediction for Testing System II. The sac of Testing System II is estimated to be 9 μM, at which the inhibition efficiency is around 90% and above which inhibition efficiency is slightly increased as the concentration continues to increase. The predicted corrosion inhibition efficiency of Testing System II using regular LA model is also presented in Fig. 2.12. However, significant deviation between prediction and experiment is observed due to the lack of

solution condition adjustment using cmc. This is attributed to the different solution conditions for Testing System I and Testing System II in which the aggregation properties, such as cmc and micelle composition, of mixed BAC are different and thus K_{ad} value differ. In MLA, K_{ad} value is replaced by incorporating the cmc value to obtain universal constant K' for homologous BAC. The corrosion inhibition efficiency prediction model is also extended to other surfactant testing systems and works very well, such as AAOA-1018 steel system [5], C_{16}TAB-copper system [24], and TCA-DDPB-J55 steel system [75], as shown in Fig. 2.12.

2.4 Summary

Based on the electrochemical measurements, thermodynamic parameters evaluation of X65 steel corrosion and associated mixed BAC surfactant adsorption in CO_2-saturated solution, DFT calculation, and corrosion inhibition modeling and prediction, the conclusions are summarized as follows:

1. Mixed BAC surfactants act as good inhibitors for the corrosion inhibition of steel in CO_2-saturated aqueous solution. Corrosion inhibition efficiency increases rapidly as the surfactant concentration increases to the sac, indicating the formation of a relatively complete surfactant monolayer around the sac that effectively protects the steel electrode from corrosion. Above the sac, inhibition efficiency slightly increases with the increase in surfactant concentration probably due to active electrode surface sites barely available for surfactant bilayers/multilayers to cover.

2. In the EIS measurements, four types of Nyquist plots were observed. The impedance plots feature a capacitive semicircle at high frequency and an inductive

semicircle at low frequency with lower surfactant concentration, typically lower than the sac. As surfactant concentration increases to the sac, the inductive semicircle gradually disappeared, and two overlapping capacitive semicircles were observed over the whole frequency range. Above the sac, the diameter of the 2nd capacitive semicircle increases due to bilayers/multilayers coverage on electrode surface.

3. Within the surfactant concentration range of 0-72 μM, the inhibition efficiency decreases by increasing the temperature from 40 to 60 °C. This phenomenon can be explained by the physisorption mechanism in which the adsorption of surfactant on steel surface becomes weaker as temperature increases. The physisorption is also supported by E_{pzc} measurement as discussed in the context. For surfactant concentrations above the sac, the inhibition efficiency barely changes over all studied temperatures and remains at a high level because of chemisorption dominated adsorption.

4. Chemisorption of the BAC molecules is made possible in part by electron-sharing between the d orbital of iron atoms and the lone sp2 electron pairs of the N atoms of the surfactants. The electron-sharing between the benzene ring of the surfactant molecules and the d orbital of iron atoms also contributes to the chemisorption.

5. The MLA features sac which is more effective in characterizing corrosion inhibition efficiency, whereas regular Langmuir, Freundlich, and Temkin adsorption models do not effectively identify the effect of the sac.

6. A new cmc prediction model for various pure, binary-, ternary-, and multi-component mixed surfactants has been developed and validated over a wide concentration range of salt. The model is simple, easy to use, and requires few input values.

7. The MLA model, which incorporates the cmc prediction model into the usual Langmuir adsorption model, provides a potential method to predict metal corrosion inhibition efficiency of various pure, binary-, ternary-, or multiple-component surfactant mixtures of interest in the presence of salt in solution at various concentration levels.

Table 2.1 Experimental condition for different testing systems of mixed BAC in CO_2-saturated solution

Testing system	Mixed molar ratio α_i ($C_{12}BzCl/C_{14}BzCl/C_{16}BzCl$)	NaCl (M)	Measured cmc (μM)	Temperature (℃)	pH	Rotation speed (RPM)
I	0.70/0.25/0.05	0.171	144	40, 50, 60	4	300
II	0.33/0.33/0.33	0.599	16.5	40, 50, 60	5	100

Table 2.2 Tafel slopes, corrosion rate, polarization resistance, and η (%) for X65 in the absence and presence of Testing System I with various surfactant concentrations at 40 ℃, 50 ℃, and 60 ℃. Concentration: *C*; temperature: *T*.

C (μM)	*T* (℃)	β_a (mV dec^{-1})[a]	β_c (mV dec^{-1})	*i* (μA cm^{-2})	η (%)[b]	R_p (ohm cm^2)	η (%)[c]
0	40	61.5	255	201	0	104	0
	50	62.1	249	238	0	87	0
	60	60.9	251	304	0	72	0
9	40	65.7	248	116	39	188	44
	50	64.8	243	165	31	126	31
	60	65.8	247	240	21	91	21
18	40	67.1	243	85	58	249	58
	50	68.9	245	131	45	167	48
	60	68.4	239	210	31	112	36
36	40	68.3	235	55	73	436	76
	50	67.2	234	100	58	225	61
	60	67.5	236	143	53	157	54
54	40	63.2	245	33	84	643	83
	50	63.5	246	50	79	426	80
	60	62.9	239	79	74	285	75
72	40	64.8	239	24	88	845	88
	50	63.2	238	33	86	685	87
	60	61.9	233	49	86	546	87
140	40	*67.9*	237	9	96	2550	96
	50	*65.8*	238	12	95	1819	95
	60	*65.1*	239	15	95	1389	95
360	40	*63.2*	233	5	97	4282	98
	50	*64.2*	229	7	97	2246	96
	60	*63.7*	241	9	96	1658	96

[a]β_a at the concentration of 140 μM and 360 μM were derived from the cathodic branch and β_c due to lack of sensible linearity in the anodic branch in potentiodynamic scans [29]; [b]η (%) calculated from potentiodynamic scans; [c]η (%) calculated from LPR.

Table 2.3 Equivalent circuit parameters of EIS plot for X65 steel for Testing System I. C (μM), T (℃), R ($\Omega \cdot cm^2$), P ($s^{1/2}$), W ($10^{-6} \cdot \Omega^{-1}\ s^{1/2}\ cm^{-2}$), Y ($10^{-6} \cdot \Omega^{-1}\ s^{n}\ cm^{-2}$), L (H cm^{-2}), η (%).

C	Blank			9			18			36			54			72			140			360		
T	40	50	60	40	50	60	40	50	60	40	50	60	40	50	60	40	50	60	40	50	60	40	50	60
R_s	7.2	6.5	5.8	7.0	6.9	6.3	5.5	7.3	6.5	8.2	7.1	6.9	9.2	8.1	7.4	9.3	8.2	7.1	8.0	8.4	7.6	8.7	8.2	8.0
P_2	--	--	--	--	--	--	--	--	--	--	--	--	--	--	--	--	--	--	3.5	3.3	2.9	3.9	3.5	3.1
W_2	--	--	--	--	--	--	--	--	--	--	--	--	--	--	--	--	--	--	65.9	57.3	51.2	69.4	50.4	48.5
Y_2	--	--	--	--	--	--	--	--	--	--	--	--	--	--	--	--	--	--	78	85	96	64	129	139
n_2	--	--	--	--	--	--	--	--	--	--	--	--	--	--	--	--	--	--	0.94	0.94	0.92	0.91	0.92	0.89
R_2	--	--	--	--	--	--	--	--	--	--	--	--	--	--	--	--	--	--	6.4	5.9	4.2	11.1	8.6	6.3
P_1	--	--	--	--	--	--	--	--	--	--	--	--	--	--	--	1225	892	646	1366	924	698	1492	1058	748
W_1	--	--	--	--	--	--	--	--	--	--	--	--	--	--	--	2453	2162	1848	308	311	317	287	305	324
Y_1	--	--	--	426	395	320	345	322	298	326	296	256	283	262	242	1895	1273	1165	120	154	172	86	175	233
n_1	--	--	--	0.84	0.82	0.81	0.83	0.81	0.80	0.78	0.77	0.76	0.83	0.83	0.81	0.96	0.95	0.91	1	1	1	1	1	1
R_1	--	--	--	4.9	4.7	3.5	6.6	5.1	4.2	17.2	14.6	9.8	22.5	16.8	10.6	88.6	72.3	46.2	12.3	9.2	8.8	18.2	15.1	10.6
L	26708	19785	12456	38002	28902	25125	65968	46565	35852	108952	95062	79012	11096	99854	88365	--	--	--	--	--	--	--	--	--
R_L	365	321	246	1072	401	346	1301	683	468	1756	1306	1156	2015	1792	1548	--	--	--	--	--	--	--	--	--
Y_{dl}	1025	1062	1102	268	288	296	231	252	268	226	240	316	206	227	265	182	256	342	138	192	236	78	98	112
n_{dl}	0.81	0.80	0.79	0.85	0.78	0.71	0.86	0.85	0.83	0.81	0.79	0.78	0.82	0.81	0.81	0.81	0.80	0.79	0.88	0.85	0.84	0.85	0.86	0.83
R_{ct}	109	91	72	185	131	86	275	1593	104	411	216	145	620	415	282	1202	820	555	2123	1678	1232	2870	1925	1524
η	0	0	0	44	32	20	61	46	34	74	59	53	83	79	75	91	89	87	95	95	94	96	96	95

Table 2.4 Activation parameters of X65 steel dissolution in CO_2-saturated 0.171 M NaCl aqueous solution.

C, μM	E_{act}, kJ mol^{-1}	ln(λ, μA cm^{-2})	ΔH_{act}, kJ mol^{-1}	ΔS_{act}, J mol^{-1} K^{-1}
0	17.9	12.2	15.2	-152.9
9	31.5	16.9	28.9	-113.7
18	38.9	19.4	36.3	-92.6
36	41.7	20.1	39.1	-87.1
54	38.1	18.1	35.4	-103.3
72	30.1	15.1	28.1	-129.2
140	23.9	11.4	21.3	-159.2
360	23.4	10.7	20.7	-165.3

Table 2.5 Thermodynamic parameters for the adsorption of mixed BAC in CO_2-saturated 0.171 M aqueous solution on X65 steel electrode at different temperatures.

T (℃)	$10^4 K_{ad}$, M^{-1}	ΔG^o_{ad}, kJ mol^{-1}	ΔH^o_{ad}, kJ mol^{-1}	ΔS^o_{ad}, J mol^{-1} K^{-1}
40	9.3	-39.8	-50.9	-34.3
50	5.1	-39.5		
60	2.9	-39.2		

Table 2.6 Model parameters (δ_i and $\Delta\mu^{o}_{ich2}$) for various surfactants

Compound	δ_i	$\Delta\mu^{o}_{ich2}/RT$
C_nTAB[a]	0.55	-1.12
$C_nH_{(2n+1)}KO_2$	0.56[b]	-1.08[c]
SDS	0.50[d]	-1.08[e]
OG	0	-1.06[f]
C_nCOOE_{12}	0	-1.08[g]
BAC	0.63	-1.03
$C_{16}E_{20}$	0	-1.08[h]

[a] Parameters of Alkyl TAB calculated based on reported cmc values from our previous work [22]; [b-h] literature reported values [68-71].

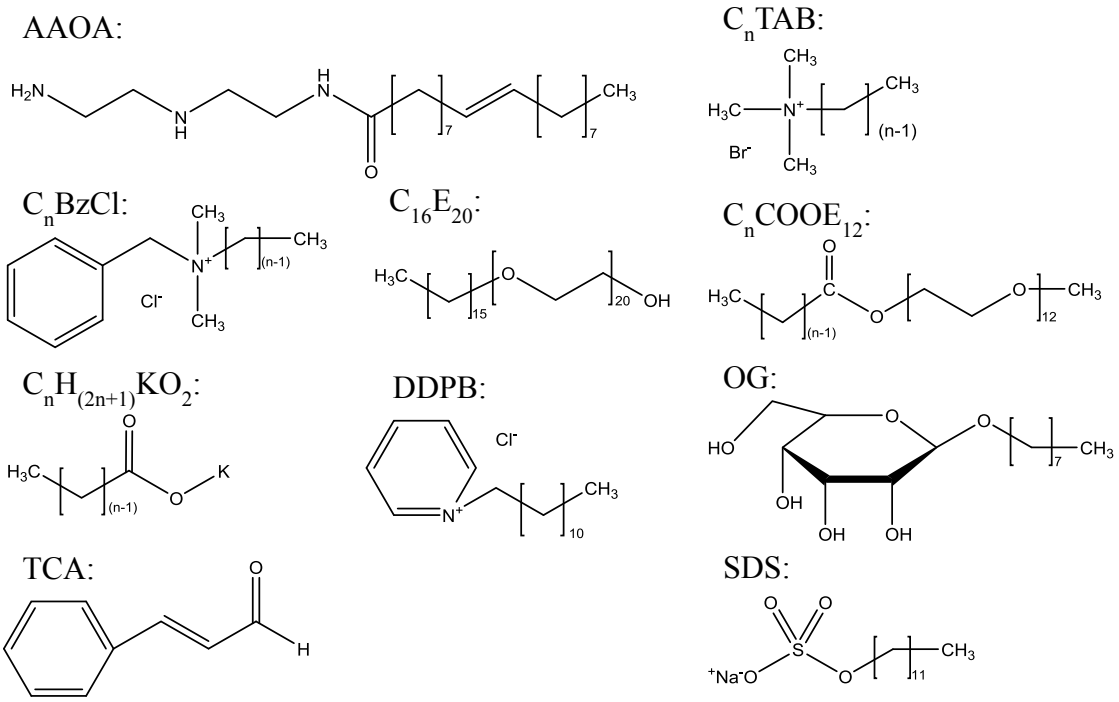

Fig. 2.1 Chemical structure of various surfactant molecules discussed in the present work. n represents hydrocarbon chain length. AAOA: N-[2-[(2-aminoethyl) amino] ethyl]-9-octadecenamide; C_nTAB: n-alkyl trimethyl ammonium bromide; C_nBzCl: n-benzalkonium chloride; $C_{16}E_{20}$: polyoxythylene cetyl ether; C_nCOOE_{12}: $C_nH_{(2n+1)}COO(CH_2CH_2O)_{12}CH_3$; OG: octylglucoside; $C_nH_{(2n+1)}KO_2$: potassium alkanoate; SDS: sodium dodecyl sulfate; TCA: trans-cinnamaldehyde; DDPB: dodecylpyridinium bromide.

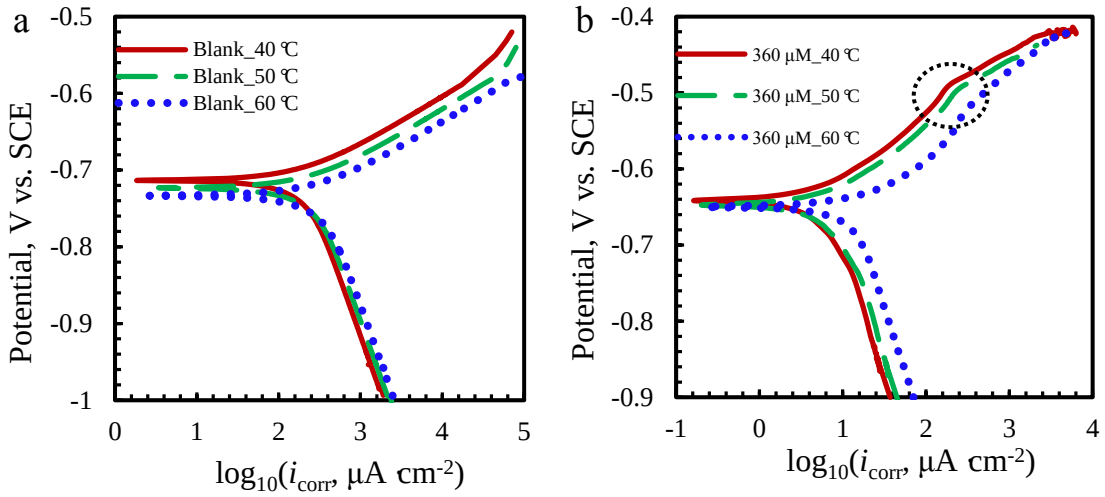

Fig. 2.2 Potentiodynamic polarization curves of X65 steel electrode exposed in CO_2-saturated 0.171 M NaCl aqueous solution containing (a) 0 μM (Blank), and (b) 360 μM mixed BAC surfactants in Testing System I at different temperatures (40 ℃, 50 ℃, and 60 ℃).

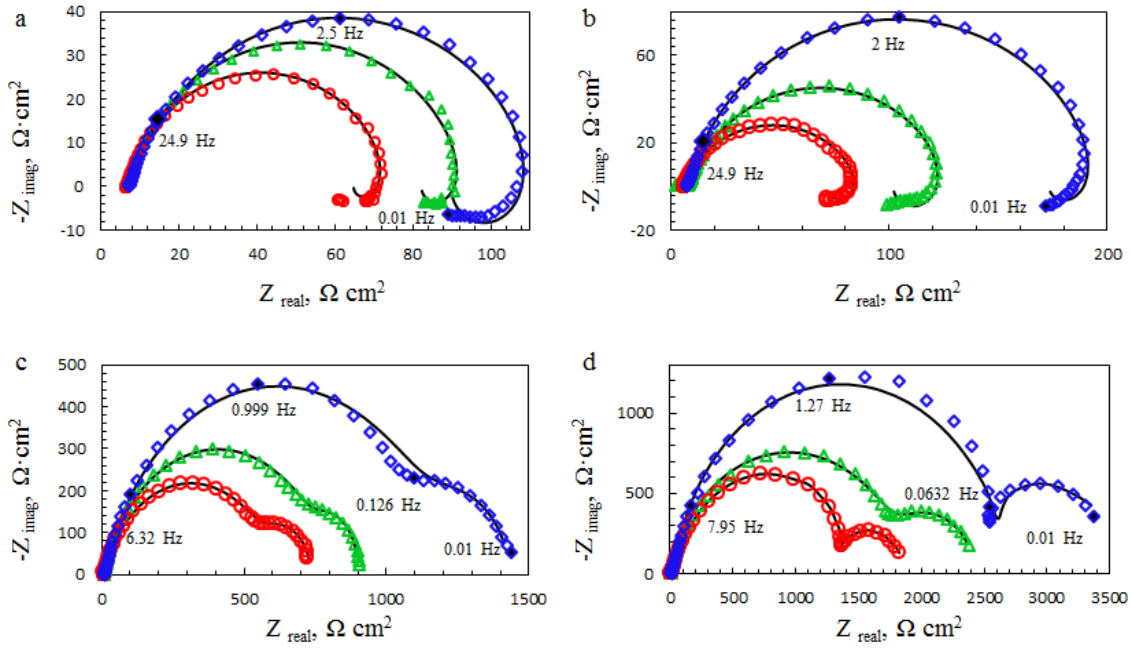

Fig. 2.3 Nyquist plot of X65 steel electrode exposed in CO_2-saturated 0.171 M NaCl aqueous solution containing (a) 0 μM (Blank), (b) 9 μM, (c) 72 μM, and (b) 360 μM mixed BAC surfactants in Testing System I at different temperatures (diamond: 40 ℃; triangle: 50 ℃; circle: 60 ℃; Solid lines: electrical circuit fitting). The number next to the solid symbol in Nyquist plots represents its corresponding frequency.

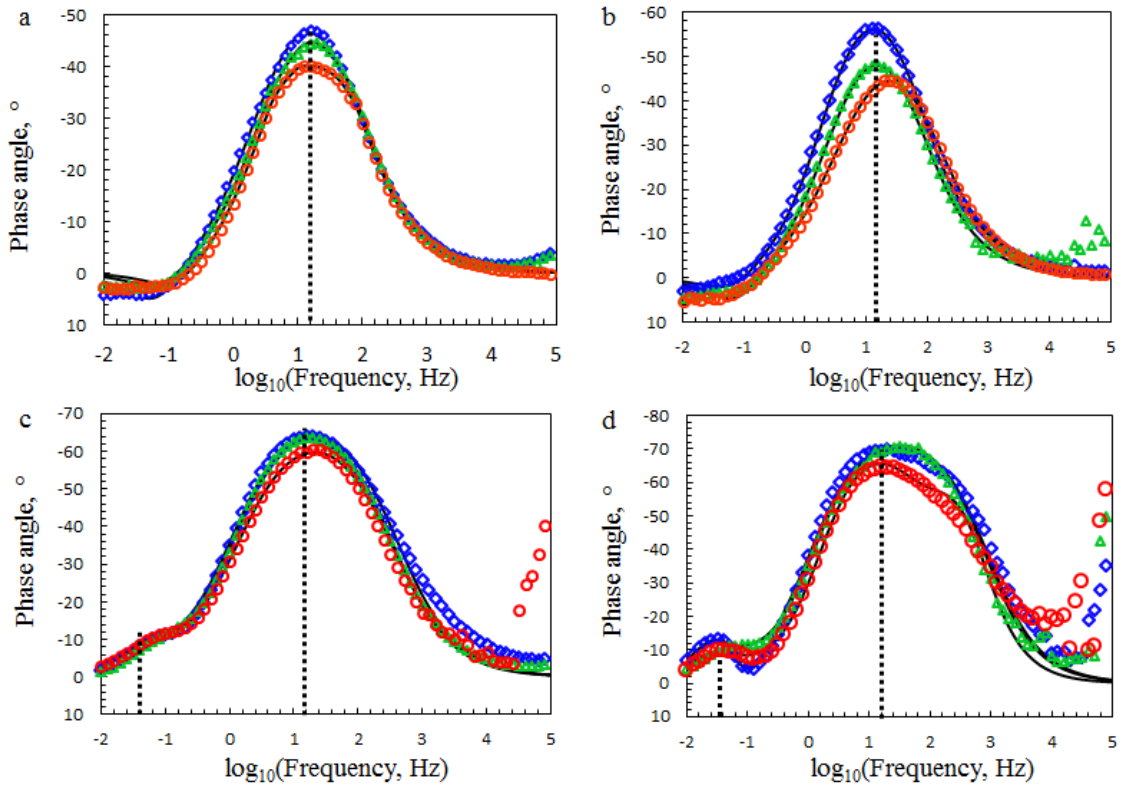

Fig. 2.4 Bode phase plot of X65 steel electrode exposed in CO_2-saturated 0.171 M NaCl aqueous solution containing (a) 0 μM (Blank), (b) 9 μM, (c) 72 μM, and (b) 360 μM mixed BAC surfactants in Testing System I at different temperatures (diamond: 40 ℃; triangle: 50 ℃; circle: 60 ℃; Solid lines: equivalent electrical circuit model fitting). Dashed-lines indicate time constant.

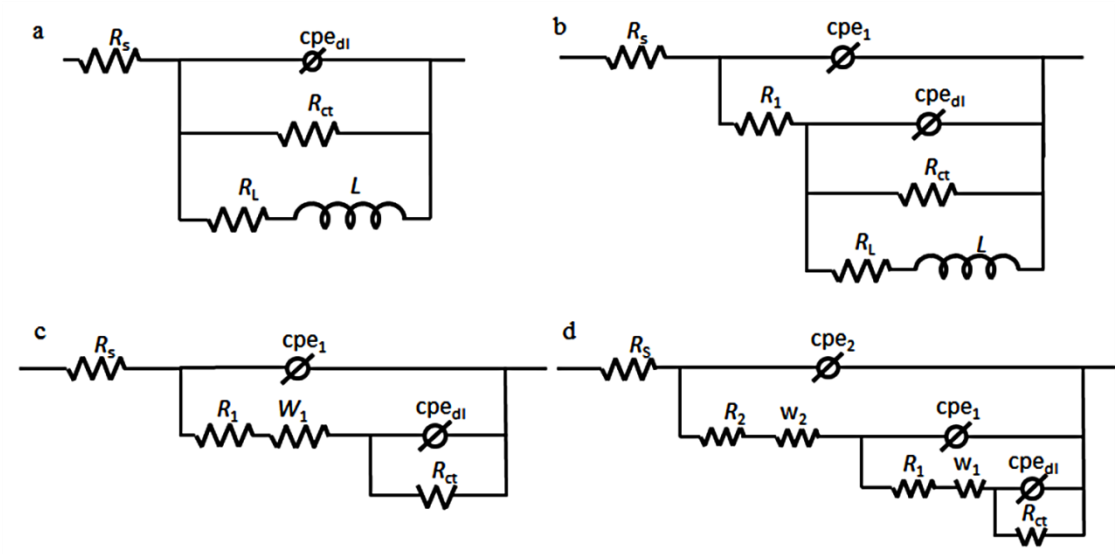

Fig. 2.5 Electrochemical equivalent circuits for the fitting of measured EIS plots: (a) without surfactant; (b) with surfactant concentration lower than sac; (c) with surfactant concentration around sac; (d) with surfactant concentration higher than sac.

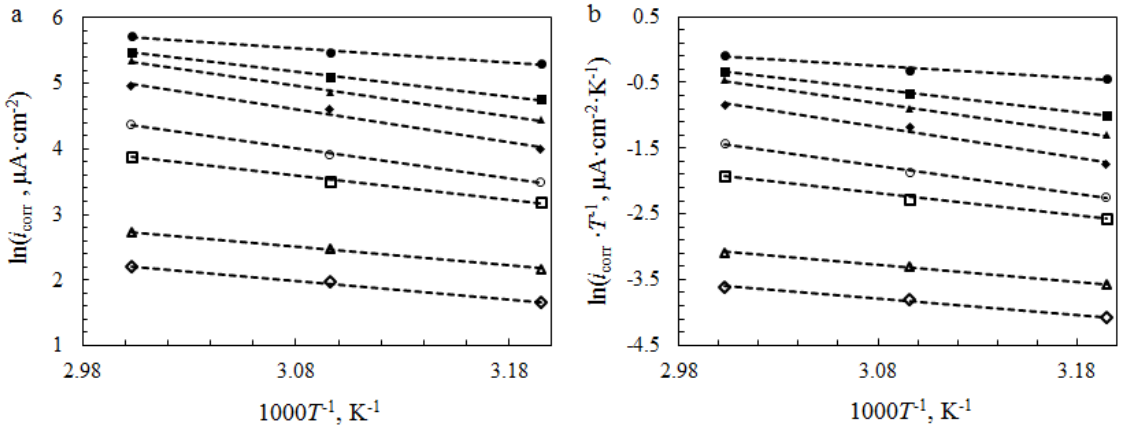

Fig. 2.6 Arrhenius plots of (a) i_{corr} vs. $1000T^{-1}$ (b) $i_{corr}T^{1}$ vs. $1000T^{-1}$ for X65 steel electrode in CO_2-saturated 0.171 NaCl M aqueous solution in presence of various total concentrations of mixed BAC in Testing System I : ●, Blank; ■, 9 μM; ▲, 18 μM; ♦, 36 μM; ○, 54 μM; □, 72 μM; Δ, 140 μM; ◊, 360 μM.

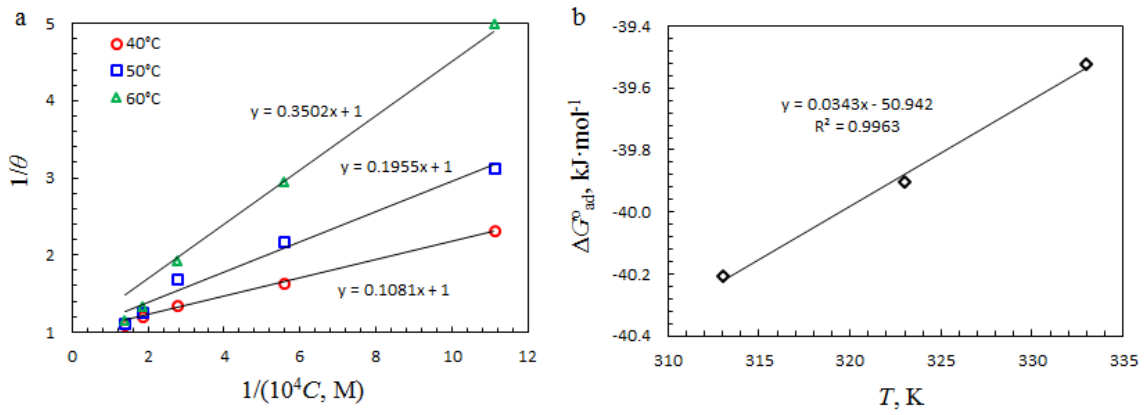

Fig. 2.7 Langmuir adsorption isotherm and free energy calculation: (a) plot of ($1/\theta$) vs. ($1/10^4C$) based on Langmuir adsorption (b) variation of $\Delta \boldsymbol{G^{o}_{ad}}$ as a function of T using EIS measurements for mixed BAC in Testing System I.

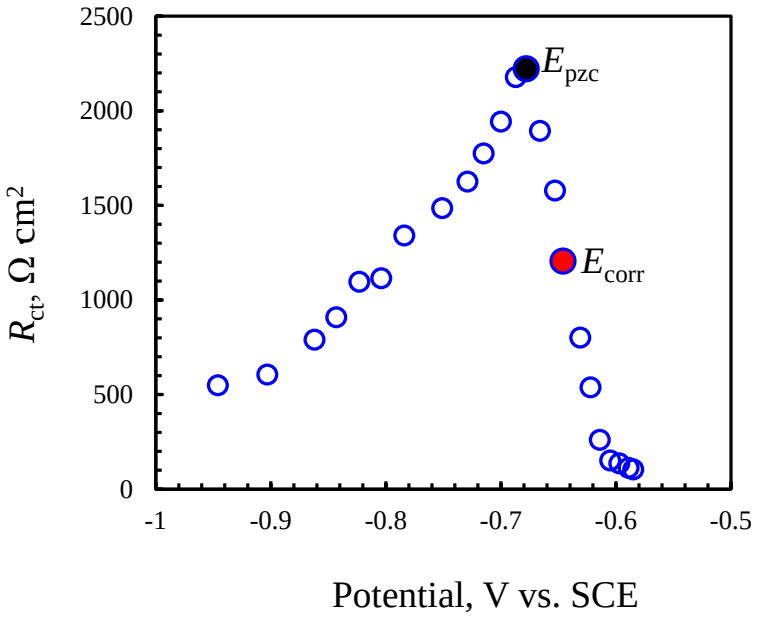

Fig. 2.8 The plot of R_{ct} vs. electrode potential for X65 steel electrode in CO_2-saturated 0.171 M NaCl solution containing 72 μM mixed BAC in Testing System I at 40 ℃.

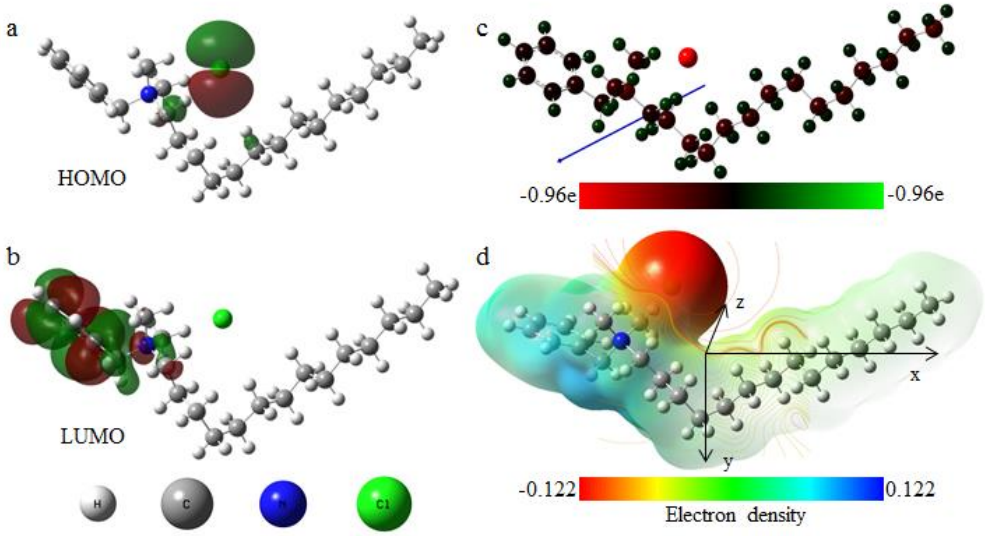

Fig. 2.9 Molecular orbitals (a) HOMO, (b) LUMO, electrostatic properties (c) Milliken charge distribution with displayed dipole, and (d) the contour with normal vector (001) and mapped surface electrostatic potential of C_{14}BzCl. e is positive elementary charge.

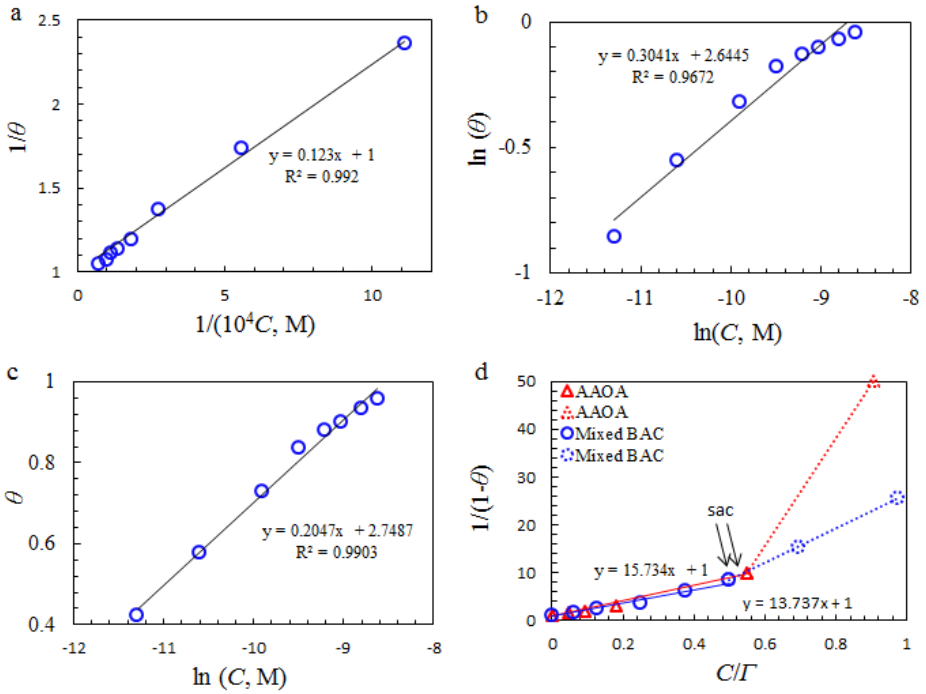

Fig. 2.10 The adsorption isotherms of mixed BAC in Testing System I at 40 ℃ on X65 steel electrode in CO_2-saturated 0.171 M NaCl solution: (a) Langmuir adsorption; (b) Freundlich adsorption; (c) Temkin adsorption; (d) Modified Langmuir adsorption. Experimental data of AAOA are cited from reference [5].

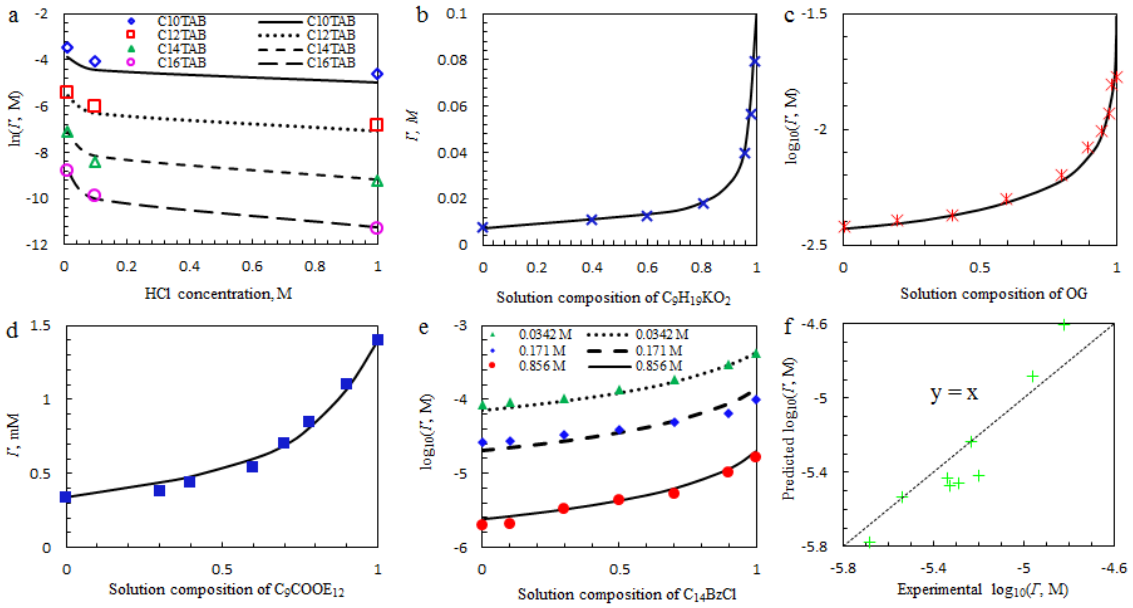

Fig. 2.11 Comparison of predicted and experimental cmc: (a) cmc of pure CnTAB as a function of HCl concentration in solution at T = 25 ℃; (b) cmc of binary mixed nonionic surfactants ($C_9H_{19}KO_2$ and $C_{11}H_{23}KO_2$) as a function of bulk mixed molar fraction of $C_9H_{19}KO_2$ at T = 25 ℃; (c) cmc of binary mixed anionic and nonionic surfactants (SDS and OG) as a function of mixed bulk solution composition of OG with 20 mM NaCl at T = 25 ℃; (d) cmc of binary mixed nonionic surfactants (C_9COOE_{12} and $C_{11}COOE_{12}$) as a function of bulk mixed molar fraction of C_9COOE_{12} at T = 25 ℃ without salt; (e) cmc of ternary mixed homologous cationic surfactants BAC ($C_{12}BzCl$, $C_{14}BzCl$, & $C_{16}BzCl$) as a function of mixed molar fraction of $C_{14}BzCl$ with NaCl concentrations of 0.0342 M, 0.171 M, or 0.856 M at T = 40 ℃; $C_{12}BzCl$ & $C_{16}BzCl$ are equal-molar mixed; (f) predicted cmc vs. experimental cmc of ternary mixed cationic, cationic, and nonionic surfactants ($C_{16}BzCl$, $C_{16}TAB$, and $C_{16}E_{20}$) at various mixed molar ratios with 30 mM NaCl in solution at T = 25 ℃. Symbols represent experimental data; lines represent model predicted data. Experimental data of cmc in Figs. (a)-(d) and (f) are cited from references [22, 68, 69, 72-74].

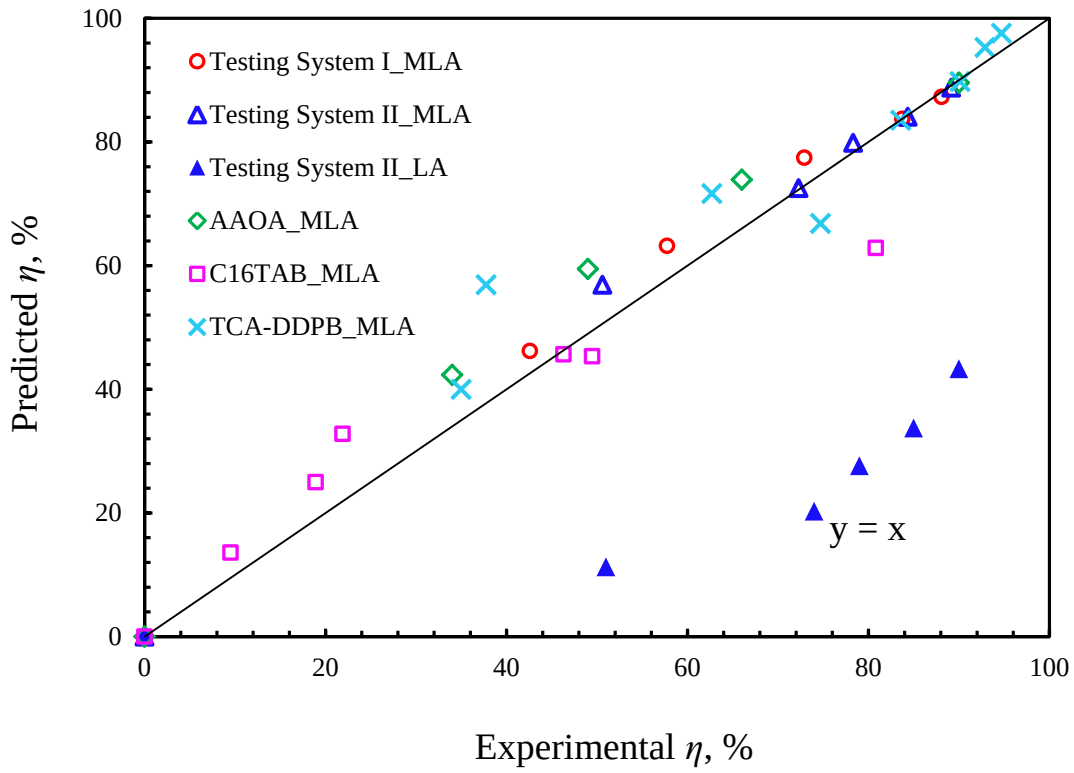

Fig. 2.12 Comparison between experimental inhibition efficiency and predicted inhibition efficiency for different testing systems as listed in Table 2.1 at 40 ℃ and reported testing system using surfactant AAOA [5] and surfactant C_{16}TAB [24] based on MLA and LA. *K′* are 15.73 for AAOA in 0.856 M NaCl aqueous solution at 25 ℃, and 2.52 for C_{16}TAB in 0.03 M $Fe(NO_3)_3$ aqueous solution at 32 ℃.

2.5 References

[1] B. Tribollet, J. Kittel, A. Meroufel, F. Ropital, F. Grosjean, E. M. M. Sutter, Electrochim. Acta 124 (2014) 46.

[2] S. Zou, X. Li, C. Dong, K. Ding, K. Xiao, Electrochim. Acta 114 (2013) 363.

[3] P. Bai, H. Zhao, S. Zheng, C. Chen, Corrosion Sci. 93 (2015) 109.

[4] Y. Zhou, Y. Zuo, Electrochim. Acta 154 (2015) 157.

[5] D.A. López, S.N. Simison, S.R. de Sánchez, Electrochim. Acta 48 (2003) 845.

[6] K.S. George, S. Nešić, Corrosion 63 (2007) 178.

[7] B.R. Linter, G.T. Burstein, Corrosion Sci. 41 (1999) 117.

[8] N. G. Thompson, Y. Mark, D. Daniel, Corrosion Rev. 25 (2007) 247.

[9] R. Fuchs-Godec, Electrochim. Acta 54 (2009) 2171.

[10] D. Gelman, D. Starosvetsky, Y. Ein-Eli, Corrosion Sci. 82 (2014) 271.

[11] B. Kronberg, Surfactant mixtures, Curr. Opin. Colloid Interface Sci. 2 (1997) 456.

[12] M.Z.A. Rafiquee, S. Khan, N. Saxena, M.A. Quraishi, J. Appl. Electrochem. 39 (2009) 1409.

[13] M.A. Quraishi, A. Singh, V.K. Singh, D.K. Yadav, A.K. Singh, Mater. Chem. Phys. 122 (2010)114.

[14] J.O. Bockris, A.K.N. Reddy, Modern Electrochemistry, 2nd ed., Kluwer Academic/Plenum Publishers, New York, 2000.

[15] A. Kokalj, S. Peljhan, M. Finsgar, I. Milosev, J. Am. Chem. Soc. 132 (2010) 16657.

[16] R. M. Hill, Mixed Surfactant systems, Marcel Dekker, New York, 1993.

[17] M. J. Rosen, Surfactants and Interfacial Phenomena, 3rd ed., John Wiley, New Jersey, 2004.

[18] Sonu, A. K. Tiwari, S. K. Saha, Ind. Eng. Chem. Res. 52 (2013) 5895.

[19] I. B. Obot, D. D. Macdonald, Z. M. Gasem, Corrosion Sci. (2015).

[20] S. Nešić, Corrosion Sci. 49 (2007) 4308.

[21] G. Gece, Corrosion Sci. 50 (2008) 2981.

[22] M. L. Free, W. Wang, D. Y. Ryu, Corrosion. 60 (2004) 837.

[23] W. Wang, M. L. Free, Corrosion. Sci. 46 (2004) 2601.

[24] M. L. Free, Corrosion. Sci. 46 (2004) 3101.

[25] M. L., Free, Corrosion. Sci. 44 (2002) 2865.

[26] Y. Zhu, M. L. Free, G. Yi, Corrosion Sci. 98 (2015) 417.

[27] W. Durnie, R. De Marco, A. Jefferson, B. Kinsella, J. Electrochem. Soc. 146 (1999) 1751.

[28] M. A. Migahed, M. A. Hegazy, A. M. Al-Sabagh, Corrosion. Sci. 61 (2012) 10.

[29] D. A. Jones, Principles, Prevention of Corrosion, Macmillan Publishing Company, 1991.

[30] V. Jovancicevic, S. Ramachandran, P. Prince, Corrosion 55 (1999) 309.

[31] X. Liu, P. C. Okafor, Y. G. Zheng, Corrosion Sci. 51 (2009) 744.

[32] Y. R. Dong, M. L. Free, J. Coll. Interf. Sci. 264 (2003) 402.

[33] Y. R. Dong, M. L. Free, Colloids Surf. A: Physicochem. Eng. Asp. 226 (2003) 17.

[34] F. Bentiss, M. Lebrini, M. Lagrenée, Corrosion. Sci. 47 (2005) 2915.

[35] K. Jüttner, Electrochim. Acta 35 (1990) 1501.

[36] D.M. Ortega-Toledo, J.G. Gonzalez-Rodriguez, M. Casales, L. Martinez, A. Martinez-Villafañe, Corrosion Sci. 53 (2011) 3780.

[37] G.A. Zhang, Y.F. Cheng, Corrosion. Sci. 51 (2009) 87.

[38] M. E. Orazem, B. Tribollet, Electrochemical Impedance Spectroscopy, Wiley, 2008, New Jersey.

[39] A. Popova, E. Sokolova, S. Raicheva, M. Christov, Corrosion Sci. 45 (2003) 33.

[40] X. Y. Zhang, F. P. Wang, Y. F. He, Y. L. Du, Corrosion Sci. 43 (2001) 1417.

[41] R. Lopes-Sesenes, G.F. Dominguez-Patiño, J.G. Gonzalez-Rodriguez, J. Uruchurtu-Chavarin, Int. J. Electrochem. Sci. 8 (2013) 477.

[42] E. E. Oguzie, Y. Li, F. H. Wang, J. Coll. Interf. Sci. 310 (2007) 90.

[43] X. Jiang, Y.G. Zheng, W. Ke, Corrosion. Sci. 47 (2005) 2636.

[44] M. Gholami, I. Danaee, M. H. Maddahy, M. RashvandAvei, Ind. Eng. Chem. Res. 52 (2013) 14875.

[45] M. P. Desimone, G. Gordillo, S. N. Simison, Corrosion Sci. 53 (2011) 4033.

[46] P. C. Okafor, X. Liu, Y. G. Zheng, Corrosion Sci. 51 (2009) 761.

[47] L. M. Vracar, D. M. Drazic, Corrosion Sci. 44 (2002) 1669.

[48] M. P. Desimone, G. Grudmeier, G. Gordillo, S. N. Simison, Electrochim. Acta 56 (2011) 2990.

[49] T. Szauer, A. Brandt, Electrochim. Acta 26 (1981) 1257.

[50] E. E. Oguzie, B. N. Okolue, E. E. Ebenso, G. N. Onuoha, A. I. Onuchukwu, Mater. Chem. Phys. 87 (2004) 394.

[51] M. Christov, A. Popova, Corrosion. Sci. 46 (2004) 1613.

[52] P. C. Okafor, Y. Zheng, Corrosion. Sci. 51 (2009) 850.

[53] M. Behpour, S.M. Ghoreishi, N. Soltani, M. Salavati-Niasari, M. Hamadanian, A. Gandomi, Corrosion. Sci. 50 (2008) 2172.

[54] E. A. Noor, A. H. Al-Moubaraki, Mater. Chem. Phys. 110 (2008) 145.

[55] R. Yıldız, Corrosion Sci. 90 (2015) 544.

[56] R. Solmaz, G. Kardas, B. Yazıcı, M. Erbil, Colloid Surf. A 312 (2008) 7.

[57] A. Lukomska, J. Sobkowski, J. Electroanal. Chem. 576 (2004) 95.

[58] J. Radilla, G. E. Negrón-Silva, M. Palomar-Pardavé, M. Romero-Romo, M. Galván, Electrochim. Acta 112 (2013) 577.

[59] A. E. Adnani, M. Mcharfi, M. Sfaira, M. Benzakour, A. T. Benjelloun, M. E. Touhami, Corrosion Sci. 68 (2013) 223.

[60] N. O. Obi-Egbedi, I. B. Obot, Mater. Chem. Phys. 12 (2010) 325.

[61] J. N. Butler, Ionic Equilibrium: Solubility and pH Calculations, Wiley, New York, 1998.

[62] J. F. Zemaitis, D. M. Clark, M. Rafal, N. C. Scrivner, Handbook of Aqueous Electrolyte Thermodynamics, AlChE, New York, 1986.

[63] K. S. Pitzer, Activity Coefficients in Electrolyte Solutions, 2nd ed., CRC Press, Boca Raton, 1991.

[64] M. Bourrel, R. S. Schechter, Microemulsions and Related System, Marcel Dekker, New York, 1988.

[65] U. P. Preiss, P. Eiden, J. Luczak, C. Jungnickel, J. Colloid Interface Sci. 412 (2013) 13.

[66] B. Lukanov, A. Firoozabadi, Langmuir 30 (2014) 6373.

[67] J. N. Phillips, Trans. Faraday Soc. 51 (1955) 561.

[68] K. Shinoda, J. Phys. Chem. 58 (1954) 541.

[69] K. Shinoda, T. Nakagawa, Colloidal Surfactants, Academic Press, New York, 1963.

[70] M. L. Corrin, W. D. Harkins, J. Am. Chem. Soc. 69 (1947) 683.

[71] J. T. Davies, Trans. Faraday Soc. 48 (1952) 1052.

[72] K. Kameyama, A. Muroya, T. Takagi, J. Colloid Interface Sci. 196 (1997) 48.

[73] H. P. Moises de Oliveira, M. H. Gehlen, Langmuir 18 (2002) 3792.

[74] A. A. Dar, G. M. Rather, S. Ghosh, A. R. Das, J. Colloid Interface Sci. 322 (2008) 572.

[75] F. B. Growcock, W. W. Frenier, J. Electrochem. Soc. 135(1988) 817.

CHAPTER 3

MLA AND MQSAR MODELS*

3.1 Introduction

Carbon steel is widely used for production and transportation pipelines in the oil and gas industries [1-4]. However, carbon steel is easily corroded in environments that contain water and carbon dioxide (CO_2) [3-7]. As one of the main corrosion types in the oil and gas industry, CO_2 related corrosion can cause tremendous damage to pipelines and structural components in water and crude oil transportation and thus threaten production and safety [3-5,7-9]. The annual direct cost of corrosion in the United States has been estimated to be around 3.1% of the gross domestic product (GDP). About 3.7% out of the total cost comes from the oil and gas industry [7,10], which is mainly due to the corrosion of carbon steel. Therefore, the cost of corrosion and safety has led to great interest in controlling CO_2-related corrosion in various oilfields around the world.

The most popular control method is to use organic inhibitors that contain heterocyclic molecules to reduce CO_2-based corrosion on carbon steel [1,2,11-14]. Many of the organic inhibitors are surfactants with hydrophilic and hydrophobic molecular sections.

The hydrophilic group of surfactant strongly prefers interaction with polar entities such as water, metals, and ions. These organic surfactants adsorb on the metal surface,

* Paper published in J. Electrochem. Soc. 168 (2015) C582-C591.

block the active surface sites, and thereby reduce corrosion attack [11,12]. The presence and structure of specific atoms, such as N and O, in surfactants determine the adsorption mechanism and corrosion inhibition efficiency [13,14]. Surfactant mixtures have received wide attention in practical applications because of their superior physicochemical properties and capabilities in efficient solubilization, dispersion, suspension, and transportation [15,16]. Solutions containing mixed surfactants can often be conveniently tuned to achieve desired properties by adjusting the composition of the mixture. More surface-active and expensive surfactants are usually mixed with less surface-active and less expensive surfactants to reduce cost [17]. However, the authors are not aware of a completely established theory or model to adequately predict corrosion inhibition using mixed surfactants despite extensive research work [3,18-24].

Because of hydrophobicity, surfactant molecules tend to adsorb at the air-liquid interface, liquid-solid interface, or liquid-liquid interface to escape from the aqueous phase by associating and aggregating hydrocarbon chains together [15-17]. The concentration at which a monolayer covers the solid-liquid interface is considered as the surface aggregation concentration (sac). Above the sac, surfactants will form aggregate structures to orient their hydrophobic tails toward those of neighboring surfactant molecules and their hydrophilic head groups toward water. The concentration at which surfactants start to form aggregates in solution is termed the critical micelles concentration (cmc) [21-25].

It is often assumed that the corrosion rate in the presence of low concentration of surfactants (usually lower than sac) can be represented by the number of available surface sites remaining after limited surfactant adsorption [21-25]. As the concentration of

surfactants increases, more and more active surface sites are covered by surfactants. Near the sac or cmc, the metal surface is assumed to be nearly covered by one monolayer or multilayers of surfactants, respectively, and metal is well protected from corrosion attack [21-26]. Thus, sac and cmc are important factors in the evaluation of the effect of surfactant concentration on surfactant adsorption and corrosion inhibition of metal. However, there is a lack of investigation and associated modeling work that illustrate how sac and cmc affect corrosion inhibition efficiency of surfactants in solutions with various dissolved salt contents.

In the present study, a new model for prediction of corrosion inhibition efficiency in salt solution using surfactants (both pure and mixture) is introduced based on previous work [21-25,27]. This model is based on utilization of either a Langmuir adsorption (LA) submodel or a Quantitative Structure Activity Relation (QSAR) submodel with a cmc prediction submodel [27]. The developed model is referred to as a modified Langmuir adsorption (MLA) [25] or modified Quantitative Structure Activity Relation (MQSAR) model, respectively, and will be introduced in the following section. The predictive MLA and MQSAR models are validated using electrochemical data collected from X65 steel corrosion inhibition testing using mixed homologous benzalkonium chlorides (BAC) surfactants as well as the reported data on other testing systems (Table 3.1). The chemical structure of various surfactant molecules discussed in the present work is given in Fig. 3.1. The predicted results from MLA and MQSAR agree well with experimental results. In addition, the effect of BAC concentration on steel corrosion inhibition as well as the associated adsorption mechanism on steel is discussed based on electrochemical measurements and density functional theory (DFT) calculations.

3.2 Model derivation

3.2.1 MLA submodel

One of the widely accepted models which is used for the adsorption of surfactants at an electrode-solution interface is the Langmuir adsorption model [21-25,30], in which the surface coverage is represented by:

$$\frac{1}{\theta} = \frac{1}{K_{\mathrm{ad}} C} + 1 \tag{3.1}$$

where K_{ad} is the equilibrium adsorption constant given by

$$K_{\mathrm{ad}} = \frac{1}{C_{\mathrm{wm}}} \exp\left(-\frac{\Delta G_{\mathrm{ad}}^{\mathrm{o}}}{RT}\right) \tag{3.2}$$

where C is the concentration of surfactant in the bulk solution, C_{wm} is the molar concentration of water which is 55.5 M, $\Delta G_{\mathrm{ad}}^{\mathrm{o}}$ is the standard free energy of adsorption, R is gas constant, and T is absolute temperature.

As mentioned in the former section, sac (represented using $\bar{\Gamma}$) and cmc (represented using Γ) are important parameters characterizing corrosion inhibition efficiency of surfactants. Therefore, MLA is introduced to evaluate corrosion inhibition efficiency of surfactants under various solution conditions by the incorporation of the cmc considering that the cmc is easier to measure and predict than sac [25]. The MLA is presented below

$$\frac{1}{1-\theta} = 1 + K' \frac{C}{\Gamma} \tag{3.3}$$

or

$$\eta\,(\%) = 100\theta = \left(1 - \frac{1}{1 + K' \frac{C}{\Gamma}}\right) \times 100 \tag{3.4}$$

where K' is equal to the adsorption constant K_{ad} multiplied by Γ, and η is corrosion inhibition efficiency. Note homologous surfactants tend to achieve similar levels of surface coverage at similar ratios of surfactant concentration to surfactant cmc, so the

value of K' barely varies for homologous surfactants and can be used as a universal constant for such homologous surfactants [25]. Note that C can increase above the sac or the cmc, but the fitting will not be as good as the fitting for C below the sac as shown in the following sections, which show that the sac is a transition point in characterizing the effectiveness of surfactants as corrosion inhibitors. The essence of Eqs. (3) and (4) is that the incorporation of cmc can successfully adjust for the effect of solution conditions and surfactant properties, such as salt concentration, solution temperature, hydrocarbon chain length, lateral surfactant interactions, and counterion binding, on surfactant adsorption and thus on corrosion inhibition efficiency.

3.2.2 MQSAR submodel

It is reported that a nonlinear relationship, QSAR, exists between a series of quantum chemical descriptors, such as HOMO and LUMO energies, and average corrosion inhibition efficiency for a specific surfactant [31-33]:

$$\eta\ (\%) = \frac{(\vec{A}\cdot\vec{Q}+\bar{B})C}{1+(\vec{A}\cdot\vec{Q}+\bar{B})C} \times 100 \qquad 3.5$$

where $\vec{A}$ is a vector of regression coefficients specific to surfactant and solution conditions (such as salt and temperature), $\vec{Q}$ is a vector of quantum chemical descriptors for a particular surfactant, and $\bar{B}$ is a regression constant. For mixture of homologous surfactants, the quantum chemical descriptors are weight-based average values.

Considering that QSAR in Eq. (3.5) was derived based on LA, it is reasonable that QSAR can also be modified to a general relation to predict η by the incorporation of cmc as presented below:

$$\eta\ (\%) = \frac{(\vec{A}' \cdot \vec{Q} + \bar{B}')C}{\Gamma + (\vec{A}' \cdot \vec{Q} + \bar{B}')C} \times 100 \quad 3.6$$

where $\vec{A}'$ is a modified vector of regression coefficients, and $\bar{B}'$ is a modified regression constant. Eq. (3.6) is termed MQSAR-1, which is similar to MLA in essence and can be adjusted for the effect of solution conditions on corrosion inhibition.

The correlation between salt concentration and cmc of surfactant is well described by the Corrin-Harkins relation as follows [34]:

$$\log_{10}(\Gamma) = a' \log_{10}(C_s) + b' \quad 3.7$$

where a' and b' are regression constants, and C_s is salt concentration.

With Corrin-Harkins relation, MQSAR-1 can be further modified to a more general form by eliminated Γ term:

$$\eta\ (\%) = \frac{(\vec{A}' \cdot \vec{Q} + \bar{B}')C}{b'' {C_s}^{a'} + (\vec{A}' \cdot \vec{Q} + \bar{B}')C} \times 100 \quad 3.8$$

$$b'' = 10^{b'} \quad 3.9$$

Eq. (3.8) is termed MQSAR-2 and is comparable to MLA and MQSAR-1 with respect to corrosion inhibition efficiency prediction. The advantage of MQSAR-2 is that it does not need the cmc as an input.

3.2.2.1 cmc prediction submodel

To use MLA and MQSAR-1 for the prediction of corrosion inhibition efficiency as mentioned above, known value of the cmc for the associated surfactant or mixed surfactants is a prerequisite. A model for the cmc prediction is briefly introduced in this section. More details about model derivation and validation can be found in Appendix A.3 and existing reference [27].

The cmc of surfactant is evaluated using the following equation:

$$\Gamma = (C_{\mathrm{mw}} + C_{\mathrm{s}})\exp^{\left(\frac{1}{kT}\Delta\mu_{\mathrm{m}}^{\mathrm{o}}\right)} \quad 3.10$$

where k is Boltzmann constant, T is temperature, and $\Delta\mu_{\mathrm{m}}^{\mathrm{o}}$ is micellization free energy which is estimated from several contributing terms as described below.

$$\Delta\mu_{\mathrm{m}}^{\mathrm{o}} = \Delta\mu_{\mathrm{trt}}^{\mathrm{o}} + \Delta\mu_{\mathrm{int}}^{\mathrm{o}} + \Delta\mu_{\mathrm{pack}}^{\mathrm{o}} + \Delta\mu_{\mathrm{st}}^{\mathrm{o}} + \Delta\mu_{\mathrm{ent}}^{\mathrm{o}} + \Delta\mu_{\mathrm{elec}}^{\mathrm{o}} + \Delta\mu_{\mathrm{act}}^{\mathrm{o}} \quad 3.11$$

where $\Delta\mu_{\mathrm{trt}}^{\mathrm{o}}$, $\Delta\mu_{\mathrm{int}}^{\mathrm{o}}$, $\Delta\mu_{\mathrm{pack}}^{\mathrm{o}}$, $\Delta\mu_{\mathrm{st}}^{\mathrm{o}}$, $\Delta\mu_{\mathrm{ent}}^{\mathrm{o}}$, and $\Delta\mu_{\mathrm{elec}}^{\mathrm{o}}$ are the free energy contributions from hydrocarbon transfer from water into micelle, formation of micellar core-water interface, hydrocarbon tail packing in the micelle, surfactant headgroup steric interaction, headgroup-counterion mixing, and electrostatic interaction, respectively [35,36]. $\Delta\mu_{\mathrm{act}}^{\mathrm{o}}$ comes from surfactant activity and counterion activity contribution.

Free energy micellization as a function of variables, including on micelle shape, micelle composition, micelle radius, and counterion binding coefficient, at given solution conditions is minimized using home-designed MATLAB code. The minimized micellization free energy is then used for the evaluation of cmc, aggregation number, counterion binding coefficient, and sphere-to-rod transition. Descriptions of model derivation, model parameters including effective area of headgroup or headgroup-ion pair, distance from the surface of the micelle to the center of charged headgroup, Stern layer thickness, as well as related calculations are found in the Appendix A.3 information and existing literature [25,27].

With the predicted cmc values of various pure surfactant and mixed surfactants, MLA and MQSAR-1 can be used for the prediction of corrosion inhibition efficiency.

3.3 Experimental

The homologous cationic benzalkonium chlorides (BAC) surfactants, including benzyl dimethyl dodecyl ammonium chloride (C_{12}BzCl), benzyl dimethyl tetradecyl ammonium chloride (C_{14}BzCl), and benzyl dimethyl hexadecyl ammonium chloride (C_{16}BzCl), were supplied by Sigma-Aldrich Co. LLC with assay values higher than 99%. The molecular structure of the surfactants are optimized and quantum parameters calculated using Gasussian09 simulation package with the method of B3LYP and the basis set of 6-311G(d, p) based on DFT. The test samples for surface tension measurements were prepared by sequential dilution of concentrated aqueous solutions of surfactants using double deionized water, made through a water purification system (Simplicity® UV made by EMD Millipore). The stock solution was prepared at a total surfactant concentration of 25 mM for electrochemical measurements using deionized water.

A piece of X65 steel, purchased from Metal Samples®, was used as the working electrode in electrochemical measurements with a surface area of 0.196 cm^2. The composition (wt %) is C 0.06%, Mn 1.33%, P 0.007%, S 0.005%, Si 0.30%, Cu 0.30%, Ni 0.10%, V 0.022%, Cb 0.046%, Al 0.019%, Cr 0.05%, Mo 0.03%, Ti 0.017%, Ca 0.0033%, and Fe (balance).

The surface of the X65 electrode was polished using SiC paper in the sequence of 400-600-800-1200 grit and followed by MicroCloth™ with grit size of ~ 5 μm supplied by Buehler. A platinum ring electrode and a single junction saturated calomel electrode (SCE) were employed as counter electrode and reference electrode, respectively. Test solutions contained 0.171 or 0.599 M NaCl and were purged with Ar (>99.999%) for 2 h

to remove oxygen followed by the purge of CO_2 (>99.999%) for 2 h to ensure CO_2 saturation prior to measurements. A flow of CO_2 was maintained during the experiments to keep a positive pressure inside the cell to avoid air ingress. The concentration of dissolved oxygen was monitored before electrochemical measurements using an Oxygen ULR CHEMets® Kit and the concentration was measured to be below 20 ppb. The pH was adjusted to 4 - 5 for different mixtures by the injection of 1.0 M $NaHCO_3$ or diluted HCl into the cell. The surfactants were added at the beginning of each measurement. The test solutions were then kept at open circuit potential (OCP), E_{corr}, for 2 h for equilibration. Experimental conditions for various testing systems are listed in Table 3.1. For time and experimental resource conservation, only Testing System II is used as an example for the results discussion from electrochemical measurements and for the inhibition efficiency prediction model derivation.

A Gamry reference 600 potentiostat was used for electrochemical measurements. Polarization resistance R_p was measured using the linear polarization resistance (LPR) method by polarizing the working electrode +/- 0.010 V (SCE) vs. E_{corr} with a sweep rate of 0.1 mV/s. Potentiodynamic scans were performed with a sweep rate of 1mV/s from -0.9 V (SCE) to -0.35 V (SCE). Electrochemical impedance spectroscopy (EIS) measurements were made with an applied alternating current (AC) potential of +/-0.010 V rms vs. E_{corr} in the frequency range of 100,000 - 0.010 Hz. The direct current (DC) potential was set as zero relative to E_{corr}. Each test was repeated at least three times as independent measurements within +/-4% deviation. The collected electrochemical data was analyzed with the Gamry Echem Analyst software package.

The surface tension of test solutions was measured within a precision of 0.1 mN/m by

the platinum ring method using a Krüss K10 ST digital tensiometer, equipped with an isothermal vessel holder. All the measurements were performed at a constant temperature of 40 ℃ ± 0.2 ℃, which has been shown to be higher than the Krafft point of the surfactants and their mixtures in aqueous media containing various concentrations of NaCl. The constant temperature was maintained through a water circulation bath using Polystat temperature controller, purchased from Cole-Parmer®. The platinum ring was rinsed with water and heated to an orange color using a Bunsen burner between tests to ensure the complete removal of contaminants. Triplicate measurements were used to confirm reproducibility within +/-2% deviation.

Nova™ Nano scanning electron microscope (SEM) equipped with energy dispersive X-ray spectroscopy (EDS) system was used to observe the surface morphology.

3.4 Results

3.4.1 cmc measurement

Upon the adsorption of surfactants at the air-water interface, the surface tension is reduced due to the amphiphilic nature of surfactants. Examples of surface tension vs. surfactant concentration curves are given in Fig. 3.2 and the cmc is determined from the interception of the two solid lines in each curve. As can be seen, the surface tension decreases with the increase in surfactant concentration until the surface tension reaches a plateau value, which is a result of surfactant assembled into aggregates, such as micelles, bilayers, or multilayers. Beyond the cmc, additional micelles form but the surface tension remains constant. Fig. 3.2 also indicates that the cmc of C_{12}BzCl decreases as the salt concentration increases because more surfactant molecules adsorb on the surface at the

higher concentration of salt. The comparison between curves b and c reveals that the ternary mixture of C_{12}BzCl, C_{14}BzCl, and C_{16}BzCl has a lower cmc value because the average hydrocarbon chain length is longer than that of pure C_{12}BzCl.

3.4.2 Electrochemical measurements

Considering E_{corr} stability is important to electrochemical measurements, the X65 steel electrode was immersed in solution and kept at OCP for equilibration before measurement. Examples of the dependence of E_{corr} of X65 steel electrode on time are given in Fig. 3.3(a). The E_{corr} stabilized at around -0.725 V (SCE) without surfactant. Upon the introduction of surfactant to CO_2-saturated aqueous solution containing salt, a positive shift of E_{corr} is usually observed [37]. In the present research, E_{corr} of Testing System II stabilized between -0.720 V (SCE) and -0.620 V (SCE) after the addition of surfactants at a wide concentration range, which includes sac and cmc. The cmc is around 16.5 μM by measurement. E_{corr} did not increase much at surfactant concentrations above cmc levels. The difference in E_{corr} in the absence and presence of surfactants indicates that the steel surface was covered and protected by the surfactant adsorption. According to Riggs Jr. [38], it is possible to classify one surfactant as anodic or cathodic if E_{corr} in the presence of surfactant shifts at least +85 mV or -85 mV, respectively, relative to E_{corr} in the absence of surfactant. However, the positive shift of E_{corr} of the investigated Testing System II at the highest concentration of 36 μM is only around 85 mV, indicating that both the dissolution of iron at the anode and the hydrogen evolution at the cathode were affected.

The LPR measurements were performed on Testing System II with various

concentrations of surfactants and the results were used to evaluate corrosion inhibition efficiency, η (%), using Eq. (3.12) [39]:

$$\eta(\%) = 100 \times \frac{R_{\mathrm{p}} - R_{\mathrm{po}}}{R_{\mathrm{p}}} \qquad 3.12$$

where R_{po} and R_{p} are polarization resistances in the absence and presence of surfactants, respectively.

Fig. 3.3(b) shows selected potentiodynamic scan curves of Testing System II. The shape of the anodic branch does not change a lot when the surfactant concentration is less than 9 μM. Above 9 μM, the anodic branch experiences a significant change. This phenomenon may be explained by coverage by the first monolayer on the steel where the monolayer effectively protects steel from corrosion. The concentration of 9 μM is interpreted as the sac of mixed surfactants in Testing System II. As the concentration continues to increase to the cmc or even higher values, the shape of the anodic branch does not shift much due to the fact that steel surface is already covered by monolayer before multilayers of surfactants form. The overall protection is slightly affected by the multilayers which form after the first monolayer [25,40].

The Tafel slopes were estimated from potentiodynamic scan curves. For those curves without anodic Tafel dependence above the sac, the anodic Tafel slopes were derived from the cathodic branches and cathodic Tafel slopes [39]. The corrosion inhibition efficiency was calculated using Eq. (3.13) based on the Tafel slope method [39].

$$\eta\ (\%) = 100 \times \frac{i_{\mathrm{ocorr}} - i_{\mathrm{corr}}}{i_{\mathrm{ocorr}}} \qquad 3.13$$

where i_{ocorr} and i_{corr} are the corrosion current density without and with surfactants in solution, respectively.

The calculated Tafel slopes, polarization resistance, corrosion rate, and inhibition

efficiency are summarized in Table 3.2 for Testing System II. Each electrochemical measurement was repeated at least three times within +/-4 % deviation. The corrosion inhibition efficiency results from potentiodynamic scans and LPR match very well. The inhibition efficiency increases rapidly to around 90% with the increase in surfactant concentration from 0 up to 72 μM. Further increase in concentration does not effectively enhance inhibition efficiency even when the concentration is much higher than the cmc, Γ. As mentioned previously, the concentration of 72 μM is interpreted as the value of the sac, F, at which a complete monolayer usually forms at the electrode-solution interface, and above which, bilayers or multilayers usually form at the electrode-solution interface [41,42]. Corrosion inhibition is usually directly related to the electrode surface coverage. Therefore, the monolayer is effective with respect to corrosion protection and the formation of bilayers and multiplayers do not contribute much to additional corrosion inhibition beyond the protection provided by monolayer coverage.

The topography of a corroded X65 steel electrode surface was examined using SEM, as shown in Fig. 3.4. The electrode surface was strongly damaged in the absence of surfactants in corrosive solution, as shown in Fig. 3.4(a). In contrast, there was much less damage on the electrode surface with surfactant addition. Moreover, the electrode was better protected with higher concentration of surfactants.

3.4.3 Determination of K' in MLA submodel

The corrosion current density as a function of (C/Γ) for various testing systems is presented in Fig. 3.5(a). As can be seen, the current density decreses rapidly with the increase in surfactant concentration in the range between 0 and the sac for each of the

testing systems. Above the sac, the current density reaches a plateau value. Fig. 3.5(a) also indicates that the surfactants in Testing Systems IV and V are not as effective in corrosion inhibition as those surfactants in Testing Systems II and III due to relatively higher plateau values of current density in the concentration range studied.

Fig. 3.5(b) presents the plots of $1/\theta$ vs. $1/C$ based on the regular LA in the concentration range between 0 and the cmc for various testing systems. The calculated adsorption free energies based on Eqs. (3.1) and (3.2) are -45.6 kJ/mol for Testing System II, -43.4 kJ $\cdot$mol^{-1} for Testing System III, -44.1 kJ $\cdot$mol^{-1} for Testing System IV, and -37.9 kJ $\cdot$mol^{-1} for Testing System V. If adsorption free energy is more positive than -20 kJ $\cdot$mol^{-1}, the interaction between surfactant and metal is usually dominated by physisorption. If adsorption free energy is more negative than -40 kJ $\cdot$mol^{-1}, the interaction is usually dominated by chemisorption in which the adsorption involves charge sharing or transfer between surfactant molecules and metal surface to form coordination bonds [43,44]. Based on the calculated adsorption free energy, it is inferred that the surfactant adsorption in Testing Systems II, III, and IV is dominated by chemisorption; the surfactant adsorption in Testing Systems V is dominated by both physicorption and chemisorption. However, physisorption can sometimes be energetically favorable and significant whereas chemisorption may sometimes have relatively weak binding energy due to various factors that influence adsorption [45,46].

Over the entire range of surfacant concentration, the linear fitting is excellent based on the regular LA model for each investigated system in Fig. 3.5(b). In contrast, the MLA model features a sharp transition around the sac, as shown in Fig. 3.5(c). Below the sac, there is a good linear correlation between $1/(1-\theta)$ and (C/Γ); above the sac, a sharp

transition appears, and after that the plot is curved and gradually reaches a plateau as the concentration increases. The transitions indicate that below the sac, the inhibition efficiency increases rapidly with the increase in surfactant concentration and that further increase in concentration above the sac does not effectively enhance inhibition efficiency even when the concentration is much higher than the cmc. These results are in accordance with electrochemical measurements. For each testing system, the linear part (C<sac) of the plot in Fig. 3.5(c) is presented in Fig. 3.5(d), in which the value of the modified adsorption constant K' is given by the slope of the linear fitting equation. The K' values are 13.97, 15.73, 0.96, and 4.84 for Testing System II, III, IV, and V, respectively. The fitted K' value will be used for the corrosion inhibition prediction model discussed in this paper. Note that homologous surfactants tend to achieve similar levels of surface coverage at similar ratios of surfactant concentration to surfactant cmc, so the value of K' does not vary a lot for homologous surfactants [25]. Considering the surfactant used in Testing Systems I and II are homologous, $K' = 13.97$ can be directly used in Testing System I.

3.4.4 Determination of $\vec{A}'$ and $\bar{B}'$ in MQSAR submodel

For better illustration of adsorption of BAC surfactants on steel surface, regular quantum chemical descriptors [19,20,31-33,47], including the energies of molecular frontier orbitals (E_{HOMO} and E_{LUMO}), energy difference between HOMO and LUMO (ΔE), Mulliken charge distribution on the backbone atoms, dipole moment of the surfactant molecule ($\bar{\mu}$), surface electrostatic potential based on electron density of the molecule, and the fraction of electrons transferred from the surfactant to the steel surface (ΔN)

[31,48,49], were determined based on DFT using Gaussian09. HOMO tends to donate electrons to suitable acceptor substances on the steel surface while LUMO tends to accept electrons from the steel surface and lower LUMO energy usually indicates stronger electron accommodation [19,20,47]. The energy gap ΔE usually characterizes the stability of the complex of surfactant and metal surface [31,48,49]. The value of ΔN describes the inhibition achieved from electron donation [31,49]. The Milliken charges and surface electrostatic potential usually shed light on the electron distribution in surfactant molecules and electrostatic interaction between surfactant and iron or steel [30-33]. The molar volume of surfactant molecule, V_{sm}, is also needed to be considered due to its potential effect on surfactant packing/aggregation efficiency and steric interactions. However, the relationship between dipole moment and corrosion inhibition is still a controversial issue [31,45].

Many existing literature articles illustrate in detail how to calculate the fraction of electrons transferred from inhibitor to the metal surface, ΔN [31,49]. The calculation process is briefly described below. The ionization potential E_{ip} and the electron affinity A_e are approximated to $-E_{HOMO}$ and $-E_{LUMO}$, respectively. The absolute electronegativity χ and the global hardness Υ are defined as

$$\chi = (E_{ip}+A_e)/2 \quad 3.14$$

$$\Upsilon = (E_{ip}-A_e)/2 \quad 3.15$$

ΔN is given by

$$\Delta N = \frac{\chi_{mel}-\chi_{inh}}{2(\Upsilon_{mel}-\Upsilon_{inh})} \quad 3.16$$

where χ_{mel} and Υ_{mel} are electronegativity and global hardness of metals (electrodes), respectively. χ_{inh} and Υ_{inh} are electronegativity and global hardness of surfactant

molecule, respectively. The reported electronegativity and global hardness of iron (4.06 eV/mol and 3.81 eV/mol, respectively) are used [50,51]. For Testing System V, the electronegativity and global hardness of copper are 5.59 eV/mol and 0.15 eV/mol, which were calculated using Gaussian09 following the same procedures for surfactants.

The values of quantum descriptors of homologous BAC surfactants as well as surfactants in other testing systems are summarized in Table 3.3. For qualitative illustration of homologous BAC surfactants, the calculated results of C_{14}BzCl are presented in Fig. 3.6 considering that the electronic properties of homologous series should be similar.

Application of Eqs. (3.5), (3.6), and (3.8) based on electrochemical data of Testing System II in Table 3.2 and calculated quantum descriptors in Table 3.3 yields the following semi-empirical equations of QSAR, MQSAR-1, and MQSAR-2, respectively:

$$\eta\,(\%) = \left(\frac{(3.97E_{\mathrm{HOMO}}+5.05E_{\mathrm{LUMO}}-10.12\Delta E+51.71\Delta \mathrm{N}+18200\bar{\mu}+0.417V_{\mathrm{sm}}+574693)C}{1+(3.97E_{\mathrm{HOMO}}+5.05E_{\mathrm{LUMO}}-10.12\Delta E+51.71\Delta N+18200\bar{\mu}+0.417V_{\mathrm{sm}}+574693)C}\right)\times 100 \quad (3.17)$$

$$\eta\,(\%) = \left(\frac{(-4.80E_{\mathrm{HOMO}}-0.656E_{\mathrm{LUMO}}-2.41\Delta E+1.15\Delta N-0.052\bar{\mu}-0.071V_{\mathrm{sm}}+2.01)C}{\Gamma+(-4.80E_{\mathrm{HOMO}}-0.656E_{\mathrm{LUMO}}-2.41\Delta E+1.15\Delta N-0.052\bar{\mu}-0.071V_{\mathrm{sm}}+2.01)C}\right)\times 100 \quad (3.18)$$

$$\eta = \left(\frac{(-30.3E_{\mathrm{HOMO}}-2.06E_{\mathrm{LUMO}}+10.1\Delta E-2.50\Delta N-0.213\bar{\mu}-0.004V_{\mathrm{sm}}+2.22)C}{0.0092{C_{\mathrm{S}}}^{-1.17}+(-30.3E_{\mathrm{HOMO}}-2.06E_{\mathrm{LUMO}}+10.1\Delta E-2.50\Delta N-0.213\bar{\mu}-0.004V_{\mathrm{sm}}+2.22)C}\right) \quad (3.19)$$

Note that Eq. (3.18) and Eq. (3.19) are comparable with respect to corrosion inhibition efficiency prediction. Similar to the above-mentioned MLA submodel, the regression parameters of $\vec{A}' = (-4.80, -0.656, -2.41, 1.15, -0.052, -0.071)$ *and* $\bar{B}' = 2.01$ in Eq. (3.18), which are the values from one fitting operation using the

experimental data of Testing System II, can be directly used in other testing systems with homologous surfactants or similar surfactants for corrosion inhibition evaluation. Without using the cmc in QSAR, the transfer of the regression parameters $\bar{A} = (3.97, 5.05, -10.12, 51.71, 18200,\ 0.417)$ *and* $\bar{B} = 574693$ in Eq. (3.17) to other testing systems is expected to fail in the evaluation of corrosion inhibition because the surfactant interaction effect is not taken into account.

3.4.5 MLA submodel and MQSAR submodel validation

To validate the MLA submodel and the MQSAR submodel, and to illustrate the advantage of MLA relative to LA, and of MQSAR relative to QSAR, examples of the applications of Eqs. (3.1) and (3.4), and Eqs. (3.17) and (3.18) to Testing System I are presented in Fig. 3.7. Note that the values of thermodynamic parameter K_{ad} in Eq. (3.1), and fitting parameters K' in Eq. (3.4), $\bar{A}$ and $\bar{B}$ in Eq. (3.5), and $\vec{A}'$ and $\bar{B}'$ in Eq. (3.6) are calculated based on experimental data of Testing System II. The calculated value of K_{ad} is 7.28×10^5 M^{-1}. The values of other parameters are as mentioned in previous sections. The predicted cmc value Γ of mixed surfactants in Testing System I is 1.44×10^{-4} M which is used in the validation of MLA submodel.

Note that the average chain length, salt concentration, and testing conditions (such as pH) are different for Testing System I and Testing System II. As can be seen from Fig. 3.7, the predicted corrosion inhibition efficiency using both MLA submodel and MQSAR-1 submodel agree well with experimental results due to the adjustment of solution environment, surfactant interactions, and surfactant chain length etc. through cmc. The prediction using LA and QSAR, however, deviates significantly from

experimental data. Note that MQSAR-2 is similar to MQSAR-1 in essence and thus is not shown in the comparison in Fig. 3.7.

As discussed above, both MLA and MQSAR need the cmc value of surfactant or surfactant mixture of discussed as an input. The validation of the well-developed cmc prediction model is exemplified in Fig. 3.8. The predicted cmc for pure, binary- and ternary-mixed BAC surfactants in the solution containing various NaCl concentrations agree well with experimental results, as shown in Figs. 3.8(a)-3.8(c). For all of the discussed testing systems listed in Table 3.1, there is excellent agreement in the value of cmc between prediction and experiment (Fig. 3.8(d)). The application of the cmc prediction model to the binary mixture of anionic and nonionic surfactants (Fig. 3.8(e)) and to the ternary mixture of cationic, cationic, and nonionic surfactants (Fig. 3.8(f)) is also successful, even though the agreement between the prediction and the experiment is not as excellent as that shown in Figs. 3.8(a)-3.8(d). Note that the experimental data of Testing Systems III, IV, and V are cited from references [21,52-56].

It is expected that the integrated model based on the MLA submodel and the cmc submodel or the integrated model based on the MQSAR submodel and the cmc submodel should be successful in the prediction of corrosion inhibition efficiency of the discussed surfactant systems. The comparison of the predicted results from the integrated model and from the experimental measurements is shown in Fig. 3.9, based on the data of corrosion inhibition from all the five testing systems as summarized in Table 3.4. The prediction agrees very well with experiment for Testing Systems I, II, III, and IV. The deviation for Testing System V is slightly higher but still falls within a reasonable range. This may be due to less effective monolayer coverage of C_{16}TAB on copper surface in

presence of slightly complicated salt $Fe(NO_3)_3$ in Testing System V. Note that the MQSAR predicted corrosion inhibition of all the five testing systems are based on Eqs. (3.18) and (3.19) with unified fitting parameters, which indicates the vastly improved applicability and robustness of developed MQSAR over regular QSAR.

3.5 Discussion

It can be seen in Table 3.3 that all the three surfactants display slight differences in quantum descriptors. In the context of simple corrosion inhibition, it is believed that alkyl chains are chemically unreactive substituents and that the homologous surfactants which vary only in alkyl chain length have very similar quantum descriptors. In other words, these quantum descriptors, calculated based on frontier orbital theory with a very strong fundamental basis, describe the characteristics of the head groups and reflect the associated adsorption properties. It is feasible to get quantum descriptors from only one type of surfactant and then apply these parameters to a series of homologous surfactants or surfactants with similar headgroups. For the surfactants of different classes with considerable differences in quantum descriptors, molar-based average quantum descriptors are recommended. In this study, the molar-based average was used to calculate the quantum descriptors of mixtures regardless of surfactant classes.

The cmc model takes into account the ion/salt effect on aggregation/adsorption, the effect of chain length of surfactant, van der Waals interactions between surfactant molecules, steric interactions between head groups, electrostatic interactions at interfacial region of micelles, and the interactions between solvent and surfactant [21,22,25,27,35,57]. Therefore, the insertion of cmc into QSAR or LA can accurately

describe the adsorption phenomena of surfactants on substrate (metal electrode) and associated effects of physical and chemical properties of surfactants and solvent environment. Mixtures of surfactants, which involve surfactant of the same or different classes, have been widely used in practical applications because of their superior physicochemical properties, capabilities, and/or economic viability [15,16]. Beyond the applicability of our model for pure surfactant and mixed homologous surfactants, the more valuable part lies in its potential to evaluate the corrosion inhibition of various surfactant mixtures of different classes at various solution conditions using only one set of experimental data.

The fitting of MQSAR only requires one set of experimental data just as MLA does. The only difference is that the fitting of MQSAR yields a set of regression parameters simultaneously but MLA only has one parameter. In terms of the number of regression parameters, the use of MLA is simpler. In other words, the MQSAR is an alternative to the MLA for corrosion inhibition modeling.

It is interesting to note that the regression parameters in QSAR/MQSAR for one class of surfactants may be transferred to other surfactants with similar head groups or similar quantum descriptors. Similarly, the MLA parameter (K') for one surfactant can be used for other surfactants with similar head groups. In addition, the parameters of one surfactant mixture can be used for the mixtures of similar surfactants. The initial evaluation of transferability of regression parameters was performed by applying Eqs. (3.18) and (3.19) to the five testing systems discussed and the results in Fig. 3.9 indicates a good agreement between experimental data and various model predictions. Other cases of parameter transfer between different classes of surfactants can be found elsewhere [58].

3.6 Summary

1. Monolayer coverage of pure surfactant or mixed surfactants in the testing systems listed in Table 3.1 provides good inhibition of metallic electrode corrosion.

2. The MLA features the sac which is more effective in characterizing corrosion inhibition efficiency of surfactants, whereas regular ML does not utilize the sac.

3. MQSAR is provided as an alternative to the MLA for the prediction of corrosion inhibition of surfactants.

4. The incorporation of the cmc into MLA, MQSAR-1, and MQSAR-2 successfully accounts for the effect of solution environment, such as salt concentration and surfactant interactions, and the effect of surfactant properties on surfactant adsorption and thus on corrosion inhibition efficiency. The integrated prediction model is efficient in predicting corrosion inhibition of surfactants in various discussed testing systems.

5. The developed corrosion inhibition prediction models provide potential methods to evaluate the effectiveness of various surfactant or surfactant mixtures in corrosion inhibition under various testing conditions.

Table 3.1 Experimental condition for different surfactant testing systems. cmc and sac are estimated values based on experiment.

Testing system	Surfactant Mixed ratio	Salt C(M)	T (℃)	pH	Electrode	Rotation (RPM)	cmc (μM)	sac (μM)	Reference
I	$C_{14}BzCl/C_{14}BzCl/C_{16}BzCl$ 0.70/0.25/0.05	NaCl 0.171	40	4	X65 steel	300	140	72	---
II	$C_{14}BzCl/C_{14}BzCl/C_{16}BzCl$ 0.33/0.33/0.33	NaCl 0.599	40	5	X65 steel	100	16.5	9	---
III	AAOA 1	NaCl 0.856	25	6	1018 steel	low	15	8.2	28, 29
IV	CPC 1	HCl 1	31	0	1018 steel	1000	1.5	1	21
V	$C_{16}TAB$ 1	$Fe(NO_3)_3$ 0.03	32	---	copper	1000	30	20	22

Table 3.2 Results obtained from polarization resistance measurements and dynamic scans for X65 steel in absence and presence of various total concentrations of surfactants in Testing System II

C (μM)	β_a (mV dec^{-1})	β_c (mV dec^{-1})	i_{corr} (μA cm^{-2})	η (%)[a]	R_p (ohm cm^2)	η (%)[b]
0	55.2±2	202±6	182±7	0	101±4	0
1.5	51.7±2	212±7	90±3	51±2	197±7	49±2
3	57.3±3	221±7	47±2	74±3	408±10	75±3
4.5	56.5±2	205±5	39±2	79±3	483±10	79±3
6	49.7±1	212±4	27±2	85±2	636±12	84±3
9	49.2±2	210±2	20±1	89±2	850±15	88±2

[a] η (%) calculated from potentiodynamic scans using Tafel slopes; [b] η (%) calculated from LPR.

Table 3.3 Quantum chemical descriptors of surfactants in aqueous phase

BAC	E_{HOMO} (eV)	E_{LUMO} (eV)	ΔE (eV)	$\bar{\mu}$ (debye)	ΔN	V_{sm} (cm^3/mol)
C_{12}BzCl	-5.185	-1.674	-3.510	13.87	0.057	351.3
C_{14}BzCl	-5.186	-1.673	-3.514	13.90	0.057	343.9
C_{16}BzCl	-5.174	-1.669	-3.505	13.80	0.057	265.8
AAOA	-5.314	0.8754	-6.189	3.998	0.133	352.3
CPC	-5.994	-2.384	-3.609	15.74	-0.012	253.9
C16TAB	-7.178	-7.122	-0.056	6.953	-4.399	335.2

Table 3.4 Experimental measured and model predicted corrosion inhibition efficiency

Testing System	Concentration, 10^{-6} M	Corrosion inhibition efficiency η, %			
		Measurement, ±4	MLA	MQSAR-1	MQSAR-2
I	0	0	0	0	0
	9	44	46	43	48
	18	58	63	60	65
	36	76	77	75	78
	54	83	84	82	85
	72	88	87	86	88
II	0	0	0	0	0
	1.5	51	57	55	52
	3	74	73	71	69
	4.5	79	80	79	77
	6	85	84	83	81
	9	90	89	88	87
III[a]	0	0	0	0	0
	0.7	34	42	35	32
	1.4	49	59	51	49
	2.7	66	74	67	65
	8.2	90	90	86	85
	14	98	93	91	90
IV[b]	0	0	0	0	0
	0.32	17	16	16	17
	0.61	30	28	26	29
	1	38	39	37	40
	1.5	44	49	47	50
V[c]	0	0	0	0	0
	1.9	11	14	14	13
	1	21	25	26	24
	5.8	31	33	33	32
	10	46	46	46	45
	12	49	48	46	46
	20	81	63	64	62

a-c: experimental data is cited from literature [21,22,28,29].

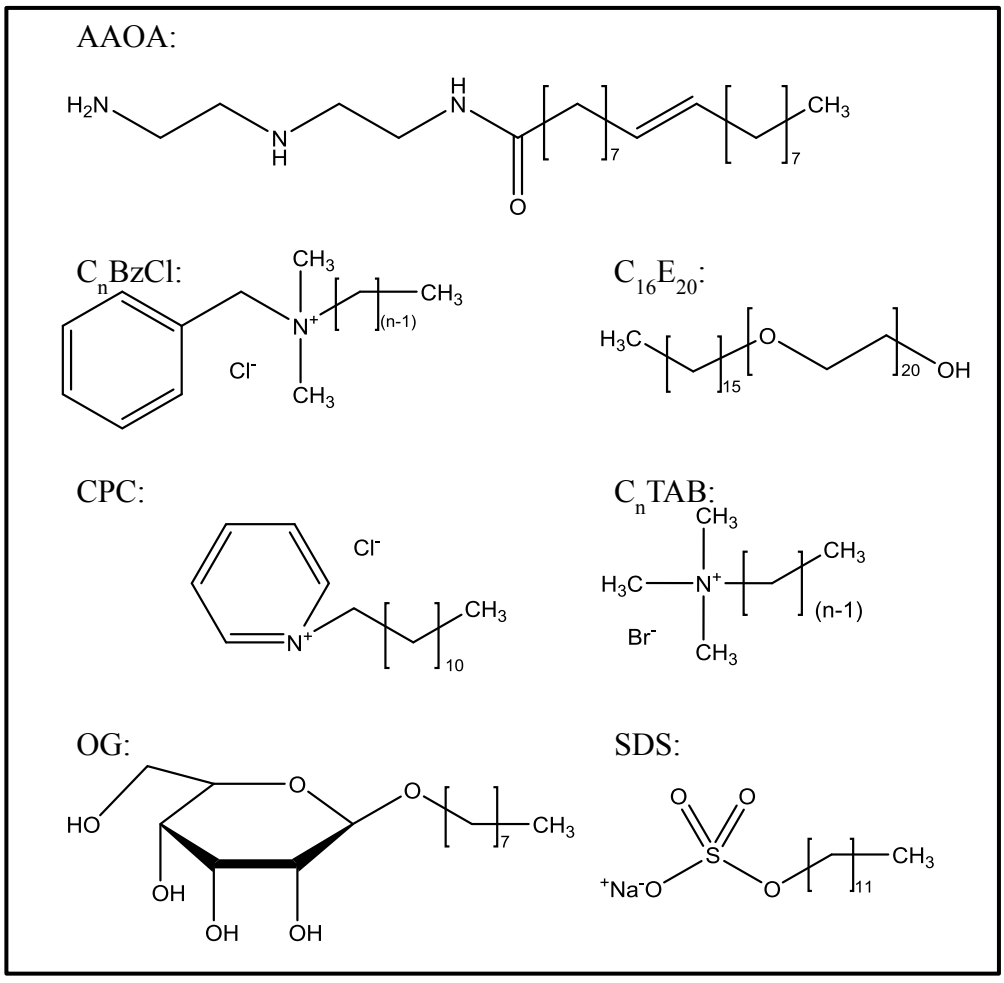

Fig. 3.1 Chemical structure of various surfactant molecules discussed in the present work. n represents hydrocarbon chain length. AAOA: N-[2-[(2-aminoethyl) amino] ethyl]-9-octadecenamide; C_nBzCl: n-benzalkonium chloride; $C_{16}E_{20}$: polyoxythylene cetyl ether; CPC: cetylpyridinium chloride; C_nTAB: n-alkyl trimethyl ammonium bromide; OG: octylglucoside; SDS: sodium dodecyl sulfate.

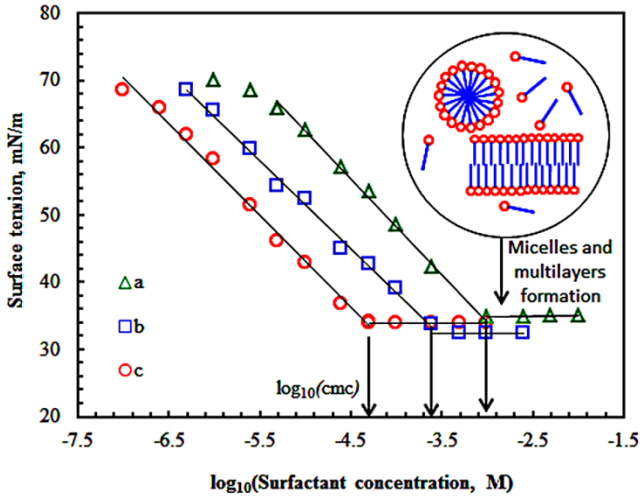

Fig. 3.2 Plots of surface tension vs. concentration of surfactants: (a) C_{12}BzCl in 0.171 M NaCl-containing aqueous solution at 40 ℃; (b) C_{12}BzCl in 0.856 M NaCl-containing aqueous solution at 40 ℃; (c) mixed C_{12}BzCl, C_{14}BzCl, & C_{16}BzCl at ratio of 0.15/0.70/0.15 in 0.171 M NaCl-containing aqueous solution at 40 ℃. The cmc value is indicated by the arrow.

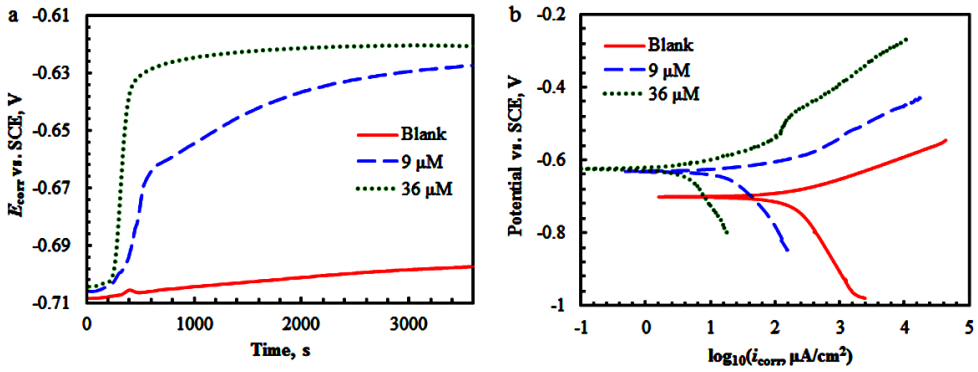

Fig. 3.3 Electrochemical measurement results: (a) variation of open circuit potential E_{corr} with time (b) potentiodynamic scans of X65 steel electrode in CO_2-saturated aqueous solution containing mixed BAC surfactants in Testing System II with total concentrations of 0, 9, and 36 μM.

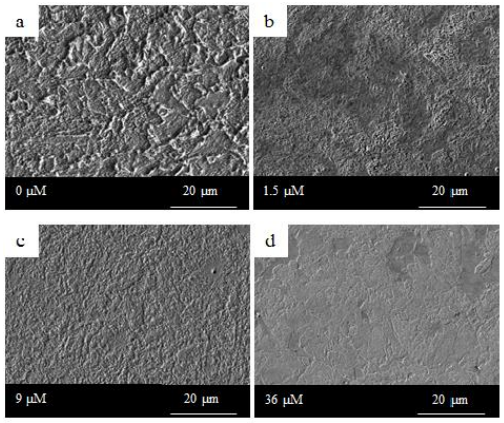

Fig. 3.4 SEM images of surface tomography with corrosion products of X65 steel electrode immersed in CO_2-saturated aqueous solution containing equal-molar mixed BAC surfactants in Testing System II with total concentrations of (a) 0, (b) 1.5, (c) 9, and (d) 36 μM.

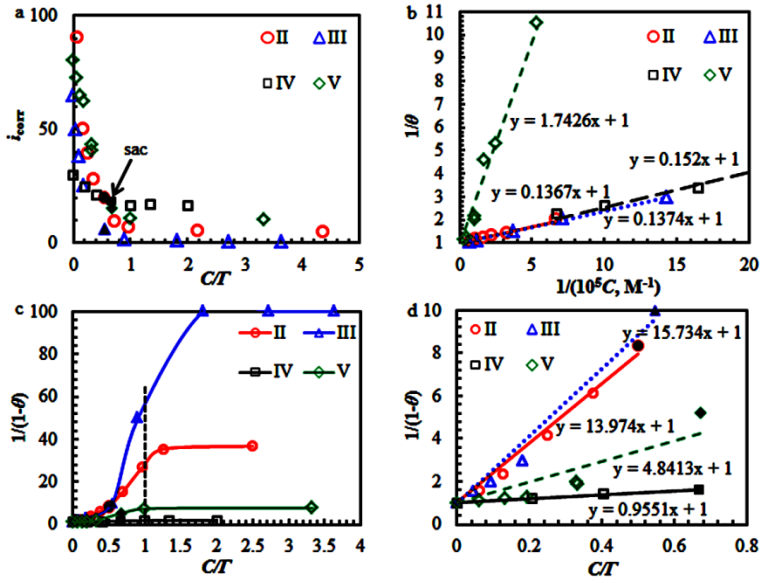

Fig. 3.5 Adsorption isotherms for various testing systems: (a) corrosion current density as a function of C/Γ (b) Langmuir adsorption model ($C<\Gamma$) (c) modified Langmuir adsorption model over the entire concentration range of surfactants (d) modified Langmuir adsorption model with surfactant concentration up to sac for different testing systems. Considering the surfactants in Testing Systems I and II are homologous, Testing System II is used for model derivation. Solid-symbols represent the sac; the intersections of solid-curves and dashed-lines in (c) represent cmc. Experimental data of Testing systems III, IV, and V is cited from references [21,22,28,29].

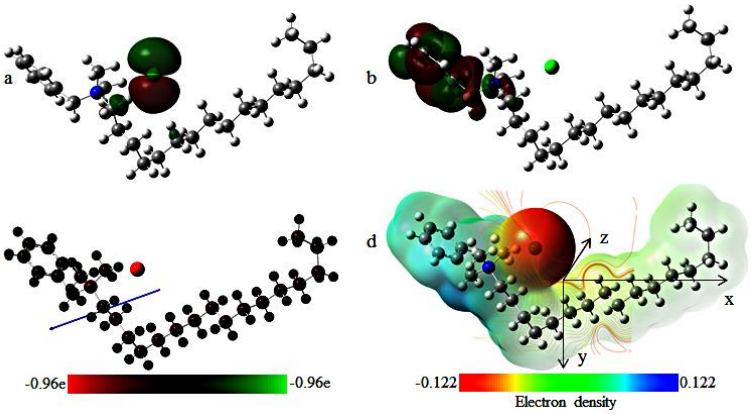

Fig. 3.6 Molecular orbitals (a) HOMO, (b) LUMO, electrostatic properties (c) Milliken charge distribution with displayed dipole, and (d) the contour (two-dimensional projection) and mapped isosurface (three-dimensional visualization) representation of electrostatic potential of C_{16}BzCl. The normal direction of two-dimensional projection is (001). The x, y, and z axis are indicated in the figure. e is positive elementary charge.

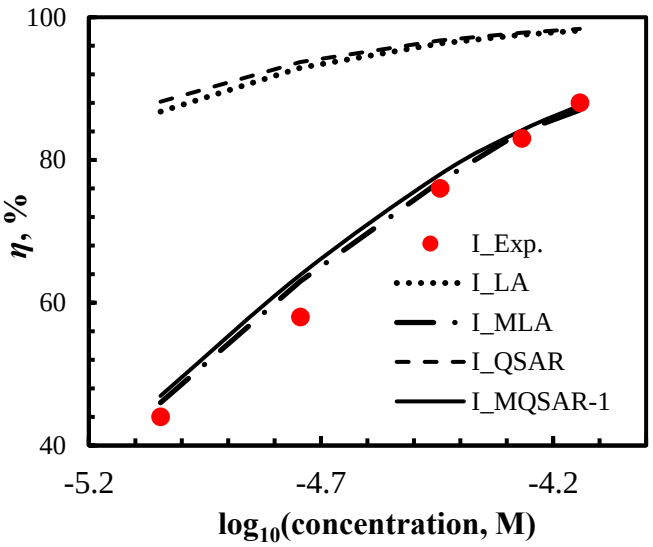

Fig. 3.7 Comparison of MLA and LA, and MQSAR-1 and QSAR based on the experimental corrosion inhibition data of X65 steel electrode in CO_2-saturated 0.171 M NaCl aqueous solution containing various concentrations (<sac) of mixed BAC surfactants in Testing System I.

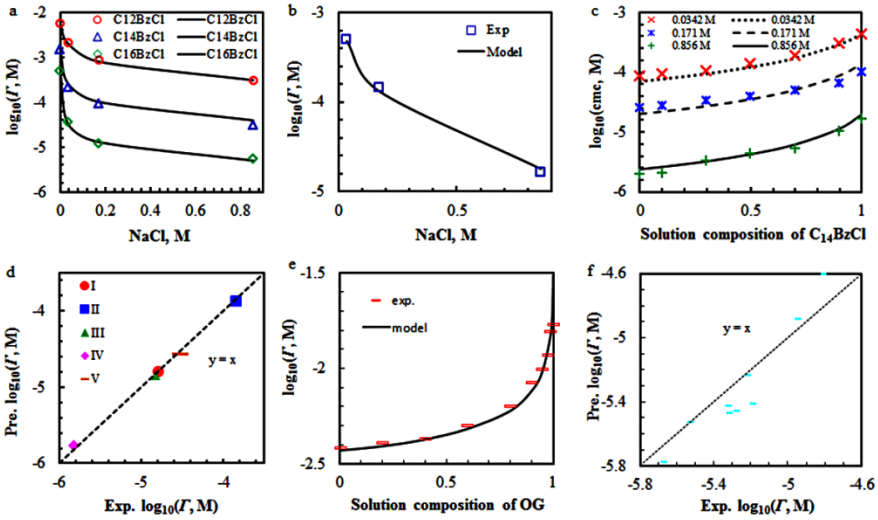

Fig. 3.8 Comparison between predicted and experimental cmc: (a) cmc of pure cationic BAC surfactants (C_nBzCl) as a function of NaCl concentration in solution at T = 40 ℃; (b) cmc of ternary mixed BAC surfactants ($C_{12}BzCl/C_{14}BzCl/C_{16}BzCl$=0.70/0.25/0.05) as a function of NaCl concentration in solution at T = 40 ℃; (c) cmc of ternary mixed BAC surfactants as a function of bulk mixed molar fraction of $C_{14}BzCl$ at NaCl concentrations of 0.0342 M, 0.171 M, or 0.856 M at T = 40 ℃; $C_{12}BzCl$ & $C_{16}BzCl$ are equal-molar mixed; (d) comparison of predicted (Pre.) and experimental (Exp.) cmc of discussed surfactants in various testing systems in Table 3.1; (e) cmc of binary mixed anionic and nonionic surfactants (SDS and OG) as a function of mixed bulk solution composition of OG with 20 mM NaCl at T = 25 ℃; (f) Pre. cmc vs. Exp. cmc of ternary mixed cationic, cationic, and nonionic surfactants ($C_{16}BzCl$, $C_{16}TAB$, and $C_{16}E_{20}$) at various mixed molar ratios with 30 mM NaCl in solution at T = 25 ℃. For Figs. 3.8(a, b, c, and e) symbols represent experimental data; lines represent model predicted data. Experimental data of testing systems III, IV, and V are cited from references [21,52-56].

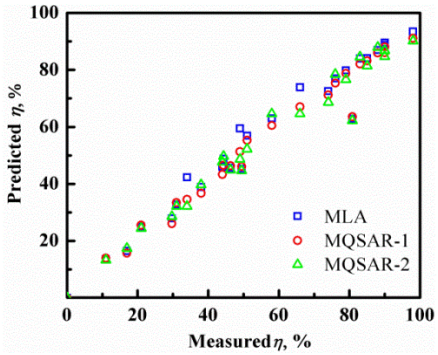

Fig. 3.9 Comparison (90 data points in total) of model predicted inhibition efficiency and experimental inhibition efficiency of pure surfactant and mixed surfactants in various testing systems listed in Table 3.1. The associated corrosion inhibition efficiency is summarized in Table 3.4. Experimental data of Testing systems III, IV, and V are cited from references [21,22,28,29].

3.7 References

[1] M. Finšgar, J. Jackson, *Corrosion Sci.* 86 (2014) 17.

[2] A. Popova, M. Christov, A. Vasilev, Corrosion Sci. 94 (2015) 70.

[3] K.S. George, S. Nešić, Corrosion 63 (2007) 178.

[4] Y. Zhou, Y. Zuo, Electrochim. Acta 154 (2015) 157.

[5] G.A. Zhang, Y.F. Cheng, Corrosion Sci. 51 (2009) 87.

[6] B.R. Linter and G.T. Burstein, Corrosion Sci. 41 (1999) 117.

[7] N. G. Thompson, Y. Mark, D. Daniel, Corrosion Rev. 25 (2007) 247.

[8] Z. Xia, K.C. Chou, Z.S. Smialowska, Corrosion 45 (1989) 636.

[9] M.B. Kermani, A. Morshed, Corrosion 59 (2003) 659.

[10] P. Bai, H. Zhao, S. Zheng, C. Chen, Corrosion Sci. 93 (2015) 109.

[11] M.Z.A. Rafiquee, S. Khan, N. Saxena, M.A. Quraishi, J. Appl. Electrochem. 39 (2009) 1409.

[12] M.A. Quraishi, A. Singh, V.K. Singh, D.K. Yadav, A.K. Singh, Mater. Chem. Phys 122 (2010) 114.

[13] J.O. Bockris, A.K.N. Reddy, Modern Electrochemistry, 2nd ed., Kluwer Academic/Plenum Publishers, New York, 2000.

[14] A. Kokalj, S. Peljhan, M. Finsgar, I. Milosev, J. Am. Chem. Soc. 132 (2010) 16657.

[15] R. M. Hill, Mixed Surfactant systems, Marcel Dekker, New York, 1993.

[16] M. J. Rosen, Surfactants and Interfacial Phenomena, 3rd ed., John Wiley, New Jersey, 2004.

[17] Sonu, A. K. Tiwari, S. K. Saha, Ind. Eng. Chem. Res. 52 (2013) 5895.

[18] S. Nešić, Corrosion Sci. 49 (2007) 4308.

[19] I. B. Obot, D. D. Macdonald, Z. M. Gasem, Corrosion Sci. (2015).

[20] G. Gece, Corrosion Sci. 50 (2008) 2981.

[21] M. L. Free, W. Wang, D. Y. Ryu, Corrosion 60 (2004) 837.

[22] W. Wang, M. L. Free, Corrosion Sci. 46 (2004) 2601.

[23] M. L. Free, Corrosion Sci. 46 (2004) 3101.

[24] M. L. Free, Corrosion Sci. 44 (2002) 2865.

[25] Y. Zhu, M. L. Free, G. Yi, Corrosion Sci. 98 (2015) 417.

[26] M. A. Migahed, M. A. Hegazy, A. M. Al-Sabagh, Corrosion Sci. 61 (2012) 10.

[27] Y. Zhu, M. L. Free, ECS Trans. 66 (2015) 53.

[28] M. P. Desimone, G. Gordillo, S. N. Simison, Corrosion Sci. 53 (2011) 4033.

[29] M. P. Desimone, G. Grudmeier, G. Gordillo, S. N. Simison, Electrochim. Acta 56 (2011) 2990.

[30] W. Durnie, R. De Marco, A. Jefferson, B. Kinsella, J. Electrochem. Soc. 146 (1999) 1751.

[31] M. Gholami, I. Danaee, M. H. Maddahy, M. RashvandAvei, Ind. Eng. Chem. Res., 52 (2013) 14875.

[32] L. Lukovits, E. Kalman, F. Zucchi, Corrosion 57 (2001) 3.

[33] K. F. Khaled, Appl. Surf. Sci. 252 (2006) 4120.

[34] M. L., Corrin, W. D. Harkins, J. Am. Chem. Soc. 69 (1947) 683.

[35] L. Moreira, A. Firoozabadi, Langmuir 26 (2010) 15177.

[36] A. Goldsipe, D. Blankschtein, Langmuir 21 (2005) 9850.

[37] M. Knag, K. Bilkova, E. Gulbrandsen, P. Carlsen, J. Sjoblom, Corrosion Sci. 48 (2006) 2592.

[38] O. L. Riggs Jr., Corrosion Inhibitors, 2nd ed., C. C. Nathan, Editor, Houston, TX, 1973.

[39] D. A. Jones, Principles, Prevention of Corrosion, Macmillan Publishing Company, 1991.

[40] V. Jovancicevic, S. Ramachandran, P. Prince, Corrosion 55 (1999) 309.

[41] Y. R. Dong, M. L. Free, J. Coll. Interf. Sci. 264 (2003) 402.

[42] Y. R. Dong, M. L. Free, Colloids Surf. A: Physicochem. Eng. Asp. 226 (2003) 17.

[43] M. Christov, A. Popova, Corrosion Sci. 46 (2004) 1613.

[44] P. C. Okafor, Y. Zheng, Corrosion Sci. 51 (2009) 850.

[45] Shi, R. Zhang, C. Minot, K. Hermann, M. A. Van Hove, W. Wang, N. Lin, J. Phys. Chem. Lett. 1 (2010) 2974.

[46] J. N. Israelachvili, Intermolecular and Surface Forces, 3rd ed., Academic Press, San Diego, 2011.

[47] D. A. Winkler, M. Breedon, A. E. Hughes, F. R. Burden, A. S. Barnard, T. G. Harvey, I. Cole, Green Chem. 16 (2014) 3349.

[48] I.B. Obot, N.O. Obi-Egbedi, Corrosion Sci. 52 (2010) 198.

[49] R. Yıldız, Corrosion Sci. 90 (2015) 544.

[50] L. Li, X. Zhang, S. Gong, H. Zhao, Y. Bai, Q. Li, L. Ji, Corrosion Sci. (2015).

[51] M. Sahin, G. Gece, F. Karci, S. Bilgc, J. Appl. Electrochem. 38 (2008) 809.

[52] K. Shinoda, J. Phys. Chem. 58 (1954) 541.

[53] K. Shinoda, T. Nakagawa, Colloidal Surfactants, Academic Press, New York, 1963.

[54] K. Kameyama, A. Muroya, and T. Takagi, J. Colloid Interface Sci. 196 (1997) 48.

[55] H. P. Moises de Oliveira, M. H. Gehlen, Langmuir 18 (2002) 3792.

[56] A. A. Dar, G. M. Rather, S. Ghosh, A. R. Das, J. Colloid Interface Sci. 322 (2008) 572.

[57] S. Ramachandran, B. Tsai, M. Blanco, H. Chen, Y. Tang, W. A. Goddard, Langmuir 12 (1996) 6419.

[58] H. Zhao, X. Zhang, L. Ji, H. Hu, Q. Li, Corrosion Sci. 83 (2014) 261.

CHAPTER 4

EFFECTS OF MICELLIZATION AND AGGREGATION*

4.1 Introduction

As an important component of the economy, the oil and gas industry has received considerable attention from researchers because oil mining and transportation have become increasingly expensive due to equipment (metallic pipelines) damage caused by corrosion, especially CO2 corrosion [1-5]. The concerns have led to great interest in industry and academia to control corrosion of metallic pipelines in various oilfields around the world. Among the existing corrosion control methods, surfactant inhibitors have widely been used for corrosion inhibition of pipelines in water-oil-steel pipe (WOS) environments [1,2]. Particularly, surfactant mixtures are well known due to the superior physicochemical properties and capabilities in efficient solubilization, adsorption, and suspension etc. [1,2,6-8]. More surface-active and expensive surfactants are often mixed with less surface-active and cheaper surfactants to reduce cost [1,2,9]. The use of surfactant inhibitors for corrosion inhibition is based on the fact that surfactant molecules adsorb on and cover metal surface and slow down one or more electrochemical reactions associated with metal dissolution and thus inhibit corrosion [1,2,9,10]. The adsorption process, however, is highly affected by the other main processes upon the

* Paper published in Ind. Eng. Chem. Res. 54 (2015) 9052-9056 and Colloid. Sur. A: Physical. Eng. Aspects (2015) doi: 10.1016/j.colsurfa.2015.11.005.

addition of surfactants to WOS environments, such as micellization and water/oil partitioning [10] which tend to deplete monomeric surfactants available for the adsorption and effective coverage on metal surface. Therefore, it is necessary to understand micellization process for a systematic evaluation of corrosion inhibition using various pure and mixed surfactants in WOS environments [1,2,10].

More recently, it has been reported that the cmc has been successfully coupled with mechanistic evaluation approaches which are modified Langmuir adsorption (MLA) and modified quantitative structure activity relation (MQSAR) to predict corrosion inhibition efficiency η (%) [1,2,9]. The MLA and MQSAR are briefly presented below. Details of derivation, validation, and application have been reported elsewhere [1,2,9].

MLA model

$$\eta\,(\%) = \left(1 - \frac{1}{1+K'\frac{C}{\Gamma^w}}\right) \times 100 \tag{4.1}$$

MQSAR model

$$\eta\,(\%) = \frac{(\vec{A}'\cdot\vec{Q}+\bar{B}')C}{\Gamma^w+(\vec{A}'\cdot\vec{Q}+\bar{B}')C} \times 100 \tag{4.2}$$

where C is the concentration of surfactants in the bulk solution, Γ^w is the aqueous cmc of surfactant mixture, K' is equal to the adsorption constant K_{ad} multiplied by Γ^w, and η is corrosion inhibition efficiency. $\vec{A}'$ is a modified vector of regression coefficients, and $\bar{B}'$ is a modified regression constant. $\vec{Q}$ is a vector of quantum chemical descriptors for a particular surfactant. For surfactant mixtures, the quantum chemical descriptors are weight-based average values. Note that for pure surfactant, Γ^w is replaced by the aqueous cmc of pure surfactant i, Γ_i^w.

Therefore, the present work is thus focused on the micellization properties of

surfactants in salt solutions. One of the challenges in the study of micellization comes from the effects of specific ions and added salts. Different counterions usually present different effects on the critical micelle concentration (cmc), micelle shape, micelle growth, micelle size and distribution, mixed micelle composition (for mixed surfactants), and phase separation [11-18]. It is reported that the counterion effect on the aggregation properties of cationic surfactants is usually stronger than that of anionic surfactants [15,16]. In addition, the cmc depression due to counterion effect usually follows the Hofmeister series: $OH^- < F^- < Cl^- < Br^- < NO_3^- < ClO_3^- < I^-$ < benzoate$^-$ < salicylate$^-$ for cationic surfactants; and $Li^+ < Na^+ < K^+ < C_s^+$ for anionic surfactants [15,16]. The specific counterion effects on micelle size and sphere-to-rod transition is usually in the same order as shown previously for cmc [16]. The counterion binding mechanism is not clear and has been a controversial issue [19].

At low salt concentration the coion effect on cmc, aggregation number, and sphere-to-rod transition is negligible [20,21]. However, as salt concentration increases, the coion effect becomes increasingly noticeable [20,21]. Particularly at relatively high salt concentration, the coion effect on aggregation properties becomes dramatic, as discussed in the text below.

The authors are not aware of a completely established theory or model to adequately describe the effects of ion specificity and binding mechanism on surfactant aggregation properties despite extensive progress in theoretical and experimental work.

In the approach proposed by Nagarajan and Ruckenstein [22] based on the work from Evans and Ninham [23], Nagarajan [22] successfully incorporates a parameter which is the distance between the surface of a hydrophobic/micellar core (the micellar core is the

micelle with hydrophobic chain and without headgroup) and the center of counterions. This parameter, according to Nagarajan [23], is dependent on headgroup size, hydrated counterion size, and the distance from the counterion to the charge of ionic surfactant. However, Nagarajan does not provide more details about these dependencies.

The molecular thermodynamic theory (MTT) [12,24-26] provides a great step in progress toward the understanding and modeling of counterion specificity on ionic surfactant micellization. In the theory, the counterion is assumed to bind to the micelle surface in terms of fractional coverage between 0 and 1, and it affects the magnitude of various free energy contributions to the micellization process. The predicted cmc as well as some other properties such as aggregation number and mixed micelle composition are in relatively good agreement with experiment. However, the theory does not clarify the specificity of headgroup-counterion pair interactions.

More recently, Moreira and Firoozabadi (MF) [20] improved to some extent the existing MTT [12,22,24-27] by the introduction of solvent-shared specific counterion-headgroup pairs. However, the MF model only applies to the spherical and globular micelles in a very narrow range of added salt concentration and does not take into account the sphere-to-rod transition and growth of micelles to long cylinders.

Koroleva and Victorov (KV) [28] developed a model that introduces the specific headgroup-counterion pair in which a geometric parameter, called the distance of the closest approach of the ion to the core, is added to take into account hydration effects. Moreover, they adopted a modified Poisson-Boltzmann equation (PB) [29] that incorporates the dispersion interactions between ions and micelles to differentiate the polarizability of different ions, which has also been considered by recently reported work

[30]. The predicted cmc, aggregation number, and sphere-to-rod transition are in reasonably good agreement with experiment. However, the incorporation of dispersion interaction between counterion and micelle in the modified PB equation does not adequately reflect the effect of counterion specificity on cmc [20].

In the present work, an alternative cmc model is developed which incorporates the surfactant activity, counterion activity, and ion effects on surfactant aggregation. The activity coefficient of ions is evaluated using Pitzer's method [31,32] or Davies [33] equation depending on the salt concentration. The activity coefficient of surfactants is evaluated from the Setchenov equation [34]. Similar to the MF model [25] and the KV model [27], the specificity of headgroup-counterion pair is considered to reflect hydration effects and the degree of counterions binding to micelles. The counterion binding coefficient is initially set as a variable and finds its optimal value by minimizing micellization free energy. The effect of coion is evaluated from salt-dependent factors, including the Setchenov coefficient k_s [28,34], the dielectric decrement of salt δ_s [25], and the correlation between the change of surface tension and the change of salt concentration in aqueous solution, $d\sigma_o/dC_s$ (σ_o is surface tension and C_s is salt concentration) [25] (symbol definition can be found in Appendix A.1.).

For validation, the developed model has been applied to various pure (anionic & cationic), binary (anionic/nonionic, & cationic/nonionic), and ternary (cationic/nonionic/nonionic) mixed surfactants in aqueous solutions containing salt concentrations up to 3 M. The predicted cmc, aggregation number, counterion binding coefficient, and sphere-to-rod transitions are in good agreement with reported values.

The article is organized as follows: the brief description and derivation of the cmc model (details in Appendix A.3); experimental procedures; application of cmc model to various pure, binary, and ternary mixed surfactants, comparison of cmc model prediction to experimental data and to other existing models, and associated discussion; integration of the cmc model with MLA and MQSAR for corrosion inhibition prediction; and conclusions from the present work.

4.2 cmc model description

Assuming the monomeric surfactant m_i (i=1, 2, or 3...) is completely dissociated in aqueous solution containing counterion m_j (j=1, 2, or 3…) but in the micelle form the surfactant is associated to some extent with counterions, therefore, the surfactant micellization is described by the following process [2,35,36]

$$N\sum_i \alpha_i m_i^{z_i} + N\sum_j \delta_j m_j^{z_j} \leftrightarrow M_N^{N(\sum_i \alpha_i z_i + \sum_j \delta_j z_j)} \quad 4.3$$

where α_i is the composition of surfactant i in the micelle, M_N, which has an aggregation number N, micelle composition α_i, and a counterion binding coefficient δ_j [12]. (For simplicity, only N is shown in the subscript.) For micelles of pure surfactant, $\alpha_i = 1$; for mixed micelles, $0 < \alpha_i < 1$. z_i and z_j are the valences of ionic surfactant i in dissociated form and counterion j. For nonionic surfactant i, $z_i = 0$ and $\delta_j = 0$.

The aqueous cmc of pure surfactant i (Γ_i^w) or of surfactant mixture (Γ^w) is calculated using the equation below (Γ^w is used for illustration) [2]

$$\Gamma^w = (C_{mw} + C_s)\exp^{\left(\frac{1}{kT}\Delta\mu_m^o\right)} \quad 4.4$$

where k is Boltzmann constant, T is temperature, and $\Delta\mu_m^o$ is micellization free energy which is calculated from several contributing thermodynamic terms.

$$\Delta\mu_{\mathrm{m}}^{\mathrm{o}} = \Delta\mu_{\mathrm{trt}}^{\mathrm{o}} + \Delta\mu_{\mathrm{int}}^{\mathrm{o}} + \Delta\mu_{\mathrm{pack}}^{\mathrm{o}} + \Delta\mu_{\mathrm{st}}^{\mathrm{o}} + \Delta\mu_{\mathrm{ent}}^{\mathrm{o}} + \Delta\mu_{\mathrm{elec}}^{\mathrm{o}} + \Delta\mu_{\mathrm{act}}^{\mathrm{o}} \quad 4.5$$

The first three terms on the right side of Eq. (4.5) are associated with the packing and interactions of hydrocarbon tails and the formation of hydrophobic micellar core: $\Delta\mu_{\mathrm{trt}}^{\mathrm{o}}$, $\Delta\mu_{\mathrm{int}}^{\mathrm{o}}$, and $\Delta\mu_{\mathrm{pack}}^{\mathrm{o}}$ represent free energy contributions from hydrocarbon transfer from water into micelle, formation of micellar core-water interface, and hydrocarbon tail packing in micelle, respectively. The next three terms are associated with surfactant headgroups and counterions in the micelle-water interfacial region: $\Delta\mu_{\mathrm{st}}^{\mathrm{o}}$, $\Delta\mu_{\mathrm{ent}}^{\mathrm{o}}$, and $\Delta\mu_{\mathrm{elec}}^{\mathrm{o}}$ represent surfactant headgroup steric interactions, headgroup-counterion mixing, and electrostatic interactions, respectively [2,38-41]. The last term $\Delta\mu_{\mathrm{act}}^{\mathrm{o}}$ represents the contribution from surfactant activity and counterion activity in the bulk solution [2]. Details of model derivation and associated calculation of energy terms and parameters are provided in Appendix A.3.

4.3 Experimental procedures

The homologous cationic benzalkonium chlorides (BAC) surfactants, including benzyl dimethyl dodecyl ammonium chloride (C_{12}BzCl), benzyl dimethyl tetradecyl ammonium chloride (C_{14}BzCl), and benzyl dimethyl hexadecyl ammonium chloride (C_{16}BzCl), were supplied by Sigma-Aldrich Co. LLC with assay values higher than 99%. The molecular structure of the surfactants are optimized and quantum parameters calculated using Gasussian09 simulation package with the method of B3LYP and the basis set of 6-311G(d, p) based on DFT. The test samples for surface tension measurements were prepared by sequential dilution of concentrated aqueous solutions of surfactants using double deionized water, made through a water purification system

(Simplicity® UV made by EMD Millipore). The stock solution was prepared at a total surfactant concentration of 25 mM for electrochemical measurements using deionized water. A piece of X65 steel, purchased from Metal Samples®, was used as the working electrode in electrochemical measurements with a surface area of 0.196 cm^2. The composition (wt %) is C 0.06%, Mn 1.33%, P 0.007%, S 0.005%, Si 0.30%, Cu 0.30%, Ni 0.10%, V 0.022%, Cb 0.046%, Al 0.019%, Cr 0.05%, Mo 0.03%, Ti 0.017%, Ca 0.0033%, and Fe (balance).

The experimental procedures for cmc measurement and electrochemical tests, including polarization resistance, potentiodynamic scan, and electrochemical impedance spectroscopy, can be found elsewhere [1,2]. The quantum calculation using Gaussian09 follows the method reported in previous work [2]. Chemical structure of various surfactant molecules discussed in the present work is given in Fig. 4.1

4.4 cmc model validation and discussion

4.4.1 Activity contribution

To illustrate the effect of surfactant activity on the micellization free energy and thus on cmc prediction, the variation of activity coefficient and the corresponding free energy contribution for pure surfactant sodium dodecyl sulfate (SDS or NaDS), polyoxythylene ether ($C_{14}E_6$), or benzalkonium chloride (C_{16}BzCl), as a function of added NaCl concentration, are plotted in Fig. 4.2. As can be seen from the plot, both activity coefficient and $\Delta\mu_{\mathrm{act}}^{\mathrm{o}}$ experience rapid changes as NaCl concentration increases, especially when salt is concentrated over about 0.5 M. Even for the salt concentration lower than 0.5 M, the activity coefficient effect cannot be neglected. For example, for

C_{16}BzCl at NaCl concentration of 0.1 M, the calculated micellization free energy is -10.04kT with the contribution of $\Delta\mu_{\mathrm{act}}^{\mathrm{o}}$ = 0.22kT, which is only 2.1% of the micellization free energy. Without the contribution from activity, the predicted cmc would shift by 25%. Slight deviation in the free energy will cause relatively significant change in the predicted aggregation properties.

4.4.2 Pure anionic surfactant

The comparison of model predicted (lines) and experimental (symbols) aggregation properties, including cmc and counterion binding coefficient δ of alkyl sulfates, are presented in Fig. 4.3. The predicted cmc of alkyl sulfate (XC_nS) with different chain length or with different alkali metals as counterions agrees well with experimental data at low to medium salt XCl concentration (~1M). Slight deviation is observed when the salt concentration is higher than 1 M, as shown in Figs. 4.2(a, c). In Figs. 4.2(b, d) only predicted counterion binding coefficients are presented due to limited experimental data. The counterion binding coefficient increases with the increase in salt concentration and approaches to unity, which means that the micelle is fully associated with counterion. A transition is manifested as salt concentration increases, which corresponds to the sphere-to-rod transition of micellization, as indicated by the arrow for $NaC_{10}S$, for example. It is found the transition is also indicated by value of optimized micellar core minor radius l_c, which gets to maximum at the sphere-to-rod transition. In addition, the degree of counterion binding of homologous surfactants increases as chain length increases. The Hofmeister series, which is $Li^+ < Na^+ < K^+ < Cs^+$ for anionic surfactants [15-16], is correctly reflected by the effect of counterions on the depression of cmc and on the

increment of counterion binding coefficient of alkali metal alkyl sulfates (Figs. 4.2(c, d)).

4.4.3 Pure cationic surfactant

The model is also applied to pure alkyltrimethylammonium surfactant alkyltrimethylammonium bromide (C_nTABr) in solution with added salt (NaBr, NaCl, or KCl) to evaluate chain length effects, counterion effects, and coion effects on aggregation properties, as shown in Fig. 4.4. The cmc (Fig. 4.4(a)) and sphere-to-rod transition threshold (Fig. 4.4(b)) decreases as chain length increases whereas N_w (Fig. 4.4(b)) increases as chain length increases. The predicted cmc for all surfactants in Fig. 4.4 match very well with experimental data except that a slight deviation appears for C_{12}TABr with added NaBr above 1 M. An excellent agreement is observed between predicted and experimental N_w. The sphere-to-rod transition is manifested by the sharp change of aggregation number, counterion binding coefficient, and core minor radius l_c (not shown here) as a function of salt concentration. The comparison of model predicted transition (salt concentration threshold) and deduced transition from experiment is summarized in Table 4.1. For C_{16}TABr with added salt KBr for example, the predicted threshold is 0.08 M and the experimental threshold is 0.1 M [53-55].

The Hofmeister series, which indicates $Cl^- < Br^-$ for cationic surfactant aggregation, is reflected by the effect of counterion on the depression of cmc, and on the increment of N_w by comparing C_{16}TABr and C_{16}TACl (see Fig. 4.4). The effect of coion is examined by adding different salts (NaBr and KBr) to the aqueous solutions containing C_{16}TABr: the coion effect on cmc and on N_w is minor at low salt concentration, whereas with increasing salt concentration increases, the coion effect becomes increasingly noticeable,

as shown in Fig. 4.4.

4.4.4 Binary anionic/nonionic surfactant mixture

The developed model is applied to anionic/nonionic surfactant mixtures of SDS and octylglucoside (OG) in the presence of NaCl in aqueous solution. The total concentration of mixed surfactants in the model is set as 25 mM with various mixed molar ratios. The NaCl concentration (20 mM) and temperature (25 ℃) follow the experimental conditions [56,57]. The predicted cmc and the experimental cmc as a function of bulk solution composition of SDS are presented in Fig. 4.5(a). The agreement between predicted and experimental cmc for various compositions of SDS is excellent.

Fig. 4.5(b) presents the aggregation number as a function of micelle SDS composition. Note that the experimental aggregation number was obtained by a time-resolved fluorescence quenching method. The quencher-based aggregation number N_Q should be equal to the weight-based aggregation number N_w [58]. The aggregation number gradually increases as micelle SDS composition decreases and experiences a sharp transition at around 40% SDS in micelle. This sphere-to-rod transition is also manifested by the counterion binding coefficient change. The aggregation number at high micelle SDS composition is slightly underestimated due to the preferred form of globular micelle, instead of spherical micelle. However, as SDS composition in micelle increases more, the micelle is associated with more counterions and more charges, and the aggregation number decreases until nearly spherical micelles form, which is indicated by the better agreement between prediction and experiment at 100% SDS micelle composition in Fig. 4.5(b).

A slight underestimation of counterion binding coefficient as a function of micelle SDS composition from the present model, compared to the experimentally deduced counterion binding coefficient based on Corrin-Harkins relation [59], is observed in Fig. 4.5(c). This deviation is probably due to the underestimation of the effects from two free energy contribution terms [25]: hydrocarbon tail transfer free energy and micelle core-water interface formation free energy. A sharp increase is observed when micelle SDS composition is above 40%. This phenomenon is most probably dominated by the electrostatic free energy change and counterion entropy change with increased binding.

4.4.5 Binary cationic/nonionic surfactant mixture

For further validation, the model was applied to binary cationic/nonionic surfactant mixtures containing C_{16}BzCl and polyoxythylene cetyl ether ($C_{16}E_{20}$) with added NaCl. The total concentration of mixed surfactants in the model is set at the cmc with various mixed molar ratios of C_{16}BzCl and $C_{16}E_{20}$. The NaCl concentration (30 mM) and temperature (25 ℃) follow the experimental conditions [60]. Fig. 4.6(a) presents the predicted cmc from various models and from experiment as a function of solution composition of C_{16}BzCl. The mixed cmc increases as the cationic surfactant (C_{16}BzCl) concentration increases. This is expected due to the weaker hydrophobicity of ionic surfactant compared to nonionic surfactant given the same hydrocarbon tail length. The Clint model [61] overestimates the cmc whereas the present model and the D.B. model [38,39] give a better evaluation with experimental data evenly distributed along the prediction curves, as shown in Fig. 4.6(a). The aggregation number is almost constant and no sphere-to-rod transition is observed in the plot of aggregation number vs. micelle

C_{16}BzCl composition in Fig. 4.6(b). The preferred micelle shape is inferred to be spheres. The aggregation number from the present model is overestimated and the reason is not clear yet. However, with one empirical formula [44] used to estimate aggregation number of spherical micelles

$$N_{\mathrm{sph}} \approx 0.4 L_{\mathrm{i}}^2 \tag{4.6}$$

the aggregation number is around 102 which is in much better agreement with the model prediction rather than experimental results.

4.4.6 Ternary surfactant mixture

The model is further applied to ternary cationic/cationic/nonionic surfactant mixtures of C_{16}TABr + C_{16}BzCl + $C_{16}E_{20}$ with added NaCl in solution. The NaCl concentration (30 mM) and temperature (25 ℃) follow the experimental conditions [60]. Fig. 4.7(a) gives the comparison of predicted cmc from various models, including the Clint model [61], Rubingh and Holland (R-H) model [62,63], and the model in the present work, and experimental cmc. The present model gives the best prediction. There is an overestimation from the Clint model [61] and an underestimation from the R-H model [62,63]. The predicted aggregation number is only calculated from the present model, which gives slightly overestimated but acceptable values.

The model is further applied to ternary mixed homologous benzalkonium chloride surfactants, C_nBzCl, and ternary mixed anionic/nonionic/nonionic surfactants, SDS/dodecyl dimethylammonium oxide (DDAO)/decyl tetra ethylene oxide ($C_{10}E_4$). C_{12}BzCl and C_{16}BzCl are equal-molar mixed with varying fractions of C_{14}BzCl at different NaCl concentrations. SDS, DDAO, and $C_{10}E_4$ are mixed at various molar ratios

as reported [62]. The predicted cmc and experimental cmc match very well for mixed C_nBzCl (Fig. 4.8(a)). For mixed SDS/DDAO/$C_{10}E_4$ the predicted cmc from the three models (Rosen model [4], D.B. model [38,39], and the present model) agrees reasonably well with experimental data (Fig. 4.8(b)). The data and its comparison with the models are presented in Fig. 4.8, which demonstrate the wide applicability of the present model.

4.5 Integration of the cmc with MLA and MQSAR

It is expected that the integrated model based on the MLA and the cmc model or that the integrated model based on the MQSAR and the cmc model will be successful in the prediction of corrosion inhibition efficiency of the discussed surfactant systems. The comparison of the predicted results from the integrated model and from the experimental measurements is shown in Fig. 4.9, based on the data of corrosion inhibition and calculated quantum descriptors from all the five testing systems (I-V) reported elsewhere [2]. The prediction from both MLA and MQSAR combined with the cmc model agrees very well with experimental data for all testing systems. Note that the MQSAR predicted corrosion inhibition is based on Eq. (3.6) [2] in which the $\vec{A}'$ and $\bar{B}'$ were obtained from best-fit of the experimental data of Testing System II [2], which indicates the transferability of regression parameters and the vastly improved applicability and robustness of developed MQSAR over regular QSAR. It is interesting to find that the regression parameters in MLA and MQSAR for one class of surfactants can be transferred to other surfactants with similar head groups, which indicates the sound fundamental basis of these models beyond semi-empirical fitting. In addition, the parameters of one surfactant mixture can be used for the mixtures of similar surfactants.

$$\eta\,(\%) = \left(\frac{(-4.80E_{\mathrm{HOMO}} - 0.656E_{\mathrm{LUMO}} - 2.41\Delta E + 1.15\Delta N - 0.052\bar{\mu} - 0.071V_{\mathrm{m}} + 2.01)C}{\Gamma^{w} + (-4.80E_{\mathrm{HOMO}} - 0.656E_{\mathrm{LUMO}} - 2.41\Delta E + 1.15\Delta N - 0.052\bar{\mu} - 0.071V_{\mathrm{sm}} + 2.01)C}\right) \times 100 \quad (4.7)$$

where E_{HOMO} and E_{LUMO} are energies of highest occupied molecular orbital and lowest unoccupied molecular orbital, respectively. ΔE is the difference between E_{HOMO} and E_{LUMO}. $\bar{\mu}$ is dipole moment, ΔN is the fraction of electrons transferred from the surfactant to the metal surface, and V_{sm} is molar volume of surfactant molecule.

Various phenomena and processes associated with surfactants are considered by the cmc model, including the salt effect on surfactant aggregation/adsorption, the effect of chain length of surfactant, van der Waals interactions between surfactant molecules, steric interactions between head groups, electrostatic interactions at interfacial region of micelles, and the interactions between solvent and surfactant [2,20]. Therefore, the combination of the cmc model with MLA or MQSAR can accurately describe the adsorption phenomena of surfactants on substrate (metal electrode) and associated effects of physical and chemical properties of surfactants and solution environment. Beyond the applicability of our model for pure surfactant and mixed homologous surfactants, the more valuable part lies in its potential to evaluate the corrosion inhibition of various surfactant mixtures of different classes at various solution conditions using only one set of experimental data.

4.6 Summary

The thermodynamic and molecular-based model developed in the present work is an alternative, and in many cases, improved version of some traditional cmc prediction methods [64-67]. The preset model successfully incorporates activities of monomeric

surfactants and ions. The headgroup-counterion pair is incorporated to take into account the ion specificity and hydration effects. The effect of coion is also evaluated. Therefore, the developed model provides a potential method to evaluate ion effects on aggregation properties of various surfactants in salt solution at various concentration levels.

The model has been applied to various pure (anionic and cationic), binary (anionic/nonionic, and cationic/nonionic), and ternary (cationic/nonionic/nonionic) mixed surfactants in aqueous solution containing simple salt up to high concentration (~3 M). The predicted cmc, aggregation number, counterion binding coefficient, and sphere-to-rod transitions are in good agreement with reported values either from experiment or from various existing prediction models mentioned in the text. The Hofmeister series is observed regarding the effect of counterion on the depression of cmc.

At the combination of the above developed cmc model and previously reported MLA and MQSAR [1,2,9], the effective surface coverage and corrosion inhibition efficiency of various pure and mixed surfactant inhibitors are predicted which are in good agreement with experimental data, which can be found elsewhere [1,2,9].

However, more work is needed to further improve the present model. The use of empirical parameters makes the present model compromised in terms of molecular basis. Another challenge is the model application to aqueous solution containing more than one salt, or containing complicated salts other than 1:1 simple salts. Branched, globular, and discoid micelle/aggregates should also be incorporated to accurately evaluate the aggregation properties of surfactants.

Table 4.1 Experimental condition for different surfactant testing systems. cmc and sac are estimated values based on experiment [2]. Con. represents concentration.

Testing system	Surfactant Mixed ratio	Salt Con.(M)	T (℃)	pH	Electrode	Rotation (RPM)	cmc (μM)	sac (μM)
I	$C_{14}BzCl/C_{14}BzCl/C_{16}BzCl$ 0.70/0.25/0.05	NaCl 0.171	40	4	X65 steel	300	140	72
II	$C_{14}BzCl/C_{14}BzCl/C_{16}BzCl$ 0.33/0.33/0.33	NaCl 0.599	40	5	X65 steel	100	16.5	9
III	AAOA 1	NaCl 0.856	25	6	1018 steel	low	15	8.2
IV	CPC 1	HCl 1	31	0	1018 steel	1000	1.5	1
V	$C_{16}TAB$ 1	$Fe(NO_3)_3$ 0.03	32	---	copper	1000	30	20

Table 4.2 Quantum chemical descriptors of surfactants in aqueous phase [2]

BAC	E_{HOMO} (eV)	E_{LUMO} (eV)	ΔE (eV)	$\bar{\mu}$ (debye)	ΔN	V_{sm} (cm^3/mol)
$C_{12}BzCl$	-5.185	-1.674	-3.510	13.87	0.057	351.3
$C_{14}BzCl$	-5.186	-1.673	-3.514	13.90	0.057	343.9
$C_{16}BzCl$	-5.174	-1.669	-3.505	13.80	0.057	265.8
AAOA	-5.314	0.8754	-6.189	3.998	0.133	352.3
CPC	-5.994	-2.384	-3.609	15.74	-0.012	253.9
C16TAB	-7.178	-7.122	-0.056	6.953	-4.399	335.2

Table 4.3 Sphere-to-rod transition, characterized by salt (NaBr and KBr) concentration threshold (M), of C_nTABr

	$C_{12}TABr$	$C_{14}TABr$	$C_{16}TABr$	$C_{16}TABr$*
Experiment [49-53]	1.8	0.12	0.06	0.1
KV model [28]	1.8	0.25	0.035	----
Present model	1.6	0.26	0.065	0.08

*Added salt is KBr.

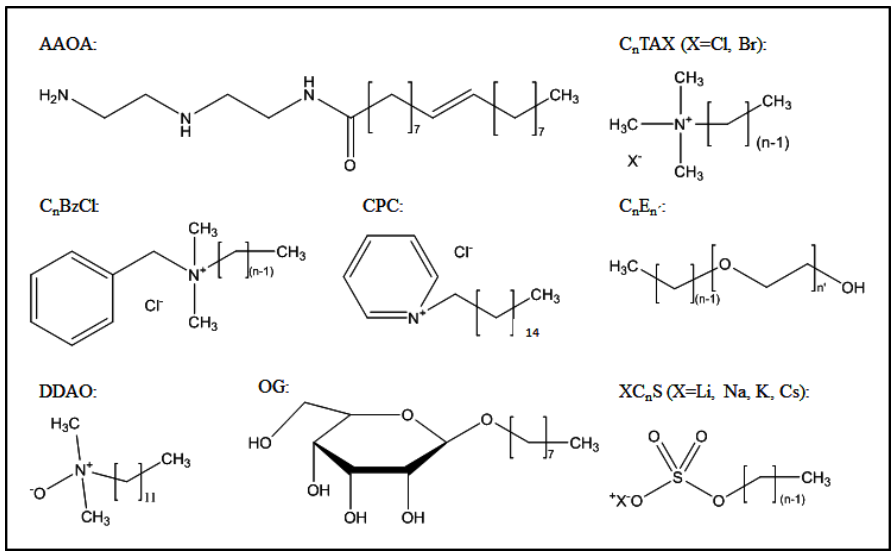

Fig. 4.1 Chemical structure of various surfactant molecules discussed in the present work. n represents the number of carbon atoms in hydrocarbon chain. n' represents the number of oxyethylene group. AAOA: N-[2-[(2-aminoethyl) amino] ethyl]-9-octadecenamide; C_nTAX (X=Cl, Br): n-alkyl trimethyl ammonium salts; C_nBzCl: n-benzalkonium chloride; $C_nE_{n'}$: polyoxythylene cetyl ether; CPC: cetylpyridinium chloride; DDAO: dodecyl dimethylammonium oxide; OG: octylglucoside; XC_nS (X=Li, Na, K, Cs): alkaline n-alkyl sulfate. For n=12, XC_nS is equivalent to XDS.

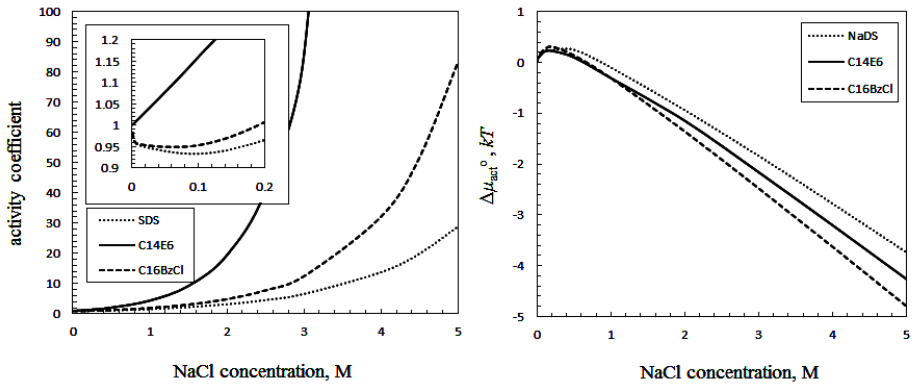

Fig. 4.2 Variation of (a) activity coefficient and (b) activity-contributing free energy of surfactants (SDS, $C_{14}E_6$, and $C_{16}BzCl$) as a function of NaCl concentration in solution.

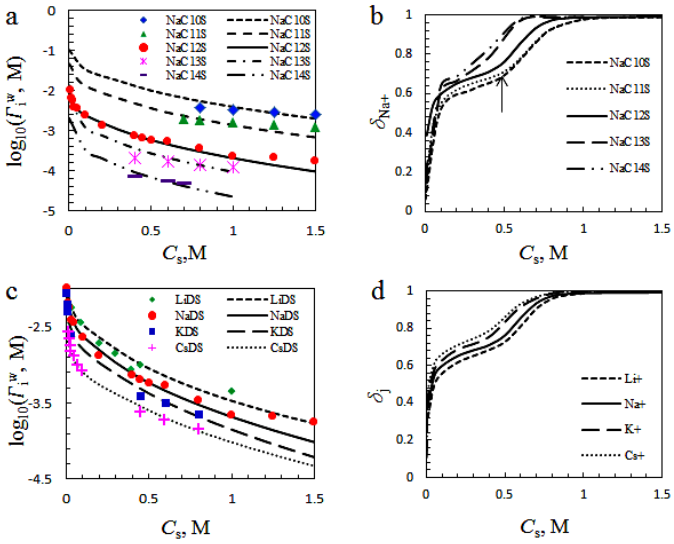

Fig. 4.3 cmc (a, c) and counterion binding coefficient (b, d) of alkyl sulfate XC_nS vs. salt XCl concentration. $X=Li^+$, Na^+, K^+, and Cs^+. Solid and dashed lines represent model prediction; symbols represent experimental data cited from references [42-47]. Inputs of model: 25-45 ℃, and total solution concentration of surfactant set at 10-100 mM depending on specific surfactant.

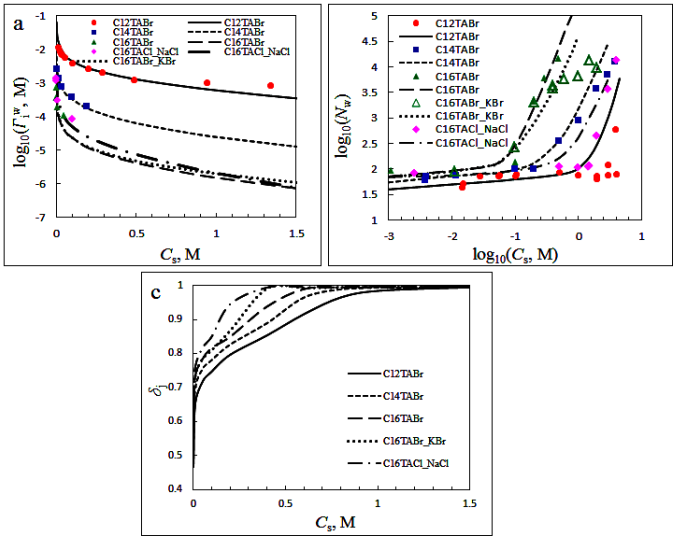

Fig. 4.4 cmc (a), weight-based aggregation number N_w (b), and counterion binding coefficient (c) of alkyltrimethylammonium bromide/chloride C_nTAX ($X=Br^-$, Cl^-) vs. salt concentration. The salt type is specified in the legend; if not specified, the default salt is NaBr. Solid and dashed lines represent model prediction; symbols represent experimental data cited from references [48-55]. Model inputs based on experimental conditions: 35 ℃, and total solution concentration of surfactant set at 10 mM for $C_{14}TABr$ and $C_{16}TABr/Cl$, and at 30 mM for $C_{12}TABr$.

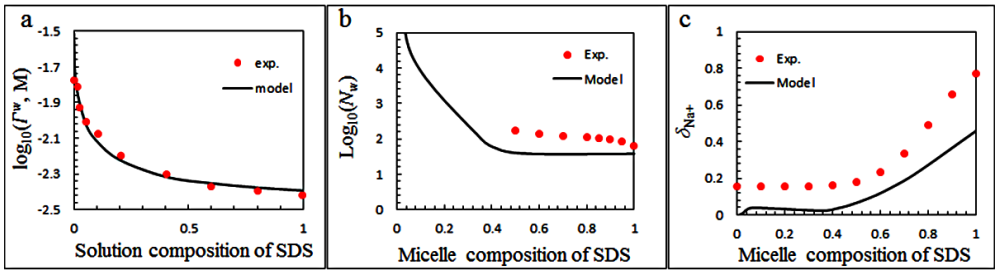

Fig. 4.5 cmc (a), aggregation number (b), and counterion binding coefficient (c) of binary mixed surfactants SDS and OG vs. solution composition (it means bulk mixed molar fraction) or micelle composition of SDS. Solid and dashed lines represent model prediction; symbols represent experimental data cited from references [56-57]. Inputs of model according to experiment conditions: 20 mM NaCl, 25 ℃, various mixed molar ratios, and total solution concentration of mixed surfactants set at 25 mM.

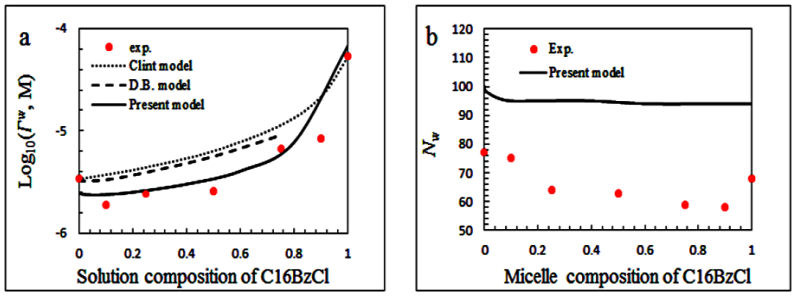

Fig. 4.6 cmc (a) and aggregation number (b) of binary mixed surfactants C_{16}BzCl and $C_{16}E_{20}$ vs. solution composition or micelle composition of C_{16}BzCl. Solid and dashed lines represent model prediction; symbols represent experimental data cited from references [60]. Inputs of model according to experiment conditions: 30 mM NaCl, 25 ℃, various mixed molar ratios, and total solution concentration of mixed surfactants set at cmc.

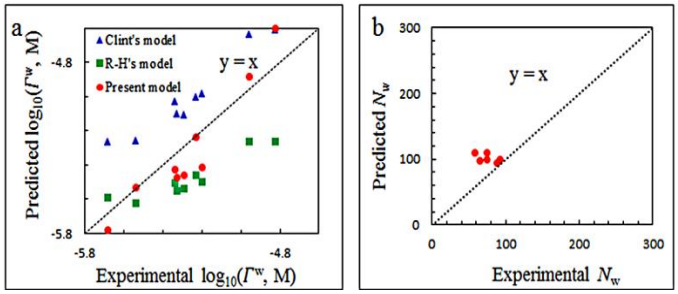

Fig. 4.7 Predicted cmc (a) and aggregation number (b) of ternary mixed surfactants C_{16}TABr, C_{16}BzCl and $C_{16}E_{20}$ vs. experimental results. In Fig. 4.7(a), solid and dashed lines represent model prediction; symbols represent experimental data cited from reference [60]. Predicted values in Fig. 4.7(b) are from our model. Inputs of model according to experiment conditions: 30 mM NaCl, 25 ℃, and total solution concentration of surfactant set at cmc.

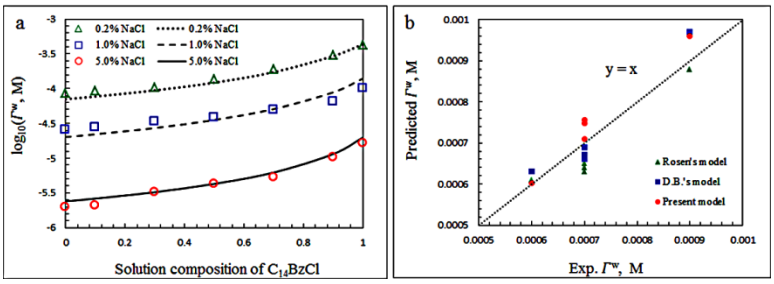

Fig. 4.8 cmc vs. solution molar composition of C_{14}BzCl in ternary mixed C_{12}BzCl, C_{14}BzCl, and C_{16}BzCl in aqueous solution, in which C_{12}BzCl & C_{16}BzCl are equal-molar mixed (a) and comparison of predicted cmc with experimental cmc of ternary mixture of DDAO, $C_{10}E_4$, and SDS with various mixed ratios (b). Solid and dashed lines represent model prediction; symbols represent experimental data. Data in Fig. 4.8(b) are cited from reference [62]. Model inputs based on experimental conditions: 40 ℃ for Fig. 4.8(a), and total solution concentration of mixed surfactants set at cmc.

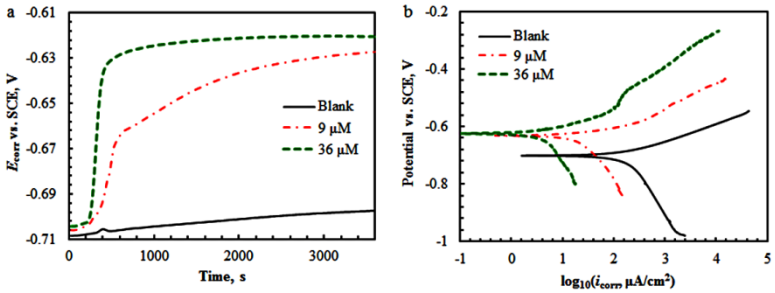

Fig. 4.9 Examples of electrochemical measurements: (a) Variation of open circuit potential E_{corr} with time (b) potentiodynamic scans of X65 steel electrode in CO_2-saturated aqueous solution containing mixed BAC surfactants in Testing System II with total concentrations of 0, 9, and 36 μM.

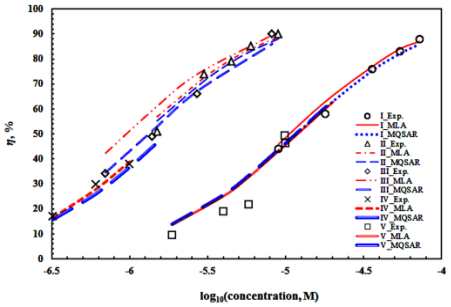

Fig. 4.10 Comparison of MLA and MQSAR model predicted inhibition efficiency and experimental inhibition efficiency as a function of concentration of pure surfactant and mixed surfactants in various testing systems. The values of the fitting parameter *K'* in MLA are 13.97, 13.97, 15.73, 0.96, and 4.84 for Testing Systems I, II, III, IV, and V, respectively.

4.7 References

[1] Y. Zhu, M. L. Free, G. Yi, Corrosion Sci. 98 (2015) 417.

[2] Y. Zhu, M. L. Free, G. Yi, J. Electrochem. Soc. 168 (2015) C582.

[3] M. Finšgar, J. Jackson, Corrosion Sci. 86 (2014) 17.

[4] D.A. López, S.N. Simison, S.R. de Sánchez, Electrochim. Acta 48 (2003) 845.

[5] I. Jevremović, M. Singer, S. Nešić, V. Mišković-Stanković, Corrosion Sci. 77 (2013) 265.

[6] L. Wolf, H. Hoffmann, K. Watanabeb, T. Okamotob, Phys. Chem. Chem. Phys. 13 (2011) 3248.

[7] M. J., Rosen, Q. Zhou, Langmuir 17 (2001) 3532.

[8] B. Kronberg, Surfactant mixtures. Curr. Opin. Colloid Interface Sci. 2 (1997) 456.

[9] Y. Zhu, M. L. Free, Electrochemical measurement and modeling of corrosion inhibition efficiency of surfactants in salt solutions, ECS Trans 66 (2015) 53.

[10] C. D. Taylor, A. Chandra, J. Vera, N. Sridhar, J. Electrochem. Soc. 162 (2015) 369.

[11] S. Ikeda, S. Hayashi, T. Imae, J. Phys. Chem. 85 (1981) 106.

[12] A. Goldsipe, D. Blankschtein, Langmuir 21 (2005) 9850.

[13] F. S. Lima, I. M. Cuccovia, D. Horinek, L. Q. Amaral, K. A. Riske, S. Schreiber, R.K. Salinas, E. L. Bastos, P. A. R. Pires, J. C. Bozelli, D. C. Favaro, A. C. B. Rodriguez, L. G. Dias, O. A. Eleoud, H. Chaimovich, Langmuir 29 (2013) 4193.

[14] F. S. Lima, F. A. Maximiano, I. M. Cuccovia, H. Chaimovich, Langmuir 27 (2011) 4319.

[15] L. Abezgauz, K. Kuperkar, P. A. Hassan, O. Ramon, P. Bahadur, D. Danino, J. Colloid Interface Sci. 342 (2010) 83-92.

[16] C. Oelschlaeger, P. Suwita, N. Willenbacher, Effect of counterion binding efficiency on structure and dynamics of wormlike micelles, Langmuir 26 (2010) 7045.

[17] N. Vlachy, B. Jagoda-Cwiklik, R. Vácha, D. Touraud, P. Jungwirth, W. Kunz, Adv. Colloid Interface Sci. 146 (2009) 42.

[18] L. J. Magid, J. Phys. Chem. B 102 (1998) 4064.

[19] R. R. Netz, D. Horinek, Annu. Rev.Phys. Chem. 63 (2012) 401.

[20] L. Moreira, A. Firoozabadi, Langmuir 26 (2010) 15177.

[21] S. V. Koroleva, A. I. Victorov, Langmuir 22 (2006) 8298.

[22] R. Nagarajan, E. Ruchenstein, Langmuir 7 (1991) 2934.

[23] R. Nagarajan, *Theory of Micelle Formation*, K. Esumi, M. Ueno, CRC Press, Boca Raton, FL, 2003.

[24] V. Srinivasan, D. Blankschtein, Langmuir 19 (2003) 9932.

[25] V. Srinivasan, D. Blankschtein, Langmuir 19 (2003) 9946.

[26] V. Srinivasan, D. Blankschtein, Langmuir 21 (2005) 1647.

[27] S. V. Koroleva, A. I. Victorov, Phys. Chem. Chem. Phys. 16 (2014) 17422.

[28] S. V. Koroleva, A. I. Victorov, Langmuir 30 (2014) 3387.

[29] M. Manciu, E. Ruckenstein, Langmuir 21 (2005) 11312.

[30] B. Lukanov, A. Firoozabadi, Langmuir 30 (2014) 6373.

[31] J. F. Zemaitis, D. M. Clark, M. Rafal, N. C. Scrivner, Handbook of Aqueous Electrolyte Thermodynamics, AlChE, New York, 1986.

[32] K. S. Pitzer, Activity Coefficients in Electrolyte Solutions, 2nd ed., CRC Press, Boca Raton, 1991.

[33] J. N. Butler, Ionic Equilibrium: Solubility and pH Calculations, Wiley, New York, 1998.

[34] R. P. Schwarzenbach, P. M. Gschwend, D. M. Imboden, Environmental Organic Chemistry, 2nd ed., John Wiley and Sons, New York, 2001.

[35] J. N. Phillips, Trans. Faraday Soc. 51 (1955) 561.

[36] M. Bourrel, R. S. Schechter, Microemulsions and Related Systems: Formation, Solvency, and Physical Properties, Marcel Dekker, Inc., New York, NY, 1988,.

[37] J. N. Israelachvili, D. J. Mitchell, B. W. Ninham, J. Chem. Soc., Faraday Trans. 2 72 (1976) 1525.

[38] A. Shiloach, D. Blankschtein, Langmuir 14 (1998) 1618.

[39] A. Shiloach, D. Blankschtein, Langmuir 14 (1988) 4105.

[40] S. Puvvada, D. Blankschtein, J. Phys. Chem. 96 (1992) 5567.

[41] C. Sarmoria, S. Puvvada, D. Blankschtein, Langmuir 8 (1992) 2690.

[42] M. F. Emerson, A. Holtzer, J. Phys. Chem. 71 (1967) 1898.

[43] S. Hayashi, S. Ikeda, J. Phys. Chem. 84 (1980) 744.

[44] P. J. Missel, N. A. Mazer, G. B. Benedek, M. C. Carey, J. Phys. Chem. 87 (1983) 1264.

[45] P. J. Missel, N. A. Mazer, M. C. Carey, G. B. Benedek, J. Phys. Chem. 93 (1989) 8354.

[46] D. Nguyen, G. L. Bertrand, J. Phys. Chem. 96 (1922) 1994.

[47] A. Y. Vlasov, K. R. Savchuk, A. A. Starikova, N. A. Smirnova, Zhidk. Krist. Ikh Prakt. Ispol'z. 4 (2011) 90.

[48] M. N. Jo Nomuranes, J. Piercy, J. Chem. Soc., Faraday Trans. 1 68 (1972) 1839.

[49] S. Ozeki, S. Ikeda, Colloid Polym. Sci. 262 (1984) 409.

[50] T. Imae, R. Kamiya, S. Ikeda, J. Colloid Interface Sci. 108 (1985) 215.

[51] T. Imae, S. Ikeda, J. Phys. Chem. 90 (1986) 5216-5223.

[52] H. Nomura, S. Koda, T. Matsuoka, T. Hiyama, R. Shibata, S. Kato, J. Colloid Interface Sci. 230 (2000) 22.

[53] Z. Weican, L. Ganzuo, M. Jianhai, S. Qiang, Z. Liqiang, L. Haojun, W. Chi, Chin. Sci. Bull. 45 (2000) 1854.

[54] A. Khatory, F. Lequeux, F. Kern, S.J. Candau, Langmuir 9 (1993) 1456.

[55] L. Magid, Z. Han, Z. Li, P. Butler, Langmuir 16 (2000) 149.

[56] K. Kameyama, A. Muroya, T. Takagi, J. Colloid Interface Sci. 196 (1997) 48.

[57] H. P. Moises de Oliveira, M. H. Gehlen, Langmuir 18 (2002) 3792.

[58] G. G. Warr, F. Grieser, J. Chem. Soc. Faraday Trans. 1 82 (1986) 1813.

[59] M. L. Corrin, W. D. Harkins, J. Am. Chem. Soc. 69 (1947) 683.

[60] A. A. Dar, G. M. Rather, S. Ghosh, A. R. Das, J. Colloid Interface Sci. 322 (2008) 572.

[61] J. H. Clint, J. Chem. Soc. Faraday Trans. 1 71 (1975) 1327.

[62] P. M. Holland, D. N. Rubingh, J. Phys. Chem. 87 (1983) 1984.

[63] A. D. Burman, T. Dey, B. Mukherjee, A. R. Das, Langmuir 16 (2000) 10020.

[64] M. L. Free, Corrosion 58 (2002) 1025.

[65] M. L. Free, W. Wang, D. Y. Ryu, Corrosion 60 (2004) 837.

[66] W. Wang, M. L. Free, Corrosion Sci. 46 (2004) 2601.

[67] M. L. Free, Corrosion Sci. 46 (2004) 3101.

[68] W. F. McDevit, F. A. Long, J. Am. Chem. Soc. 74 (1952) 1773.

[69] R. Aveyard, D. A. Haydon, Trans. Faraday Soc. 61 (1965) 2255.

[70] S. Zeppieri, J. Rodrı´guez, A. L. L. de Ramos, J. Chem. Eng. Data 46 (2001) 1086.

[71] B. Janczuk, T. Bialopiotrowicz, W. Wojcik, Colloids Surf. 36 (1989) 391.

[72] R. Aveyard, S. M. Saleem, J. Chem. Soc., Faraday Trans. 1 72 (1976) 1609.

[73] N. B. Vargaftik, B. N. Volkov, L. D. Voljak, J. Phys. Chem. Ref. Data 12 (1983) 817.

[74] P. K. Weissenborn, R. J. Pugh, J. Colloid Interface Sci. 184 (1996) 550.

[75] E. R. Nightingale, J. Phys. Chem. 63 (1959) 1381.

[76] J. B. Hasted, Aqueous dielectrics, 1st ed., Chapman and Hall Ltd., London, 1973.

[77] E. D. R Lide, CRC Handbook of Chemistry and Physics, 84th ed., CRC Press, Boca Raton, FL, 2004.

[78] K. Giese, U. Kaatze, R. Pottel, J. Phys. Chem. 74 (1970) 3718.

[79] G. B. Arfken, H. J. Webber, Mathematical Methods for Physicists, 5th ed., Academic Press, London, 2001.

[80] J. N. Israelachvili, Intermolecular and Surface Forces, 3rd ed., Academic Press, San Diego, 2011.

[81] S. May, A. Ben-Shaul, Giant Micelles: Properties and Applications, R. Zana, E. W. Kaler, CRC Press, Boca Raton, FL, 2007.

[82] P. J. Mlssel, N. A. Mazer, G. B. Benedek, C. Y. Young, J. Phys. Chem. 84 (1980) 1044.

[83] D. Blankschtein, G. M. Thurston, G. B. Benedek, J. Chem. Phys. 85 (1986) 7268.

CHAPTER 5

EFFECTS OF SURFACTANT PARTITIONING AND DISTRIBUTION*

5.1 Introduction

The use of surfactant inhibitors has received extensive attention in the oil and gas industry for corrosion inhibition of production and transportation pipes (metallic materials, such as steel and copper) in a way that surfactant molecules usually adsorb on steel surface and form a protective film which acts as a barrier to prevent corrosive media penetration and attack [1-4]. Compared to the production and use of pure surfactants, surfactant mixtures are well known due to the superior physicochemical properties and capabilities in efficient solubilization, adsorption, suspension, and transportation [5-8]. The solutions of surfactant mixtures can often be conveniently tuned to achieve desired properties by adjusting the mixed surfactant types and molar ratios. More surface-active and expensive surfactants are often mixed with less surface-active and cheaper surfactants to reduce cost [9, 10]. Natural mixtures of surfactants are sometimes used to avoid the investment in separation processes. However, further studies are required in order to optimize inhibition efficiency of surfactant mixtures and minimize environmental impact.

Surfactant molecules have hydrophilic and hydrophobic sections [7,11,12], which are

* Paper published in J. Electrochem. Soc. 168 (2015) C702-C717.

critical to the adsorption on metal surface and associated corrosion inhibition [2-4]. The hydrophilic functional group of surfactant molecules strongly prefers interaction with polar entities such as metals, which is helpful in corrosion inhibition. The hydrophobic portion, which is nonpolar, strongly prefers interaction with hydrophobic entities such as hydrocarbon phase. Because of this, surfactant molecules tend to escape from polar environments, such as water, by associating and aggregating hydrocarbon chains together, which compromises the surfactant adsorption on metal surface and corrosion inhibition efficiency.

When an aqueous surfactant solution comes into contact with an immiscible organic liquid in one environment, such as water-oil-metal pipe environments, surfactant monomers may prefer partitioning into organic liquid until equilibrium is reached [13-15], which usually depletes the surfactants available in aqueous phase for adsorption on metal surface and for corrosion inhibiton [4]. Considering the behavior of surfactant partitioning in oil-water environments and associated interfacial phenomena, the determination of surfactant partitioning between water and oil usually serves as the basis of the hydrophobic-hydrophilic balance [13,14,16,17] and is critical for the evaluation of corrosion inhibition efficiency of surfactants [4].

For pure surfactant, the partitioning is usually characterized by the partitioning coefficient, which is defined as the ratio of monomeric surfactant concentration in oil to that in aqueous phase [14,16,18,19]. Extensive research has been performed on low concentration (typically lower than aqueous critical micelle concentration (cmc)) partitioning of nonionic surfactants [14,16,17,20-27]. The partitioning research on higher surfactant concentration solutions, however, has been rarely reported and is limited

[19,28-30]. The relevant report on the partitioning of ionic surfactant at high concentration level is even less [31]. The investigation of partitioning above the aqueous cmc (it means no oil phase) and apparent cmc is important (the apparent cmc is the average concentration in water-oil environments of pure or mixed surfactants at which micelles start to form): the portioning is a monomer process, and the partitioning coefficient is determined by monomer concentrations in two phases, which are limited by micelle formation.

For mixed surfactants, the phenomenon becomes more complicated. The effect of individual mixed species on the partitioning, and the adsorption of each surfactant at the oil/water interface involves many factors. It has been shown that for most pure surfactants, a plateau concentration of monomer is reached either in oil phase or in aqueous phase with increasing total surfactant concentration beyond the aqueous cmc [29,32,33]. However, it is also reported that for mixed surfactants, the amount of surfactants partitioned into oil phase continues to increase beyond aqueous cmc [19,30,32]. The different partitioning behavior of mixed surfactants above the aqueous cmc is reported to arise from the selective partitioning of more hydrophobic components into oil phase, which makes the experimental investigation and quantitative modeling work more challenging [19,30,32].

In the present research, a water-oil surfactant distribution model is proposed to evaluate the associated water-oil partitioning phenomena of mixed surfactants. This model is applicable over a wide total surfactant concentration range, including the aqueous cmc, oil cmc, and apparent cmc. The model inputs are the aqueous cmc of pure surfactant, total surfactant concentration, water and oil volume ratio, and mixed molar

ratio in bulk solution, the last three of which are known partitioning conditions. The partitioning coefficient can either be directly measured from experiment or calculated from different methods that are introduced in the text. The aqueous cmc can also be measured from experiment. However, it usually can be calculated from well-developed prediction models that are introduced in the text [34,35]. The model outputs include monomer concentrations at equilibrium in oil and in water, the apparent cmc value of mixtures in water-oil environment, and molar fraction of each mixed surfactant component in mixed micelles. The surfactant distribution model, which is a combination of a partitioning submodel, a partitioning coefficient calculation method, and the developed cmc prediction submodel based on previous work [34,35], provides a potential tool to evaluate the partitioning of surfactant mixtures in water-oil environment. The developed water-oil surfactant distribution model is validated using experimental data of pure and mixed benzalkonium chloride (C_{12}, C_{14}, and C_{16}) surfactants in water (containing salt)-oil (toluene) environments. The effects of surfactant concentration, experimental temperature, and bulk mixed molar ratio of surfactants are investigated. The application of the surfactant distribution model is also extended to other surfactants in water-oil environments in which the model prediction and experimental/reported data agree very well. The effect of partitioning on corrosion inhibition efficiency of mixed surfactants was initially evaluated by modified Langmuir adsorption and by electrochemical measurements.

5.2 Water-oil surfactant distribution model

5.2.1 Surfactant partitioning submodel derivation

A mass balance of total mixed surfactants in the water-oil environment is (see List of Symbols for symbol definition)

$$C_{\mathrm{tol}}V_{\mathrm{w}} = \bar{C}\,(V_{\mathrm{w}} + V_{\mathrm{o}}) \tag{5.1}$$

When $\bar{C} < \Gamma_{\mathrm{app}}$, mass balance of each mixed surfactant 'i' at partitioning equilibrium is given by

$$x_{\mathrm{i}}C_{\mathrm{tol}}V_{\mathrm{w}} = C_{\mathrm{mi}}^{\mathrm{w}}V_{\mathrm{w}} + C_{\mathrm{mi}}^{\mathrm{o}}V_{\mathrm{o}} \tag{5.2}$$

where $\bar{C}$ is the overall concentration of mixed surfactants in water-oil environment and Γ_{app} is the apparent cmc of the surfactant mixture in water-oil environment.

Alternatively,

$$x_{\mathrm{i}} = \frac{C_{\mathrm{mi}}^{\mathrm{w}}V_{\mathrm{w}} + C_{\mathrm{mi}}^{\mathrm{o}}V_{\mathrm{o}}}{C_{\mathrm{tal}}V_{\mathrm{w}}} \tag{5.3}$$

The partitioning coefficient of pure surfactant 'i' is defined as

$$K_{\mathrm{i}} = \frac{C_{\mathrm{mi}}^{\mathrm{o}}}{C_{\mathrm{mi}}^{\mathrm{w}}} \tag{5.4}$$

Partitioning coefficient of surfactant mixture is termed apparent partitioning coefficient and is given by

$$K_{\mathrm{mix}} = \frac{C_{\mathrm{m}}^{\mathrm{o}}}{C_{\mathrm{m}}^{\mathrm{w}}} = \frac{\sum C_{\mathrm{mi}}^{\mathrm{o}}}{\sum C_{\mathrm{mi}}^{\mathrm{w}}} \tag{5.5}$$

Substitution of Eqs. (5.3) and (5.4) into Eq. (5.5) leads to

$$K_{\mathrm{mix}} = \frac{\sum K_{\mathrm{i}}x_{\mathrm{i}}/(V_{\mathrm{w}}+V_{\mathrm{o}}K_{\mathrm{i}})}{\sum x_{\mathrm{i}}/(V_{\mathrm{w}}+V_{\mathrm{o}}K_{\mathrm{i}})} \tag{5.6}$$

Eqs. (5.2) - (5.3) and (5.5) - (5.6) are only applicable to the condition of $\bar{C} < \Gamma_{\mathrm{app}}$, whereas, Eq. (5.4) applies to all values of $\bar{C}$.

When $\bar{C} > \Gamma_{\mathrm{app}}$, it is assumed that partitioning process between water and oil only

involves monomers. For ionic surfactant, the partitioning involves surfactant molecule and the associated counterion. On the other hand, there is no dissociation in the process of partitioning.

The chemical potential of monomeric surfactant 'i' in water and oil phase, and the chemical potential of counterion 'j' in water can be written, respectively, as

$$\mu_{\mathrm{i}}^{\mathrm{w}} = \mu_{\mathrm{i}}^{\mathrm{w,o}} + RT\ln(\gamma_{\mathrm{mi}}^{\mathrm{w}} X_{\mathrm{mi}}^{\mathrm{w}}) \approx \mu_{\mathrm{i}}^{\mathrm{w,o}} + RT\ln(\gamma_{\mathrm{mi}}^{\mathrm{w}} C_{\mathrm{mi}}^{\mathrm{w}}/C_{\mathrm{mw}}) \quad 5.7$$

$$\mu_{\mathrm{i}}^{\mathrm{o}} = \mu_{\mathrm{i}}^{\mathrm{o,o}} + RT\ln(\gamma_{\mathrm{mi}}^{\mathrm{o}} X_{\mathrm{mi}}^{\mathrm{o}}) \approx \mu_{\mathrm{i}}^{\mathrm{o,o}} + RT\ln(\gamma_{\mathrm{mi}}^{\mathrm{o}} C_{\mathrm{mi}}^{\mathrm{o}}/C_{\mathrm{mo}}) \quad 5.8$$

$$\mu_{\mathrm{j}}^{\mathrm{w}} = \mu_{\mathrm{j}}^{\mathrm{w,o}} + RT\ln\left(\gamma_{\mathrm{mj}}^{\mathrm{w}} X_{\mathrm{j}}^{\mathrm{w}}\right) \approx \mu_{\mathrm{j}}^{\mathrm{w,o}} + RT\ln\left(\gamma_{\mathrm{mj}}^{\mathrm{w}} C_{\mathrm{j}}^{\mathrm{w}}/C_{\mathrm{mw}}\right) \quad 5.9$$

The chemical potential of surfactant i in mixed micelles is given by

$$\mu_{\mathrm{i}}^{\mathrm{m}} = \mu_{\mathrm{i}}^{\mathrm{pm}} + RT\ln(f_{\mathrm{i}}\alpha_{\mathrm{i}}) \quad 5.10$$

When micelles form, a saturation concentration for monomer is reached both in water and oil phase. Therefore, when partitioning equilibrium between micelle and water is reached for surfactant 'i', the chemical potentials of surfactant 'i' in mixed micelles is equal to the sum of the chemical potential of surfactant 'i' and the chemical potential of associated counterion 'j' in water

$$\mu_{\mathrm{i}}^{\mathrm{m}} = \mu_{\mathrm{i}}^{\mathrm{w}} + \delta_{\mathrm{j}}\mu_{\mathrm{j}}^{\mathrm{w}} \quad 5.11$$

where δ_{j} represents binding coefficient of counterion 'j' to micelles. Note that ionic surfactant is assumed to be completely dissociated when dissolved in aqueous phase as a monomer, but in the micelles form, the surfactant is associated to some extent with a counterion. Therefore, δ_{j}=0 for micelles of nonionic surfactant and $0<\delta_{\mathrm{j}}<1$ for micelles of ionic surfactant.

The cmc is interpreted as the monomer concentration at saturation for surfactant 'i'. Considering the equilibrium condition among pure micelles, water, and oil phases for

surfactant ‘i’, we have

$$\mu_{\mathrm{i}}^{\mathrm{pm}} = \mu_{\mathrm{i}}^{\mathrm{w,o}} + RT\ln(\gamma_{\mathrm{mi}}^{\mathrm{w}}\Gamma_{\mathrm{i}}^{\mathrm{w}}/C_{\mathrm{mw}}) + \delta_{\mathrm{j}}\mu_{\mathrm{j}}^{\mathrm{w}} = \mu_{\mathrm{i}}^{\mathrm{o,o}} + RT\ln(\gamma_{\mathrm{mi}}^{\mathrm{o}}\Gamma_{\mathrm{i}}^{\mathrm{o}}/C_{\mathrm{mo}}) \quad 5.12$$

With Eqs. (5.7), (5.8), and (5.10) - (5.12), it is obtained

$$C_{\mathrm{mi}}^{\mathrm{w}} = f_{\mathrm{i}}\alpha_{\mathrm{i}}\Gamma_{\mathrm{i}}^{\mathrm{w}} \quad 5.13$$

$$C_{\mathrm{mi}}^{\mathrm{o}} = f_{\mathrm{i}}\alpha_{\mathrm{i}}\Gamma_{\mathrm{i}}^{\mathrm{o}} \quad 5.14$$

Molar fraction of surfactant ‘i’ in mixed micelles is written as

$$\alpha_{\mathrm{i}} = \frac{x_{\mathrm{i}}C_{\mathrm{tol}}V_{\mathrm{w}} - (C_{\mathrm{mi}}^{\mathrm{w}}V_{\mathrm{w}} + C_{\mathrm{mi}}^{\mathrm{o}}V_{\mathrm{o}})}{C_{\mathrm{tol}}V_{\mathrm{w}} - C_{\mathrm{m}}(V_{\mathrm{o}} + V_{\mathrm{w}})} \quad 5.15$$

Substitution of Eqs. (5.13) and (5.14) into Eq. (5.15) and arrangement leads to

$$\alpha_{\mathrm{i}} = \frac{x_{\mathrm{i}}C_{\mathrm{tol}}}{C_{\mathrm{tol}} - C_{\mathrm{m}}(1 + V_{\mathrm{o}}/V_{\mathrm{w}}) + f_{\mathrm{i}}\Gamma_{\mathrm{i}}^{\mathrm{w}} + f_{\mathrm{i}}\Gamma_{\mathrm{i}}^{\mathrm{o}}V_{\mathrm{o}}/V_{\mathrm{w}}} \quad 5.16$$

Summation of molar fraction of surfactant ‘i’ in mixed micelles should result in unity

$$\sum \alpha_{\mathrm{i}} = 1 \quad (5.17)$$

and thus

$$\sum \frac{x_{\mathrm{i}}C_{\mathrm{tol}}}{C_{\mathrm{tol}} - C_{\mathrm{m}}(1 + V_{\mathrm{o}}/V_{\mathrm{w}}) + f_{\mathrm{i}}\Gamma_{\mathrm{i}}^{\mathrm{w}} + f_{\mathrm{i}}\Gamma_{\mathrm{i}}^{\mathrm{o}}V_{\mathrm{o}}/V_{\mathrm{w}}} = 1 \quad 5.18$$

Given other parameters, Eq. (5.18) is a polynomial function of C_{m}. For surfactant mixtures with multiple components, C_{m} has multiple corresponding mathematical values. However, in reality, C_{m} should only have one value and should be confined to

$$\Gamma_{\mathrm{app}} < C_{\mathrm{m}} < \bar{C} \quad 5.19$$

Eqs. (5.18) and (5.19) is solved simultaneously with respect to C_{m} using designed MATLAB code. The value of Γ_{app} can be calculated using the method described below.

At the mixed cmc, the following equations apply

$$x_{\mathrm{i}}\Gamma_{\mathrm{app}}(V_{\mathrm{w}} + V_{\mathrm{o}}) = C_{\mathrm{mi}}^{\mathrm{w}}V_{\mathrm{w}} + C_{\mathrm{mi}}^{\mathrm{o}}V_{\mathrm{o}} \quad 5.20$$

$$\frac{x_i\Gamma_{app}(V_w + V_o)}{f_{\mathrm{i}}\Gamma_{\mathrm{i}}^{\mathrm{w}}V_{\mathrm{w}} + f_{\mathrm{i}}\Gamma_{\mathrm{i}}^{\mathrm{o}}V_{\mathrm{o}}} = \frac{C_{\mathrm{mi}}^{\mathrm{w}}V_{\mathrm{w}} + C_{\mathrm{mi}}^{\mathrm{o}}V_{\mathrm{o}}}{f_{\mathrm{i}}\Gamma_{\mathrm{i}}^{\mathrm{w}}V_{\mathrm{w}} + f_{\mathrm{i}}\Gamma_{\mathrm{i}}^{\mathrm{o}}V_{\mathrm{o}}} \quad 2.21$$

The sum of Eqs. (5.13) and (5.14) leads to

$$C_{\mathrm{mi}}^{\mathrm{w}}V_{\mathrm{w}} + C_{\mathrm{mi}}^{\mathrm{o}}V_{\mathrm{o}} = \alpha_i(f_{\mathrm{i}}\Gamma_{\mathrm{i}}^{\mathrm{w}}V_{\mathrm{w}} + f_{\mathrm{i}}\Gamma_{\mathrm{i}}^{\mathrm{o}}V_{\mathrm{o}}) \quad 5.22$$

Replacement of mole fraction of surfactant 'i' in micelles using Eq. (5.17) and rearrangement yield

$$\sum \frac{C_{\mathrm{mi}}^{\mathrm{w}}V_{\mathrm{w}}+C_{\mathrm{mi}}^{\mathrm{o}}V_{\mathrm{o}}}{f_{\mathrm{i}}\Gamma_{\mathrm{i}}^{\mathrm{w}}V_{\mathrm{w}}+K_{\mathrm{i}}f_{\mathrm{i}}\Gamma_{\mathrm{i}}^{\mathrm{w}}V_{\mathrm{o}}} = 1 \quad 5.23$$

Combination of Eqs. (5.21) and (5.23) and rearrangement leads to

$$\sum \frac{x_{\mathrm{i}}\Gamma_{\mathrm{app}}(V_{\mathrm{w}}+V_{\mathrm{o}})}{f_{\mathrm{i}}\Gamma_{\mathrm{i}}^{\mathrm{w}}V_{\mathrm{w}}+f_{\mathrm{i}}\Gamma_{\mathrm{i}}^{\mathrm{o}}V_{\mathrm{o}}} = 1 \quad 5.24$$

Rearrangement leads to

$$\Gamma_{\mathrm{app}} = \frac{1}{\sum \frac{x_{\mathrm{i}}}{f_{\mathrm{i}}\Gamma_{\mathrm{i}}^{\mathrm{w}}V_{\mathrm{w}}/(V_{\mathrm{w}}+V_{\mathrm{o}})+f_{\mathrm{i}}\Gamma_{\mathrm{i}}^{\mathrm{o}}V_{\mathrm{o}}/(V_{\mathrm{w}}+V_{\mathrm{o}})}} \quad 5.25$$

The above derivation is a general form of the partitioning submodel. However, some surfactants may not form micelles in both aqueous phase and in oil phase when $\bar{C} > \Gamma_{\mathrm{app}}$. If no micelle formation in aqueous phase, $\Gamma_{\mathrm{i}}^{\mathrm{w}}$ should be replaced by $\Gamma_{\mathrm{i}}^{\mathrm{o}}/K_{\mathrm{i}}$; if no micelle formation in oil phase, $\Gamma_{\mathrm{i}}^{\mathrm{o}}$ should be replaced by $\Gamma_{\mathrm{i}}^{\mathrm{w}}K_{\mathrm{i}}$. It is also important to be aware that $\Gamma_{\mathrm{i}}^{\mathrm{o}}$ can still be replaced using $\Gamma_{\mathrm{i}}^{\mathrm{w}}K_{\mathrm{i}}$ even if micelles form in oil phase provided that $\Gamma_{\mathrm{i}}^{\mathrm{w}}$ is in isolated aqueous phase that can be measured from experiment or predicted from existing models. Here the isolated aqueous phase means the aqueous phase is not in contact with the oil phase and there is no partitioning process. The activity coefficient, f_{i}, of surfactant, 'i', arises from the interaction between surfactant molecules, which is considered by the cmc prediction submodel (see following sections) [35], and therefore, it is assumed to be unity in the present research without any compromise of the overall model performance.

5.2.2 Partitioning coefficient determination method

The partitioning submodel requires the input of the partitioning coefficient of surfactant 'i', which can be determined from experimental measurement (see Eq. (5.4)) or from model estimation. Here one model is briefly introduced for the estimation of partitioning coefficient.

As previously mentioned, the chemical potential of surfactant 'i' in water and in oil should be equal at partitioning equilibrium:

$$\mu_{\mathrm{i}}^{\mathrm{w}} = \mu_{\mathrm{i}}^{\mathrm{o}} \tag{5.26}$$

Substitution of Eqs. (5.7) and (5.8) leads to

$$\mu_{\mathrm{i}}^{\mathrm{w,o}} + RT\ln(\gamma_{\mathrm{mi}}^{\mathrm{w}} C_{\mathrm{mi}}^{\mathrm{w}}/C_{\mathrm{mw}}) = \mu_{\mathrm{i}}^{\mathrm{o,o}} + RT\ln(\gamma_{\mathrm{mi}}^{\mathrm{o}} C_{\mathrm{mi}}^{\mathrm{o}}/C_{\mathrm{mo}}) \tag{5.27}$$

Standard free energy change of transfer of surfactant i from aqueous phase to oil phase is given by

$$\Delta\mu_{\mathrm{tri}}^{\mathrm{o}} = \mu_{\mathrm{i}}^{\mathrm{o,o}} - \mu_{\mathrm{i}}^{\mathrm{w,o}} \tag{5.28}$$

Combination of Eqs. (5.4), (5.27), and (5.28) leads to

$$\Delta\mu_{\mathrm{tri}}^{\mathrm{o}} = RT\ln\left(\frac{1}{K_{\mathrm{i}}}\frac{\gamma_{\mathrm{mi}}^{\mathrm{w}} C_{\mathrm{mo}}}{\gamma_{\mathrm{mi}}^{\mathrm{o}} C_{\mathrm{mw}}}\right) \tag{5.29}$$

Further rearrangement leads to

$$K_{\mathrm{i}} = \frac{\gamma_{\mathrm{mi}}^{\mathrm{w}} C_{\mathrm{mo}}}{\gamma_{\mathrm{mi}}^{\mathrm{o}} C_{\mathrm{mw}}} \exp\left(-\frac{\Delta\mu_{\mathrm{tri}}^{\mathrm{o}}}{RT}\right) \tag{5.30}$$

where $\gamma_{\mathrm{mi}}^{\mathrm{o}}$ is assumed to be unity, and C_{mo} and C_{mw} are molar concentration of oil and water, respectively. The essence of $\gamma_{\mathrm{mi}}^{\mathrm{w}}$is to take into account the effect of dissolved salt in water on water-oil partitioning of surfactants.

For ionic surfactant,

$$\gamma_{\mathrm{mi}}^{\mathrm{w}} = \sqrt{\gamma_{\mathrm{hmi}}^{\mathrm{w}} \gamma_{\mathrm{tmi}}^{\mathrm{w}}} \tag{5.31}$$

For nonionic surfactant,

$$\gamma_{\mathrm{mi}}^{\mathrm{w}} = \gamma_{\mathrm{tmi}}^{\mathrm{w}} \quad 5.32$$

where $\gamma_{\mathrm{hmi}}^{\mathrm{w}}$ is the functional headgroup activity coefficient and $\gamma_{\mathrm{tmi}}^{\mathrm{w}}$ is the hydrocarbon chain tail activity coefficient. $\gamma_{\mathrm{hmi}}^{\mathrm{w}}$ can be calculated from Pitzer's method [36,37] or Davies equation [38]. $\gamma_{\mathrm{tmi}}^{\mathrm{w}}$ is estimated from the Setchenov equation shown as below [39].

$$\gamma_{\mathrm{tmi}}^{\mathrm{w}} = 10^{Ik_{\mathrm{s}}} \quad 5.33$$

where I is ionic strength of solution. k_{s} is Setchenov coefficient specific to added salt in water [39,40].

The standard transfer free energy $\Delta\mu_{\mathrm{tri}}^{\mathrm{o}}$ can be determined by different methods. Two methods are briefly described below.

Method I: free energy transfer method. $\Delta\mu_{\mathrm{tri}}^{\mathrm{o}}$ is the sum of two contributing parts: head group part $\Delta\mu_{\mathrm{trhi}}^{\mathrm{o}}$ and hydrocarbon tail part $\Delta\mu_{\mathrm{trti}}^{\mathrm{o}}$. The 1st part is the transfer free energy of hydrocarbon tail from salt water to organic phase, which is calculated in two steps using the reported methodology for alkanes [40].

Step one is the transfer of hydrocarbon chain from salt water to pure water [40]:

$$\frac{\Delta\mu_{\mathrm{i,s/w}}^{\mathrm{o}}}{RT} = -k_{\mathrm{s}}C_{\mathrm{s}} \quad 5.34$$

Step two is the transfer of hydrocarbon chain from pure water to oil/organic phase [40]:

$$\frac{\Delta\mu_{\mathrm{i,w/o}}^{\mathrm{o}}}{RT} = \frac{\Delta\mu_{\mathrm{ch3}}^{\mathrm{o}}}{RT} + (L_{\mathrm{i}} - 1)\frac{\Delta\mu_{\mathrm{ch2}}^{\mathrm{o}}}{RT} \quad 5.35$$

$$\frac{\Delta\mu_{\mathrm{ch3}}^{\mathrm{o}}}{RT} = 3.38lnT + \frac{4064}{T} - 44.13 + 0.02595T \quad 5.36$$

$$\frac{\Delta\mu_{\mathrm{ch2}}^{\mathrm{o}}}{RT} = 5.85lnT + \frac{896}{T} - 36.15 - 0.0056T \quad 5.37$$

The second part is the transfer free energy of the headgroup, which is estimated either

from reported experimental data [24,25,41-44] or from quantum calculation, as summarized in Table 5.1. The quantum calculation of transfer free energy of headgroups followed the reported procedure [4], in which the transfer free energy $\Delta\mu_{\mathrm{tri}}^{\mathrm{o}}$ is interpreted as the difference in solvation energy of surfactant 'i' in oil and in water based on the quantum chemical calculations using Gasussian09.

Method II: group contribution method, in which the aqueous solubility of a molecule is empirically related to structural descriptors [45]. The transfer free energy contribution of each group in a molecule to its solubility is calculated. The sum of free energy contribution of all groups is considered as the free energy of transfer [45,46].

Once the standard transfer free energy of surfactant 'i' from aqueous phase to oil phase is calculated based on the methods described above, the partitioning coefficient can be determined using Eq. (5.30) at given conditions of water-oil environment.

5.2.3 cmc prediction submodel

The aqueous cmc of pure surfactant or mixed surfactants in the absence of oil phase is usually very close to the aqueous cmc in the presence of nonpolar oil phase, which is confirmed for the discussed surfactants in the present work by experiment. On the other hand, the nonpolar oil phase does not contribute to the micelle formation in aqueous phase. It is actually reported that for nonionic surfactants with nonpolar organic as oil phase, such as heptane and toluene, the aqueous cmc has been observed to be very similar to the corresponding cmc without oil phase [47] and that for certain anionic surfactants with nonpolar organic (such as heptane) as oil phase, the aqueous cmc has also been found to be very close to the cmc measured in water in the absence of oil [48]. For certain

cationic surfactants with polar oil phase (dichloromethane), however, the aqueous cmc is significantly different from the corresponding cmc with oil phase [49].

As previously discussed, the cmc of each mixed surfactant component in aqueous phase is required as an input. The required cmc values can either be measured using traditional methods, such as surface tension measurement and conductivity measurement, or be predicted using simplified molecular thermodynamic model [34] or more advanced molecular thermodynamic model [35]. The advanced model is briefly described below.

The aqueous cmc of mixed surfactants (taken as one example) is evaluated using the following equation:

$$\Gamma^{\mathrm{w}} = (C_{\mathrm{mw}} + C_{\mathrm{s}})\exp^{\left(\frac{1}{kT}\Delta\mu_{\mathrm{m}}^{\mathrm{o}}\right)} \qquad 5.38$$

where k is Boltzmann constant, T is temperature, and $\Delta\mu_{\mathrm{m}}^{\mathrm{o}}$ is micellization free energy which is estimated from several contributing terms as described below.

$$\Delta\mu_{\mathrm{m}}^{\mathrm{o}} = \Delta\mu_{\mathrm{tr}}^{\mathrm{o}} + \Delta\mu_{\mathrm{int}}^{\mathrm{o}} + \Delta\mu_{\mathrm{pack}}^{\mathrm{o}} + \Delta\mu_{\mathrm{st}}^{\mathrm{o}} + \Delta\mu_{\mathrm{ent}}^{\mathrm{o}} + \Delta\mu_{\mathrm{elec}}^{\mathrm{o}} + \Delta\mu_{\mathrm{act}}^{\mathrm{o}} \qquad 5.39$$

where $\Delta\mu_{\mathrm{tr}}^{\mathrm{o}}$, $\Delta\mu_{\mathrm{int}}^{\mathrm{o}}$, $\Delta\mu_{\mathrm{pack}}^{\mathrm{o}}$, $\Delta\mu_{\mathrm{st}}^{\mathrm{o}}$, $\Delta\mu_{\mathrm{ent}}^{\mathrm{o}}$, $\Delta\mu_{\mathrm{elec}}^{\mathrm{o}}$, and $\Delta\mu_{\mathrm{act}}^{\mathrm{o}}$ are the free energy contributions from hydrocarbon transfer from water into micelle, formation of micellar core-water interface, hydrocarbon tail packing in the micelle, surfactant headgroup steric interaction, headgroup-counterion mixing, electrostatic interaction, and surfactant activity and counterion activity contribution, respectively [34]. Details of the cmc prediction submodel can be found elsewhere [34,35].

The developed cmc prediction submodel takes into account hydrocarbon chain length, head group steric interactions, van der Waals force between surfactant molecules, electrostatic force between micelles and monomeric surfactant, and entropy of mixing. The cmc submodel takes into account the ion/salt effect on surfactant aggregation, the

effect of chain length, van der Waals interactions between surfactant molecules, steric interactions between head groups, electrostatic interactions at the interfacial region of micelles, and the interactions between solvent and surfactant.

By the integration of partitioning submodel, partitioning coefficient calculation method, and the cmc prediction submodel, the water-oil surfactant distribution model is developed. With this developed model, partitioning coefficient K_i of surfactant 'i', the aqueous cmc of surfactant 'i', the apparent cmc of mixed surfactants in water-oil environment, Γ_{app}, monomer concentration of surfactant 'i' in water and in oil phase, C_{mi}^{w} and C_{mi}^{o}, and molar fraction of surfactant 'i' in the mixed micelles, α_i, can be predicted at given inputs, which include total surfactant concentration C_{tol} and mixed molar ratio x_i in bulk solution. If no experimental data are available, methods introduced above can be used to predict the aqueous cmc and partitioning coefficient values and the values can be substituted into the surfactant distribution model.

5.3 Experiment

All the chemicals were used as received. The homologous cationic benzalkonium chlorides (BAC) surfactants, including benzyl dimethyl dodecyl ammonium chloride (C12 or C_{12}), benzyl dimethyl tetradecyl ammonium chloride (C14 or C_{14}), benzyl dimethyl hexadecyl ammonium chloride (C16 or C_{16}), and polyoxyethylene n-cetyl ether ($C_nE_{n'}$) were supplied by Sigma-Aldrich Co. LLC with assay values higher than 99%. Primary alcohol ethoxylate ($C_{12}OE_n$) was provided by Witco Corporation. Benzyl dimethyl tetradecyl ammonium-d7 chloride (C_{14}') was provided by Santa Cruz Biotechnology with compound purity higher than 98% and isotopic purity higher than

99%.

For the partitioning tests, equal volumes (5 ml) of aqueous phase and oil phase (toluene or heptane) were separately added to a partitioning cell. The cell is a glass cylinder, one inch in diameter, which has two ports (top and bottom) for the sampling of oil and aqueous phase separately without contamination from each other. The cell was kept in a water bath at the desired temperatures (25, 40, 50, and 60 ℃) for at least 12 h. Gentle stir (25-30 rpm) using a magnetic stirrer was applied for to accelerate partitioning equilibration but prevent emulsification. In this study, it was confirmed that the partitioning equilibrium is reached within 12 h. The constant temperature was maintained through a water circulation bath using a Polystat temperature controller, purchased from Cole-Parmer®. The initial concentration of pure surfactant or mixed surfactants in aqueous phase is known. No surfactant was initially added to the oil phase. The aqueous phase contains different concentrations of NaCl (0, 0.03, 0.0342, 0.171, 0.599, 0.804, and 0.856 M). The sampled aqueous and oil phases were centrifuged following partitioning equilibration and were then injected into a liquid chromatography instrument for analysis.

The sample analysis was conducted using an Ultra Performance Liquid Chromatography (Waters ACQUITY®) coupled with a UV detector and a triple quadripole mass spectrometry (Waters TQD®). The separation was performed with a 100x2.1um i.d. (1.7 um) Acquity UPLC® BEH C18 column purchased from by Waters. The flow rate was controlled at 0.6 ml/min and the target column temperature was maintained at 40 ℃. The mobile phase consisted of water and acetonitrile with 0.1% formic acid. Ionization was performed with an electrospray source in positive mode and acquisition was achieved in multiple reactions monitoring (MRM).

The data analysis was performed using MassLynx 4.1 Software. The internal calibration method was adopted for quantification. The C_{14}' were used as internal references at constant concentration of $5x10^{-7}$ M in all tested samples (added after partitioning and before liquid chromatography and mass spectrometry analysis) and standard samples. The concentration of standard solution for tested surfactants ranged between $2.5x10^{-8}$ M and $2.5x10^{-5}$ M. All the tested aqueous samples were diluted to this calibration range for partitioning equilibrium quantification. Surfactant concentration at equilibrium in oil phase is calculated based on a mass balance. Note that surfactant concentration of certain oil samples was also determined experimentally for verification. The error is within 5% between calculation and experimental measurement.

A dynamic light scattering instrument ‘‘Wyatt Dynopro NanoStar’’ was used for the detection of surfactant aggregation in the oil phase. The detection temperature was controlled at the same temperature as partitioning tests.

The experimental cmc was obtained from surface tension measurements. The surface tension of test solutions was measured within a precision of 0.1 mN/m by the platinum ring method using a Krüss K10 ST digital tensiometer, equipped with an isothermal vessel holder. The test samples for surface tension measurements were prepared by sequential dilution of concentrated aqueous solutions of surfactants using double deionized water, made through a water purification system (Simplicity® UV made by EMD Millipore). All measurements were performed at desired constant temperatures, which have been confirmed to be higher than the Krafft point of the surfactants and their mixtures in aqueous media. The platinum ring was rinsed with water and heated to an orange color using a Bunsen burner between tests to ensure the complete removal of

organic contaminants. Triplicate measurements were used to confirm reproducibility.

In the electrochemical measurements, a piece of X65 steel, purchased from Metal Samples®, was used as the working electrode in electrochemical measurements with a surface area of 0.196 cm^2. The composition (wt %) is C 0.06%, Mn 1.33%, P 0.007%, S 0.005%, Si 0.30%, Cu 0.30%, Ni 0.10%, V 0.022%, Cb 0.046%, Al 0.019%, Cr 0.05%, Mo 0.03%, Ti 0.017%, Ca 0.0033%, and Fe (balance). The surface of the X65 electrode was polished using SiC paper in the sequence of 400-600-800-1200 grit, and followed by polishing using MicroCloth™ with a particle size of ~ 5 μm supplied by Buehler. A platinum ring electrode and a single junction saturated calomel electrode (SCE) were employed as counter and reference electrodes, respectively.

The glass cell of 150 mL volume for electrochemical measurements is designed with a water jacket for isothermal test. Aqueous solutions in the cell for tests contained 0-1 M NaCl and were purged with Ar (>99.999%) for 2 h to remove oxygen followed by a purge of CO_2 (>99.999%) for 2 h to ensure CO_2 saturation prior to measurements. The concentration of dissolved oxygen was monitored before electrochemical measurements using an Oxygen ULR CHEMets® Kit, and the concentration was measured and found to be below 20 ppb. The pH was adjusted to 4 - 5 for different mixtures by the addition of 1.0 M $NaHCO_3$ or diluted HCl. The three electrodes and pH meter were in direct contact with the aqueous phase in the glass cell during equilibration and measurements. The surfactants were added to the aqueous phase at the beginning of each measurement. The effect of partitioning and aggregation on steel corrosion rate and on corrosion inhibition efficiency of inhibitors was evaluated by the addition of desired volume of toluene into the cell following the addition of surfactants. Care was taken to ensure that the added

toluene did not contact the electrodes. The working electrode was rotated at very low speed (25-30 rpm) considering the rotation can facilitate partitioning process but the speed is not high enough to cause microemulsions. For the electrochemical tests without toluene, the step for the addition of toluene is skipped.

A Gamry reference 600 potentiostat was then used for electrochemical measurements. Polarization resistance R_p was measured every 20 minutes in 15 h using the linear polarization resistance (LPR) method by polarizing the working electrode +/- 0.010 V (SCE) vs. E_{corr} with a sweep rate of 0.1 mV/s for the evaluation of corrosion rate as a function of time. At the end of the 15-hour measurement, potentiodynamic scans (PDS) were performed with a sweep rate of 1mV/s from -0.9 V (SCE) to -0.35 V (SCE). Electrochemical impedance spectroscopy (EIS) measurements were then made with an applied alternating current (AC) potential of +/-0.010 V rms vs. E_{corr} in the frequency range of 100,000 - 0.010 Hz. The direct current (DC) potential was set as zero relative to E_{corr}. Each test was repeated at least three times as an independent measurement within deviation of +/- 3%. The collected electrochemical data were analyzed using software package Gamry Echem Analyst.

5.4 Results and discussion

Fig. 5.1 shows the calibration curves based on internal reference C_{14}' for the three homologous BAC surfactants between the concentrations of 2.5×10^{-8} M and 2.5×10^{-5} M. As can be seen, the linearity of the calibration curves over three orders of magnitude is excellent for all three surfactants. Based on the experimental data, the concentration of all tested samples was higher than 2.5×10^{-8} M. For samples with concentrations higher than

$2.5x10^{-5}$ M, dilution was applied, which assured the accuracy of quantitative determination of surfactant concentration in aqueous phase at equilibrium. Surfactant concentration at equilibrium in oil phase is calculated based on mass balance within the error of 5% as mentioned previously.

The partitioning results of pure BAC surfactants, C_{12}, C_{14}, and C_{16}, in water-oil partitioning are shown in Fig. 5.2(a). The experimental partitioning coefficients at 40 ℃ are 0.041 for C_{12}, 0.598 for C_{14}, and 8.802 for C_{16}, respectively. The equilibrium concentration of pure surfactant in aqueous phase increases linearly with the initial concentration up to around the aqueous cmc, which is consistent with previous reports [29,32,33]. Above the aqueous cmc, extra C_{12} and C_{14} accumulated in aqueous phase, as indicated by the arrow for C_{14}, for example. Extra C_{16} partitioned into oil phase probably because of stronger hydrophobicity. It is inferred that C_{12} and C_{14} form micelles in aqueous phase but not in the oil phase, whereas C_{16} mainly forms inverse micelles in the oil phase and the cmc of C_{16} in the oil phase is estimated as $1.08x10^{-4}$ M, which is calculated using the value of $1.2x10^{-4}$ M minus $1.2x10^{-5}$ M. Note $1.2x10^{-4}$ M is the highest value of C_{tol} and that $1.2x10^{-5}$ is the saturation value of concentration of C_{16} in aqueous phase before micellization of C_{16} in water-oil partitioning process at 40 ℃, as indicated by the arrows in Fig. 5.2(a).

The temperature effect on the water-oil partitioning of C_{16} was also investigated. As can be seen in Fig. 5.2(a), the equilibrium concentration in aqueous phase decreases with increasing temperature, which means K_{16} increases with increasing temperature.

The thermodynamic relation between entropy, enthalpy, and free energy of transfer is given by

$$\Delta\mu_{\mathrm{tri}}^{\mathrm{o}} = \Delta H_{\mathrm{tri}}^{\mathrm{o}} - T\Delta S_{\mathrm{tri}}^{\mathrm{o}} \quad 5.40$$

Combination of Eqs. (5.29) and (5.40) leads to

$$\ln K_{\mathrm{i}} = -\frac{\Delta H_{\mathrm{tri}}^{\mathrm{o}}}{RT} + \frac{\Delta S_{\mathrm{tri}}^{\mathrm{o}}}{R} + \ln\left(\frac{\gamma_{\mathrm{mi}}^{\mathrm{w}} C_{\mathrm{mo}}}{\gamma_{\mathrm{mi}}^{\mathrm{o}} C_{\mathrm{mw}}}\right) \quad 5.41$$

It is assumed that the values of $\Delta H_{\mathrm{tri}}^{\mathrm{o}}$ and $\Delta S_{\mathrm{tri}}^{\mathrm{o}}$ do not vary much within the temperature range of discussed. The plot of $\ln K_{\mathrm{i}}$ vs. $1/T$ is a straight line which yields a slope for the calculation of $\Delta H_{\mathrm{tri}}^{\mathrm{o}}$ and an intercept for the calculation of $\Delta S_{\mathrm{tri}}^{\mathrm{o}}$, as shown in Fig. 5.2(b). The calculated entropy and enthalpy of C_{16} partitioning are 0.203 kJ/(mol K) and 53.9 kJ/mol. The calculated free energy of transfer is -9.64, -11.67, and 13.69 kJ/mol at 40, 50, and 60 ℃, respectively. It is thus concluded that at the temperature range discussed, the partitioning of C_{16} is in favor of the oil phase and the partitioning coefficient increases with the increasing temperature. In combination with Eqs. (5.34)-(5.37) as introduced in the Method I, the transfer free energy of the C_{16} functional head group $\Delta\mu_{\mathrm{trhi}}^{\mathrm{o}}$ can be calculated and summarized as presented in Table 5.1. The values of $\Delta\mu_{\mathrm{trhi}}^{\mathrm{o}}$ are used for the following calculation of partitioning coefficients of BAC surfactants under various partitioning conditions.

The aggregation properties of BAC surfactants in toluene were examined using dynamic light scattering. Fig. 5.3 presents the DLS testing results, including aggregate radius and intensity of collected light signal, of C_{12}, C_{14}, and C_{16} in toluene which was sampled from oil phase at water-oil partitioning equilibrium of pure BAC surfactants. As can be seen, both the particle radius and signal intensity of C_{12} and C_{14} barely changed in the concentration range evaluated, which indicates C_{12} and C_{14} in toluene do not form micelles. For C_{16}, however, micelles started to form at the added initial concentration of around $1.20\text{x}10^{-4}$ M, as indicated both by the aggregate radius and by the intensity. These

results support the findings in Fig. 5.2 that C_{12} and C_{14} form micelles in aqueous phase while C_{16} mainly forms inverse micelles in oil phase. According to Fig. 5.3(a), the diameter of micelles of C_{16} (assumed as spherical micelles) is estimated to be 0.45 nm which is close to twice the extended length of hydrocarbon tail of C_{16} (2.17 nm). The extended length of hydrocarbon tail is calculated using a group contribution of 0.1265 nm for methylene group and 0.2765 nm for the methyl group [40,50].

The comparison of predicted partitioning coefficient and experimental partitioning coefficient of pure BAC surfactants (C_{12}, C_{14}, and C_{16}) in water (salt containing) - oil environment is shown in Fig. 5.4(a). The predicted partitioning coefficients at various conditions based on the transfer free energy calculated using the two aforementioned methods match experimental data reasonably well. Note that the transfer free energy of polar functional group of BAC surfactants is 55.3 kJ/mol at 40 ℃ which is based on the partitioning coefficients of C_{16} as shown in Fig. 5.2 and the associated calculations. This value is much lower than the reported value of polar functional group ($>N(CH_3)_2^+$) transferring from 0.1 M aqueous sodium hydroxide to heptane.[45] This is probably because the functional group in BAC surfactants has one extra benzene group and one extra methylene group which prefer the nonpolar organic phase and thus decrease the free energy of transfer. The affinity of functional group to different organic phases also contributes to the energy difference. In Method II, the transfer free energy of a surfactant molecule is estimated from the solubility which is calculated from a few contributing groups, including -CH< and >C< in a ring, $-CH_2-$ and CH_3- in linear alkane, and -N-. The predicted partitioning coefficients from Method I will be used in the overall partitioning model because it deviates less from experimental results.

The method to determine the transfer free energy for the partitioning coefficient was also tested on other surfactants. Fig. 5.4(b) presents the predicted and experimental partitioning coefficients of homologous polyoxyethylene glycol n-dodecyl ether $C_{12}H_{25}(OCH_2CH_2)_nOH$ (or $C_{12}E_n$) surfactants in pure water and isooctane environments; Fig. 5.4(c) presents the predicted and experimental partitioning coefficients of N-based alkyl amines and derivatives in 0.1 M NaOH water and heptane environments. As can be seen, there is an excellent agreement between predicted and experimental partitioning coefficients.

The partitioning model requires the aqueous cmc of pure surfactant as input as discussed previously. The aqueous cmc in isolated aqueous phase can either be determined from experimental measurement or predicted from the existing model [34,35]. In experimental measurement, the aqueous cmc in isolated aqueous phase is calculated from the interception of the two solid lines in the curve of surface tension vs. surfactant concentration as shown in Fig. 5.5(a). As can be seen, the surface tension decreases with the increase in surfactant concentration until the surface tension reaches a plateau value, which is the result of surfactant assembled into aggregates, such as micelles, bilayers, or multilayers. Alternatively, the aqueous cmc can be predicted from the well-developed model based on our previous work [34,35]. The comparison of the measured cmc and the predicted cmc of pure BAC surfactants as a function of NaCl concentration in aqueous phase is shown in Fig. 5.5(b). The predicted cmc values will be used in the partitioning model. Note that the predicted cmc of C_{16} in 0.171 NaCl aqueous phase is $1.20\text{x}10^{-5}$ M, which is very close to the oil cmc of C_{16} divided by partitioning coefficient, $1.08\text{x}10^{-4}$ M/8.802=$1.22\text{x}10^{-5}$ M. It is confirmed by experiment that the aqueous cmc of surfactants

in isolated aqueous phase can be used in the partitioning model and that the oil cmc can be calculated using the aqueous cmc and partitioning coefficient, rather than using direct measurement from experiment.

As previously discussed, the use of the surfactant distribution model in water and oil phases requires the inputs of the aqueous cmc of surfactant 'i', volume ratio, total surfactant concentration, and mixed molar ratio in bulk solution. With all required inputs provided the model application to the water-oil partitioning of equal-molar ternary mixtures of BAC surfactants are shown in Fig. 5.6. Figs. 5.6(a) and 5.6(b) present equilibrium concentrations of monomeric surfactants in water and in oil vs. total initial concentration of mixed surfactants added to the aqueous phase. The intersection of the vertical dash line and horizontal axis identifies the aqueous cmc of surfactant mixture, which is $\Gamma^{w} = 3.40\text{x}10^{-5}$ M. As can be seen, the partitioning of each mixed component as well as the overall partitioning continues without any change when C_{tol} reaches Γ^{w}. This is consistent with the reported view that the amount of surfactants partitioned into oil phase continues to increase beyond the aqueous cmc of that mixture [19,29,32]. It is easy to understand that the partitioning of surfactants into oil phase depletes the surfactants in aqueous phase to an extent that causes micelles to fail to form in aqueous phase at $C_{tol} < 2\Gamma_{app}$. $2\Gamma_{app}$ is used as upper limit rather than Γ_{app} considering that water and oil are equal-volume mixed and that the horizontal axis represents the total initial concentration of surfactants, C_{tol}, added to the aqueous phase.

Above $2\Gamma_{app}$ which is suggested by the dot line, the partitioning behavior of each mixed surfactant component starts to change, as indicated by the transition point in Figs. 5.6(a)-5.6(c). The mixed surfactants form micelles in aqueous phase as indicated by Fig.

5.6(c). It is also interesting to observe that above the transition point monomeric concentrations of C_{14} and C_{16} in both phases decrease while the concentrations of more hydrophilic C_{12} in both phases continue to increase to some extent, and that the total monomeric concentration in aqueous phase ($C_{\mathrm{m}}^{\mathrm{w}}$) increases and the counterpart in oil ($C_{\mathrm{m}}^{\mathrm{o}}$) phase decreases slightly before reaching a plateau. This phenomenon can be explained by the fact that surfactant molecules in micellar form are generally more thermodynamically stable than existing in monomeric form with respect to relatively hydrophobic species and that C_{16} and C_{14} prefer to exist in micellar form, which leads to the leveling off of monomeric surfactant concentration in water and oil phases. The preference of micellar form of C_{16} and C_{14} is reflected by the much higher molar fraction in micelles at the beginning of micelle formation, as shown in Fig. 5.6(d), indicating the formation of more hydrophobic micelle at the beginning. As the total surfactant concentration increases, the micelles become less hydrophobic.

The molar fraction change of C_{12}, C_{14}, and C_{16} in mixed micelles seems to be contrary to the report that more hydrophilic micelles form at first and then become more hydrophobic as the total initial concentration C_{tol} increases for mixed surfactants in a water-oil system [29,51]. However, the relative hydrophobicity/hydrophilicity in one-phase system, such as in water phase, may or may not be the same as that in a two-phase system, such as in water-oil phases for one particular surfactant relative the other. The hydrophobicity/hydrophilicity of surfactant can usually be reflected by the value of the cmc in the environment discussed. To clarify this statement, the apparent cmc of pure surfactant ‘i’ in water-oil environment is defined as

$$\Gamma_{\mathrm{app,i}} = \frac{\Gamma_{\mathrm{i}}^{\mathrm{o}} V_{\mathrm{o}} + \Gamma_{\mathrm{i}}^{\mathrm{w}} V_{\mathrm{w}}}{x_{\mathrm{i}}(V_{\mathrm{o}} + V_{\mathrm{w}})} \qquad 5.42$$

If Γ_i^o is not available, replace Γ_i^o with $\Gamma_i^w K_i$; if Γ_i^w is not available, replace Γ_i^w with Γ_i^o / K_i as stated previously. This defined apparent cmc of one pure surfactant in water-oil environment can reflect the relative hydrophobicity/hydrophilicity of that surfactant. The higher the apparent cmc of one pure surfactant, the lower the hydrophobicity of that surfactant in water-oil environments. The reverse is also true.

For mixed BAC surfactants in water-oil environments, the apparent cmc of each mixed component is calculated based on aqueous cmc and partitioning coefficient, and the relative values are shown below

$$\Gamma_{app,C12} > \Gamma_{app,C14} > \Gamma_{app,C16} \quad 5.43$$

Therefore, C_{16} is still the most hydrophobic surfactant among the three in water-oil environments, as well as in water only. It is thus easy to understand that C_{16} has the highest mixed molar fraction at the beginning of micelle formation in water-oil environments, followed by the mixed molar fractions of C_{14} and C_{12}. As C_{tol} increases, the molar fraction α_i in mixed micelles of each mixed component approaches the initial mixed molar ratio x_i in the bulk solution. The relative value of $\Gamma_{app,i}$ of BAC surfactants also shed light on the continuing increase of the concentration of monomeric C_{12} and the decrease of that of C_{14} and C_{16} after mixed micelles start to form as shown in Figs. 5.6(a) and 5.6(b).

It is confirmed from the results in Fig. 5.6 that mixed micelles barely forms in oil phase at $C_{tol} > 2\Gamma_{app}$ and therefore, it is easy to understand most surfactant molecules, including monomeric form and micellar form, exist in aqueous phase (especially at $C_{tol} >> 2\Gamma_{app}$). At $C_{tol} >> 2\Gamma_{app}$, the distribution of monomeric surfactants in water and oil phase approach plateau values (Figs. 5.6(a) and 5.6(b)), extra surfactant molecules exist in

micellar form in aqueous (Fig. 5.6(c)), and the molar fraction of surfactant i in mixed micelles (α_i) approaches to a plateau value which is actually infinitely getting close to the initial mixed molar ratio (x_i) in bulk aqueous phase (Fig. 5.6(d)).

The partitioning model application to various BAC surfactant mixtures is shown in Fig. 5.7. Vertical lines in Fig. 5.7(a) indicate the transition point ($C_{tol} = 2\Gamma_{app}$). For each studied mixture, the concentration change of monomeric surfactants as well as the concentration change of total surfactants in water and in oil follows a similar tendency presented in Fig. 5.6 as the C_{tol} increases. The mixed micelles start to form only in aqueous phase after the transition point. For different mixtures, the partitioning coefficient of each mixed surfactant component is barely affected by mixed molar ratio. The transition point can be interpreted as a characteristic of hydrophobicity of surfactant mixture. The higher the transition point, the less hydrophobicity of that mixture, and the less surfactant molecules partitioning into oil phase.

The model application is also extended to water-oil partitioning of other surfactants, as shown in Figs. 5.8(a) and 5.8(b) for mixed $C_{12}OE_{14}$ and $C_{12}OE_{30}$, Figs. 5.8(c) and 5.8(d) for mixed hexaoxyethylene nonyl phenyl ether (NPE_6) and octaoxyethylene nonyl phenyl ether (NPE_8), and Figs. 5.8(e) and 5.8(f) for mixed C_{16} and polyoxyethylene 20 cetyl ether ($C_{16}E_{20}$) in water-oil environments. As can be seen from Fig. 5.8(a), the predicted and experimental [19,29] surfactant (monomers) distribution in oil phase (trichloroethylene) for mixed $C_{12}OE_{14}$ and $C_{12}OE_{30}$ agree reasonably well. The ethoxylate group (EO) average per molecule in oil phase based on prediction agrees well experimental data whereas the experimental EO average is slightly higher in aqueous phase probably due to experimental error considering that EO average should never be

higher than 30. The partitioning into oil phase continues above the reported aqueous cmc value of 240 mg/L for the mixture [28], which is mainly because the selective partitioning of more hydrophobic component $C_{12}OE_{14}$ into oil phase. This is also accompanied by EO average increase in aqueous phase and decrease in oil phase relative to the initial EO average as indicated by the arrow in Fig. 5.8(b). An excellent agreement between the predicted and reported [32,46] monomeric surfactant distribution and molar fraction in micelles is observed in Figs. 5.8(c) and 5.8(d) for mixed NPE_6 and NPE_8 in equal volume of water/oil (cyclohexane) environment. When C_{tol} reaches $2\Gamma_{app}$ (Γ_{app} = $2.5x10^{-3}$ M), more hydrophilic micelles with a higher molar fraction of NPE_8 start to form, which seems to be contrary to the initial formation of more hydrophobic micelles of mixed BAC surfactants in the water-oil environments. By examining the apparent cmc of pure NPE_6 and NPE_8, however, it is found that NPE_8 has a lower apparent cmc ($2.89x10^{-3}$ M) than NPE_6 ($1.30x10^{-2}$ M) in water-oil environment. Therefore, it is expected that NPE_8 has a higher molar fraction in mixed micelles at the beginning of micelle formation. Similar interpretation is applicable to mixed $C_{12}OE_{14}$ and $C_{12}OE_{30}$ in water-oil phase.

It is interesting to note that when the surfactant distribution model is applied to nonhomologous mixed C_{16} and $C_{16}E_{20}$ in water-oil (heptane) environment, good agreement between experiment and model prediction is observed with respect to the monomer distribution in each phase. The aqueous phase cmc and partitioning coefficient are predicted from the developed the cmc submodel and the partitioning coefficient determination method as described earlier. The authors believe that this is the first time that the partitioning and distribution of nonhomologous mixed surfactants in oil-water environments are evaluated both theoretically and experimentally, which is actually

critical to industrial production process in terms of contamination control and investment minimization.

The apparent cmc of pure surfactant is effective in characterizing the hydrophobicity/hydrophilicity of that surfactant in water-oil environment. Thus it is summarized that the higher the apparent cmc of one surfactant, the higher the hydrophobicity, and thus the higher the mixed molar fraction in micelles of that surfactant. The micellar molar fraction α_i eventually approaches initial mixed molar ratio x_i as total concentration increases. It applies both to one-phase (water) and two-phase (water and oil) environment. All the surfactant mixtures discussed above follow this rule very well.

The effect of partitioning on corrosion inhibition efficiency of mixed surfactants was initially evaluated by the electrochemical measurements performed in an electrochemical glass cell which contains water and oil. The working electrode was exposed to aqueous phase only. At the partitioning equilibrium, the total monomer concentration C_m^w of surfactants in aqueous phase can be calculated using the surfactant distribution model. Considering the equilibrium between monomers in aqueous phase and the adsorbed monomers on steel surface, the corrosion inhibition efficiency can also be estimated using the modified Langmuir adsorption (MLA) model in Eq. (5.44)

$$\eta\,(\%) = 100 \cdot \theta = \left(1 - \frac{1}{1+K'\frac{C_m^w}{\Gamma^w}}\right) \times 100 \qquad 5.44$$

The comparison of predicted and experimental corrosion current density as a function of time of equal-molar mixed BAC surfactants (C12, C14, and C16) at C_{tol}=1.50x10^{-5} M with water/oil volume ratio of 2:1 is shown in Fig. 5.9(a). The experimental adsorption equilibrium was reached within 3 h and after that the corrosion current density remained

almost constant. The fluctuation is probably caused by the dynamic adsorption/desorption processes of surfactants. The predicted current density based on MLA, which agrees with the experimental current density at adsorption equilibrium, does not reflect the kinetics of surfactant adsorption but the equilibrium surface coverage and the associated corrosion inhibition efficiency.

The MLA model predicted results and experimental results of corrosion inhibition efficiency as a function of surfactant concentration is given in Fig. 5.9(b), in which the vertical line represents the transition concentration (C_{tol}=1.5Γ_{app}) at which micelles start to form. The predicted corrosion inhibition efficiency agrees with experimental data reasonably well. The slightly higher prediction of η (%) at C_{tol}<1.5Γ_{app} can probably be explained by the slight overestimation of monomer surfactants in bulk aqueous phase due to the neglect of the surfactants adsorbed at water/oil interface. On the other hand, η (%) is slightly underestimated at C_{tol}>1.5Γ_{app} due to micelle formation in water-oil environments where the MLA model is no longer applicable and the predicted η (%) becomes constant as C_{tol} increases. Please note that the molar ratio of mixed BAC surfactants in bulk aqueous phase at equilibrium, which is constant (0.58/0.37/0.05) at C_{tol}<1.5Γ_{app}, is different from the initial molar ratio which is 0.33/0.33/0.33, because of partitioning process. When C_{tol}>1.5Γ_{app}, the equilibrium mixed molar ratio in the bulk aqueous phase is not constant and changes with the change in C_{tol}. Therefore, the corresponding aqueous cmc of mixed surfactant changes as C_{tol} changes in the bulk aqueous phase.

The predicted corrosion inhibition efficiency based on the modified quantitative structure activity relation (MQSAR) for mixed BAC surfactants which is cited from

reported work [35] is also presented in Fig. 5.9(b) and is comparable to the experimental data and MLA prediction. The associated results are also summarized in Table 5.2.

5.5 Conclusions

1. One water-oil surfactant distribution model for the evaluation of the water-oil partitioning of surfactant is proposed and validated. This model is applicable over a wide total surfactant concentration range, including aqueous cmc, oil cmc, and apparent cmc. The surfactant distribution model, which is a combination of a surfactant partitioning submodel, a partitioning coefficient calculation method, and the developed cmc prediction submodel based on previous work, provides one potential tool to evaluate the partitioning of surfactant mixture (either homologous or nonhomologous) in water-oil environment. The model predicted data and experimental/reported data of surfactant distribution in water-oil environment agree very well.

2. For pure surfactant partitioning in water-oil environment, the equilibrium concentration in aqueous/oil phase of surfactant increases linearly with the initial concentration added to the system up to around the aqueous cmc value. Above the aqueous cmc, surfactant starts to accumulate and form micelles in either aqueous phase, oil phase, or both phases. It is confirmed that C_{12} and C_{14} form micelles in aqueous phase and C_{16} mainly in oil phase.

3. The temperature effect on the water-oil partitioning of C_{16} was also evaluated. K_{16} increases with increasing temperature. The calculated transfer free energy of head group is validated in the calculation of partitioning coefficients of BAC surfactants under various partitioning conditions.

4. Different methods to calculate partitioning coefficient are introduced, which includes an experimental measurement, a transfer free energy method, and a group contribution method. The experimental data and calculated data based on transfer free energy agree very well.

5. The mixed micelles start to form only after the transition point (apparent cmc of mixture) is reached in water-oil partitioning of mixed surfactants. The partitioning coefficient of each mixed surfactant component is barely affected by the bulk mixed molar ratio. The apparent cmc of surfactant mixture can be interpreted as a characteristic of hydrophobicity/hydrophilicity of that mixture. The higher the apparent cmc, the less hydrophobicity of that mixture, and the less surfactant molecules partitioning into oil phase.

6. The higher the apparent cmc of one surfactant in water-oil environment, the higher the hydrophobicity, and thus the higher the mixed molar fraction α_i in micelles of that surfactant at the initiation of micelle formation. The molar fraction α_i in micelles eventually approaches the initial bulk mixed molar ratio x_i as total concentration increases. It is applicable to both one-phase (water) and two-phase (water and oil) environments. The apparent cmc of pure surfactant can also explain the selective partitioning of mixed surfactants.

7. The effect of partitioning on corrosion inhibition efficiency of mixed surfactants was initially evaluated by modified Langmuir adsorption and by electrochemical measurements. The corrosion inhibition efficiency from the model prediction and from the experimental measurements is comparable.

Table 5.1 Standard transfer free energy of functional groups

surfactant	structure	functional group	organic phase	T (°C)	energy (kJ/mol)	Ref.
BAC	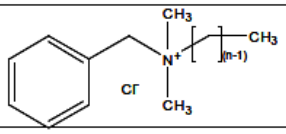	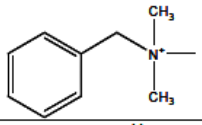	Toluene	40 50 60	55.3 53.9 52.4	Present work
Polyoxyethylene glycol n-dodecyl ether ($C_{12}En$)	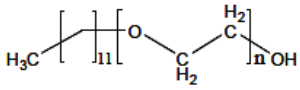	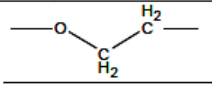 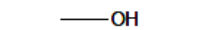	isooctane	25	2.61 15.5	24
Primary alcohol ethoxylate ($C_{12}OEn$)	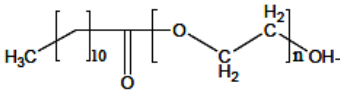	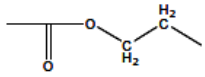 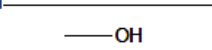	heptane	20	2.68 14.1	29,41,43
N-based alkyl amines and derivatives*	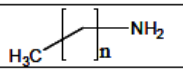	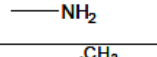	Heptane	20	11.5	Present work, 42-44
	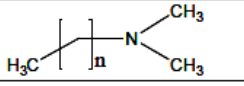	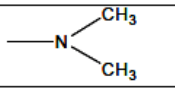			2.28	
	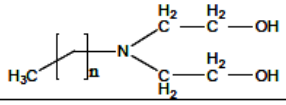	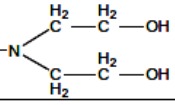			21.8	
	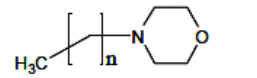	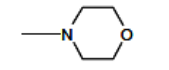			6.04	
	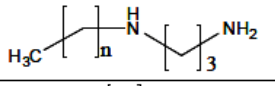	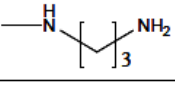			18.8	
	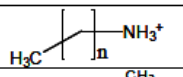	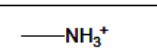			52.4	
	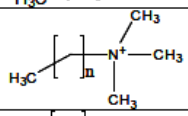	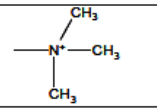			54.4	
	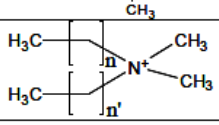	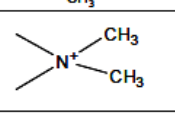			131	
Alkyl ether isosorbide (CnIso-endo/exo)	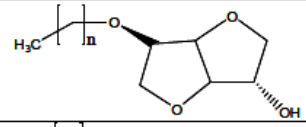	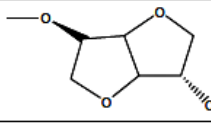	cyclohexane	25	27.1	25
	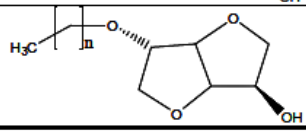	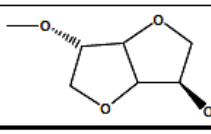			18.0	

Table 5.2 Equilibrium concentrations of total monomers in aqueous phase at partitioning equilibrium and the corrosion inhibition efficiency from electrochemical measurements and model prediction for equal-molar mixed BAC surfactants (C12, C14, and C16) in water (0.171 M NaCl)-toluene-steel electrode environments at 40 ℃. Volume of water and toluene are 80 mL and 40 mL, respectively.

Initial concentration C_{tol}, µM	Aqueous monomer concentration C_m^w, µM	η, %*			
		LPR	PDS	EIS	MLA Prediction
0.5	0.28	4	5	7	6
1	0.55	11	9	10	12
2.5	1.38	21	19	24	26
5	2.76	38	42	39	41
10	5.53	52	48	53	58
16	8.85	67	71	70	69
55	27.6	87	90	90	88
100	55.3	96	95	97	93
250	80.6	98	97	98	93
500	102	99	98	99	93

* Each experimental test was repeated at least three times as an independent measurement within deviation of +/- 3%. Average anodic (58 mV dec^{-1})) and cathodic (220 mV dec^{-1}) Tafel slopes were used in corrosion current density calculation which were estimated from potentiodynamic scan curves using the reported method [34].

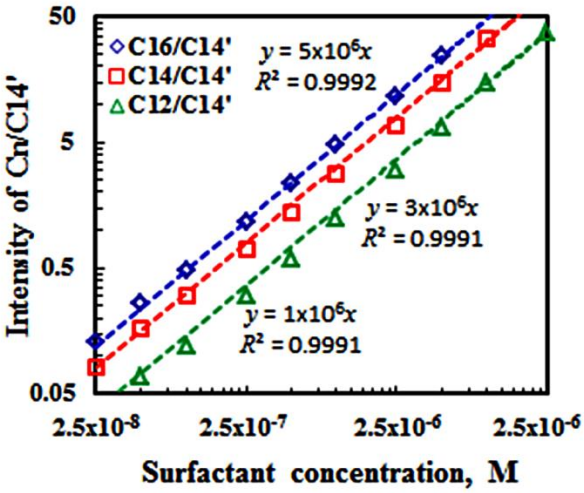

Fig. 5.1 Calibration curves with internal reference for the three homologous BAC surfactants between the concentration of 2.5×10^{-8} M and 2.5×10^{-5} M.

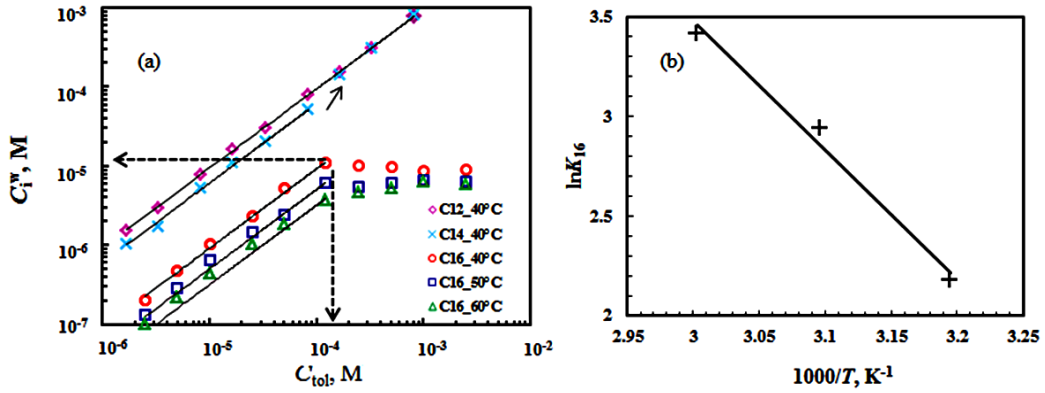

Fig. 5.2 Equilibrium concentration C_i^w vs. initial concentration C_{tol} of pure BAC surfactants in 0.171 NaCl aqueous phase at equilibrated water-oil partitioning at different temperatures (a) and partitioning coefficient of C16 vs. $1/T$ (b). Solid lines in (a) are linear fitting before micellization for the determination of partitioning coefficient. Arrow indicates linear-to-nonlinear transition for C14. Solid line is linear fitting (b).

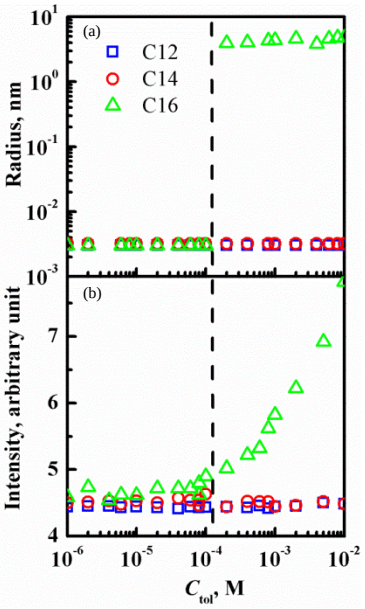

Fig. 5.3 Dynamic light scattering testing results of C12, C14, and C16 from the sampled oil phase after water-oil partitioning equilibrium of pure BAC surfactants: (a) particle radius (b) dimensionless intensity vs. initial concentration of surfactants added to water. Dash line indicates micelle formation concentration. C_{tol} here represents concentration of pure surfactant.

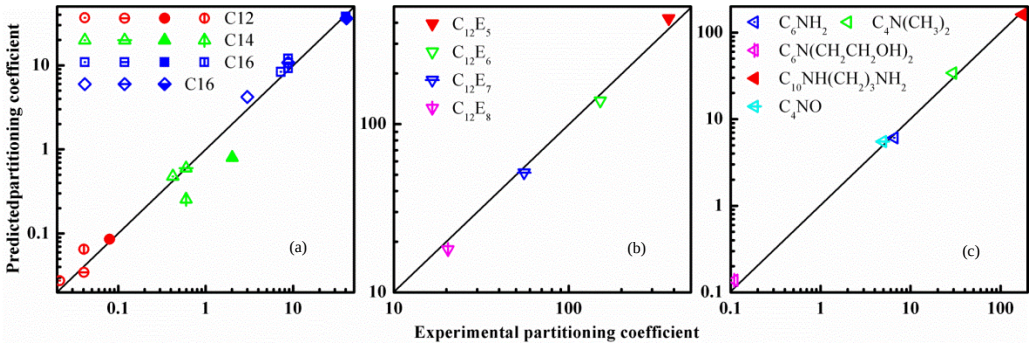

Fig. 5.4 Comparison of predicted partitioning coefficient and experimental partitioning coefficient. (a) Pure C12, C14, and C16 partitioning in water and oil environment at 40 ℃. Open symbols with vertical center cross line: transfer free energy calculated using Method II; all other symbols: transfer free energy calculated using Method I. Open symbols: 0 M NaCl water and oil partitioning; open symbols with center dot: 0.0342 M NaCl water and oil partitioning; open symbols with (vertical and horizontal) center cross line: 0.171 M NaCl water and oil partitioning; half-filled symbols: 0.804 M NaCl water and oil partitioning; solid-filled symbols: 0.856 M NaCl water and oil partitioning. All diamond symbols: literature reported data [33]. (b) Polyoxyethylene glycol n-dodecyl ether ($C_{12}E_n$) partitioning in pure water and isooctane environment at 25 ℃ [24]. (c) Alkyl amines partitioning in 0.1 M NaOH water and heptane at 20°C [41]. "–NO" see Table 5.1.

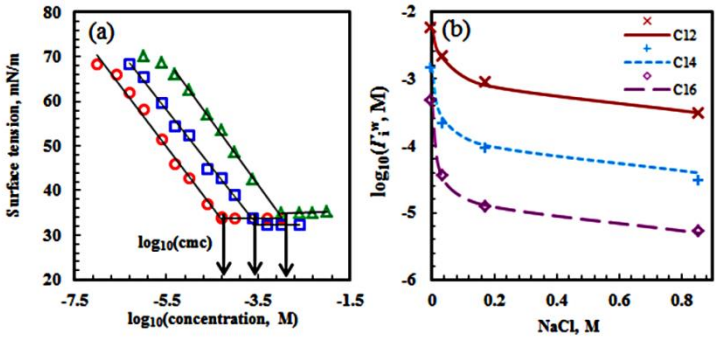

Fig. 5.5 Plots of surface tension vs. concentration of surfactants (a): triangle—C12 in 0.171 M NaCl aqueous solution at 40 ℃; square—C12 in 0.856 M NaCl aqueous solution at 40 ℃; circle--mixed C12, C14, and C16 at molar ratio of 0.15/0.70/0.15 in 0.171 M NaCl aqueous solution at 40 ℃. The aqueous cmc value is indicated by the arrow. Aqueous phase cmc of pure BAC surfactants as a function of NaCl concentration in solution at T = 40 ℃ (b). Symbols represent experimental values; lines represent predicted values in (b) [34,35].

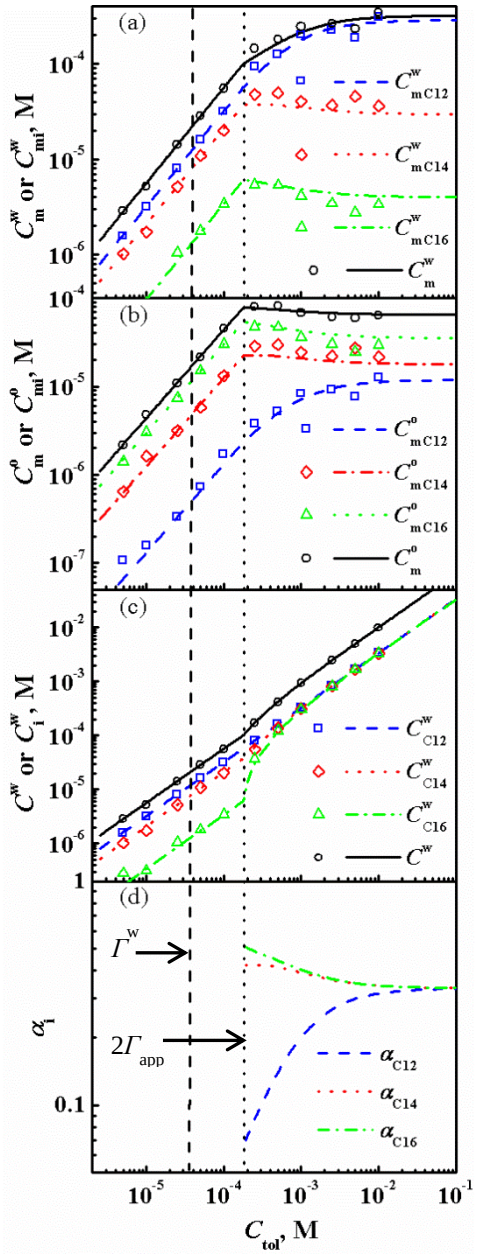

Fig. 5.6 Equilibrium partitioning properties of equal-molar mixed BAC surfactants (C12, C14, and C16) in water (0.171 M NaCl)-oil environments at 40 ℃: (a) equilibrium concentration of monomeric surfactants in water, (b) in oil, (c) equilibrium concentration of total surfactants in water, including monomer and micellized form, and (d) micelle composition of surfactant i as functions of total initial concentration of surfactants added to water. Symbols: experiment; lines: model prediction. Vertical dash line represents the cmc of surfactant mixture in aqueous phase: Γ^w; vertical dot line represents twice of the apparent cmc of surfactant mixture in water-oil environment: $2\Gamma_{app.}$

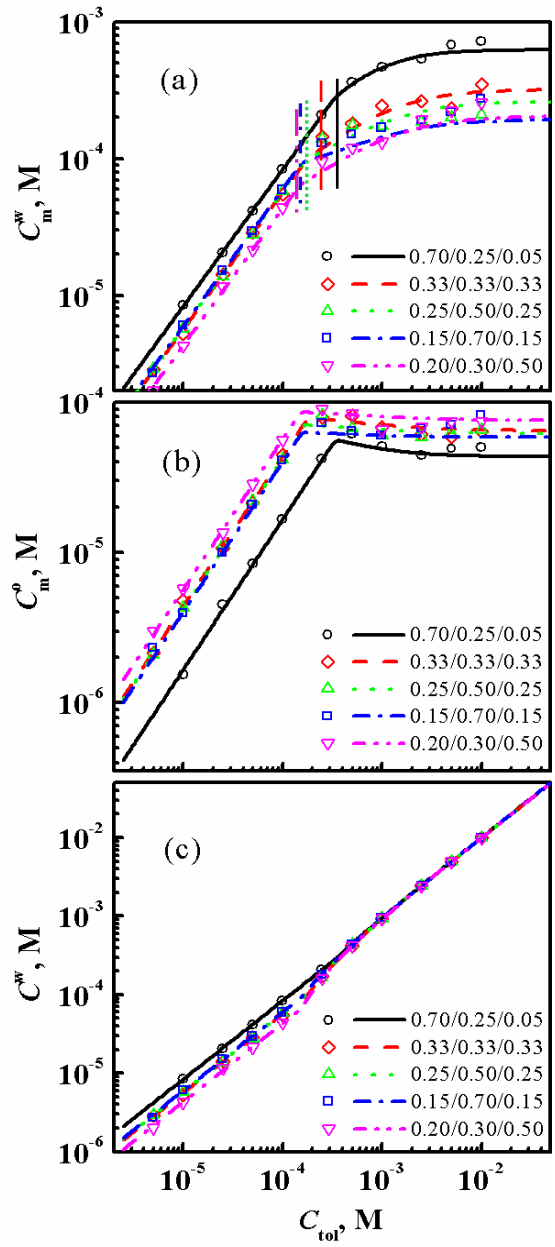

Fig. 5.7 Equilibrium partitioning properties of mixed BAC surfactants (C12, C14, and C16) at various mixed molar ratios in water (0.171 M NaCl) - oil environments at 40 ℃: (a) equilibrium concentration of total monomeric surfactants in water, (b) in oil, (c) equilibrium concentration of total surfactants, including monomer and micellized form, in water as functions of total initial concentration of surfactants added to water. Symbols: experiment; lines: model prediction. Legend represents various mixed molar ratios of C12/C14/C16. Vertical lines in (a) indicate $2\Gamma_{app}$ for each mixture.

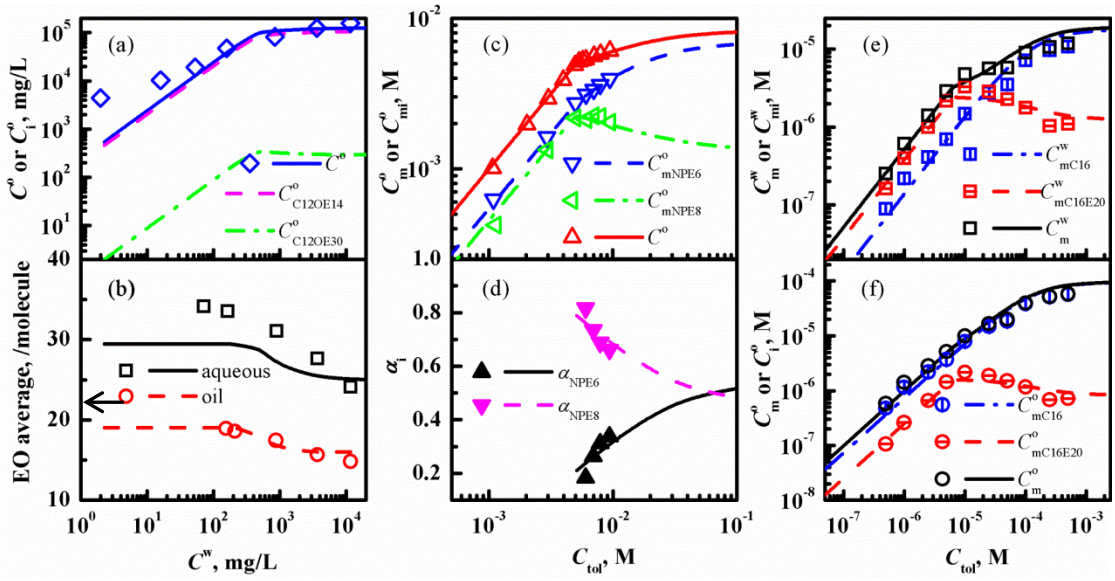

Fig. 5.8 Comparison between predicted and experimental partitioning properties of surfactants. (a) and (b) are equilibrium partitioning properties of mixed $C_{12}OE_{14}$ and $C_{12}OE_{30}$ surfactants in water-oil (trichloroethylene) environments at 25 ℃: (a) concentration of surfactants (b) average ethoxylate group (EO) distribution in aqueous and oil phase as a function of equilibrium aqueous concentration C^w. The values of aqueous cmc are 123.2 mg/L and 560 mg/L for $C_{12}OE_{14}$ and $C_{12}OE_{30}$, respectively. Mixed ratio: 0.475/0.525. The arrow in (b) indicates the initial EO average in water-oil environment. (c) and (d) are equilibrium partitioning properties of mixed NPE_6 and NPE_8 surfactants in water-oil (cyclohexane) environments at 25 ℃: (c) concentration of monomeric surfactants in oil phase (d) molar fraction of surfactants in mixed micelles as a function of C_{tol}. The values of aqueous cmc and partitioning coefficients are 2.70×10^{-5} M and 4.05×10^{-5} M, and 481 and 70 for NPE_6 and NPE_8, respectively. Mixed ratio: 0.542/0.458. Water/oil volume ratio: 1/1. (e) and (f) are equilibrium partitioning properties of mixed C16 and $C_{16}E_{20}$ surfactants in water-oil (heptane) environments at 25 ℃: (e) concentration of monomeric surfactants in 0.03 M NaCl aqueous phase (f) in oil phase as a function of C_{tol}. The predicted values of aqueous cmc and partitioning coefficients from previous work are 3.61×10^{-5} M and 2.47×10^{-6} M, and 5.32 and 0.66 for C16 and $C_{16}E_{20}$, respectively. Mixed ratio: 0.542/0.458. Water/oil volume ratio: 2/1. Lines: model prediction; symbols: reported data. Reported data in Figs. 5.8(a)-5.8(d) are cited from literature [19,29,32,51].

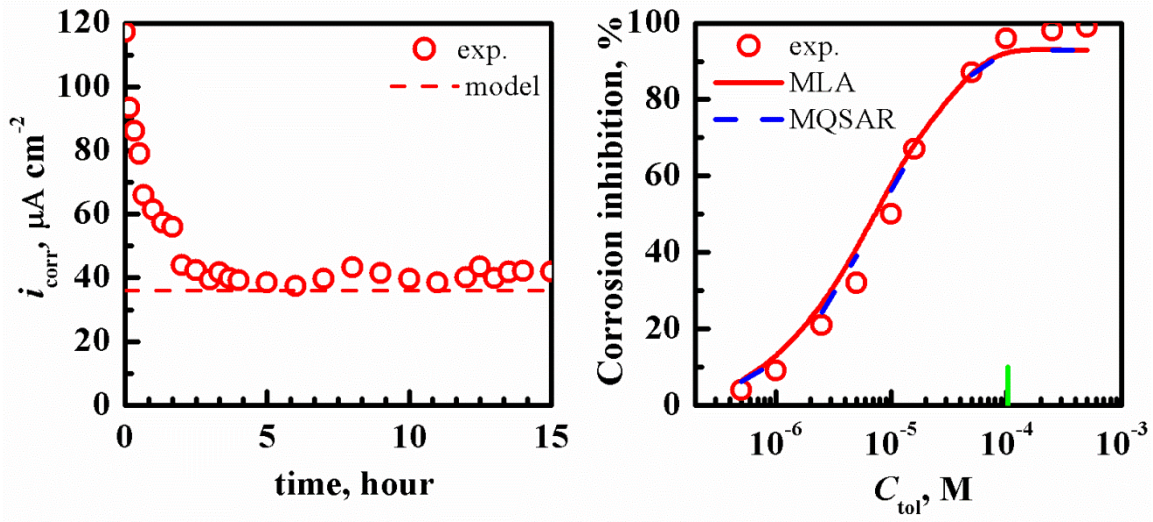

Fig. 5.9 Comparison of predicted and experimental corrosion current density as a function of time of equal-molar mixed BAC surfactants (C12, C14, and C16) at C_{tol}=1.50x10^{-5} M with water/oil volume ratio of 2:1 (a) and comparison of predicted inhibition efficiency from MLA and MQSAR and experimental inhibition efficiency on steel corrosion of mixed surfactant systems in water-oil environment (b). Symbols: experiment; curves: prediction. Vertical line indicates the transition potion at C_{tol}=1.5Γ_{app}, where micelles form in water-oil environments. K'=13.74 in MLA model for mixed BAC surfactants [34]. The quantum descriptors of mixed BAC surfactants are molar-based average values of the reported quantum descriptors of pure BAC surfactants and regression coefficients in MQSAR are reported values [35].

5.5 References

[1] M. J. Rosen, Surfactants and Interfacial Phenomena, 3rd ed. Wiley: New York, 2004.

[2] A. Kokalj, S. Peljhan, M. Finsgar, I. Milosev, J. Am. Chem. Soc. 132 (2010) 16657.

[3] M. L. Free, Corrosion. Sci. 46 (2004) 3101.

[4] C. D. Taylor, A. Chandra, J. Vera, N. Sridhara, J. Electrochem. Soc. 162 (2015) C347.

[5] X. Ye, C. Zheng, J. Chen, Y. Gao, C. B. Murray, Nano Lett. 13 (2013) 765.

[6] M. J. Rosen, Q. Zhou, Langmuir 17 (2001) 3532.

[7] B. Kronberg, Curr. Opin. Colloid Interface Sci. 2 (1997) 456.

[8] L. Wolf, H. Hoffmann, K. Watanabeb, T. Okamotob, Phys. Chem. Chem. Phys. 13 (2011) 3248.

[9] I. M. Zin, S. B. Lyon, V. I. Pokhmurskii, Corrosion Sci. 45 (2003) 777.

[10] Sonu, A. K. Tiwari, S. K. Saha, Ind. Eng. Chem. Res. 52 (2013) 5895.

[11] R. Fuchs-Godec, Electrochim. Acta 54 (2009) 2171.

[12] D. Gelman, D. Starosvetsky, Y. Ein-Eli, Corrosion Sci. 82 (2014) 271.

[13] M. Ben Ghoulam, N. Moatadid, A. Graciaa, J. Lachaise, Langmuir 20 (2004) 2584.

[14] A. Graciaa, J. Andérez, C. Bracho, J. Lachaise, J. Salager, L. Tolosa, F. Ysambertt, Adv. Colloid Interface Sci. 123-126 (2006) 63.

[15] S. Endo, K. Goss, Environ. Sci. Technol. 48 (2014) 2776.

[16] J. Salager, N. Marquez, A. Graciaa, J. Lachaise, Langmuir 16 (2000) 5534.

[17] J. Gomez del Rio, D. Hayes, V. S. Urban, J. Colloid Interface Sci. 352 (2010) 424.

[18] E. H. Crook, D. B. Fordyce, G. F. Trebbi, J. Colloid Interface Sci. 20 (1965) 191.

[19] T. C. G. Kibbey, L. Chen, Colloids Surf. A: Physicochem. Eng. Aspects 326 (2008) 73.

[20] B. W. Brooks, H. N. Richmond, J. Colloid Interface Sci. 162 (1994) 59.

[21] B. W. Brooks, H. N. Richmond, J. Colloid Interface Sci. 162 (1994) 67.

[22] J. L. Salager, N. Marquez, R. E. Anton, A. Graciaa, J. Lachaise, Langmuir 11 (1995) 37.

[23] F. Ravera, M. Ferrari, L. Liggieri, R. Miller, A. Passerone, Langmuir 13 (1997) 4817.

[24] M. Ben Ghoulam, N. Moatadid, A. Graciaa, J. Lachaise, Langmuir 18 (2002) 4367.

[25] Y. Zhu, V. Molinier, M. Durand, A. Lavergne, J. Aubry, Langmuir 25 (2009) 13419.

[26] A. Van de Voorde, C. Lorgeous, M. Gromaire, G. Chebbo, Environ. Pollution 164 (2012) 150.

[27] G. G. Warr, F. Grieser, T. W. Healy, J. Phys. Chem. 87 (1983) 4520.

[28] A. Graciaa, J. Lachaise, J. G. Sayous, P. Grenier, S. Yiv, R. S. Schechter, W. H. Wade, J. Colloid Interface Sci. 93 (1983), 474.

[29] M. A. Cowell, T. G. C. Kibbey, J. B. Zimmerman, K. F. Hayes, Environ. Sci. Technol. 34 (2000) 1583.

[30] M. Balcan, D. Anghel, Colloid Polym. Sci. 283 (2005) 982.

[31] V. Pradines, S. Despous, C. Claparols, N. Martins, J. Micheau, D. Lavabre, V. Pimienta, J. Phys. Org. Chem. 19 (2006) 350.

[32] F. Harusawa, T. Saito, H. Nakajima, S. Fukushima, J. Colloid Interface Sci. 74 (1980) 435.

[33] P. Alaei, B. P. Binks, P. D. I. Fletcher, NACE Corrosion Conference, 2013, Orlando, Paper No. 2158.

[34] Y. Zhu, M. L. Free, G. Yi, Corrosion Sci. 98 (2015) 417.

[35] Y. Zhu, M. L. Free, G. Yi, J. Electrochem. Soc. 168 (2015) C582.

[36] J. F. Zemaitis, D. M. Clark, M. Rafal, N. C. Scrivner, Handbook of Aqueous Electrolyte Thermodynamics, AlChE, New York, 1986.

[37] K. S. Pitzer, Activity Coefficients in Electrolyte Solutions, 2nd ed., CRC Press, Boca Raton, 1991.

[38] J. N. Butler, Ionic Equilibrium: Solubility and pH Calculations, Wiley, New York, 1998.

[39] R. P. Schwarzenbach, P. M. Gschwend, D. M. Imboden, Environmental Organic Chemistry, 2nd ed., John Wiley and Sons, New York, 2001.

[40] L. Moreira, A. Firoozabadi, Langmuir 26 (2010) 15177.

[41] T. C. G. KIBBEY, K. F. HAYES, Environ. Sci. Technol. 31 (1997) 1171.

[42] J. M. Pollard, A. J. Shi, K. E. Goklen, J. Chem. Eng. Data 51 (2006) 230.

[43] A. D. James, J. M. Wates, E. W. Jones, J. Colloid Interface Sci. 160 (1993) 158.

[44] F. A. Vilallonga, R. J. Koftan, J. P. O'Connell, J. Colloid Interface Sci. 90 (1982) 539.

[45] G. Klopman, H. Zhu, J. Chem. Inf. Comput. Sci. 41 (2001) 439.

[46] M. Feig, Modeling Solvent Environments: Applications to Simulations of Biomolecules, 1st ed., Wiley, 2010.

[47] R. Aveyard, B. P. Binks, S. Clark, P. D. I. Fletcher, J. Chem. Soc. Faraday Trans. 1 86 (1990) 3111.

[48] R. Aveyard, B. P. Binks, S. Clark, J. Mead, J. Chem. Soc. Faraday Trans. 1 82 (1986) 125.

[49] R. Tadmouri, C. Zedde, C. Routaboul, J. C. Micheau, V. Pimienta, J. Phys. Chem. B 112 (2008) 12318.

[50] R. Nagarajan, E. Ruchenstein, Langmuir 7 (1991) 2934.

[51] F. Harusawa, M. Tanaka, J. Phys. Chem. 85 (1981) 882.

CHAPTER 6

INTEGRATED MODELING OF SURFACTANT CORROSION INHIBITION*

6.1 Introduction

Carbon steel is one of the most widely used metals in production and transportation in the oil and gas industries [1-3]. However, carbon steel is highly susceptible to corrosive environments that contain water, CO_2, H_2S, and various ions (such as Cl^-), etc. [4,5]. The presence of CO_2 in oil pipe lines exposes carbon steel components to substantial damage due to the accelerated corrosion, which eventually threatens production and safety [4,6,7]. An illustrated example of corroding sample, a piece of X65 steel used in oil pipeline, is shown in Fig. 6.1(a).

Various methods for CO2-related corrosion control have been developed. One of these methods is to use surfactant inhibitors, which contain heterocyclic molecules to reduce corrosion, and has proven to be economical and effective [1-4,8,9]. Surfactant mixtures have been used in wide ranging applications due to their superior physicochemical properties and capabilities in efficient solubilization, dispersion, suspension, and transportation [4,10,11]. Surfactant mixtures can often be conveniently tuned to achieve desired properties by adjusting surfactant type and mixture ratios [12]. Many of the organic inhibitors are surfactants with hydrophilic and hydrophobic

* Manuscript submitted.

molecular sections which increases the complexity of their use in water-oil-steel pipe (WOS) environments.

The hydrophilic portion of surfactants strongly favors interactions with polar entities such as water, metals, and ions, which facilitates the adsorption of surfactants on metal surfaces, blocks active surface sites, and thereby protects metal from corrosion [8,9]. On the other hand, surfactant molecules tend to escape from polar aqueous phase and adsorb at surfaces and interfaces by associating and aggregating hydrocarbon chains together [9,13].

Upon addition of surfactants to WOS environments, the inhibition performance of surfactants is usually affected by different phenomena (see Figs. 6.1(b) and 6.1(c)) such as surfactant partitioning between oil and water, micellization, surfactant-corrosion product precipitation, adsorption/desorption, fluid flow, surfactant-solvent interactions, surfactant-counterion pairing, and lateral interactions between surfactant molecules. These phenomena are incorporated into three main processes: partitioning between oil and water, micellization/precipitation, and effective adsorption on metal surface and water/oil interface. Fluid flow is simulated using rotating disc test. The last three phenomena in the domain of multilayer/micelle-water interfaces can be incorporated into effective adsorption processes using associated modeling. Note that the critical micelle concentration (cmc) is defined as the concentration at which surfactant molecules start to form micelles (the apparent cmc is defined as the average concentration of mixed surfactants at which mixed micelles start to form for WOS environments, the aqueous cmc for the aqueous phase, and the oil cmc for the oil phase). When surfactant concentration reaches the cmc, bilayers/multilayers/micelles adsorb on metal surface and

micelles also form in water phase or oil phase or both phases [14]. The steel corrosion inhibition is directly determined by the monomeric surfactant adsorption and effective coverage on steel [4,8,9] The adsorption process, however, is affected by the other two main processes: partitioning and micellization, which tend to deplete monomeric surfactants available for the adsorption and effective coverage on steel. Therefore, it is necessary to consider these three main processes simultaneously for a systematic evaluation and modeling of steel corrosion inhibition using mixed surfactants in WOS environments.

Extensive research work has been performed in each of these processes [15-21]. Regarding partitioning, however, the research over a wider surfactant concentration range (above and below the apparent cmc) of various mixed homologous/nonhomologous surfactants has not been systemically reported [14]. A comprehensive theory or model to adequately describe the effects of ions and binding mechanisms on micellization of mixed surfactants over a wide concentration range of salt has not been well developed [4,17,18]. At present, the modeling of corrosion inhibition efficiency of surfactant inhibitors is limited to traditional methods, including Langmuir adsorption isotherm, quantitative structure activity relation (QSAR), and combined QSAR and mechanistic approaches etc. [19-21], each of which is at different stages of maturity and has potential limitations.

With these points in mind, one multiphysics model, integrated corrosion inhibition (ICI) model, in this work, has been provided for the modeling and prediction of corrosion inhibition efficiency of mixed surfactant inhibitors based on a few previously developed submodels, including the water-oil surfactant distribution submodel [14], the aqueous

cmc prediction submodel [4,22,23], and the modified Langmuir adsorption (MLA) submodel and modified QSAR (MQSAR) submodel [4,14]. The developed ICI model has been validated using existing experimental data and literature reported results, which demonstrate the robustness of this approach to corrosion inhibition prediction.

6.2 Framework of ICI model

At the partitioning equilibrium, all of the mixed surfactants in WOS environments should conform to a mass balance equation

$$M_{\mathrm{tol}} = M_{\mathrm{w}} + M_{\mathrm{o}} + M_{\mathrm{ad}} \tag{6.1}$$

where M_{tol} is the total quality of all surfactants added to the WOS environments, M_{w} is the surfactants (both monomeric and micellar forms) distributed in the water phase, M_{o} is the surfactants (both monomeric and micellar forms) distributed in the oil phase, and M_{ad} is the surfactants adsorbed on steel surface and water/oil interface. The amount of surfactants adsorbed on the water-oil interface is unlikely to significantly impact the mass balance [24] and thus has become neglected in Eq. (6.1). Similarly, the amount of adsorbed surfactants in the form of monolayer, bilayers, multilayers, and micelles on steel surface is also negligible. Therefore, Eq. (6.1) can be simplified to the following format without the compromise of surfactant mass balance in WOS environments. The model predicted results based on Eq. (6.1) and Eq. (6.2) are compared and the difference (< 3%) is negligible.

$$M_{\mathrm{tol}} = M_{\mathrm{w}} + M_{\mathrm{o}} \tag{6.2}$$

Alternatively, the equivalent form of Eq. (6.2) is given by the water-oil surfactant distribution submodel (details can be found elsewhere) as follows [14]

$$C_{\mathrm{tol}}V_{\mathrm{w}} = \bar{C}\ (V_{\mathrm{w}} + V_{\mathrm{o}}) \tag{6.3}$$

where C_{tol} is the initial concentration (not at equilibrium) of total surfactants added to aqueous phase. $\bar{C}$ is the overall average concentration of total surfactants in water and oil phases. V_{o} and V_{w} are volumes of oil and water, respectively.

With this developed surfactant distribution submodel, the apparent cmc of mixed surfactants in WOS environments (Γ_{app}), the apparent partitioning coefficient of the mixture (K_{mix}), monomer concentration of surfactant 'i' in water and in oil phase ($C_{\mathrm{mi}}^{\mathrm{w}}$ and $C_{\mathrm{mi}}^{\mathrm{o}}$), and molar fraction of surfactant i in mixed micelles (α_{i}), can be predicted at given inputs which include partitioning coefficient K_{i} and the aqueous cmc Γ_i^w of pure surfactant 'i' at given C_{tol} and mixed surfactant molar ratio x_{i} in bulk solution. K_{i} can be determined by the Partitioning Coefficient Determination Method which is developed and validated in previous work [14]. The aqueous cmc of pure and mixed surfactants in salt solution can be calculated using the traditional cmc submodel [4] or more advanced molecular thermodynamic cmc submodel [22,23]. The thermodynamic framework of the latter cmc submodel is briefly described below.

The aqueous cmc of pure surfactant i (Γ_i^w), or of surfactant mixture (Γ^w), is calculated using the equation below (Γ^w is used for illustration) [22,23]

$$\Gamma^{\mathrm{w}} = (C_{\mathrm{mw}} + C_{\mathrm{s}})\exp^{\left(\frac{1}{kT}\Delta\mu_{\mathrm{m}}^{\mathrm{o}}\right)} \tag{6.4}$$

where C_{mw} is molar concentration of water, C_{s} is concentration of salt, k is Boltzmann constant, T is temperature, and $\Delta\mu_{\mathrm{m}}^{\mathrm{o}}$ is micellization free energy which is calculated from several contributing thermodynamic terms.

$$\Delta\mu_{\mathrm{m}}^{\mathrm{o}} = \Delta\mu_{\mathrm{trt}}^{\mathrm{o}} + \Delta\mu_{\mathrm{int}}^{\mathrm{o}} + \Delta\mu_{\mathrm{pack}}^{\mathrm{o}} + \Delta\mu_{\mathrm{st}}^{\mathrm{o}} + \Delta\mu_{\mathrm{ent}}^{\mathrm{o}} + \Delta\mu_{\mathrm{elec}}^{\mathrm{o}} + \Delta\mu_{\mathrm{act}}^{\mathrm{o}} \tag{6.5}$$

The first three terms on the right side of Eq. (6.5) are associated with the packing and

interactions of hydrocarbon tails and the formation of the hydrophobic micellar core: $\Delta\mu^{o}_{trt}$, $\Delta\mu^{o}_{int}$, and $\Delta\mu^{o}_{pack}$ represent free energy contributions from hydrocarbon transfer from water into the micelle, formation of the micellar core-water interface, and hydrocarbon tail packing in the micelle, respectively. The next three terms are associated with surfactant headgroups and counterions in the micelle-water interfacial region: $\Delta\mu^{o}_{st}$, $\Delta\mu^{o}_{ent}$, and $\Delta\mu^{o}_{elec}$ represent surfactant headgroup steric interactions, headgroup-counterion mixing, and electrostatic interactions, respectively [17,18,22,23]. The last term $\Delta\mu^{o}_{act}$ represents the contribution from surfactant activity and counterion activity in the bulk solution [22,23].

The micellization free energy as a function of a few variables, which include micelle radius, micelle composition, micelle shape, and counterion binding coefficient, is minimized at known solution conditions using home-designed MATLAB code, and is then used to calculate the aqueous cmc, aggregation number, and sphere-to-rod transition.

The aqueous cmc at partitioning, adsorption, and aggregation equilibrium is critical in the evaluation of corrosion inhibition efficiency of surfactants. Therefore, MLA is introduced by incorporating the aqueous cmc to evaluate surfactant adsorption and inhibition performance under various solution conditions and is presented below [4, 22]

$$\frac{1}{1-\theta} = 1 + K' \frac{C^{w}_{m}}{\Gamma^{w}}, (C^{w}_{m} \leq \Gamma^{w}) \qquad 6.6$$

where θ is effective surface coverage that is assumed to be equal to corrosion inhibition. K' is equal to the equilibrium adsorption constant K_{ad} multiplied by Γ^{w}, C^{w}_{m} is concentration of total monomers in aqueous phase and is determined from the surfactant distribution submodel. The advantage of MLA is that the incorporation of the cmc submodel considers the ion effect on aggregation/adsorption, the effect of chain length,

van der Waals interactions between surfactant molecules, headgroup steric interactions, and electrostatic interactions at interfacial region etc. [18,22,25], thereby making it very useful in inhibition prediction over a wide range of conditions.

Based on the described ICI model and associated submodels, a schematic flow chart is presented in Scheme 1 to illustrate how corrosion inhibition efficiency $\eta(\%)$ of mixed surfactants in WOS environments is predicted. First, given a corrosive environments of WOS, mixed surfactants are added to aqueous phase. At the equilibrium of surfactant partitioning, aggregation, and adsorption, the surfactant distribution submodel combined with the cmc submodel is then used to calculate equilibrium monomeric concentration of each mixed surfactant component i in water and oil phases. The MLA submodel and the cmc submodel along with the calculated results from previous steps are used to evaluate surfactant adsorption/coverage on steel surface. Finally, $\eta(\%)$ is predicted using Eq. (6.7) with the assumption of effective surface coverage (mainly due to self-assembled monolayer) equal to inhibition [2,4,9]. The validation of developed ICI model and associated comparison to experimental data which are obtained from testing systems listed in Table 6.1 are as follows.

$$\eta\ (\%) = 100 \cdot \theta = \left(1 - \frac{1}{1+K'\frac{C_{\mathrm{m}}^{w}}{\Gamma^{w}}}\right) \times 100 \qquad 6.7$$

6.3 Validation of ICI model

It is found that the all the predicted aqueous cmc values of various pure surfactants and associated mixtures match experimental data very well in Figs. 6.2(a) and 6.2(b). Note that for each surfactant mixture in Fig. 6.2(b), the aqueous cmc varied before (solid symbol) and after (open symbol) partitioning due to the change in bulk mixed molar ratio

of surfactants, which is originally caused by the partitioning of a certain amount of surfactants into oil phase. Considering the partitioning coefficient of each surfactant is constant, the new aqueous cmc Γ^{w} is constant if no micelle formation occurs in WOS environments ($\bar{C} < \Gamma_{app}$ or $C_{tol} \leq 1.5\Gamma_{app}$ in the case of V_o/V_w = 1/2). The new Γ^{w} would vary as a function of C_{tol} if $C_{tol} > 1.5\Gamma_{app}$ where the bulk mixed molar ratio is affected by both partitioning and micellization. Eventually, the change in the micellar mixed molar ratio as a function of C_{tol} leads to the change in the bulk mixed molar ratio.

The predicted K_i in Fig. 6.2(c) is based on the following equation [14]

$$K_i = \frac{\gamma_{mi}^{w} C_{mo}}{\gamma_{mi}^{o} C_{mw}} \exp\left(-\frac{\Delta\mu_{tri}^{o}}{RT}\right) \qquad 6.8$$

where γ_{mi}^{o} and γ_{mi}^{w} are activity coefficients of monomeric surfactant 'i' in oil phase and water phase, respectively. γ_{mi}^{o} is assumed to be unity. γ_{mi}^{w} is calculated using Pitzer's method to take into account the effect of dissolved salt in water on the partitioning process [4,27]. C_{mo} and C_{mw} are molar concentrations of oil and water, respectively. The standard free energy change $\Delta\mu_{tri}^{o}$ of surfactant i transfer from water to oil is estimated from the free energy transfer method [14]. An excellent agreement is observed between predicted and experimental values of K_i in Fig. 6.2(c).

This study is the first time the partitioning of nonhomologous ternary mixed surfactants in water-oil environments has been evaluated both experimentally and theoretically (see Fig. 6.3 for Testing System iv). The partitioning of each mixed surfactant component 'i' as well as the overall partitioning continues without any change when C_{tol} increases from zero to $1.5\Gamma_{app}$ (note that $1.5\Gamma_{app} > \Gamma^{w'}$), which is consistent with the reported partitioning behavior of mixed homologous surfactants [24,28]. The corresponding new aqueous cmc Γ^{w} at partitioning equilibrium is also indicated in the

figure, which, along with the total monomer concentration in aqueous phase $C_{\mathrm{m}}^{\mathrm{w}}$, will be used for corrosion inhibition prediction using Eq. (6.7).

Above $1.5\Gamma_{app}$ the partitioning behavior of surfactant 'i' experiences changes as a function of C_{tol}. The monomer concentration of $C_{16}E_{20}$, for example, in aqueous phase and oil phase reaches a maximum followed by a slight decrease due to the consumption of most monomeric $C_{16}E_{20}$ by the micelle formation in aqueous phase (see Fig. 6.3(c)). The much higher micellar molar fraction of $C_{16}E_{20}$ at the initial stage of micelle formation (Fig. 6.3(d)) can be explained by its lower apparent cmc in water-oil environments ($2.19\text{x}10^{-6}$ M) than that of the other two mixed components ($1.28\text{x}10^{-4}$ M for C_{16}TAB and $8.81\text{x}10^{-5}$ M for C_{16}) and thus, $C_{16}E_{20}$ in micellar form is generally more thermodynamically stable than in monomeric form [14]. As C_{tol} increases, the micellar molar ratio of the three surfactants approaches the initial bulk mixed molar ratio, which leads to the leveling off of monomeric surfactant concentration in water and oil phases.

Fig. 6.4(a) presents the corrosion current density of surfactant mixture ($C_{tol}=1.50\text{x}10^{-5}$ M) in Testing System i as a function of time. The concentration of $C_{tol}=1.50\text{x}10^{-5}$ M which is slightly less than $\Gamma^{w'}$ and a lot less than $1.5\Gamma_{app}$ assures of the absence of micelles in the tested environments (both aqueous phase without oil and WOS environments) and thus assures the applicability of ICI model to the discussed testing system. The predicted current density for this testing system agrees with the experimental data reasonably well. The slight underestimation in the presence of oil is probably due to the slight overestimation of monomeric surfactants present in bulk aqueous phase because of the neglect of corrosion product-surfactant precipitates and adsorbed surfactants at water-oil interface. The overall prediction of corrosion inhibition efficiency

as a function of C_{tol} matches experimental data well for all testing systems, as shown in Fig. 6.4(b). The slightly higher prediction of η (%) at $C_{tol}<1.5\Gamma_{app}$ can be explained by the same reason for the underestimation of corrosion current density mentioned previously. On the other hand, η (%) is slightly underestimated at $C_{tol}>1.5\Gamma_{app}$ due to micelle formation in WOS environments where the ICI model is no longer applicable and the predicted η (%) becomes constant as C_{tol} increases. In reality, η (%) should still increase with C_{tol} increasing due to potential extra steel surface coverage by multilayers/micelles. However, η (%) is usually high enough (provided the discussed surfactants act as good inhibitors) around $C_{tol}=1.5\Gamma_{app}$, where monolayer covers steel surface well and multilayer/micelle coverage does not contribute much to additional corrosion inhibition [4,9,22]. Therefore, experimental data are only slightly higher than the prediction.

6.4 Summary

In summary, one multiphysics model, ICI model, is theoretically developed and experimentally validated for the evaluation of partitioning, aggregation, adsorption, and corrosion inhibition of mixed surfactant inhibitors (both homologous and nonhomologous) in water (containing salt)-oil-steel pipe environments for the first time. The framework of ICI model is based on three associated submodels which actually take into account water-oil surfactant partitioning, micellization, effective adsorption/desorption on substrate, surfactant-solvent interactions, surfactant-counterion pair, and lateral surfactant interactions etc., and serves as a basic framework for development of a more powerful predictive overall model/tool in the understanding of design, selection, optimization, and

utilization of various pure and mixed surfactant inhibitors with a focus on the application in salt-containing WOS environments.

The ICI model, however, has a few limitations and still needs improvements in the aspects 1) that the current model is only derived and validated in WOS environments containing simple 1:1 salts, such as NaCl; however, crude oil usually contains mixture of various salts such as 1:1, 2:1, and 2:2 salts/ions, and 2) that surfactant-corrosion product precipitation is neglected by the present model.

Table 6.1 Testing Systems of mixed surfactant partitioning in water-oil environment and associated inhibition on steel corrosion in water

Testing System (TS)	Surfactants	Mixed molar ratio in water		NaCl, M	T, ℃	Oil	Volume ratio (oil/water)
		initial ratio	after partitioning*				
i	$C_{12}/C_{14}/C_{16}$	1/1/1	20/7/1	0.599	40	toluene	0/1, 1/2, 2/1
ii	$C_{12}/C_{14}/C_{16}$	6/3/1	35/14/1	0.0855	40	toluene	1/2
iii	$C_{16}/C_{16}E_{20}$	1/1	0.36/1	0.03	25	heptane	1/2
iv	$C_{16}TAB/C_{16}/C_{16}E_{20}$	1/3/6	0.14/0.33/1	0.03	25	heptane	1/2

*Note that the mixed molar ratio in the bulk after partitioning is constant if no micelle formation. Once micelle forms (if C_{tol} is high enough), the ratio changes as a function of C_{tol}. Here it means the former case. Chemicals C_n: benzalkonium chlorides; $C_{16}TAB$: hexadecyl trimethyl ammonium bromide; $C_{16}E_{20}$: poly (20) oxyethylene 16-cetyl ether.

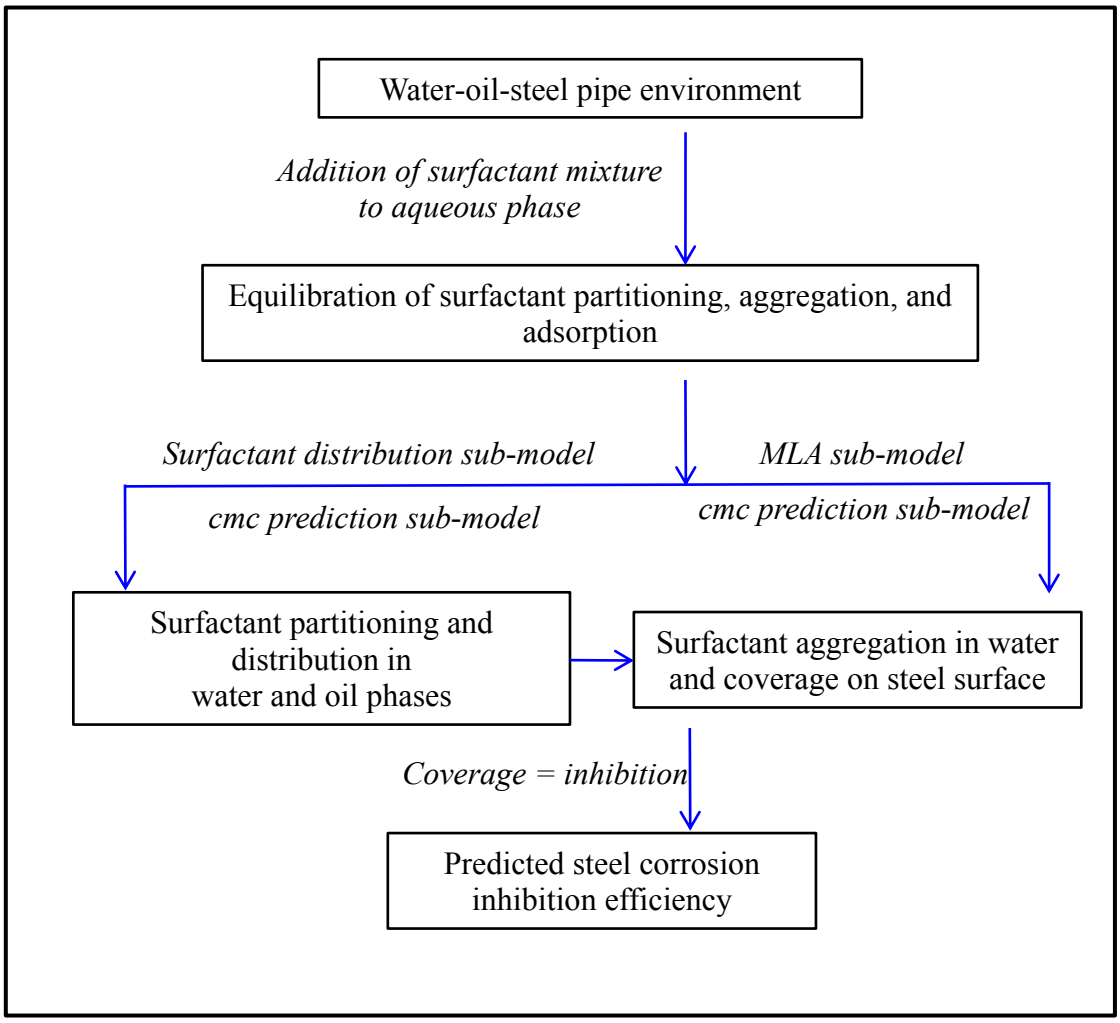

Scheme 6.1 Flow chart of ICI model for steel corrosion inhibition using mixed surfactants in WOS environment

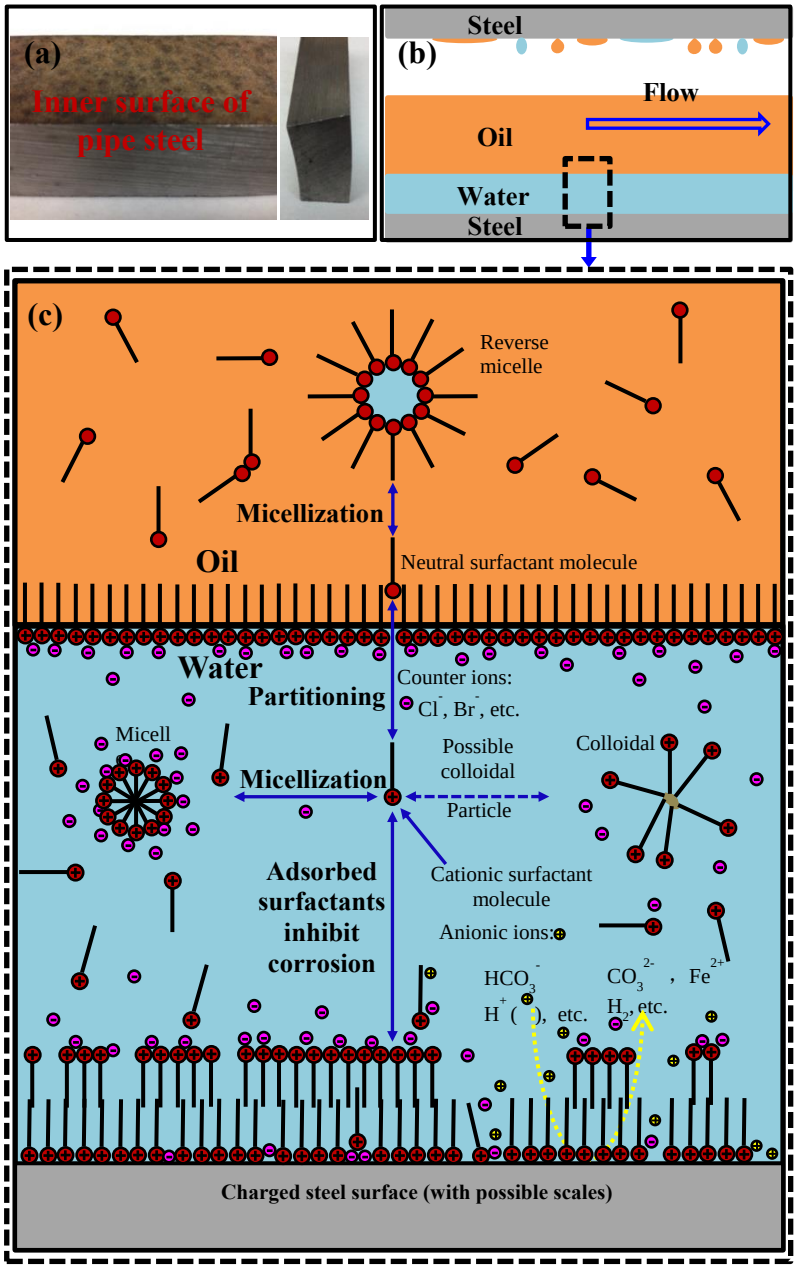

Fig. 6.1 One piece of corroded X65 steel pipe (a). Cross section of steel pipe containing water, oil, and some oil vapor (b). Schematic illustration of cationic surfactant distribution and various processes in water-oil-steel (WOS) pipe environment with dissolved CO_2 at the average surfactant concentration above the apparent cmc (c).

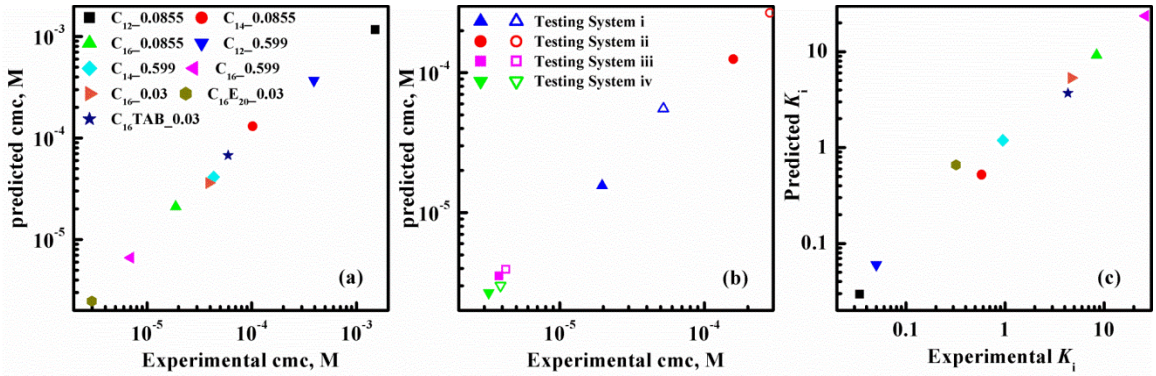

Fig. 6.2 Comparison of predicted aqueous cmc and experimental aqueous cmc of various pure surfactants (a) and of different testing systems of surfactant mixtures (b) in NaCl-containing aqueous solution. The number in the legend in (a) is NaCl concentration in unit M. Solid symbols represent the initial aqueous cmc of added surfactant mixture before paritioning, $\Gamma^{w'}$; open symbols represent the equilibrated aqueous cmc of surfactant mixture at partitioning and aggregation equilibrium, Γ^{w}. Note that for mixtures in (b) the total initial concentration C_{tol} is less than 1.5 times of the apparent aqueous cmc Γ_{app} (it means no micelle formation in water-oil environment.). 1.5 is calculated based on mass balance and oil/water volume ratio (1/2). Γ^{w} is calculated at the critical point of C_{tol} = 1.5Γ_{app}. Comparison of predicted and experimental partitioning coefficients of various pure surfactants (c). The legend is the same with that in (a). Experimental cmc of mixtures in Testing Systems iii and iv are reported data [26].

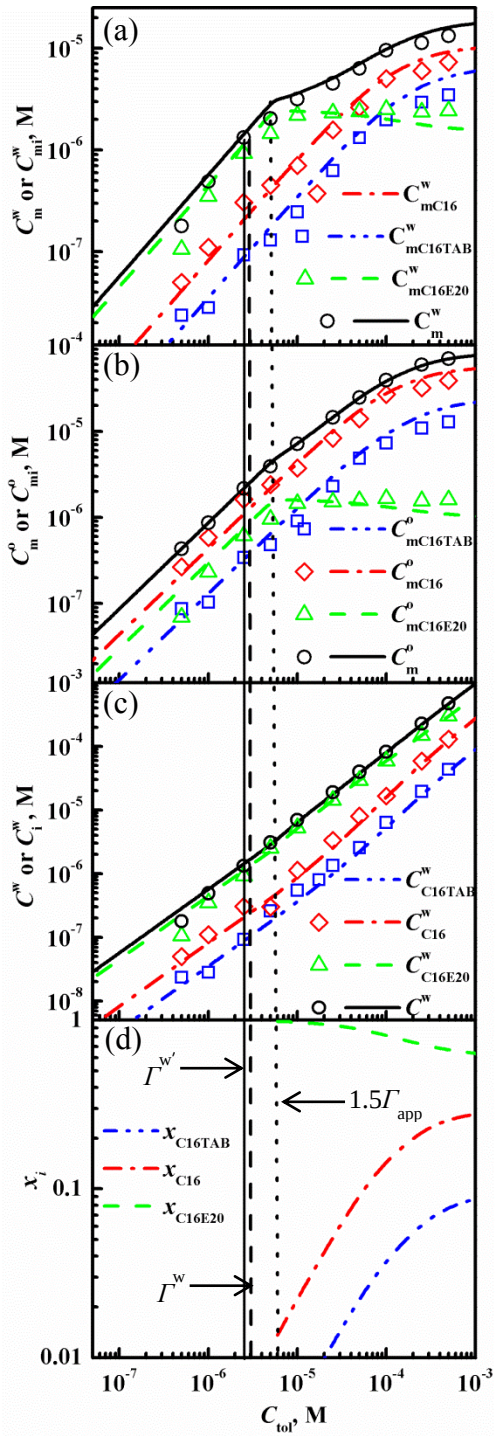

Fig. 6.3 Equilibrium partitioning properties of Testing System iv: (a) equilibrium concentration of monomeric surfactants in water, (b) in oil, (c) equilibrium concentration of total surfactants in water, including monomer and micellized form, and (d) molar fraction of surfactant i in mixed micelle as functions of C_{tol}. Symbols: experiment; curves: model prediction. Vertical dot line: $C_{tol}=1.5\Gamma_{app}=5.39\text{x}10^{-6}$ M. Vertical solid line: $\Gamma^{w'}=2.65\text{x}10^{-6}$ M. Vertical dash line: $\Gamma^{w}=3.01\text{x}10^{-6}$ M when $C_{tol} < 1.5\Gamma_{app}$.

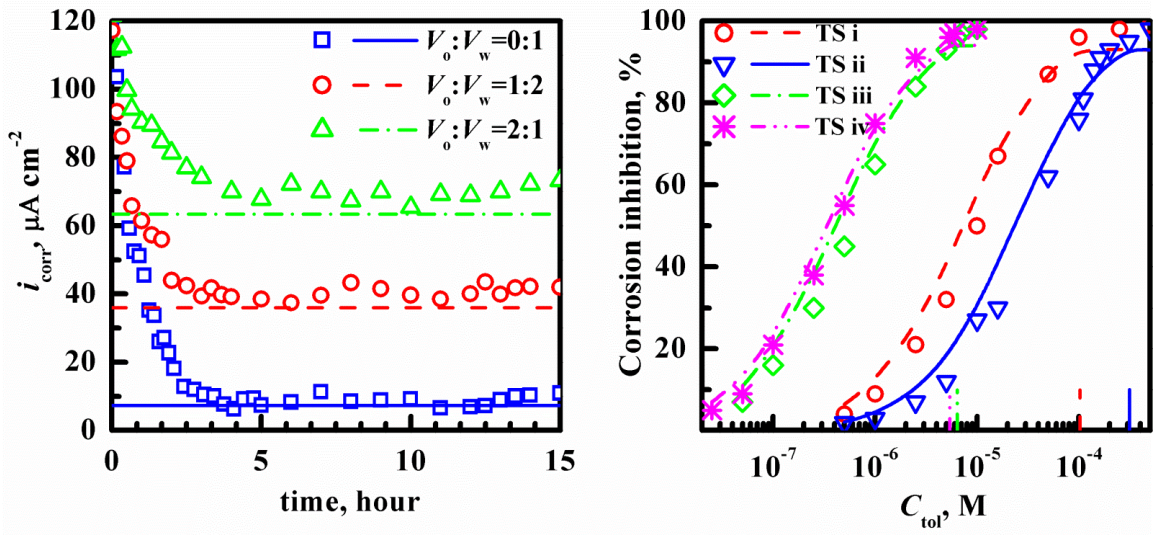

Fig. 6.4 Comparison of predicted and experimental corrosion current density as a function of time of the surfactant mixture (C_{tol}=1.50x10^{-5} M) in Testing System i with different water/oil volume ratios (a) and comparison of predicted and experimental inhibition efficiency on steel corrosion of mixed surfactant systems in water-oil environment (b). Symbols: experiment; curves: prediction. TS represents Testing System. Vertical lines indicate C_{tol}=1.5Γ_{app}. K'= 4.84 [22], 13.74 [22], and 23.59 for C_{16}TAB, BAC, and $C_{16}E_{20}$, respectively. The molar fraction-based average value of K' is used for different testing systems.

6.5 Reference

[1] M. Finšgar, J. Jackson, Corrosion Sci. 86 (2014) 17.

[2] H. N. Shubha, T. V. Venkatesha, K. Vathsala, M. K. Pavitra, M. K. Punith Kumar, ACS Appl. Mater. Interfaces 5 (2013) 10738.

[3] D. Snihirova, S. V. Lamaka, M. Taryba, A. N. Salak, S. Kallip, M. L. Zheludkevich, M. G. S. Ferreira, M .F. Montemor, ACS Appl. Mater. Interfaces 2 (2010) 3011.

[4] Y. Zhu, M. L. Free, G. Yi, Corrosion Sci. 98 (2015) 417.

[5] Y. Zhou, Y. Zuo, Electrochim. Acta 154 (2015) 157.

[6] K. S. George, S. Nešić, Corrosion 63 (2007) 178.

[7] N. G. Thompson, Y. Mark, D. Daniel, Corrosion Rev. 25 (2007) 247.

[8] D. V. Andreeva, E. V. Skorb, D. G. Shchukin, ACS Appl. Mater. Interfaces 2 (2010) 1954.

[9] S. Ramachandran, B. Tsai, M. Blanco, H. Chen, Y. Tang, W. A. Goddard, Langmuir 12 (1996) 6419.

[10] M. J. Rosen, Surfactants and Interfacial Phenomena, 3rd ed., John Wiley, New Jersey, 2004.

[11] X. Ye, C. Zheng, J. Chen, Y. Gao, C. B. Murray, Nano Lett. 13 (2013) 765.

[12] Sonu, A. K. Tiwari, S. K. Saha, Ind. Eng. Chem. Res. 52 (2013) 5895.

[13] T. Ishizaki, M. Okido, Y. Masuda, N. Saito, M. Sakamoto, Langmuir 27 (2011) 6009.

[14] Y. Zhu, M. L. Free, J. Electrochem. Soc. submitted.

[15] S. Endo, K. Goss, Environ. Sci. Technol. 48 (2014) 2776.

[16] M. A. Cowell, T. C. G. Kibbey, J. B. Zimmerman, K. F. Hayes, Environ. Sci. Technol. 34 (2000) 1583.

[17] J. Iyer, D. Blankschtein, J. Phys. Chem. B, 118 (2014) 2377.

[18] L. Moreira, A. Firoozabadi, Langmuir 26 (2010) 15177.

[19] C. D. Taylor, A. Chandra, J. Vera, N. Sridhar, J. Electrochem. Soc. 162 (2015) C369.

[20] A. Kokalj, S. Peljhan, M. Finsgar, I. Milosev, J. Am. Chem. Soc. 132 (2010) 16657.

[21] D. A. Winkler, M. Breedon, A. E. Hughes, F. R. Burden, A. S. Barnard, T. G. Harvey, I. Cole, Green Chem. 16 (2014) 3349.

[22] Y. Zhu, M. L. Free, G. Yi, J. Electrochem. Soc.168 (2015) C582.

[23] Y. Zhu, M. L. Free, Ind. Eng. Chem. Res. (2015).

[24] T. C. G. Kibbey, L. Chen, Colloids Surf. A: Physicochem. Eng. Aspects 326 (2008) 73.

[25] A. Shiloach, D. Blankschtein, Langmuir 14 (1998) 1618.

[26] A. A. Dar, G. M. Rather, S. Ghosh, A. R. Das, J. Colloid Interface Sci. 322 (2008) 572.

[27] K. S. Pitzer, Activity Coefficients in Electrolyte Solutions, 2nd ed., CRC Press, Boca Raton, 1991.

[28] B. W. Brooks, H. N. Richmond, J. Colloid Interface Sci. 162 (1994) 59.

CHAPTER 7

CONCLUSIONS

The oil and gas industry has received considerable attention from researchers because oil, mining, and transportation have become increasingly expensive due to equipment (metallic pipelines) damage caused by corrosion-especially CO_2 corrosion. The corrosion issues have led to great interest in industry and academia to control corrosion of metallic pipelines in various oilfields around the world. Among the existing corrosion control methods, surfactant inhibitors have widely been used for corrosion inhibition of pipelines in water-oil-steel pipe (WOS) environments. This dissertation includes a systemic review of the causes of pipeline corrosion in WOS environments with CO_2, general corrosion control using surfactant inhibitors and associated concerns, and commonly used classes of surfactants and their properties, and various processes and phenomena that affect overall surfactant performance, various developed models (semi-empirical model, mechanistic model, and multiphysics model) in evaluation of surfactant inhibition efficiency.

A multiphysics integrated corrosion inhibition (ICI) model is proposed, developed, and validated based on the current understanding of the inhibition of CO_2 corrosion in WOS environments using surfactants. This multiphysics model is the integration of several submodels, including the aqueous cmc prediction submodel, the MLA/MQSAR

submodels, and a water-oil surfactant distribution submodel. The aqueous cmc submodel is developed and validated to study micellization of various pure and mixed surfactants in aqueous solution containing salts (0-3M). The effects of counterion and coion specificity, various physical and chemical properties of surfactants, and solution environments on aggregation properties are successfully evaluated. The predicted aggregation properties, including cmc, micelle shape, micelle aggregation number, and sphere-to-rod transition, agree well with experimental data.

The MLA/MQSAR submodels, which consider the effects of major processes such as micellization and aggregation on surfactant adsorption, and the effects of solution environments, provide a potential tool to determine the ultimate effective surface coverage and predict corrosion inhibition efficiency of various pure, binary-, ternary-, or multiple-component surfactant mixtures of interest in the presence of salt in solution at various concentration levels.

The water-oil surfactant distribution submodel has been developed and validated for the evaluation of surfactant partitioning and distribution in water-oil environment. The surfactant distribution submodel, which is a combination of partitioning process, partitioning coefficient, and the aqueous cmc of surfactants, provides one tool to evaluate the partitioning of mixed surfactants in water-oil environments.

The phenomena and processes integrated into the ICI model include surfactant partitioning between oil and water, micellization and precipitation, adsorption/desorption at surfaces and interfaces, surfactant-solvent interactions, surfactant-counterion pairing, lateral interactions between surfactant molecules, and fluid flow. These phenomena are incorporated into three main processes and associated modeling: partitioning between oil

and water, micellization/precipitation, and effective adsorption on metal substrate and water/oil interface. The ICI model does not focus on the surfactant injection process/frequency and adsorption kinetics.

The framework of multiphysics ICI model is intended to serve as a basic framework in the understanding and modeling of mixed surfactant inhibitor performance with a focus on the application in salt-containing WOS environments. Beyond this, other potential applications may be extended to the design of surfactants, selection of optimal surfactants for specific applications, experimental validation of developed models, simulation of conceivable processes and phenomena, and the integration into more comprehensive lifetime prediction models in which all the surfactant efficiency-affecting factors may be evaluated.

The ICI model, however, has a few limitations and still needs improvements in the aspects 1) that the current model is only derived and validated in WOS environments containing simple 1:1 salts, such as NaCl; however, crude oil usually contains mixture of various salts such as 1:1, 2:1, and 2:2 salts/ions, and 2) that the flow rate is simulated using a rotating disc test without multiphase flow and microemulsion formation which are normally present in real WOS environments.

APPENDIX

A.1 Traditional cmc model*

A.1.1 Pure surfactant

Assuming the monomeric cationic surfactant is completely dissociated in solution, but in the micelle form, the surfactant is associated to some extent with counterions. The counterion dissociates from 1:1 electrolyte and surfactant. Therefore, the micellization process is described by the following reaction

$$N\mathrm{m}_{\mathrm{i}}^{+} + N\delta_{\mathrm{i}}\mathrm{C}^{-} \leftrightarrow \mathrm{M}^{N(1-\delta_{\mathrm{i}})^{+}} \qquad \text{A.1}$$

The chemical potential of micelle, monomer, and counterion in solution can be written, respectively, as

$$\mu_{\mathrm{M}} = N\mu_{\mathrm{Mi}}^{\mathrm{o}} + RT\ln(a_{\mathrm{M}}) \qquad \text{A.2}$$

$$\mu_{\mathrm{i}} = \mu_{\mathrm{i}}^{\mathrm{o}} + RT\ln(\gamma_{\mathrm{i}}X_{\mathrm{i}}) \qquad \text{A.3}$$

$$\mu_{\mathrm{c}} = \mu_{\mathrm{c}}^{\mathrm{o}} + RT\ln\left(\gamma_{\mathrm{c}}(X_{\mathrm{c}} + X_{\mathrm{i}})\right) \qquad \text{A.4}$$

At equilibrium

$$\mu_{\mathrm{M}} = N\mu_{\mathrm{i}} + N\delta_{\mathrm{i}}\mu_{\mathrm{c}} \qquad \text{A.5}$$

Substitution of Eqs. (A.2)-(A.4) and rearrangement lead to

$$\mu_{\mathrm{Mi}}^{\mathrm{o}} + \frac{RT}{N}\ln(a_{\mathrm{M}}) = \mu_{\mathrm{i}}^{\mathrm{o}} + RT\ln(\gamma_{\mathrm{i}}X_{\mathrm{i}}) + \delta_{\mathrm{i}}\mu_{\mathrm{c}}^{\mathrm{o}} + \delta_{\mathrm{i}}RT\ln\left(\gamma_{\mathrm{c}}(X_{\mathrm{c}} + X_{\mathrm{i}})\right) \qquad \text{A.6}$$

Then mole standard free energy change of micellization is given by

* Partially published in Corros. Sci. 98 (2015) 417-429 and Corros. Sci. (2015) doi: 10.1016/j.corsci.2015.10.012.

$$\Delta\mu_{\mathrm{mic}}^{\mathrm{o}} = \mu_{\mathrm{Mi}}^{\mathrm{o}} - \mu_{\mathrm{i}}^{\mathrm{o}} - \delta_{\mathrm{i}}\mu_{\mathrm{c}}^{\mathrm{o}} \quad \text{A.7}$$

Therefore,

$$\Delta\mu_{\mathrm{mic}}^{\mathrm{o}} = RT\ln(\gamma_{\mathrm{i}}X_{\mathrm{i}}) + \delta_{\mathrm{i}}RT\ln\big(\gamma_{\mathrm{c}}(X_{\mathrm{c}} + X_{\mathrm{i}})\big) - \frac{RT}{N}\ln(a_{\mathrm{M}}) \quad \text{A.8}$$

Activity of the micelle is set as a unit considering that the micelle does not dissolve in water and is treated as precipitates. Alternatively, the micelle can be interpreted as a second phase. Thus, the last term on the right-hand side of Eq. (A.8) is neglected and the equation is simplified to

$$\Delta\mu_{\mathrm{mic}}^{\mathrm{o}} = RT\ln(\gamma_{\mathrm{i}}X_{\mathrm{i}}) + \delta_{\mathrm{i}}RT\ln\big(\gamma_{\mathrm{c}}(X_{\mathrm{c}} + X_{\mathrm{i}})\big) \quad \text{A.9}$$

Assume the cmc is equal to the concentration of monomeric surfactant i at micellization, and we should have

$$\Delta\mu_{\mathrm{mic}}^{\mathrm{o}} = RT\ln\left(\gamma_{\mathrm{i}}\frac{\Gamma_{\mathrm{i}}^{\mathrm{w}}}{C_{\mathrm{mw}}}\right) + \delta_{\mathrm{i}}RT\ln(\gamma_{\mathrm{c}}\left(\frac{C_{\mathrm{c}}+\Gamma_{\mathrm{i}}^{\mathrm{w}}}{C_{\mathrm{mw}}}\right) \quad \text{A.10}$$

The activity coefficient of ions calculated using Davies equation or Pitzer's method is usually less than unit in electrolyte solution. The functional head group of surfactant is polar and behaves like ions, and its activity coefficient is assumed to be equal to that of ions in solution whereas the hydrocarbon chain tries to escape from electrolyte solution and its activity coefficient is usually higher than unit. Therefore, it is assumed that the activity coefficient $\gamma_{\mathrm{i}}$of a whole surfactant molecule is unit. Rearrangement of Eq. (A.10) leads to

$$\ln(\Gamma_{\mathrm{i}}^{\mathrm{w}}) = \frac{\Delta\mu_{\mathrm{mic}}^{\mathrm{o}}}{RT} - \delta_{\mathrm{i}}\ln\big(\gamma_{\mathrm{c}}(C_{\mathrm{c}} + \Gamma_{\mathrm{i}}^{\mathrm{w}})\big) + (1 + \delta_{\mathrm{i}})\ln(C_{\mathrm{mw}}) \quad \text{A.11}$$

Considering the surfactant hydrocarbon chain contains (L_{i}-1) methylene group, one methyl group, and one functional group, thus Eq. (A.11) is further rearranged to

$$\ln(\Gamma_{\mathrm{i}}^{\mathrm{w}}) = -\delta_{\mathrm{i}}\ln\big(\gamma_{\mathrm{c}}(C_{\mathrm{c}} + \Gamma_{\mathrm{i}}^{\mathrm{w}})\big) + (L_{\mathrm{i}} - 1)\frac{\Delta\mu_{\mathrm{ch2}}^{\mathrm{o}}}{RT} + \frac{\Delta\mu_{\mathrm{ch3}}^{\mathrm{o}}}{RT} + \frac{\Delta\mu_{\mathrm{f}}^{\mathrm{o}}}{RT} + (1 + \delta_{\mathrm{i}})\ln(C_{\mathrm{mw}})$$

A.12

Suppose we have a series of homologous surfactant i with chain length L_i. For surfactant i, plot of $\ln(\Gamma_i^w)$ vs. (vs.) $\ln\left(\gamma_c(C_c+\Gamma_i^w)\right)$ using Eq. (A.12) based on the measurements of cmc values with different electrolyte concentrations in solution gives a slope S_i (see Eq. (A.13)), and an intercept D_i (see Eq. (A.14)). Following this method, we can get a series of slopes S_i and a series of intercepts D_i for a series of homologous surfactants with different chain length. δ_m is equal to the average of a series values of δ_i which is calculated from Eq. (A.13). Plot of (D_i vs. (L_i-1)) in Eq. (A.14) yields one slope to calculate $\Delta\mu^o_{ch2}$. The intercept of the plot of (D_i vs. (L_i-1)) should be a constant at given temperature for homologous surfactants according to Eq. (A.14).

$$S_i = -\delta_i \tag{A.13}$$

$$D_i = (L_i - 1)\frac{\Delta\mu^o_{ch2}}{RT} + \frac{\Delta\mu^o_{ch3}}{RT} + \frac{\Delta\mu^o_f}{RT} + (1+\delta_i)\ln(C_{mw}) \tag{A.14}$$

$$D'' = \frac{\Delta\mu^o_{ch3}}{RT} + \frac{\Delta\mu^o_f}{RT} + (1+\delta_i)\ln(C_{mw}) \tag{A.15}$$

Eq. (A.12) simplifies to

$$\ln(\Gamma_i^w) = -\delta_m \ln\left(\gamma_c(C_c+\Gamma_i)\right) + (L_i - 1)\frac{\Delta\mu^o_{ch2}}{RT} + D'' \tag{A.16}$$

$$\ln(\Gamma_i^w) = -\delta_m \ln\left(\gamma_c(C_c+\Gamma_i)\right) + L_i\frac{\Delta\mu^o_{ch2}}{RT} + D' \tag{A.17}$$

$$D' = D'' - \frac{\Delta\mu^o_{ch2}}{RT} \tag{A.18}$$

Eqs. (A.16) or (A.17) is cmc prediction model for pure surfactant. The inputs of this model are cmc values of a series of homologous surfactants (at least three) in solutions with different electrolyte concentrations (at least three concentrations).

A.1.2 Binary homologous surfactant mixture

The cmc prediction model of binary mixture of homologous surfactants is derived as follows. If no electrolyte is added to solution, the term $\ln\left(\gamma_{\mathrm{c}}(C_{\mathrm{c}}+\Gamma_{\mathrm{i}}^{\mathrm{w}})\right)$ is replaced by $\ln(\Gamma_{\mathrm{i}}^{\mathrm{p}})$ in the above equations. The cmc of pure homologous surfactants 1 and 2 in aqueous solution without electrolyte addition are then given by Eqs. (A.19) and (A.20)

$$\ln\left(\Gamma_1^{\mathrm{p}}\right)=-\delta_{\mathrm{m}}\ln\left(\Gamma_1^{\mathrm{p}}\right)+L_1\frac{\Delta\mu_{\mathrm{ch2}}^{\mathrm{o}}}{RT}+D' \qquad \text{A.19}$$

$$\ln\left(\Gamma_2^{\mathrm{p}}\right)=-\delta_{\mathrm{m}}\ln\left(\Gamma_2^{\mathrm{p}}\right)+L_2\frac{\Delta\mu_{\mathrm{ch2}}^{\mathrm{o}}}{RT}+D' \qquad \text{A.20}$$

The mole fraction of surfactant i (i=1, 2) in mixed micelle is represented by x_{i}. The concentration of surfactant i in bulk solution of mixed surfactants at equilibrium is C_{mi}. At equilibrium, Eqs. (A.21) and (A.22) can be derived according to Eq. (A.17) if one mixing term $\ln\alpha_{\mathrm{i}}$ is added with the assumption of ideal mixing in the micelle.

$$\ln(C_{\mathrm{m1}})=-\delta_{\mathrm{m}}\ln(\gamma_{\mathrm{c}}C_{\mathrm{c}})+L_1\frac{\Delta\mu_{\mathrm{ch2}}^{\mathrm{o}}}{RT}+D'+\ln\alpha_1 \qquad \text{A.21}$$

$$\ln(C_{\mathrm{m2}})=-\delta_{\mathrm{m}}\ln(\gamma_{\mathrm{c}}C_{\mathrm{c}})+L_2\frac{\Delta\mu_{\mathrm{ch2}}^{\mathrm{o}}}{RT}+D'+\ln\alpha_2 \qquad \text{A.22}$$

Considering the mass balance of surfactants in micelle, we have

$$\alpha_1+\alpha_2=1 \qquad \text{A.23}$$

At the cmc, micelle starts to form. However, most surfactants exist as monomers and very few micelles form. With this consideration, Eq. (A.24) holds

$$C_{\mathrm{m1}}+C_{\mathrm{m2}}=\Gamma^{\mathrm{w}} \qquad \text{A.24}$$

Substitution of Eqs. (A.19) and (A.20) into Eqs. (A.21) and (A.22) to remove D' and $\Delta\mu_{\mathrm{ch2}}^{\mathrm{o}}$

$$\ln(C_{\mathrm{m1}})=-\delta_{\mathrm{m}}\ln(\gamma_{\mathrm{c}}C_{\mathrm{c}})+(1+\delta_{\mathrm{m}})\ln\left(\Gamma_1^{\mathrm{p}}\right)+\ln\alpha_1 \qquad \text{A.25}$$

$$\ln(C_{\mathrm{m2}})=-\delta_{\mathrm{m}}\ln(\gamma_{\mathrm{c}}C_{\mathrm{c}})+(1+\delta_{\mathrm{m}})\ln\left(\Gamma_2^{\mathrm{p}}\right)+\ln\alpha_2 \qquad \text{A.26}$$

Replacement of C_{m1} and C_{m2} in Eq. (A.24) leads to

$$\left(\frac{1}{\gamma_c C_c}\right)^{\delta_m}\left(\Gamma_1^{p(1+\delta_m)}\,\alpha_1+\Gamma_2^{p(1+\delta_m)}\,\alpha_2\right)=\Gamma^w \tag{A.27}$$

If we assume the mole fraction of surfactant i in the total amount of mixed surfactants is x_i (i=1, 2), the following equations hold

$$x_1+x_2=1 \tag{A.28}$$

$$\frac{C_{m1}}{C_{m2}}=\frac{x_1}{x_2} \tag{A.29}$$

From Eqs. (A.21) and (A.22) it is obtained

$$\frac{C_{m1}}{C_{m2}}=\frac{\alpha_1\exp\left(L_1\frac{\Delta\mu^o_{ch2}}{RT}\right)}{\alpha_2\exp\left(L_2\frac{\Delta\mu^o_{ch2}}{RT}\right)} \tag{A.30}$$

Thus,

$$\frac{x_1}{x_2}=\frac{\alpha_1\exp\left(L_1\frac{\Delta\mu^o_{ch2}}{RT}\right)}{\alpha_2\exp\left(L_2\frac{\Delta\mu^o_{ch2}}{RT}\right)} \tag{A.31}$$

Solve x_i using Eqs. (A.23) and (A.31) and substitute the results into Eq. (A.27) to get

$$\alpha_1=\frac{x_1\exp\left(-L_1\frac{\Delta\mu^o_{ch2}}{RT}\right)}{x_1\exp\left(-L_1\frac{\Delta\mu^o_{ch2}}{RT}\right)+x_2\exp\left(-L_2\frac{\Delta\mu^o_{ch2}}{RT}\right)} \tag{A.32}$$

$$\alpha_2=\frac{x_2\exp\left(-L_2\frac{\Delta\mu^o_{ch2}}{RT}\right)}{x_1\exp\left(-L_1\frac{\Delta\mu^o_{ch2}}{RT}\right)+x_2\exp\left(-L_2\frac{\Delta\mu^o_{ch2}}{RT}\right)} \tag{A.33}$$

$$\Gamma^w=\left(\frac{1}{\gamma_c C_c}\right)^{\delta_m}\left(\frac{\Gamma_{1o}{}^{(1+\delta_m)}\,\alpha_1\exp\left(-L_1\frac{\Delta\mu^o_{ch2}}{RT}\right)+\Gamma_{2o}{}^{(1+\delta_m)}\,\alpha_2\exp\left(-L_2\frac{\Delta\mu^o_{ch2}}{RT}\right)}{\alpha_1\exp\left(-L_1\frac{\Delta\mu^o_{ch2}}{RT}\right)+\alpha_2\exp\left(-L_2\frac{\Delta\mu^o_{ch2}}{RT}\right)}\right) \tag{A.34}$$

Eq. (A.34) can be used for the cmc prediction of binary homologous ionic surfactant mixture. For nonionic surfactant, counterion binding coefficient δ_m or δ_i is equal to zero.

Alternatively, from Eqs. (A.25) and (A.26) it is obtained

$$\frac{C_{\mathrm{m1}}}{C_{\mathrm{m2}}} = \frac{\alpha_1 \Gamma_{\mathrm{i}}^{\mathrm{p}(1+\delta_{\mathrm{m}})}}{\alpha_2 \Gamma_{\mathrm{i}}^{\mathrm{p}(1+\delta_{\mathrm{m}})}} \tag{A.35}$$

Combination of Eq. (A.35) and Eq. (A.29) leads to

$$\frac{\alpha_1}{\alpha_2} = \frac{x_1 \Gamma_1^{\mathrm{p}-(1+\delta_{\mathrm{m}})}}{x_2 \Gamma_2^{\mathrm{p}-(1+\delta_{\mathrm{m}})}} \tag{A.36}$$

Eq. (A.23) and Eq. (A.36) can be solved simultaneously with respect to x_{i}

$$\alpha_1 = \frac{x_1 \Gamma_1^{\mathrm{o}-(1+\delta_{\mathrm{m}})}}{x_1 \Gamma_1^{\mathrm{o}-(1+\delta_{\mathrm{m}})} + x_2 \Gamma_2^{\mathrm{o}-(1+\delta_{\mathrm{m}})}} \tag{A.37}$$

$$\alpha_2 = \frac{x_2 \Gamma_2^{\mathrm{p}-(1+\delta_{\mathrm{m}})}}{x_1 \Gamma_1^{\mathrm{p}-(1+\delta_{\mathrm{m}})} + x_2 \Gamma_2^{\mathrm{p}-(1+\delta_{\mathrm{m}})}} \tag{A.38}$$

Substitution of Eq. (A.37) and Eq. (A.38) into Eq. (A.27) leads to

$$\Gamma^{\mathrm{w}} = \left(\frac{1}{\gamma_{\mathrm{c}} C_{\mathrm{c}}}\right)^{\delta_{\mathrm{m}}} \frac{1}{x_1 \Gamma_1^{\mathrm{p}-(1+\delta_{\mathrm{m}})} + x_2 \Gamma_2^{\mathrm{p}-(1+\delta_{\mathrm{m}})}} \tag{A.39}$$

Eqs. (A.32-A.34) and Eqs. (A.37-A.39) are equivalent with respect to the calculation of mixed cmc Γ^{w} and molar fraction α_{i}. However, Eqs. (A.37-A.39) are easier to use because of less variables. It is also found that the following equations stand for homologous surfactant i and for arbitrary surfactant i (either homologous or nonhomologous), respectively

$$\Gamma_{\mathrm{i}}^{\mathrm{p}-(1+\delta_{\mathrm{m}})} = k_{\mathrm{m}} \exp\left(-L_{\mathrm{i}} \frac{\Delta\mu_{\mathrm{ch2}}^{\mathrm{o}}}{RT}\right) \tag{A.40}$$

$$\Gamma_{\mathrm{i}}^{\mathrm{p}-(1+\delta_{\mathrm{i}})} = k_{\mathrm{i}} \exp\left(-L_{\mathrm{i}} \frac{\Delta\mu_{\mathrm{ich2}}^{\mathrm{o}}}{RT}\right) \tag{A.41}$$

where k_{m} is mean proportional constant for homologous surfactants and k_{i} is proportional constant for arbitrary surfactant i.

A.1.3 Ternary and multiple homologous surfactant mixture

Similarly, the cmc prediction model for mixtures of ternary or multiple homologous surfactants can be derived in the same manner. Using surfactant i to replace surfactants 1 and 2, the mixed cmc and mixed micelle molar fraction α_i are given by the following equations, respectively

$$\Gamma^w = \left(\frac{1}{\gamma_c C_c}\right)^{\delta_m} \frac{1}{\sum_i\left(x_i \Gamma_i^{p-(1+\delta_m)}\right)} \tag{A.42}$$

$$\alpha_i = \frac{x_i \Gamma_i^{p-(1+\delta_m)}}{\sum_i\left(x_i \Gamma_i^{p-(1+\delta_m)}\right)} \tag{A.43}$$

A.1.4 Binary nonhomologous surfactant mixture

From the previous discussion, the counterion binding coefficient δ_i is different for nonhomologous surfactants. If two such surfactants 1 and 2 are mixed, the cmc prediction model should be modified. Eqs. (A.25) and (A.26) should have the following format when it applies to binary nonhomologous mixed surfactants 1 and 2, respectively

$$\ln(C_{m1}) = -\delta_1 \ln(\gamma_c C_c) + (1+\delta_1)\ln\left(\Gamma_1^p\right) + \ln\alpha_1 \tag{A.44}$$

$$\ln(C_{m2}) = -\delta_2 \ln(\gamma_c C_c) + (1+\delta_2)\ln\left(\Gamma_2^p\right) + \ln\alpha_2 \tag{A.45}$$

Combination with Eq. (A.24) leads to

$$\left(\frac{1}{\gamma_c C_c}\right)^{\delta_1} \alpha_1 \Gamma_1^{p(1+\delta_1)} + \left(\frac{1}{\gamma_c C_c}\right)^{\delta_2} \alpha_2 \Gamma_2^{p(1+\delta_2)} = \Gamma^w \tag{A.46}$$

Combination of Eqs. (A.44) and (A.45) leads to

$$\frac{C_{m1}}{C_{m2}} = \frac{\left(\frac{1}{\gamma_c C_c}\right)^{\delta_1} \alpha_1 \Gamma_1^{p(1+\delta_1)}}{\left(\frac{1}{\gamma_c C_c}\right)^{\delta_2} \alpha_2 \Gamma_2^{p(1+\delta_2)}} \tag{A.47}$$

Eq. (A.47) in combination with Eqs. (A.23) and (A.29) can solve α_1 and α_2 as follows

$$\alpha_1 = \frac{x_1(\gamma_c C_c)^{\delta_1}\Gamma_1^{p-(1+\delta_1)}}{x_1(\gamma_c C_c)^{\delta_1}\Gamma_1^{p-(1+\delta_1)} + x_2(\gamma_c C_c)^{\delta_2}\Gamma_2^{p-(1+\delta_2)}} \tag{A.48}$$

$$\alpha_2 = \frac{x_2(\gamma_c C_c)^{\delta_2}\Gamma_2^{p-(1+\delta_2)}}{x_1(\gamma_c C_c)^{\delta_1}\Gamma_1^{p-(1+\delta_1)} + x_2(\gamma_c C_c)^{\delta_2}\Gamma_2^{p-(1+\delta_2)}} \tag{A.49}$$

Substitute x_1 and x_2 into Eq. (A.46) to get mixed cmc

$$\Gamma^w = \frac{1}{x_1(\gamma_c C_c)^{\delta_1}\Gamma_1^{p-(1+\delta_1)} + x_2(\gamma_c C_c)^{\delta_2}\Gamma_2^{p-(1+\delta_2)}} \tag{A.50}$$

An alternative expression is given as follows based on Eq. (A.41)

$$\Gamma^w = \frac{1}{x_1(\gamma_c C_c)^{\delta_1}k_1\exp\left(-L_1\frac{\Delta\mu^o_{1ch2}}{RT}\right) + x_2(\gamma_c C_c)^{\delta_2}k_2\exp\left(-L_2\frac{\Delta\mu^o_{2ch2}}{RT}\right)} \tag{A.51}$$

A.1.5 Multicomponent nonhomologous surfactant mixture

Similarly, for ternary and multiple nonhomologous surfactant mixture with i components, cmc and corresponding mixed micelle composition is given by

$$\Gamma^w = \frac{1}{\sum_i\left(x_i(\gamma_c C_c)^{\delta_i}\Gamma_i^{p-(1+\delta_i)}\right)} \tag{A.52}$$

$$\alpha_i = \frac{x_i(\gamma_c C_c)^{\delta_i}\Gamma_i^{p-(1+\delta_i)}}{\sum_i\left(x_i(\gamma_c C_c)^{\delta_i}\Gamma_i^{p-(1+\delta_i)}\right)} \tag{A.53}$$

The equivalent expressions of Eq. (A.52) and Eq. (A.53) are given as follows

$$\Gamma^w = \frac{1}{\sum_i\left(x_i(\gamma_c C_c)^{\delta_i}k_i\exp\left(-L_i\frac{\Delta\mu^o_{ich2}}{RT}\right)\right)} \tag{A.54}$$

$$\alpha_i = \frac{x_i(\gamma_c C_c)^{\delta_i}k_i\exp\left(-L_i\frac{\Delta\mu^o_{ich2}}{RT}\right)}{\sum_i\left(x_i(\gamma_c C_c)^{\delta_i}k_i\exp\left(-L_i\frac{\Delta\mu^o_{ich2}}{RT}\right)\right)} \tag{A.55}$$

In summary, for various cmc prediction models introduced above, the inputs include bulk mixed molar fraction x_i, counterion binding coefficient δ_i, activity coefficient of

counterion γ_c, concentration of counterion C_c, and the cmc of surfactant i (in pure water) Γ_i^p which can be directly measured or replaced by $\Delta\mu_{ich2}^o$ and k_i. x_i and C_c are known parameters, γ_c can be easily calculated given solution conditions, and δ_i and $\Delta\mu_{ich2}^o$ are usually readily available in existing literature. The outputs include cmc and mixed micelle composition. Please note that the model derivation is based on ionic surfactant. However, the developed model is also applicable to nonionic surfactant with counterion binding coefficient fixed at zero.

A.2 Molecular thermodynamic cmc model*

A.2.1 cmc model derivation

A.2.1.1 General description

Assuming the monomeric surfactant m_i (i=1, 2, or 3...) is completely dissociated in aqueous solution containing counterion m_j (j=1, 2, or 3…), but in the micelle form, the surfactant is associated to some extent with counterions, therefore, the surfactant micellization is described by the following process

$$N\sum_i \alpha_i m_i^{z_i} + N\sum_j \delta_j m_j^{z_j} \leftrightarrow M_N^{N(\sum_i \alpha_i z_i + \sum_j \delta_j z_j)} \quad \text{A.56}$$

where α_i is the composition of surfactant i in the micelle, M_N, which has an aggregation number N, micelle composition α_i, and a counterion binding coefficient δ_j. (For simplicity, only N is shown in the subscript.) For micelles of pure surfactant, $\alpha_i = 1$; for mixed micelles, $0 < \alpha_i < 1$. z_i and z_j are the valences of ionic surfactant i in dissociated form and counterion j. For nonionic surfactant i, $z_i = 0$ and $\delta_j = 0$.

By the consideration of activity coefficient, the chemical potential of micelle M_N,

* Content published in J. Electrochem. Soc. 168 (2015) C582, Ind. Eng. Chem. Res. 54 (2015) 9052-9056, and Colloid. Sur. A: Physical. Eng. Aspects (2015) doi: 10.1016/j.colsurfa.2015.11.005.

monomeric surfactant i, and counterion j in solution can be written, respectively, as

$$\mu_{\mathrm{M}} = \mu_{\mathrm{M}}^{\mathrm{o}} + kT\ln(a_{\mathrm{M}}) = \mu_{\mathrm{M}}^{\mathrm{o}} + kT\ln(\gamma_{\mathrm{M}}X_{\mathrm{M}}) \quad \text{A.57}$$

$$\mu_{\mathrm{mi}} = \mu_{\mathrm{mi}}^{\mathrm{o}} + kT\ln(a_{\mathrm{mi}}) = \mu_{\mathrm{mi}}^{\mathrm{o}} + kT\ln(\gamma_{\mathrm{mi}}X_{\mathrm{mi}}) \quad \text{A.58}$$

$$\mu_{\mathrm{mj}} = \mu_{\mathrm{mj}}^{\mathrm{o}} + kT\ln(a_{\mathrm{mj}}) = \mu_{\mathrm{mj}}^{\mathrm{o}} + kT\ln(\gamma_{\mathrm{mj}}X_{\mathrm{mj}}) \quad \text{A.59}$$

where $\mu_{\mathrm{M}}^{\mathrm{o}}$, $\mu_{\mathrm{mi}}^{\mathrm{o}}$, and $\mu_{\mathrm{mj}}^{\mathrm{o}}$ are the standard chemical potentials of micelle, monomeric surfactant, and counterion in solution, respectively. The standard state of water is defined as pure liquid while the standard state of all other species is defined for an infinitely dilute solution. a_{M}, a_{mi}, and a_{mj} are the corresponding activities. γ_{M}, γ_{mi}, and γ_{mj} are the corresponding activity coefficients. Micelle is treated as one separate phase from aqueous solution and thus γ_{M} = 1. X_{M}, X_{mi}, and X_{mj} are mole fractions of micelle, monomeric surfactant, and counterion in bulk solution, respectively.

Assume the activity coefficient of ionic surfactant i, γ_{mi}, in bulk solution is given by the quadratic mean of the product of functional headgroup activity coefficient γ_{hmi} and hydrocarbon chain tail activity coefficient γ_{tmi}. γ_{hmi} can be calculated from Pitzer's method or Davies equation. γ_{tmi} is estimated from the Setchenov equation shown as below

$$\gamma_{\mathrm{mi}} = \sqrt{\gamma_{\mathrm{hmi}}\gamma_{\mathrm{tmi}}} \quad \text{A.60}$$

$$\gamma_{\mathrm{tmi}} = 10^{I\sum_{\mathrm{s}}\alpha_{\mathrm{s}}k_{\mathrm{s}}L_{\mathrm{i}}} \quad \text{A.61}$$

where I is ionic strength of solution. k_{s} and α_{s} are Setchenov coefficient and mole fraction of salt s in total added salts, respectively. k_{s} is salt-dependent and therefore, salts with one ion in common should have different k_{s}. It is expected that the effect of counterion and coion on aggregation properties might be reflected through k_{s}. α_{s}= 1 for pure salt added to solution; $0 < \alpha_{\mathrm{s}} < 1$ if more than one type of salt is added. Note that the activity

coefficient of nonionic surfactant is assumed as γ_{tmi}. The volume of a hydrocarbon tail of surfactant i with tail length of L_{i} is estimated by

$$v_{\mathrm{ti}} = v_{\mathrm{CH_3}} + (L_{\mathrm{i}} - 1)v_{\mathrm{CH_2}} \quad \text{A.62}$$

$$v_{\mathrm{CH_3}} = 54.6 + 0.124(T - 298) \quad \text{A.63}$$

$$v_{\mathrm{CH_2}} = 26.9 + 0.146(T - 298) \quad \text{A.64}$$

At equilibrium of micelle formation

$$\mu_{\mathrm{M}} = N\sum_{\mathrm{i}} \alpha_{\mathrm{i}}\mu_{\mathrm{mi}} + N\sum_{\mathrm{j}} \delta_{\mathrm{j}}\mu_{\mathrm{mj}} \quad \text{A.65}$$

$$\mu_{\mathrm{M}}^{\mathrm{o}} + kT\ln(X_{\mathrm{M}}) = N\sum_{\mathrm{i}} \alpha_{\mathrm{i}}(\mu_{\mathrm{mi}}^{\mathrm{o}} + kT\ln(\gamma_{\mathrm{mi}}X_{\mathrm{mi}})) + N\sum_{\mathrm{j}} \delta_{\mathrm{mj}}\left(\mu_{\mathrm{mj}}^{\mathrm{o}} + kT\ln(\gamma_{\mathrm{mj}}X_{\mathrm{mj}})\right) \quad \text{A.66}$$

Standard micellization free energy per surfactant molecule is given by

$$\Delta\mu_{\mathrm{mic}}^{\mathrm{o}} = \frac{1}{N}\mu_{\mathrm{M}}^{\mathrm{o}} - \sum_{\mathrm{i}} \alpha_{\mathrm{i}}\mu_{\mathrm{mi}}^{\mathrm{o}} - \sum_{\mathrm{j}} \delta_{\mathrm{j}}\mu_{\mathrm{mj}}^{\mathrm{o}} \quad \text{A.67}$$

Substitution of Eq. (A.59) into Eq. (A.58) leads to

$$\Delta\mu_{\mathrm{mic}}^{\mathrm{o}} = kT\sum_{\mathrm{i}} \alpha_{\mathrm{i}}\ln(\gamma_{\mathrm{mi}}X_{\mathrm{mi}}) + kT\sum_{\mathrm{j}} \delta_{\mathrm{j}}\ln(\gamma_{\mathrm{mj}}X_{\mathrm{mj}}) - \frac{kT}{N}\ln X_{\mathrm{M}} \quad \text{A.68}$$

Rearrangement of Eq. (A.68) leads to

$$X_{\mathrm{M}} = \prod_{\mathrm{i}}(\gamma_{\mathrm{mi}}X_{\mathrm{mi}})^{N\alpha_{\mathrm{i}}} \prod_{\mathrm{j}}(\gamma_{\mathrm{mj}}X_{\mathrm{mj}})^{N\delta_{\mathrm{j}}} \exp\left(-\frac{N}{kT}\Delta\mu_{\mathrm{mic}}^{\mathrm{o}}\right) \quad \text{A.69}$$

Further rearrangement leads to

$$X_{\mathrm{M}} = \prod_{\mathrm{i}}(X_{\mathrm{mi}})^{N\alpha_{\mathrm{i}}} \prod_{\mathrm{j}}(X_{\mathrm{mj}})^{N\delta_{\mathrm{j}}} \exp\left(-\frac{N}{kT}\left(\Delta\mu_{\mathrm{mic}}^{\mathrm{o}} + kT\ln\left(\prod_{\mathrm{i}}(\gamma_{\mathrm{mi}})^{-\alpha_{\mathrm{i}}} \prod_{\mathrm{j}}(\gamma_{\mathrm{mj}})^{-\delta_{\mathrm{j}}}\right)\right)\right) \quad \text{A.70}$$

where X_{mi} is the mole fraction of monomeric surfactant i in bulk solution and is equal to

$$X_{\mathrm{mi}} = x_{\mathrm{mi}}\sum_{\mathrm{i}} X_{\mathrm{mi}} \quad \text{A.71}$$

where x_{mi} is interpreted as the mole fraction of monomeric surfactant i in the total mixed monomeric surfactants. X_{m} is the total mole fraction of monomeric surfactants in bulk

solution. Only monomeric surfactants are taken into account in Eq. (A.68) considering that the mole fraction of micelles is negligible compared to that of monomers.

Eq. (A.70) is simplified to

$$X_{\mathrm{M}} = \prod_{\mathrm{i}}(X_{\mathrm{mi}})^{N\alpha_{\mathrm{i}}} \prod_{\mathrm{j}}(X_{\mathrm{mj}})^{N\delta_{\mathrm{j}}} \exp\left(-\frac{N}{kT}\Delta\mu_{\mathrm{m}}^{\mathrm{o}}\right) \quad \text{A.72}$$

where $\Delta\mu_{\mathrm{m}}^{\mathrm{o}}$ is the modified standard micellization free energy by the consideration of surfactant and ion activities and estimated by summing the contributing terms as described below

$$\Delta\mu_{\mathrm{m}}^{\mathrm{o}} = \Delta\mu_{\mathrm{trt}}^{\mathrm{o}} + \Delta\mu_{\mathrm{int}}^{\mathrm{o}} + \Delta\mu_{\mathrm{pack}}^{\mathrm{o}} + \Delta\mu_{\mathrm{st}}^{\mathrm{o}} + \Delta\mu_{\mathrm{ent}}^{\mathrm{o}} + \Delta\mu_{\mathrm{elec}}^{\mathrm{o}} + \Delta\mu_{\mathrm{act}}^{\mathrm{o}} \quad \text{A.73}$$

where $\Delta\mu_{\mathrm{trt}}^{\mathrm{o}}$, $\Delta\mu_{\mathrm{int}}^{\mathrm{o}}$, $\Delta\mu_{\mathrm{pack}}^{\mathrm{o}}$, $\Delta\mu_{\mathrm{st}}^{\mathrm{o}}$, $\Delta\mu_{\mathrm{ent}}^{\mathrm{o}}$, and $\Delta\mu_{\mathrm{elec}}^{\mathrm{o}}$ are the standard free energy contributions from hydrocarbon transfer from water into micelle, formation of micellar core-water interface, hydrocarbon tail packing in the micelle, surfactant headgroup steric interaction, headgroup-counterion mixing, and electrostatic interaction, respectively. $\Delta\mu_{\mathrm{act}}^{\mathrm{o}}$ comes from the activity contribution. The calculation of these energy terms are introduced below in detail with respect to surfactant mixture.

A.2.1.2 Hydrocarbon tail transfer contribution $\Delta\mu_{\mathrm{trt}}^{\mathrm{o}}$

$$\Delta\mu_{\mathrm{trt}}^{\mathrm{o}} = \sum_{\mathrm{i}} \alpha_{\mathrm{i}}\Delta\mu_{\mathrm{trti}}^{\mathrm{o}} \quad \text{A.74}$$

where $\Delta\mu_{\mathrm{trti}}^{\mathrm{o}}$ is hydrocarbon tail transfer contribution of surfactant i.

Specifically, $\Delta\mu_{\mathrm{trti}}^{\mathrm{o}}$ consists of two parts: (a) the hydrocarbon tail transfer from aqueous solution containing salts to pure water $\Delta\mu_{\mathrm{i,s/w}}^{\mathrm{o}}$; (b) the subsequent transfer from pure water to the micellar core $\Delta\mu_{\mathrm{i,w/o}}^{\mathrm{o}}$. The Setchenov coefficient k_{s} for the calculation of $\Delta\mu_{\mathrm{i,s/w}}^{\mathrm{o}}$ is per CH_2 group based, which is different from the hydrocarbon tail volume-based k_{s}. Considering the CH_2 group adjacent to headgroup possesses weaker

hydrophobicity than the CH_2 groups away from headgroup and that the CH_3 group at the end of the tail may have stronger hydrophobicity, k_s multiplied by tail length should give a reasonable estimation of the salt effect on the entire hydrocarbon tail transfer. $\Delta\mu^{o}_{trti}$ is calculated following reported procedures as below:

$$\Delta\mu^{o}_{trti} = \Delta\mu^{o}_{i,s/w} + \Delta\mu^{o}_{i,w/o} \quad \text{A.75}$$

$$\frac{\Delta\mu^{o}_{i,s/w}}{kT} = -L_i \sum_s \alpha_s k_s C_s \quad \text{A.76}$$

$$\frac{\Delta\mu^{o}_{i,w/o}}{kT} = \frac{\Delta\mu^{o}_{ch3}}{kT} + (L_i - 1)\frac{\Delta\mu^{o}_{ch2}}{kT} \quad \text{A.77}$$

$$\frac{\Delta\mu^{o}_{ch3}}{kT} = 3.38lnT + \frac{4064}{T} - 44.13 + 0.02595T \quad \text{A.78}$$

$$\frac{\Delta\mu^{o}_{ch2}}{kT} = 5.85lnT + \frac{896}{T} - 36.15 - 0.0056T \quad \text{A.79}$$

where α_s is the molar fraction of salt s in total salts added to aqueous solution. In the present work, only one type of salt is added and thus, $\alpha_s = 1$. $\Delta\mu^{o}_{ch2}$ and $\Delta\mu^{o}_{ch3}$ are transfer energy contribution from methylene group and methyl group, respectively.

A.2.1.3 Micellar core-water interface formation contribution μ^{o}_{int}

The interfacial free energy contribution is calculated by the equation

$$\frac{\Delta\mu^{o}_{int}}{kT} = \sum_i \alpha_i \sigma_{ini}(a - a_{oi}) \quad \text{A.80}$$

where a is the area per surfactant molecule i at micellar core-water interface; a_{oi} is the area per surfactant molecule i at the interface shielded by the headgroup. a_{oi} = min (L_o^2, a_{hi}). L_o is the characteristic methylene segment length of the tail (L_o =0.46 nm), and a_{hi} is the effective cross-sectional area of the hydrated headgroup of surfactant i.

$$a = \frac{S\sum_i \alpha_i v_{ti}}{l_c} \quad \text{A.81}$$

$$a_{\mathrm{hi}} = \sum_{\mathrm{j}} \frac{C_{\mathrm{j}}}{\sum_{\mathrm{j}} C_{\mathrm{j}}} a_{\mathrm{ij}} \qquad \text{A.82}$$

where S is shape factor: S=3 for sphere; S=2 for cylinder; S=1 for disk. v_{ti} is the hydrocarbon tail volume of surfactant i. l_{c} is micellar core minor radius. C_{j} is molar fraction of counterion j in total counterions. a_{ij} is the effective cross-sectional area of the headgroup of surfactant i associated with counterion j as summarized in Table A.1 for ionic surfactants and Table A.2 for nonionic surfactants. The cross-sectional area of Octylglucoside (OG) and polyoxythylene (C_nE_n) use reported values.

In Eq. (A.80), σ_{ini} is the interfacial tension between water and surfactant i in micelle phase and is given by

$$\sigma_{\mathrm{ini}} = 0.7562(\sigma_{\mathrm{sui}} + \sum_{\mathrm{s}} \alpha_{\mathrm{s}}\, \sigma_{\mathrm{s}}) - 0.4906(\sigma_{\mathrm{sui}} \sum_{\mathrm{s}} \alpha_{\mathrm{s}}\, \sigma_{\mathrm{s}})^{0.5} \qquad \text{A.83}$$

$$\sigma_{\mathrm{sui}} = 29.7003[1 - \exp(-0.1532 L_{\mathrm{i}})] - 0.0896(T - 298.15) \qquad \text{A.84}$$

$$\sigma_{\mathrm{s}} = \sigma_{\mathrm{w}} + \left(\frac{d\sigma_{\mathrm{s}}}{dC_{\mathrm{s}}}\right) C_{\mathrm{s}} \qquad \text{A.85}$$

$$\sigma_{\mathrm{w}} = 235.8\left(1 - \frac{T}{647.15}\right)^{1.256} \left[1 - 0.625\left(1 - \frac{T}{647.15}\right)\right] \qquad \text{A.86}$$

where σ_{sui} is the surface tension of normal alkane tails from surfactant i. σ_{s} is the surface tension of aqueous solution with added salt s. σ_{w} is the surface tension of pure water. L_{i} is the hydrocarbon chain length of surfactant i. T is the absolute temperature. C_{s} is the salt concentration in unit M. ($d\sigma_{\mathrm{s}}/dC_{\mathrm{s}}$) is the correlation between surface tension and salt concentration as listed in Table A.3. Setchenov coefficients of different salts are also listed in Table A.3.

A.2.1.4 Hydrocarbon tail packing contribution $\Delta\mu^{o}_{pack}$

The packing free energy arises from the constraint of one end of surfactant tail at the micelle core-water interface, while the entire tail assumes a uniform conformation in the micelle core. For mixed surfactants, an averaged-number of segments in the tail was used based on mixed composition.

$$\frac{\Delta\mu^{o}_{pack}}{kT} = \frac{9P_p\pi^2}{80n_s}\left(\frac{l_c}{L_o}\right)^2 \quad \text{A.87}$$

where P_p is the packing factor (P_p =1/3 for spherical micelle; P_p =1/2 for cylindrical micelle; P_p =1 for planar micelle); l_c is micellar core minor radius as defined above; L_o is the characteristic segment length of the tail; n_s is the average number of segments in the tail and is calculated by

$$n_s = \frac{\sum_i \alpha_i l_{oi}}{L_o} \quad \text{A.88}$$

$$l_{oi} = 0.2765 + 0.1265(L_i - 1) \quad \text{A.89}$$

where l_{oi} is the extended hydrocarbon tail length (in nm) of surfactant i.

Substitution of Eq. (A.88) and Eq. (A.89) into Eq. (A.87) leads to

$$\frac{\Delta\mu^{o}_{pack}}{kT} = \frac{9P_p\pi^2 l_c^2}{80L_o\sum_i \alpha_i l_{oi}} \quad \text{A.90}$$

It is clearly seen that the packing free energy is dependent on micelle packing factor P_p which is dependent on micelle shape factor *S*, mixed micelle composition α_i, and micellar core minor radius l_c which changes with solution composition x_i and therefore with α_i.

A.2.1.5 Headgroup steric interaction $\Delta\mu_{\mathrm{st}}^{\mathrm{o}}$

The steric free energy considers the interaction between headgroups and counterions at the micellar core-water interface based on the assumption that the surfactants and counterions are components of an ideal monolayer at the interface. The radius of hydrated counterions is summarized in Table A.4, which are very close to reported results.

$$\frac{\Delta\mu_{\mathrm{st}}^{\mathrm{o}}}{kT} = -(1+\sum_{\mathrm{j}}\delta_{\mathrm{j}})[1-\frac{\sum_{\mathrm{i}}\alpha_{\mathrm{i}}a_{\mathrm{hi}}+\sum_{\mathrm{j}}\delta_{\mathrm{i}}a_{\mathrm{hj}}}{a}] \qquad \text{A.91}$$

A.2.1.6 Headgroup-counterion mixing entropy $\Delta\mu_{\mathrm{ent}}^{\mathrm{o}}$

The free energy contribution accounts for the entropy gain associated with the mixing of surfactant components and counterions and is modeled by ideal mixing in which all the components are randomly distributed on the micelle surface.

$$\frac{\Delta\mu_{\mathrm{ent}}^{\mathrm{o}}}{kT} = \sum_{\mathrm{i}}\alpha_{\mathrm{i}}\ln\frac{\alpha_{\mathrm{i}}}{1+\sum_{\mathrm{j}}\delta_{\mathrm{j}}} + \sum_{\mathrm{j}}\delta_{\mathrm{j}}\ln\frac{\delta_{\mathrm{j}}}{1+\sum_{\mathrm{j}}\delta_{\mathrm{j}}} \qquad \text{A.92}$$

A.2.1.7 Electrostatic contribution $\Delta\mu_{\mathrm{elec}}^{\mathrm{o}}$

The electrostatic free energy contribution arises from the building of an electrical double layer around micelles and is evaluated for spherical and cylindrical micelle respectively by

$$\frac{\Delta\mu_{\mathrm{elec}}^{\mathrm{o}}}{kT} = \frac{2\pi q^2 d_{\mathrm{st}}}{a\epsilon\left(1+\frac{d_{\mathrm{st}}}{l_{\mathrm{c}}}\right)} + \frac{a_{\mathrm{ch}}\kappa}{4\pi\lambda_{\mathrm{B}}}\int_0^t \varphi(d_{\mathrm{o}})\,dt \qquad \text{A.93}$$

$$\frac{\Delta\mu_{\mathrm{elec}}^{\mathrm{o}}}{kT} = \frac{2\pi q^2 l_{\mathrm{c}}}{a\epsilon}\ln\left(1+\frac{d_{\mathrm{st}}}{l_{\mathrm{c}}}\right) + \frac{a_{\mathrm{ch}}\kappa}{4\pi\lambda_{\mathrm{B}}}\int_0^t \varphi(d_{\mathrm{o}})\,dt \qquad \text{A.94}$$

The first term on the right side of Eq. (A.93) and Eq. (A.94) represents the contribution from Stern layer; the 2nd term represents electrostatic interaction between micelle and ions. d_{st} is the thickness of the Stern layer and is estimated from the structure

of hydrated headgroup and hydrated counterion. The value of d_{st} used in the present model is either estimated from surfactant structure or adopted from MF model. a_{ch} is the area per surfactant molecule at the micelle surface of charge. κ is the inversed Debye length. λ_B is the Bjerrum length. t is a function of micelle surface charge density σ. $\varphi(d_o)$ is the surface electrical potential at the micelle surface of charge. These parameters are described below.

$$a_{ch} \approx \frac{S(v_t+v_h)}{r_{ch}} \quad \text{A.95}$$

$$r_{ch} = d_{ch} + l_c \quad \text{A.96}$$

$$v_t = \sum_i \alpha_i v_{ti} \quad \text{A.97}$$

$$v_h = \sum_i \alpha_i v_{hi} \quad \text{A.98}$$

$$v_{hi} \approx \frac{4\pi\left(\frac{a_{ij}}{\pi}\right)^{3/2}}{3} \quad \text{A.99}$$

$$\kappa = \left(\frac{2e^2 I}{\epsilon\epsilon_o kT}\right)^{1/2} \quad \text{A.100}$$

$$\epsilon = \epsilon_w + \sum_s \delta_s \alpha_s C_s \quad \text{A.101}$$

$$\epsilon_w = -1.0677 + 306.4670\exp(-4.52 \times 10^{-3}T) \quad \text{A.102}$$

$$\lambda_B = \frac{e^2}{4\pi\epsilon\epsilon_o kT} \quad \text{A.103}$$

$$t = \frac{4\pi\sigma\lambda_B}{e\kappa} \quad \text{A.104}$$

$$\sigma = \frac{e(\sum_i \alpha_i z_i + \sum_j z_j \delta_j)}{a_{ch}} \quad \text{A.105}$$

where v_t is the average volume of hydrocarbon tails of mixed surfactants. v_h is the average volume of hydrated headgroups of mixed surfactants associated with counterions. r_{ch} is the radius of the micelle surface of charge. The electrostatic contribution barely changes with and without v_h in Eq. (A.95). v_{hi} is the volume of headgroup of surfactant i.

d_{ch} is the distance from the surface of micellar core to the center of charged headgroup (see Table A.5 for different surfactants). Therefore, d_{ch} is zero for nonionic surfactant. For mixture, d_{ch} is the average value based on mixed composition. The schematic representation of interfacial region with d_{ch} and d_{st} can be found elsewhere. e is the elementary positive charge. I is ionic strength. ϵ, ϵ_w, and ϵ_o are the dielectric constant of solvent, water, and vacuum, respectively. δ_s is the dielectric decrement of added salt s as listed in Table A.3. δ_s is salt-dependent and therefore, salts with one ion in common should have different δ_s. It is expected that the effect of coion on aggregation properties might be reflected through δ_s. It is actually expected that all salt-dependent factors may exhibit the coion effects on aggregation properties.

To calculate the integration in Eq. (A.93) and Eq. (A.94), the linearized PB equation is solved with respect to surface potential $\varphi(d_o)$. Because the linearized PB equation can only be numerically solved for one-dimensional problem, the analytical solution of surface potential from PB equation of two- and three-dimensional problems are more interested in. Three-dimensional problems are reduced to an effective one-dimensional problem by the introduction of an angle-averaged Laplacian operator. An effective generalized one-dimensional form of PB equation for spherical, cylindrical, and planar geometries is given by

$$\frac{d^2\varphi}{dd^2} + \left(\frac{S-1}{d}\right)\frac{d\varphi}{dd} = u \qquad \text{A.106}$$

with the boundary conditions of

$$\frac{d\varphi}{dd}\Big|_{d=\infty} = 0 \qquad \text{A.107}$$

and

$$\frac{d\varphi}{dd}\Big|_{d=d_o} = -t \qquad \text{A.108}$$

The solution of Eq. (A.103) is given by

$$\varphi(d) = \frac{e\sigma}{\varepsilon\epsilon_{\mathrm{o}}\kappa kT}\left(\frac{d_{\mathrm{o}}}{d}\right)^{\upsilon}\frac{K_{\upsilon}(d)}{K_{\upsilon+1}(d_{\mathrm{o}})} \qquad \text{A.109}$$

where $K_{\upsilon}(d)$ is modified Bessel function of the second kind and $\upsilon = (S-2)/2$. Given the values of υ and d, $K_{\upsilon}(d)$ can be estimated. Substitution of $\varphi(d)$ at $d=d_{\mathrm{o}}$ into the Eq. (A.93) and Eq. (A.94) leads to

$$\frac{\Delta\mu^{\mathrm{o}}_{\mathrm{elec}}}{kT} = \frac{a_{\mathrm{ch}}\kappa}{8\pi\lambda_{\mathrm{B}}}\frac{K_{\upsilon}(d_{\mathrm{o}})}{K_{\upsilon+1}(d_{\mathrm{o}})}t^{2} \qquad \text{A.110}$$

with

$$d_{\mathrm{o}} = r_{\mathrm{ch}}\kappa \qquad \text{A.111}$$

A.2.1.8 Activity coefficient contribution $\Delta\mu^{\mathrm{o}}_{\mathrm{act}}$

The activity coefficient contribution comes from the incorporation of activity coefficient term into exponential part in Eq. (A.69) and is given by

$$\frac{\Delta\mu^{\mathrm{o}}_{\mathrm{act}}}{kT} = \ln\left(\prod_{\mathrm{i}}(\gamma_{\mathrm{mi}})^{-\alpha_i}\prod_{\mathrm{j}}(\gamma_{\mathrm{mj}})^{-\delta_{\mathrm{j}}}\right) \qquad \text{A.112}$$

A.2.2 Free energy minimization and parameter determination

The standard micellization free energy $\Delta\mu^{\mathrm{o}}_{\mathrm{m}}$ depends on micelle shape S, micelle composition α_{i}, micellar core minor radius l_{c}, and counterion binding coefficient δ_{j}, at given solution conditions (model inputs), which include the composition of surfactant i in total mixed surfactants in bulk solution x_{mi}, temperature T, salt or mixed salts concentration C_{s}. In the present research, the minimization of $\Delta\mu^{\mathrm{o}}_{\mathrm{m}}$ is only performed for spherical micelles (S=3), and infinite cylindrical micelles (S=2), respectively, with respect to independent variables S, α_{i}, l_{c}, and δ_{j} under the constraints of $0<\alpha_{\mathrm{i}}<1$(for pure

surfactant α_i = 1), $0<l_c<l_o$ (l_o is the longest extended chain length among all the surfactants i), and $0< \delta_j <1$. The minimization is calculated using MATLAB code, which is a process of multiple-variable (S, α_i, l_c, and δ_j) nonlinear optimization. The required model inputs are solution conditions mentioned above, surfactant structural properties in Tables A.1 or A.2, salt-associated parameters in Table A.3, and ion radius in Table A.4. The outputs include a set of optimized variables S, α_i, l_c, and δ_j, the minimized micellization free energy $\Delta\mu_m^o$, cmc, aggregation number, and sphere-to-rod transition.

If the standard micellization free energy of spherical micelle is minimum, optimized shape should be sphere (S=3). The cmc is calculated by (here this is the mole fraction):

$$X_{msp} = \exp\left(\frac{1}{kT}\Delta\mu_{msp}^o\right) \quad \text{A.113}$$

The micelle size distribution is assumed to be monodisperse and is given by

$$X_{Msp} = \frac{X - X_{msp}}{N_{sp}} \quad \text{A.114}$$

The micelle aggregation number given by

$$N_{sp} = \frac{\frac{4}{3}\pi(l_{sp})^3}{v_{tsp}} \quad \text{A.115}$$

If the standard micellization free energy of cylindrical micelle is minimum, the optimized shape should be a cylinder (S=2). The mass balance equations (A.116)-(A.118) as well as Eq. (A.72) need to be solved simultaneously with respect to X_m, X_{mi}, and X_{mj}:

$$X = X_m + \sum_{N=N_{sp}}^{\infty} N X_M \quad \text{A.116}$$

$$X_i = X_{mi} + \sum_{N=N_{sp}}^{\infty} N\alpha_i X_M \quad \text{A.117}$$

$$X_j = X_{mj} + \sum_{N=N_{sp}}^{\infty} N\delta_j X_M \quad \text{A.118}$$

The ladder model is used to solve the micelle size distribution and micellization free energy $\Delta\mu_{mcy}^o$ in terms of a finite cylindrical micelle. The corresponding cmc is evaluated

by replacing $\Delta\mu^{o}_{msp}$ using $\Delta\mu^{o}_{mcy}$ in Eq. (A.114).

With the determined X_m, X_{mi}, and X_{mj}, micelle size distribution can be completely evaluated using Eq. (A.72). Several commonly used micelle aggregation numbers are calculated as follows

$$N_n = \frac{M_1}{M_0} \quad \text{A.119}$$

$$N_w = \frac{M_2}{M_1} \quad \text{A.120}$$

$$N_z = \frac{M_3}{M_2} \quad \text{A.121}$$

where N_n, N_w, and N_z are the number-based, weight-based, and z-based aggregation number, respectively. $M_{k'}$ (k' = 1, 2, or 3) is defined as

$$M_{k'} = \sum_{N=N_{sp}}^{\infty} N^{k'} X_M \quad \text{A.122}$$

A.3 Tables of parameters of the cmc model

Table A. 1 Effective cross-sectional area (in nm^2) of the headgroup-counterion pair. Alkyl sulfate: XC_nS; benzalkonium chloride: C_nBzX; alkyltrimethyl ammonium: C_nTAX. X represents counterion.

	XC_nS	C_nBzX	C_nTAX
Li^+	0.45	----	----
Na^+	0.45	----	----
K^+	0.45	----	----
Cs^+	0.45	----	----
Cl^-	----	0.62	0.58
Br^-	----	0.62	0.58

Table A. 2 Effective cross-sectional area (in nm^2) of the headgroup of nonionic surfactants. Octylglucoside: OG; polyoxythylene: C_nE_n

OG	$C_{16}E_{20}$
0.40	0.53

Table A. 3 Model parameters of specific salt

Salt	k_s (L/mol)	$d\sigma_o/dC_s$ (mN/(m M))	δ_s
LiCl	0.11	2.2	-13.07
NaCl	0.05	2.1	-11.27
KCl	0.04	1.84	-9.67
CsCl	0.03	1.6	-7.87
NaBr	0.03	1.89	-11.87

Table A. 4 Radius of hydrated ions

Ions	Li^+	Na^+	K^+	Cs^+	Cl^-	Br^-
Radius (nm)	0.238	0.184	0.125	0.119	0.121	0.118

Table A. 5 Values of d_{ch} (nm) for different surfactants. Head of group of alkyl sulfate C_nS^-, alkyl dimethyl benzyl ammonium C_nBz^+, and alkyl trimethyl ammonium: C_nTA^+.

surfactants	CnS^- [20]	$CnBz^+$	$CnTA^+$
d_{ch} (nm)	0.4	0.2	0.1

A.4 Software

Software is developed based on ICI model and computational and programming resources for the prediction of mixed surfactants' distribution and associated corrosion inhibition efficiency in WOS environment. The front panel of software is shown in Fig. A.1.

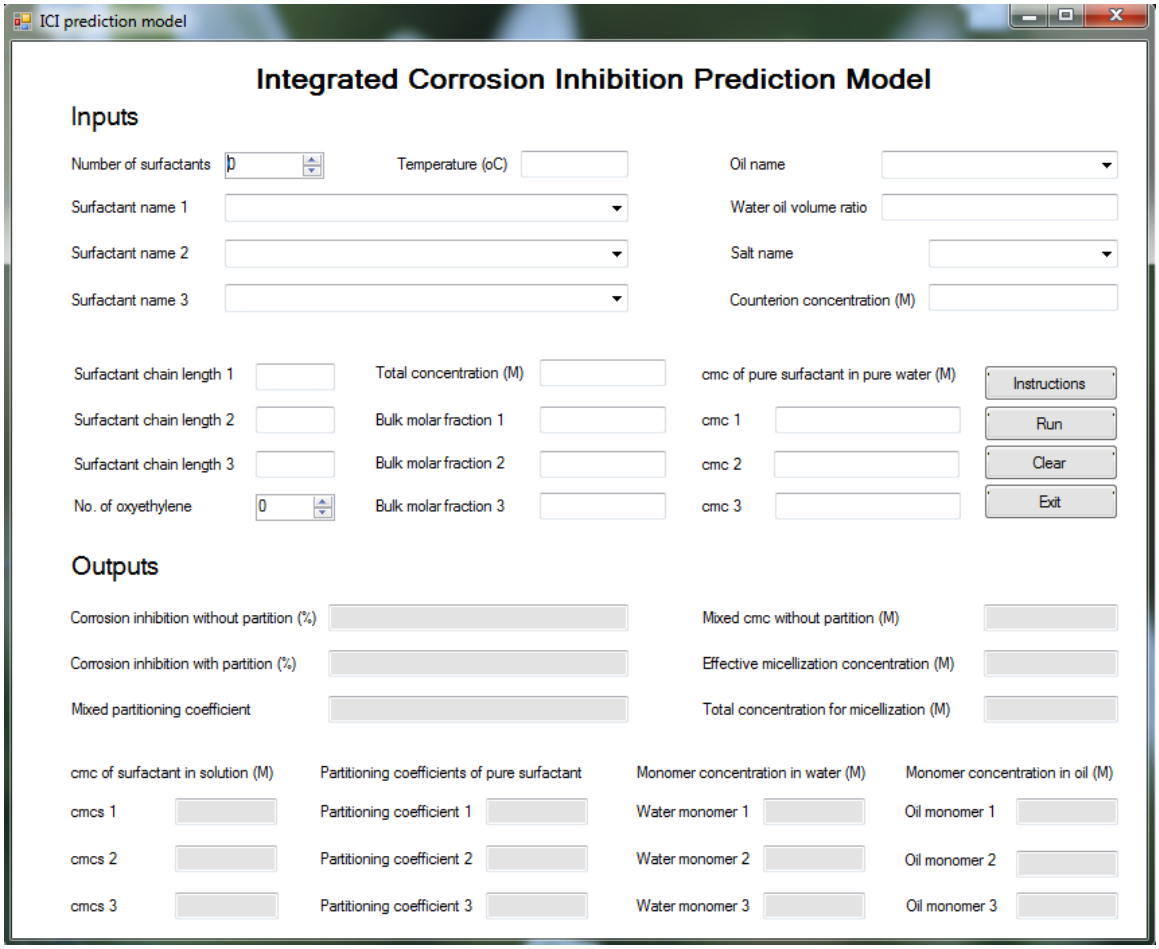

Fig. A.1 Front panel of software developed based on ICI model.

A.5 Visual basic code of software

```
Public Class LabelICIpredictionmodel
'instructions  %%%%
```

```
        Dim Cc As Double ' concontration of NaCl. Other salts will be added in a
improved version in the future
        Dim T As Double ' temperature in celcius degree
        Dim R As Double = 8.314 ' gas constant
        Dim Vra As Double ' water oil volume ratio
        Dim Cmw As Double ' molar concontration of water
        Dim Cmo As Double ' molar concentration of oil
        Dim ga As Double     ' activity coefficient of counterion. Estimate using
Davies' equation.
        Dim Ist As Double ' ionic strength of solution
        Dim x(N) As Double ' initial bulk mixed molar fraction of surfactants in
the value of 0-1
        Dim L(N) As Integer 'chain length
        Dim cmcp(N) As Double ' cmc of pure surfactant in pure water
        Dim cmcs(N) As Double ' cmc of pure surfactant in aqueous solution that
may or may not contain salt
        Dim Kmad(N) As Double ' modified adsorption constant
        Dim d(N) As Double ' counterion binding coefficient
        Dim ks As Double ' ks is Setchenov coefficient specific to  salt added in
water
        Dim Etr(N) As Double 'transfer free energy of molecule in unit RT
        Dim Etrt(N) As Double 'transfer free energy of molecule hydrocarbon tail
in unit RT
        Dim Etrh(N) As Double 'transfer free energy of molecule head group in unit
RT
        Dim gah(N) As Double 'activity coefficient of head group, which is assumed
to equal to ga
        Dim gat(N) As Double 'activity coeficient of hydrocarbon tail, which is
calculated using Setchenov equation
```

```
        Dim gam(N) As Double ' activity coefficient of surfactant molecule, which
is equal to geometric mean of gah*gat
        Dim Kp(N) As Double ' partitioning coefficient
        Dim Cwm(N) As Double 'concentration of monomeric surfactant in water
        Dim Com(N) As Double 'concentration of monomeric surfactant in oil
        Dim xnew(N) As Double ' new bluk mixed molar fraction of surfactants after
partitioning.
        Dim Kmadav As Double ' average value of Kmad
        Dim Kmadavn As Double ' average value of Kmad after partitioning
        Dim Cwmt As Double  ' total concentration of monomeric surfactant in water
        Dim Comt As Double  ' total concentration of monomeric surfactant in oil
        Dim cmcmixn As Double ' effective micellization concentration after
partitioning
        Dim Neo As Double = CDbl(NumericUpDownNumberofEO.Text) ' number of
oxyethylene group in polyoxythylene cetyl ether
'inputs %%%%%%%%%%%%%%%%%%%%%%%%%%%%%%%%%%%%%%%%%%%%%%%%%%%%%%%%%%%%%%%%%%%%%%%%
        Ctol = CDbl(Boxtotalconcentration.Text)
        Cc = CDbl(Boxcounterionconcentration.Text)
        T = CDbl(Boxtemperature.Text) + 273.15
        Vra = CDbl(Boxwateroilvolumeratio.Text)
        Cmw = 55.5
        If ComboBoxOilname.SelectedItem = "Heptane" Then
            Cmo = 6.83
        ElseIf ComboBoxOilname.SelectedItem = "Hexane" Then
            Cmo = 7.6
        ElseIf ComboBoxOilname.SelectedItem = "Toluene" Then
            Cmo = 9.43
        End If
        If N = 1 Then
```

```
            x(0) = CDbl(Boxbulkmolarfraction1.Text)
            L(0) = CDbl(Boxsurfactantchainlength1.Text)
            cmcp(0) = CDbl(Boxcmc1.Text)
            If ComboBoxSurfactant1.SelectedItem = "Alkyl trimethyl ammonium
surfactant (cationic)" Then
                Kmad(0) = 2.52
                d(0) = 0.55
                Etrh(0) = -0.1164 * T + 58.347
            ElseIf ComboBoxSurfactant1.SelectedItem = "Benzalkonium surfactant
(cationic)" Then
                Kmad(0) = 13.74
                d(0) = 0.6348
                Etrh(0) = -0.1184 * T + 58
            ElseIf ComboBoxSurfactant1.SelectedItem = "Polyoxythylene cetyl ether
surfactant (non-ionic)" Then
                Kmad(0) = 15.73
                d(0) = 0
                Etrh(0) = -0.0837 * T + 31.188 + (-0.0036 * T + 2.128) * Neo
            End If
        End If
        If N = 2 Then
            x(0) = CDbl(Boxbulkmolarfraction1.Text)
            x(1) = CDbl(Boxbulkmolarfraction2.Text)
            L(0) = CDbl(Boxsurfactantchainlength1.Text)
            L(1) = CDbl(Boxsurfactantchainlength2.Text)
            cmcp(0) = CDbl(Boxcmc1.Text)
            cmcp(1) = CDbl(Boxcmc2.Text)

            If ComboBoxSurfactant1.SelectedItem = "Alkyl trimethyl ammonium
```

```
surfactant (cationic)" Then
                Kmad(0) = 2.52
                d(0) = 0.55
                Etrh(0) = -0.1164 * T + 58.347
            ElseIf ComboBoxSurfactant1.SelectedItem = "Benzalkonium surfactant
(cationic)" Then
                Kmad(0) = 13.74
                d(0) = 0.6348
                Etrh(0) = -0.1184 * T + 58
            ElseIf ComboBoxSurfactant1.SelectedItem = "Polyoxythylene cetyl ether
surfactant (non-ionic)" Then
                Kmad(0) = 15.73
                d(0) = 0
                Etrh(0) = -0.0837 * T + 31.188 + (-0.0036 * T + 2.128) * Neo
            End If
            If ComboBoxSurfactant2.SelectedItem = "Alkyl trimethyl ammonium
surfactant (cationic)" Then
                Kmad(1) = 2.52
                d(1) = 0.55
                Etrh(1) = -0.1164 * T + 58.347
            ElseIf ComboBoxSurfactant2.SelectedItem = "Benzalkonium surfactant
(cationic)" Then
                Kmad(1) = 13.74
                d(1) = 0.6348
                Etrh(1) = -0.1184 * T + 58
            ElseIf ComboBoxSurfactant2.SelectedItem = "Polyoxythylene cetyl ether
surfactant (non-ionic)" Then
                Kmad(1) = 15.73
                d(1) = 0
```

```
                Etrh(1) = -0.0837 * T + 31.188 + (-0.0036 * T + 2.128) * Neo
            End If
        End If
        If N = 3 Then
            x(0) = CDbl(Boxbulkmolarfraction1.Text)
            x(1) = CDbl(Boxbulkmolarfraction2.Text)
            x(2) = CDbl(Boxbulkmolarfraction3.Text)
            L(0) = CDbl(Boxsurfactantchainlength1.Text)
            L(1) = CDbl(Boxsurfactantchainlength2.Text)
            L(2) = CDbl(Boxsurfactantchainlength3.Text)
            cmcp(0) = CDbl(Boxcmc1.Text)
            cmcp(1) = CDbl(Boxcmc2.Text)
            cmcp(2) = CDbl(Boxcmc3.Text)
            If ComboBoxSurfactant1.SelectedItem = "Alkyl trimethyl ammonium
surfactant (cationic)" Then
                Kmad(0) = 2.52
                d(0) = 0.55
                Etrh(0) = -0.1164 * T + 58.347
            ElseIf ComboBoxSurfactant1.SelectedItem = "Benzalkonium surfactant
(cationic)" Then
                Kmad(0) = 13.74
                d(0) = 0.6348
                Etrh(0) = -0.1184 * T + 58
            ElseIf ComboBoxSurfactant1.SelectedItem = "Polyoxythylene cetyl ether
surfactant (non-ionic)" Then
                Kmad(0) = 15.73
                d(0) = 0
                Etrh(0) = -0.0837 * T + 31.188 + (-0.0036 * T + 2.128) * Neo
            End If
```

```
            If ComboBoxSurfactant2.SelectedItem = "Alkyl trimethyl ammonium
surfactant (cationic)" Then
                Kmad(1) = 2.52
                d(1) = 0.55
                Etrh(1) = -0.1164 * T + 58.347
            ElseIf ComboBoxSurfactant2.SelectedItem = "Benzalkonium surfactant
(cationic)" Then
                Kmad(1) = 13.74
                d(1) = 0.6348
                Etrh(1) = -0.1184 * T + 58
            ElseIf ComboBoxSurfactant2.SelectedItem = "Polyoxythylene cetyl ether
surfactant (non-ionic)" Then
                Kmad(1) = 15.73
                d(1) = 0
                Etrh(1) = -0.0837 * T + 31.188 + (-0.0036 * T + 2.128) * Neo
            End If
            If ComboBoxSurfactant3.SelectedItem = "Alkyl trimethyl ammonium
surfactant (cationic)" Then
                Kmad(2) = 2.52
                d(2) = 0.55
                Etrh(2) = -0.1164 * T + 58.347
            ElseIf ComboBoxSurfactant3.SelectedItem = "Benzalkonium surfactant
(cationic)" Then
                Kmad(2) = 13.74
                d(2) = 0.6348
                Etrh(2) = -0.1184 * T + 58
            ElseIf ComboBoxSurfactant3.SelectedItem = "Polyoxythylene cetyl ether
surfactant (non-ionic)" Then
                Kmad(2) = 15.73
```

```
                d(2) = 0
                Etrh(2) = -0.0837 * T + 31.188 + (-0.0036 * T + 2.128) * Neo
            End If
        End If
'calculation of activity coefficient using Debye-Huckel equation %%%%%%%%%%%%%%%%%%
        Ist = 1 / 2 * (Cc * 1 ^ 2 + Cc * 1 ^ 2)
        Dim SqrIst As Double = Math.Sqrt(Ist)
        ga = 10 ^ (-(0.2409 + 9.01 * 10 ^ (-4) * T) * Cc ^ 2 * SqrIst / (1 + 3 *
10 ^ (-8) * (0.28 + 1.62 * 10 ^ (-4) * T) * SqrIst))
'calculation of mixed cmc in aqueous solution before partitioning %%%%%%%%%%%%%%%%%%
        Dim sum1 As Double = 0
        Dim i As Integer
        For i = 0 To (N - 1) Step 1
            sum1 = sum1 + x(i) * (ga * Cc) ^ d(i) * cmcp(i) ^ (-1 - d(i))
        Next
        Boxmixedcmcwithoutpartition.Text = (1 / sum1).ToString("e2")
'calculation of modified adsorption constant for mixture %%%%%%%%%%%%%%%%%%%%%%%%%%
        Kmadav = 0
        For i = 0 To (N - 1) Step 1
            Kmadav = Kmadav + x(i) * Kmad(i)
        Next
'calculation of corrosion inhibition without partitioning process %%%%%%%%%%%%%%%%%%
        If Ctol <= 1 / sum1 Then
            Boxcorrosioninhibitionwithoutpartition.Text = (100 * (1 - 1 / (1 +
Kmadav * Ctol / (1 / sum1)))).ToString("f2")
        End If
        If Ctol > 1 / sum1 Then
            Boxcorrosioninhibitionwithoutpartition.Text = "constant value above
cmc: " & (100 * (1 - 1 / (1 + Kmadav))).ToString("f2")
```

```
        End If
'selection of Setchenov coefficient which is specific to  salt %%%%%%%%%%%%%%%%%%%%
        If ComboBoxSaltname.SelectedItem = "NaCl" Then
            ks = 0.05
        ElseIf ComboBoxSaltname.SelectedItem = "NaBr" Then
            ks = 0.03
        ElseIf ComboBoxSaltname.SelectedItem = "NaI" Then
            ks = 0
        ElseIf ComboBoxSaltname.SelectedItem = "NaOH" Then
            ks = 0.1
        ElseIf ComboBoxSaltname.SelectedItem = "NaNO3" Then
            ks = 0.03
        ElseIf ComboBoxSaltname.SelectedItem = "LiCl" Then
            ks = 0.11
        ElseIf ComboBoxSaltname.SelectedItem = "KCl" Then
            ks = 0.04
        ElseIf ComboBoxSaltname.SelectedItem = "CsCl" Then
            ks = 0.03
        End If
'calculation of partitioning coefficient of pure surfactant in solution %%%%%%%%%%
        For i = 0 To (N - 1) Step 1
            Etrt(i) = -L(i) * ks * Cc + 3.38 * Math.Log(T) + 4064 / T - 44.13 +
0.02595 * T + (L(i) - 1) * (5.85 * Math.Log(T) + 896 / T - 36.15 - 0.0056 * T)
            gah(i) = ga
            gat(i) = 10 ^ (Ist * L(i) * ks)
            gam(i) = Math.Sqrt(gah(i) * gat(i))
            Kp(i) = Cmo * gam(i) / Cmw * Math.Exp(-(Etrt(i) + Etrh(i)))
        Next
'calculation of cmc of pure surfactant in salt solution %%%%%%%%%%%%%%%%%%%%%%%%%%%
```

```
        For i = 0 To (N - 1) Step 1
            cmcs(i) = 1 / ((ga * Cc) ^ d(i) * cmcp(i) ^ (-1 - d(i)))
        Next
'calculation of partitioning coefficient of surfactant mixture %%%%%%%%%%%%%%%%%%%
        Dim sum2 As Double = 0
        Dim sum3 As Double = 0
        Dim sum4 As Double = 0
        For i = 0 To (N - 1) Step 1
            sum2 = sum2 + x(i) / (cmcs(i) / (1 + 1 / Vra) + Kp(i) * cmcs(i) / (Vra
+ 1))
            sum3 = sum3 + Kp(i) * x(i) / (Vra + Kp(i))
            sum4 = sum4 + x(i) / (Vra + Kp(i))
        Next
        Boxmixedpartitioningcoefficient.Text = (sum3 / sum4).ToString("e2")
'calculation of total concentration for micellization initially added to water for
micelliation in oil-water environment %%%%%%%%%%%%%%%%%%%%%%%%%%%%%%%%%%%%%%%%%%%%
        Dim cmcapp As Double 'total concentration for micellization in water-oil
environment
        cmcapp = 1 / sum2
        Boxtotalconcentrationformicellization.Text = cmcapp.ToString("e2")
'calculation of monomer concentration in water and oil and new mixed molar
concnetration in water  %%%%%%%%%%%%%%%%%%%%%%%%%%%%%%%%%%%%%%%%%%%%%%%%%%%%%%%%%%%
        For i = 0 To (N - 1) Step 1
            Cwm(i) = x(i) * Ctol / (1 + Kp(i) / Vra)
            Com(i) = Cwm(i) * Kp(i)
        Next
        Cwmt = 0
        Comt = 0
        For i = 0 To (N - 1) Step 1
```

```
            Cwmt = Cwmt + Cwm(i)
            Comt = Comt + Com(i)
        Next
        For i = 0 To (N - 1) Step 1
            xnew(i) = Cwm(i) / Cwmt
        Next
'calculation of effective micellization concentration after partitioning %%%%%%%%%%
        Dim sum5 As Double = 0
        For i = 0 To (N - 1) Step 1
            sum5 = sum5 + xnew(i) * (ga * Cc) ^ d(i) * cmcp(i) ^ (-1 - d(i))
        Next
        cmcmixn = 1 / sum5
        Boxeffectivemicellizationconcentration.Text = cmcmixn.ToString("e2")
'calculation of modified adsorption constant for new mixture after partitioning %%%
        Kmadavn = 0
        For i = 0 To (N - 1) Step 1
            Kmadavn = Kmadavn + xnew(i) * Kmad(i)
        Next
'calculation of corrosion inhibition considering partitioning process  %%%%%%%%%%%%
        If Ctol <= cmcapp * (1 / Vra + 1) Then
            Boxcorrosioninhibitionwithpartition.Text = (100 * (1 - 1 / (1 +
Kmadavn * Cwmt / cmcmixn))).ToString("f2")
        End If
        If Ctol > cmcapp * (1 / Vra + 1) Then
            MessageBox.Show("Total surfactant concentration initially added into
water is above the effective concentration for micellization, which gives constant
corrosion inhibition.")
            Boxcorrosioninhibitionwithpartition.Text = "constant value above cmc:
" & (100 * (1 - 1 / (1 + Kmadavn))).ToString("f2") ' constant value given at Cwmt
```

```
= cmcmixn
        End If
'outputs %%%%
```

```
            Boxoilmonomer1.Text = Com(0).ToString("e2")
            Boxoilmonomer2.Text = Com(1).ToString("e2")
            Boxoilmonomer3.Text = Com(2).ToString("e2")
        End If
    End Sub
    Private Sub Clear_Click(sender As Object, e As EventArgs) Handles
ButtonClear.Click
        Boxtotalconcentration.Clear()
        Boxcounterionconcentration.Clear()
        Boxtemperature.Clear()
        Boxwateroilvolumeratio.Clear()
        Boxbulkmolarfraction1.Clear()
        Boxbulkmolarfraction2.Clear()
        Boxbulkmolarfraction3.Clear()
        Boxsurfactantchainlength1.Clear()
        Boxsurfactantchainlength2.Clear()
        Boxsurfactantchainlength3.Clear()
        Boxcmc1.Clear()
        Boxcmc2.Clear()
        Boxcmc3.Clear()
        Boxcorrosioninhibitionwithoutpartition.Clear()
        Boxcorrosioninhibitionwithpartition.Clear()
        Boxmixedcmcwithoutpartition.Clear()
        Boxeffectivemicellizationconcentration.Clear()
        Boxtotalconcentrationformicellization.Clear()
        Boxmixedpartitioningcoefficient.Clear()
        Boxcmcs1.Clear()
        Boxcmcs2.Clear()
        Boxcmcs3.Clear()
```

```
        Boxpartitioningcoefficient1.Clear()
        Boxpartitioningcoefficient2.Clear()
        Boxpartitioningcoefficient3.Clear()
        Boxwatermonomer1.Clear()
        Boxwatermonomer2.Clear()
        Boxwatermonomer3.Clear()
        Boxoilmonomer1.Clear()
        Boxoilmonomer2.Clear()
        Boxoilmonomer3.Clear()
        NumericUpDownnumberofsurfactant.Focus()
        NumericUpDownnumberofsurfactant.Value = 0
        NumericUpDownNumberofEO.Value = 0
        ComboBoxSurfactant1.Items.Remove(ComboBoxSurfactant1.SelectedItem)
        ComboBoxSurfactant2.Items.Remove(ComboBoxSurfactant2.SelectedItem)
        ComboBoxSurfactant3.Items.Remove(ComboBoxSurfactant3.SelectedItem)
        ComboBoxOilname.Items.Remove(ComboBoxOilname.SelectedItem)
        ComboBoxSaltname.Items.Remove(ComboBoxSaltname.SelectedItem)
    End Sub
    Private Sub Labelexit_Click(sender As Object, e As EventArgs) Handles
Buttonexit.Click
        Me.Close()
    End Sub
    Private Sub LabelICImodelBackup_Load(sender As Object, e As EventArgs) Handles
MyBase.Load
    End Sub
End Class
```